Universidad de Navarra

FACULTAD DE FARMACIA Y NUTRICIÓN

DEPARTAMENTO DE TECNOLOGÍA Y QUÍMICA FARMACÉUTICAS

Improvement of the bioavailability of quercetin encapsulated in zein-based nanoparticles. Effects on a Diet-Induced Obesity model

TESIS DOCTORAL

Raquel Campión Rodríguez

Pamplona, 2022

Universidad de Navarra

FACULTAD DE FARMACIA

DEPARTAMENTO DE TECNOLOGÍA Y QUÍMICA FARMACÉUTICAS

TESIS DOCTORAL

Improvement of the bioavailability of quercetin encapsulated in zein-based nanoparticles. Effects on a Diet-Induced Obesity model

Memoria presentada por **D.ª Raquel Campión Rodríguez** para aspirar al grado de Doctor por la Universidad de Navarra.

Pamplona, a 31 de agosto de 2022

Fdo. Raquel Campión

Universidad de Navarra

FACULTAD DE FARMACIA Y NUTRICIÓN

DEPARTAMENTO DE TECNOLOGÍA Y QUÍMICA FARMACÉUTICAS

El presente trabajo de investigación titulado:

Improvement of the bioavailability of quercetin encapsulated in zein-based nanoparticles. Effects on a Diet-Induced Obesity model

que presenta D./ª Raquel Campión Rodríguez para aspirar al grado de Doctor por la Universidad de Navarra, ha sido realizado en el Departamento de Tecnología y Química Farmacéuticas de la Facultad de Farmacia y Nutrición, bajo la dirección de el/la Dr/a. Juan M. Irache y Carlos J. González. Considerando finalizado el trabajo, autorizan su presentación a fin de que pueda ser juzgado y calificado por el Tribunal correspondiente.

Pamplona, a 31 de agosto de 2022

VºBº Director
Dr. Juan M. Irache Garreta

VºBº Director
Dr. Carlos J. González Navarro

"No tengas miedo del trabajo duro. Nada que merezca la pena es fácil. No dejes que otros te desalienten o te digan que no puedes hacerlo. En su día me dijeron que las mujeres no podían ser químicas. No encontré ninguna razón por la que no pudiéramos."

Gertrude B. Elion

(Química y farmacóloga estadounidense, 1918-1999)

A mis padres

A mi hermana

A César

Agradecimientos

En primer lugar, me gustaría dar las gracias a la Universidad de Navarra y al Departamento de Tecnología y Química Farmacéuticas de la Facultad de Farmacia, por permitirme realizar esta tesis. Especialmente quiero dar las gracias a mis directores, Juanma y Carlos, por confiar en mí sin apenas conocerme, y darme la oportunidad de comenzar esta aventura.

Gracias también a todos los profesionales con los que he tenido la oportunidad de trabajar en el Departamento de Tecnología y Química Farmacéuticas, en el Departamento de Ciencias de la Alimentación y Fisiología, en el Departamento de Química y en la plataforma de imagen del CIMA. Gracias también al Centro Nacional de Tecnología y Seguridad Alimentaria (CNTA), a Nucaps Nanotechnology, S.L. y al equipo de Radiofarmacia de la Clínica Universidad de Navarra.

Por supuesto, este trabajo no hubiera salido adelante sin la ayuda de mis compañeras y compañeros. Cristina, mi compañera de batallas, gracias por estar ahí, por ayudarme y por animarme en todo momento. Ana Luisa, nuestro referente en el laboratorio, gracias por toda tu ayuda y por responder a mis miles de preguntas siempre con buena cara y alegría. Esta tesis también ha salido adelante gracias a vosotras. Cristian, la alegría del laboratorio, gracias por hacernos las interminables jornadas más amenas. ¡Ha sido un placer trabajar con vosotros!

Gracias a toda la gente con la que he coincidido en el laboratorio: Alba, Esther, Souhaila, Jorge, Pablo Torres, Camila, Silvia, Irati, María, Jonathan, Carmen, Soco, Inés, Lecnia… Ha sido un placer. Gracias también a Pablo Rosas, por la alegría que transmites y los ánimos que siempre nos das. Gracias a Natalia, Sara y Zinnia, gracias por vuestros consejos y por compartir conmigo vuestras experiencias. Gracias a Hugo, por resolver todas mis dudas durante estos años, y sobre todo, gracias por tu ayuda y dedicación en el macro estudio de eficacia. No hubiese salido adelante sin ti. Gracias a Paula Aranaz, por enseñarme y responder a todas mis preguntas cuando me quedé sola frente a los gusanos cuando para mí era un mundo desconocido.

Gracias a mis químicas: Bea, Esther, Joan, Laura y Marcela. Vosotras mejor que nadie sabéis lo que es sufrir las alegrías y las penas de un Doctorado, y me alegro de haber vivido esta aventura al mismo tiempo que vosotras (y Laura, gracias por aguantarnos). Gracias por esos planes que nos ayudaban a desconectar y desahogarnos.

Gracias a Iratxe, aunque no sepas exactamente qué es lo que hago, gracias por estar siempre ahí, escucharme, apoyarme y animarme.

Gracias a Marta. Sin ti, esta tesis no hubiera sido posible. Has hecho que aprenda muchas cosas sobre mí misma, y durante esta etapa he crecido en lo personal gracias a ti.

Quiero dar las gracias también a mi familia, que, aunque no entiendan qué es eso del Doctorado, siempre me preguntan por “los estudios” o “el trabajo”.

Gracias a César. Gracias por escucharme y apoyarme, por interesarte por mis proyectos, gracias por tu paciencia. Gracias por intentar entenderme, en lo profesional y en lo personal. Ahora comienza una nueva aventura para los dos, sea cual sea.

Y por último y más importante, gracias a esas tres personas que me han apoyado desde que, con 18 años, decidí que quería ser química.

Gracias a mis padres, Josetxo y Maryan. Gracias por darme la oportunidad de estudiar lo que me gustaba, aunque eso os supusiera un esfuerzo, y por apoyarme en todas las fases de este difícil mundo que es la ciencia. Gracias por animarme siempre a hacer lo que me gusta. No hubiese llegado hasta aquí sin vosotros.

Gracias a mi hermana, María. Hermana, amiga, psicóloga, estilista… Y muchas cosas más. Gracias por tu sabiduría y tu ayuda en los momentos difíciles. Gracias por todo lo que haces por mí. No estaría aquí sin ti, y es un orgullo ser tu hermana.

Gracias a los tres por todo lo que habéis hecho por mí durante todos estos años, desde aguantar mi humor hasta escuchar mis presentaciones. Gracias por creer siempre en mí, y por cuidarme y animarme siempre. Gracias por estar ahí.

Gracias a todos vosotros y a los que de una u otra manera han puesto su granito de arena en esta tesis, y que seguro me he dejado en el tintero.

¡GRACIAS! MILA ESKER!

Table of contents

Abbreviations

ACN	Acetonitrile
ACOT	Acyl-CoA thioestherase
ACOX1	Peroxisomal Acyl-CoA oxidase 1
AESAN	Spanish Agency for Food Safety and Nutrition
AIP	Atherogenic index of plasma
ALT	Alanine transaminase
AST	Aspartate transaminase
AUC	Area under the curve
BMI	Body-mass index
CBG	Cytosolic β-glucosidase
C_{max}	Maximum concentration
CoA	Coenzyme A
COMT	Catechol-O-methyltransferase
COPD	Chronic obstructive pulmonary disease
CPT2	Carnitine palmitoyltranferase-2
D°	Diffusion coefficient in water
Deff	Effective Diffusion Coefficient
DIO	Diet-Induced Obesity
DLS	Dynamic Light Scattering
DMSO	Dimethyl sulfoxide
EE	Encapsulation efficiency
EFSA	European Food Safety Authority
ELISA	Enzyme-linked immunosorbent assay
ELS	Electrophoretic Light Scattering
EMA	European Medicines Agency
FASN	Fatty acid synthase
FDA	U.S. Food and Drug Administration
Fr	Relative oral bioavailability

FTIR	Fourier Transform Infrared spectroscopy
GLP-1	Glucagon-like peptide-1
GRAS	Generally Recognized as Safe
HDL	High density lipoprotein
HFS	High fat/high sucrose diet
HOMA-IR	Homeostasis model of insulin resistance
HPLC	High Performance Liquid Chromatography
HP-β-CD	2-hydroxypropyl-β-cyclodextrin
i.v.	Intravenous administration
LOQ	Limit of quantification
LPH	Lactase-phlorizin hydrolase
MCP-1	Monocyte chemoattractant protein-1
MFE-2	Multifunctional protein 2
MPT	Multiple particle tracking
MRT	Mean residence time
MSD	Mean square displacement
NAFLD	Non-alcoholic fatty liver disease
NC	Zein nanocapsules
NF-κB	Nuclear factor kappa B
NGM	Nematode Growth Medium
NS	Zein nanospheres
NS-PEG25	PEG-coated zein nanospheres (25%)
NS-PEG50	PEG-coated zein nanospheres (50%)
OATP	Organic anion transporting polypeptide
OGTT	Oral glucose tolerance test
OSA	Obstructive sleep apnoea
PBS	Phosphate Buffered Saline
PBST	0.01% Triton X-100 in Phosphate Buffered Saline
PDI	Polydispersity index
PEG	Polyethylene glycol

PLGA	Poly(lactic-co-glycolic acid)
PPARγ	Peroxisome proliferator-activated receptor γ
PQ	Partitioning quotient
ROS	Reactive oxygen species
SCP-2	Sterol carrier protein-2
SD (MPT)	Squared displacement
SEM	Scanning Electron Microscopy
SGF	Simulated gastric fluid
SGLT1	Sodium-glucose co-transporter type 1
SIF	Simulated intestinal fluid
SLN	Solid lipid nanoparticles
SPECT	Single photon emission computed tomography
SREBPs	Sterol regulatory element-binding proteins
SULT	Sulphotransferase
Q-NC	Quercetin-loaded zein nanocapsules
Q-NS	Quercetin-loaded zein nanospheres
Q-NS-PEG25	PEG-coated quercetin-loaded zein nanospheres (25%)
Q-NS-PEG50	PEG-coated quercetin-loaded zein nanospheres (50%)
Q-NS-PEG	PEG-coated Q-NS (25%) in the efficacy study
Q-Susp	Quercetin aqueous suspension
TAG	Triglycerides
TFA	Trifluoracetic acid
T_{max}	Time to reach C_{max}
TSA	Total surface area
$t_{1/2}$	Half-life
T2DM	Type 2 diabetes mellitus
UCP1	Uncoupling protein 1
UGT	Uridine 5’-diphospho-glucuronyltransferase
WAT	White adipose tissue
WHO	World Health Organization

Chapter 1

Introduction

1. Introduction

1.1. Obesity

Obesity is defined by the World Health Organization (WHO) as a complex multifactorial disease defined by excessive adiposity that presents a risk to health (1). The excess of adiposity is usually measured by anthropometric methods and expressed as the body-mass index (BMI), calculated as a relationship between the weight and the height of the person as in Equation 1 (2,3). In adults (age > 18), overweight is considered when the BMI is between 25 and 30 kg/m^2, and obesity when BMI is higher than 30 kg/m^2, with independence of age or sex. Following this definition, obesity is classified in three groups: Class I (BMI 30.0 - 34.9 kg/m^2), Class II (BMI 35.0 - 39.9 kg/m^2), and Class III (BMI ≥ 40 kg/m^2) (4–6). For children and adolescents, BMI is also used, but standard limits cannot be used, due to the changes in growth that occur during this period. Limits have been changed according to age and sex and are usually referred to as child growth reference curves (7).

$$BMI = \frac{Weight\ (kg)}{[Height\ (m)]^2} \qquad \text{[Eq. 1]}$$

BMI is widely used in clinical practice because it is non-invasive and it does not require specialized skills or expensive equipment (1). However, it is not a direct measurement of adiposity and its distribution, so it does not distinguish between adipose tissue or other kinds of tissue (3,8). In this way, two individuals may have the same BMI with different amount of fat, so differences can be found between individuals and populations, particularly by sex, age, and ethnic group. To overcome this limitation, WHO suggests combining the BMI with the measurement of waist circumference, as it has been demonstrated to be a better predictor of future health problems (1).

Obesity is caused by an energy imbalance when the intake of energy is higher than the consumption, usually caused by overeating and a sedentary lifestyle (9). However, body weight depends on genetic and environmental factors. It is estimated that for adiposity the heritability is 40-70%, but environmental factors have the major importance on obesity, having higher effects in genetically predisposed people. Among the environmental factors, socioeconomic factors, increased marketing, access to calorically dense and refined food, and a reduction of the physical activity are present (8). The exposure to some chemical compounds (called obesogens) is also associated with an increase in the body weight, and can interrupt the function of the endocrine system (9).

Adipose tissue can be classified into white adipose tissue (the most abundant form of adipose tissue) or brown adipose tissue. At the same time, white adipose tissue can be classified in visceral or subcutaneous, depending on the anatomic location. In humans, visceral fat is located in the peritoneal cavity, while subcutaneous fat is located below the skin (10). The adipose tissue is a metabolically active endocrine organ, in

which fat cells (adipocytes) are receiving and releasing hormones. These adipocytes release the substances called adipocytokines, and these have systemic or local actions such as glucose and lipid metabolism, cell development, inflammation, and oxidative stress, which can cause some health problems (1,10).

Regarding the type of adipose tissue, visceral fat is more biologically active than subcutaneous fat, with a higher density of cells, carries more blood flow, and is located near the portal vein, what makes a rise in the fatty acids reaching the liver. Because of this, the impact of visceral fat on health is higher than for subcutaneous fat (1). Also, the composition and functioning of the adipose tissue change in response to weight fluctuations and aging. Obesity and aging cause the decrease of the tissue to respond to changes, so it loses the ability to respond to bodily cues, what is related to health problems. As an example, when the adipose tissue has a fast growth, it exceeds its blood supply, leading to a decrease in oxygen in cells and causing the accumulation of these that cannot divide anymore, causing some metabolic issues (10).

1.1.1. Impact of obesity

Worldwide, 1.9 billion people live with overweight or obesity, being the 39% of the total population. 650 million of these people are obese (13% of the population), being more common in females (15%) than in males (11%). For children under 5 years old, 38.2 million people have overweight or obesity, and for people between 5 and 19 years, 340 million (11). These data have doubled in more than 70 countries between 1980 and 2015 (8), and if this tendency continues, it is estimated that 38% of adults will live with overweight and 20% with obesity by 2030 (9). Obesity is higher in countries with high sociodemographic index (8), and according to WHO, is a more severe world health problem than malnutrition (12).

The prevalence of obesity tends to be higher in richer countries of Europe, North America, and Oceania (13,14). In 2016, it was estimated that the WHO European Region had the highest obesity prevalence of the WHO regions, except the Region of Americas (14). Overweight and obesity affect almost 60% of the adult population in WHO European Region, reaching epidemic proportions. This value is lower for females (54%) than for males (63%), reaching the 70% for males in some countries. In the case of obesity, 23% of adults live with this disease, being higher the prevalence in females (24%) than in males (22%) (15). Inside the European Region, the Mediterranean and eastern European countries have the highest levels of overweight and obesity (13,14). Also, the prevalence of obesity is higher in people with lower educational attainment (15).

For paediatric population in the WHO European Region, in children under 5 years, 4.4 million people have overweight or obesity, being the 8% of all children in this group (16). For children from 5 to 9 years, 29% suffer from overweight or obesity, and 11% obesity. For adolescents from 10 to 19 years, this value decreases to 24% for overweight and obesity, and 7% live with obesity (14). Obesity in children is probable to remain in the

adulthood, resulting in a population with overweight and obesity that have been exposed to an excess of adiposity for a long period of time and increasing the risk to suffer other diseases in the adulthood (1,17).

The prevalence of overweight and obesity in adults has importantly increased in the WHO European Region in recent years, increasing an 8% from 2006 to 2016 and a 51% since 1975. For obesity, this rise is even higher, with an increase of 21% from 2006 to 2016 and 138% since 1975. In the case of children and adolescents from 5 to 19 years, overweight and obesity in males increased almost three times between 1975 and 2016, and two times in females, with obesity rising five times. Also, between 2006 and 2016 overweight and obesity increased a 20%, while the prevalence of obesity increased a 40% (1,13,14).

In Spain, overweight and obesity have decreased since 2011, with a stabilisation since 2015, but the prevalence in 6 to 9 year children is still high (40.6%) even if it decreased from 2011 to 2015 (17). In 2019, the prevalence of overweight in this range of age was 23.3% and 17.3% for obesity, being significantly higher the overweight in females and obesity in males. Among the reasons for these values are bad nutritional habits and a lack of physical activity. It should be pointed out that in Spain, as contrary to low incomes countries, the prevalence of child obesity in low-income families (23.2%) was almost two times higher than in families with higher incomes (11.9%) (17,18).

In the case of adults, as shown in Figure 1, the prevalence of overweight is being around 37% for the latest 20 years, being this value higher for males (around 45%) than for females (around 30%). In the case of obesity, a general tendency to increase is observed, as shown in Figure 2, with a decrease since 2017. Since 2006, males had a higher prevalence of obesity, except in 2014, when the prevalence was similar. In 2020, 16% of adults in Spain suffered from obesity (16.5% for males and 15.5% for females).

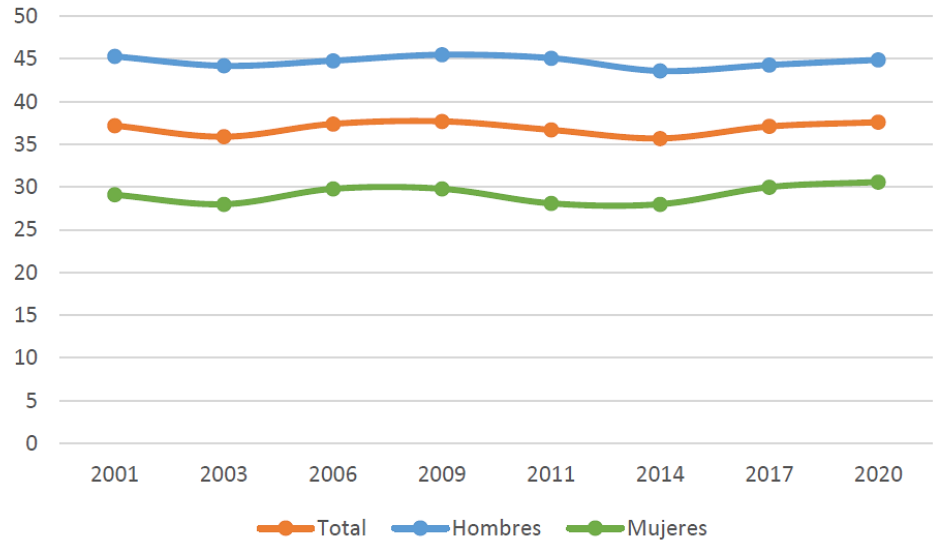

Figure 1. Overweight in adults (in percentage) by sex in Spain during the years 2001 to 2020. Obtained from the Spanish Agency for Food Safety and Nutrition (AESAN) (19). Hombres: men; Mujeres: women.

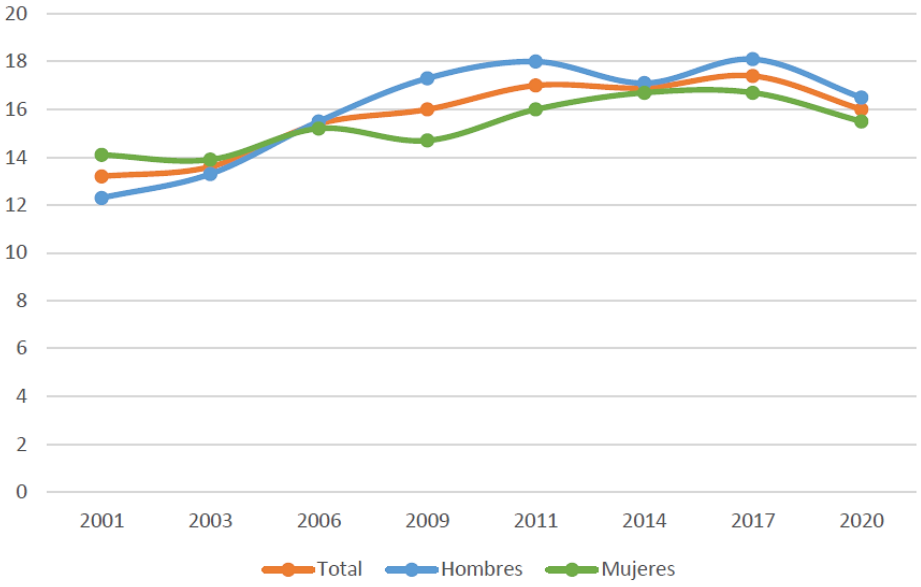

Figure 2. Obesity in adults (in percentage) by sex in Spain during the years 2001 to 2020. Obtained from the Spanish Agency for Food Safety and Nutrition (AESAN) (19). Hombres: men; Mujeres: women.

In addition, obesity and related comorbidities have financial implications due to the treatment of obesity-related ill health. Treatment costs for people with obesity are 30% higher than for people without it (20), and in 2014 obesity was estimated to be responsible for the 8% of health costs in the EU Member States (21). Among the economic impact of overweight and obesity, apart from direct medical costs, other costs must be taken into account, such as costs on premature mortality or productivity losses.

For example, in Spain, in 2019 the total costs related to obesity were more than 29 billion US$, the 2% of the gross domestic product (GDP), and will continue increasing (22).

1.1.2. Obesity and comorbidities

In 2020, obesity was considered a chronic disease by the European Commission (23), and it has been demonstrated that increases the probability of suffering other diseases and conditions, such as metabolic diseases, cardiovascular diseases, cancer, or respiratory diseases (4), as summarized in Figure 3, whose risk generally increase with increasing BMI (8,24). It is estimated that overweight and obesity cause more than 1.2 million deaths across the WHO European Region every year, being more than 13% of total deaths, the fourth cause after high blood pressure, dietary risks, and tobacco (25). Worldwide, more than 5 million people dead in 2019 due to obesity and related comorbidities, being 8.9% of total deaths (26).

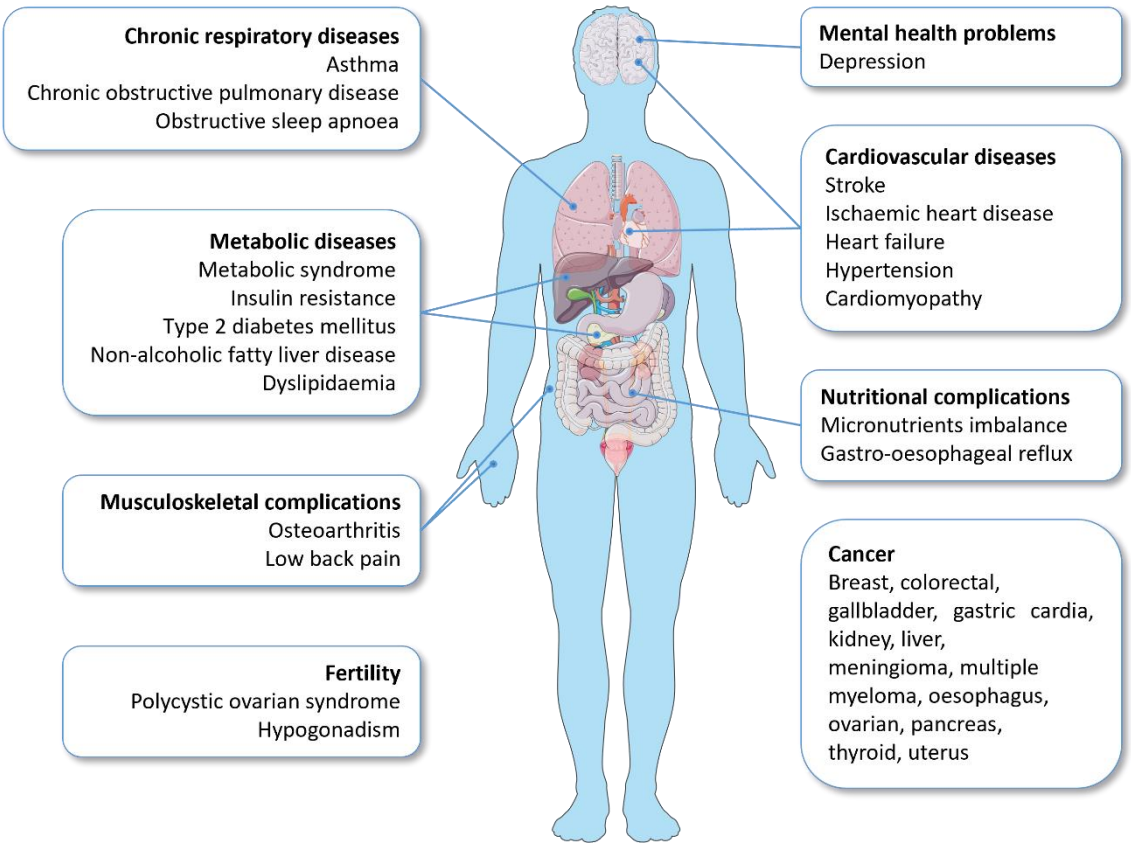

Figure 3. Some of the adverse effects caused by obesity. Based on the WHO European Regional Obesity Report 2022 (1) and Sarma *et al.* (8).

1.1.2.1. Metabolic diseases

Obesity can be the cause of metabolic diseases, such as metabolic syndrome, type 2 diabetes mellitus (T2DM), or non-alcoholic fatty liver disease (NAFLD) (27).

Metabolic syndrome is a clinical condition that is characterized by a cluster of metabolic risk factors (28). Five criteria are followed to consider that a person suffers from metabolic syndrome. He or she must have central (abdominal) obesity (defined as waist circumference with ethnicity-specific values) or BMI > 30 kg/m^2, and at least two of these factors (29):

- Increased triglycerides (≥ 150 mg/dL) or specific treatment for this lipid abnormality.
- Reduced HDL-cholesterol levels (< 40 mg/dL in males and < 50 mg/dL in females) or specific treatment for this lipid abnormality.
- Increased blood pressure (systolic BP ≥ 130 or diastolic BP ≥ 85 mm Hg) or treatment of previously diagnosed hypertension.
- Increased fasting plasma glucose levels (≥ 100 mg/dL) or previously diagnosed type 2 diabetes.

In Europe, 24.3% of the adult population suffers from metabolic syndrome (30), and the incidence increases with age (28). Visceral adiposity is the most important cause for the development of this disease (31). Studies show that among the factors associated with metabolic syndrome, abdominal fat was the most common among women, and the phenotype of the disease varies between countries, being hypertension the most common characteristic (30). Besides, metabolic syndrome rises the risk of suffering T2DM, cardiovascular events, cancer, neurodegenerative disorders, atherosclerosis, and all cause-mortality (28).

T2DM, previously called “noninsulin-dependent diabetes”, represents the 90-95% of all diabetes, and it is characterized by a hyperglycaemia (fasting glucose levels ≥ 126 mg/dL or random plasma glucose ≥ 200 mg/dL), caused by a progressive loss of pancreatic β-cell insulin secretion. T2DM patients have relative insulin deficiency and peripheral insulin resistance (32). Excess of weight itself can cause some degree of insulin resistance (32); high accumulation of free fatty acids in insulin-sensitive nonadipose tissues results in ectopic lipid deposition, which results in lipotoxicity, that causes insulin resistance (27). Other processes can also cause insulin resistance: chronic inflammation (inflammatory factors can inhibit insulin signaling), neural alteration, or intracellular disturbance (such as ectopic fat storage, oxidative stress, or mitochondrial dysfunction) (27). In Europe, 60 million people (9% of the adult population) are affected by T2DM (33). It is estimated that 44% of cases of T2DM are attributed to overweight or obesity, and by 2025, the prevalence of obesity-related diabetes is expected to double to 300 million (12).

NAFLD is defined by fat accumulation (steatosis) in > 5% of hepatocytes, in the absence of other causes including alcohol overconsumption or chronic hepatitis C (34,35). It can be divided in two groups: only steatosis (NAFL) and non-alcoholic

steatohepatitis (NASH), where steatosis appears with inflammation, hepatocyte ballooning, liver cirrhosis, and/or hepatocellular carcinoma (35,36). NAFLD affects 25% of the global adult population, and is the first cause of chronic liver disease in developed countries (35). In Europe, about 19-30% of adults have NAFLD (35). This disease is directly related to obesity, metabolic syndrome, T2DM, and dyslipidaemias, and these have an effect on the incidence and progression severity of NAFLD (34). Due to this relationship between non-alcoholic fatty liver disease, obesity, and metabolic syndrome, the prevalence will probably continue increasing during the next decade (36). Cardiovascular disease is the main cause of death in people with this pathology (34), but NAFLD is preventable and can be reversed (depending on the clinical stage of progression) by multidisciplinary health care (1,36).

Mechanisms under NAFLD are not completely understood (37,38), but some mechanisms have been proposed, where insulin resistance seems to be essential (38). In obesity, an expansion of adipose depots and accumulation of ectopic fat (pathological expansion of white adipose tissue in areas that it should not be (39)) is present, what can cause NAFLD (37). In this context, macrophage infiltration of the visceral adipose tissue creates a proinflammatory state that promotes insulin resistance. Inappropriate lipolysis in this context results in a continuous delivery of fatty acids to the liver, which overwhelms its metabolic capacity. The imbalance in lipid metabolism results in the formation of lipotoxic lipids that contribute to cellular stress, inflammasome activation and apoptotic cell death, with subsequent stimulation of inflammation, tissue regeneration, and fibrogenesis. These pathogenic pathways of NAFLD are influenced by metabolic, genetic, and microbiome-related factors (37).

1.1.2.2. Cardiovascular diseases

Obesity is related to some illnesses that increase cardiovascular disease risk (3), the most common cause of death in Europe (40). These include coronary heart disease, heart failure, hypertension, cerebrovascular disease, cardiomyopathy, atrial fibrillation, ventricular arrhythmias, stroke, and sudden cardiac death (3,8). It is estimated that 23% of cases of ischemic heart disease are caused by overweight or obesity (12). Obesity can increase the morbidity and mortality of cardiovascular diseases in a direct or indirect way. Direct effects are mediated by structural and functional adaptations of the cardiovascular system to accommodate excess body weight and by adipokine effects on inflammation and vascular homeostasis, leading to a pro-inflammatory and prothrombotic environment. Indirect effects are mediated by the presence of risk factors like visceral adiposity, hypertension, dyslipidaemia, insulin resistance, and T2DM (3).

1.1.2.3. Cancer

Obesity can also be the cause of 13 types of cancer, such as breast, colorectum, kidney, liver, ovary, multiple myeloma, and meningioma cancers (41). It is estimated that up to 41% of some cancers are attributable to overweight or obesity (12). It is known that ectopic fat deposition can cause metabolic, inflammatory, and immunologic alterations that affect DNA repair, gene function, or cell mutation that allows the malignant transformation and progression. However, the role of obesity in cancer is not well stablished, but some pathways have been defined. Among others, the following factors would be involved: (i) the hyperinsulinemia or insulin resistance, and abnormalities of the insulin-like growth factor-I (IGF-I) system and signaling; (ii) subclinical chronic low-grade inflammation and oxidative stress; (iii) alterations in adipocytokine pathophysiology; (iv) factors deriving from ectopic fat deposition; (v) microenvironment and cellular perturbations; and (vi) altered intestinal microbiome; or mechanic factors in obesity (39).

1.1.2.4. Respiratory diseases

Respiratory issues are other adverse effects related to obesity, being asthma, chronic obstructive pulmonary disease (COPD), and obstructive sleep apnoea (OSA) the most important ones. In obesity, the mechanical properties of the lungs and chest wall are modified, because of the fat deposition in the mediastinum and the abdominal cavities. These alterations reduce the compliance of the lungs, chest wall, and entire respiratory system, and contribute to respiratory symptoms (42).

COPD is one of the leading causes of mortality, morbidity, and disability, affecting 328 million people worldwide (43). Even if smoking is the first cause of COPD, other factors can influence its development (44). The role of obesity in COPD is not well understood, but it is demonstrated that extreme obesity has higher mortality in COPD adult patients (45). For OSA, this role is better understood, being a clear relationship between overweight and obesity with the risk of the disease (46). It has got a detrimental effect on health and well-being, and it is a risk factor for stroke and its recovery (47,48). It is also related to metabolic syndrome and type 2 diabetes (48). OSA affects between 9% and 38% of the adult population (49). Obesity is related to a two times higher increased risk of OSA and the prevalence of OSA in people with obesity has been reported to be ~45% (8).

1.1.2.5. Musculoskeletal diseases

Obesity is also associated with musculoskeletal complications that affect bones, joints, or soft tissue, such as osteoarthritis, rheumatoid arthritis, psoriatic arthritis, lower back pain, and osteoporosis (1,50). In fact, overweight or obese people had a three times higher risk of incident knee osteoarthritis compared to people with normal weight (51). Musculoskeletal diseases have increased parallelly to overweight and

obesity, suggesting a dose-response relationship (50,52). The mechanism of how high weight affects musculoskeletal functions is not clear, but it is known that affects mobility and functionality (50). For example, osteoarthritis is influenced by obesity because of the impact on mechanical movement and inflammation, which is the central characteristic of osteoarthritis (51,52).

1.1.2.6. Other diseases

Obesity increases the risk of other diseases, such as reproductive issues and effects on mental health (8). It is demonstrated that obesity and depression are strongly related, although the biological mechanisms are not completely understood. This relationship is bidirectional; obesity increases the risk of having depression, and depression increases the risk of having obesity (53).

In addition, overweight and obesity are related to higher mortality; it has been demonstrated that people with obesity have 5 years shorter life expectancy than people with a healthy BMI (18.5 - 24.9 kg/m^2) (54,55). Overweight and obesity are also risk factors for disability, being the 7% of *total years lived with disability* in the WHO European Region (56). Recent experience has shown also that people with overweight or obesity had a greater risk to suffer severe COVID-19 (higher risk of hospitalization, need for intubation, and death) (8,57).

Nutritional imbalances are another consequence of obesity. The risk of deficiency of some micronutrients is higher due to different factors, such as consumption of unhealthy food or imbalanced diets (1). Serum zinc (58), selenium (59), vitamin B12 (60), folate (61), and vitamin D (62) can be lower in people with obesity. All these micronutrients are involved in regulating immune and metabolic homeostasis and cardiovascular function, and their deficiency is related to a higher prevalence of infection, metabolic complications, and some noncommunicable diseases (1).

Also, excess of adipose tissue produced pro-inflammatory and pro-oxidative metabolic derangements, as well as the presence of obesity-induced comorbidities, are associated with skeletal muscle protein-catabolic changes and may lead to a loss of muscle mass and function (63). This low muscle mass together with obesity (called sarcopenic obesity) is related to a high risk of frailty and dependency, with high mortality for some comorbidities (63).

Obesity in pregnancy is also remarkable. The 7-25% of women start pregnancy with 30 kg/m^2 of BMI (64). When a pregnant woman lives with obesity, the child is exposed to a suboptimal environment since it is in the uterus, and these adversities in early life extend to adulthood and can cause cardiometabolic (cardiovascular disease and obesity) or psychiatric illnesses (65–67). Besides, the mother can suffer some complications, such as gestational diabetes and hypertension (65).

1.1.3. Treatments for obesity

For the treatment of obesity, three main strategies are followed: behavioural intervention, pharmacotherapy, and bariatric surgery. The use of these is regulated depending on the age of the patient (adult or child/adolescent). In general, lifestyle modification is considered the best choice, but these strategies can be used in combination (4). However, robust criteria are followed for the use of pharmacotherapy and bariatric surgery (6).

Apart from treatments, the prevention of obesity is also important, not only in an individual way but also in targeting the whole population. Long-term strategies must be applied for the creation of environments that support and facilitate healthy behaviours, through different policies that address social, physical, cultural, economic, and political factors, with a particular focus on income and socioeconomic inequalities. Children must also be the target of these strategies, because small changes can become in larger impacts on morbidity and mortality, since obesity increases with age, and the next generations would present better overall health (1).

1.1.3.1. Treatments for obesity in adults

In adults, people with obesity may receive individualized care plans, after medical evaluation, that address the causes of the obesity and provide support for behavioural change (eating behaviours, physical activity, etc.) and adjunctive therapies (psychological, pharmacological, and surgical interventions). This plan ideally should be created by a multidisciplinary team and could move towards improving health outcomes rather than weight loss alone. Some clinical guidelines have been published to help clinical practice (5,68). Nevertheless, to have a successful and long-lasting effect, the aim must not be the weight loss in a short period of time, because it is demonstrated that a weight loss of 5-10% is enough to achieve substantial health benefits. In addition, the reduction of waist circumference is even more important than losing weight, due to the relationship between visceral fat and cardiometabolic diseases. It should be mentioned that the prevention of weight regain is important for all techniques (5). Aerobic exercise of moderate intensity is also recommended, even if the loss of weight is only 3 kg on average. To save the lean mass through the process of losing weight, it is recommended training based on resistance; to improve muscular fitness, resistance training is advised, alone or combined with aerobic exercise (69).

In Europe, pharmacotherapy is used for weight loss and maintenance in people with a BMI higher than 30 kg/m^2 or BMI ≥ 27 kg/m^2 with complications related to obesity, to support behavioural and psychological interventions (4–6). Pharmacotherapy can complement lifestyle therapy but can never be used alone (5). Until today, only a few drugs have the European Medicines Agency (EMA) approval for their use in obesity, using three different approaches:

- Fat absorption inhibitors:

  Gastric and pancreatic lipases are enzymes secreted to the gastrointestinal tract and play important roles in the digestion of the ingested fats. Lipases hydrolyse triglycerides to free fatty acid chains and monoglyceride to be absorbed. The drug orlistat reduces the absorption of fat by inhibiting these gastric and pancreatic lipases in a reversible way, forming covalent bonds with the serine residues of the lipase active sites, inactivating them (5,70). Some adverse effects have been seen, such as faecal fat loss, gastrointestinal symptoms (fatty diarrhoea or oily rectal leakage), or abdominal pain and distress (5,71).

- GLP-1 (glucagon-like peptide-1) analogues:

  GLP-1 is an incretin hormone (from the class of satiety hormones) that is secreted by the L cells of the ileum and colon in response to a meal. It induces an increase of insulin secretion by the β-cells of the pancreas and sends a message of satiety to the brain (5,70,72). It reduces the glucagon release, the gastric emptying, and the food intake (70,72).

  Two GLP-1 analogues are commercialized; liraglutide and semaglutide. Liraglutide was initially approved for the treatment of type 2 diabetes (70), and semaglutide is the most recently approved GLP-1 analogue (73). Liraglutide is administered once daily, while semaglutide presents a longer half-life, allowing its administration once weekly (73). However, they can exert some upper gastrointestinal adverse effects, such as diarrhoea, nausea, abdominal fullness, and vomiting (72).

- Other:

  The combination of the drugs bupropion and naltrexone is also used for the treatment of obesity. Bupropion is a centrally acting drug (nonselective inhibitor of dopamine) used to treat depression and help give up smoking, that inhibits the reuptake of dopamine and norepinephrine, which will stimulate the proopiomelanocortin (POMC) release, that acts as a precursor of the α-melanocyte-stimulating hormone (α-MSH), that has an appetite suppressing effect. Naltrexone is an opioid receptor antagonist, that acts mainly on μ-type opioid receptors. It is used for the dependence on alcohol and opioids, and its side effect is a decrease in appetite (5,70). The exact mechanism of these drugs is not well understood, but effects could be obtained from the action on brain areas involved in the food intake regulation: the hypothalamus (appetite regulatory centre) and the mesolimbic dopamine circuit (reward system) (71). Like other drugs, this combination can cause nausea, headache, dizziness, insomnia, vomiting, or dry mouth (5,71).

Finally, when weight loss is not achieved by lifestyle changes, bariatric surgery can be used, and it has been demonstrated that its benefits are wider than only losing weight (4). However, some criteria must be followed (74). For example, laparoscopic bariatric surgery can be considered in adults whose BMI is higher than 40 kg/m^2 or with a BMI

higher than 35 kg/m^2 with associated comorbidities that could improve with the loss of weight (74). Bariatric surgery includes endoscopic interventions (such as the intragastric balloon, sleeve gastroplasty, or duodenal mucosal resurfacing) and surgical interventions (such as sleeve gastrectomy or Roux-en-Y gastric bypass) (70).

1.1.3.2. Treatments for obesity in children and adolescents

In children and adolescents, the aim of the treatments for obesity includes the reduction of energy intake and rising of energy consumption, reduction of weight gain, improving body composition, physical function, and quality of life, and the prevention or reduction of obesity adverse effects (1). For that purpose, several guidelines have been created (75,76).

For children and adolescents who live with overweight, WHO recommends giving advice to parents and caregivers about physical exercise and nutrition, that is, a behavioural intervention. For children with obesity, they should be evaluated in depth and an appropriate plan should be developed. The addition of pharmacotherapy is also possible (75). For adolescents with severe obesity, behavioural intervention, bariatric surgery, and pharmacotherapy can be recommended (7). To choose the most appropriate treatment, a careful medical evaluation is needed, and some parameters must take into account, such as age, sex, pubertal status, the severity of obesity, or comorbidities (76).

In general, multicomponent behavioural interventions (change in diet, physical activity, psychological therapies…) are considered the best treatment for children and adolescents. However, pharmacotherapy is proposed for adolescents with obesity that do not respond optimally to these multicomponent behavioural interventions (7). Nevertheless, options are limited in the WHO European Region (1). Orlistat is the only drug approved by the U.S. Food & Drug Administration (FDA) but not by the EMA, for long-term obesity treatments in children higher than 12 years old. Its use is limited due to its modest efficacy (3% reduction of BMI in a year) and its adverse effects. Phentermine (a norepinephrine reuptake inhibitor) is another drug approved by the FDA but not by the EMA, with limited efficacy (77). Also, FDA has recently approved an updated label of liraglutide for the treatment of obesity in adolescents between 12 and 17 years old (with weight ≥ 60 kg and BMI ≥ 30 kg/m^2), and EMA has recommended the approval. All these drugs must be accompanied by behavioural support for patients and families (1).

Regarding metabolic and bariatric surgery, it has been seen that this treatment is safe and effective in children. Patients have a reduction in BMI, an improvement in the quality of life, and a decrease in the comorbidities associated with obesity. To put into practice this treatment, some issues must be taken into account, such as psychological and physical maturity, the ability to provide informed consent and the availability of family support, and continuing postoperative behavioural intervention (78).

Apart from all these treatments, studies have demonstrated that the consumption of medicinal herbs and vegetables can reduce the prevalence of obesity-related comorbidities due to antioxidant and anti-inflammatory ingredients (79). Thus, dietary interventions using natural bioactive compounds present in food have been presented as a promising therapeutic tool for obesity and metabolic diseases, due to the limited adverse effects. Particularly, polyphenols present in food (such as fruits, vegetables, tea, chocolate, or wine) have demonstrated to reduce the weight gain (12). Flavonoids, a class of polyphenols (such as catechin, cyanidin, or quercetin), are the bioactive compounds more related to a reduced risk of all-cause mortality, T2DM, cardiovascular diseases, obesity, and obesity-related comorbidities, and also have been recently proposed as therapeutic agents against pathologies like Alzheimer's disease or cerebrovascular alterations (80).

1.2. Polyphenols and quercetin

Polyphenols are the most common and widespread group of substances in plants. They are secondary metabolites and have no specific metabolic function in plant cells. Nevertheless, these molecules are essential for the survival of plants, such as defending against microbial attacks or becoming the plants disagreeable for predators (81). Polyphenols can be classified as phenolic acids, flavonoids, and non-flavonoids, as shown in Figure 4. At the same time, flavonoids can be separated into flavonols, flavones, flavanols, flavanones, isoflavones, and anthocyanidins (82).

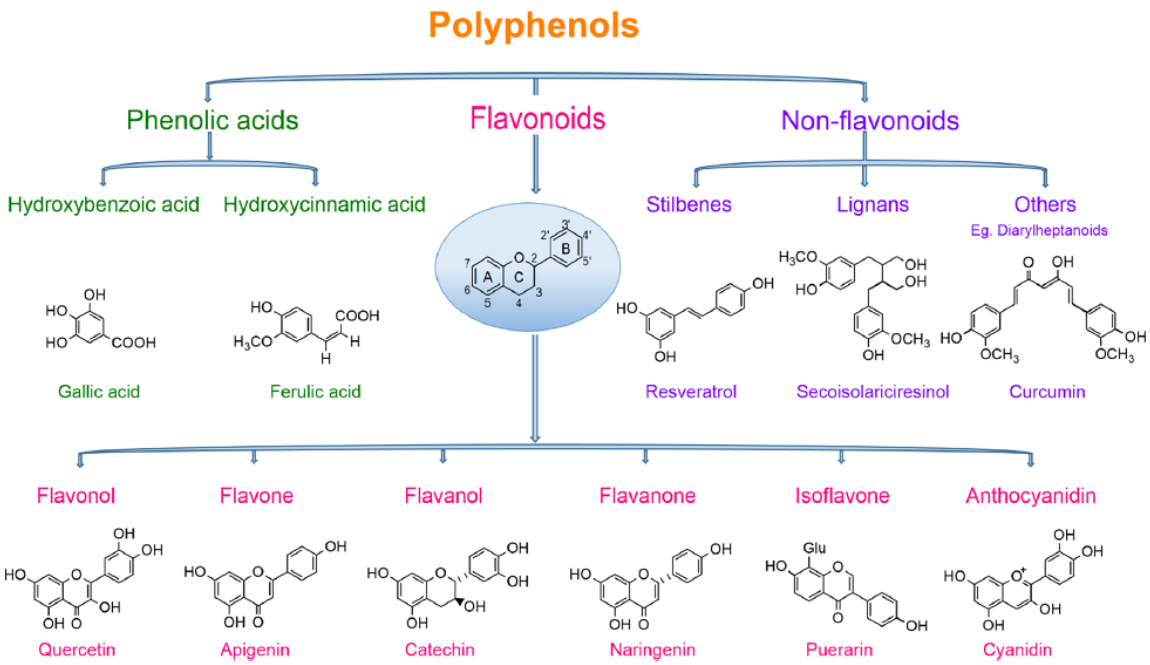

Figure 4. Classification and examples of polyphenols. Figure obtained from Rambaran (82).

Flavonoids have a common structure consisting of two benzene rings (rings A and B) linked to a heterocyclic pyran (ring C) (Figure 5A) (83). Quercetin (3,3',4',5,7-pentahydroxyflavone, Figure 5A, 302.23 g/mol) is a dietary flavonoid present in some fruits and vegetables, such as tomato, lettuce, onion, black chokeberry, apples, or wine (84,85). In fruits and vegetables, quercetin appears as quercetin glycoside, that is, quercetin aglycone conjugated to sugar moieties, such as rutin and quercetrin (quercetin esterified with rutinose (Figure 5B) and rhamnose (Figure 5C), respectively), being the first the most common and important glycoside form found in plants (86,87). The extraction of quercetin from plants can be done by extracting the quercetin glycosides followed by hydrolysis to release the aglycone (83).

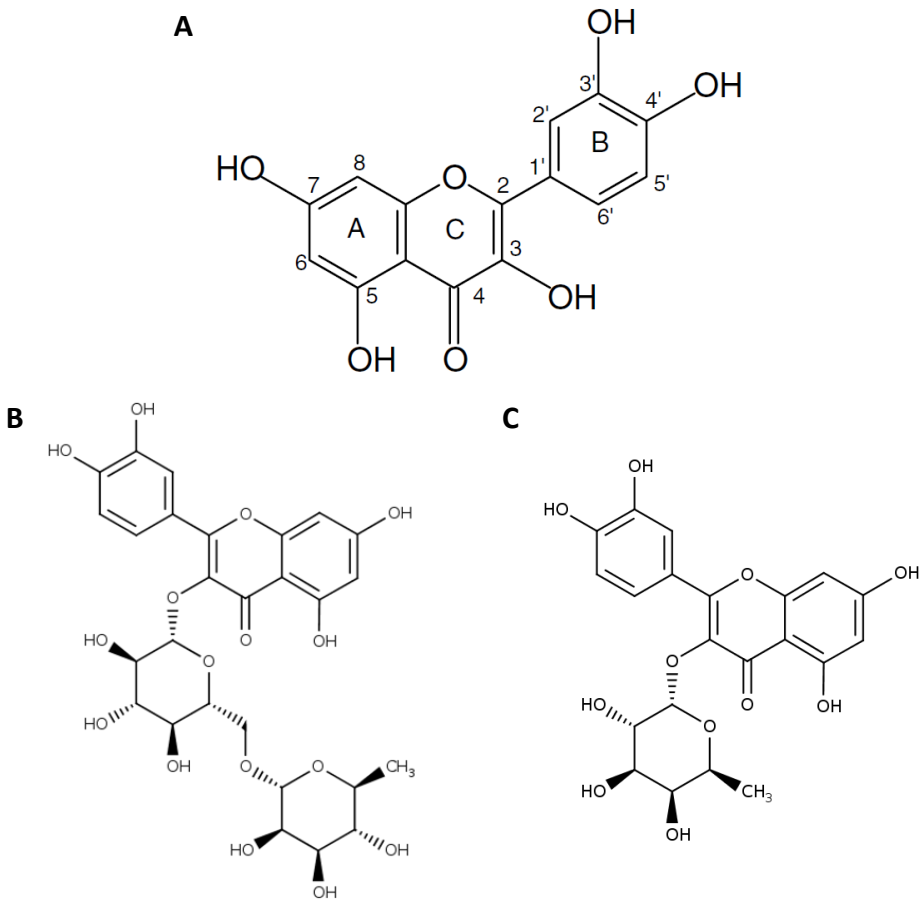

Figure 5. Chemical structure of quercetin (**A**), rutin (quercetin 3-O-rutinoside, **B**), and quercetrin (Quercetin 3-O-rhamnoside, **C**). Obtained from Harwood *et al.* (83) and Phenol-Explorer (88,89).

Quercetin appears as a yellow powder or needles, whose melting point is 316 °C (85). It is a hydrophobic compound, being its solubility in water only 0.01 mg/mL at 25 °C, but is soluble in methanol, ethanol, acetone, or dimethyl sulfoxide (84,85). Also, quercetin is sensible to temperature and chemicals, and degrades quickly in the presence of light, warm temperature, or alkaline media (90).

In the Western diet, the daily intake of quercetin is about 15 mg (91). The amount of quercetin administered by diet is between 5 and 40 mg per day, being between 200 and 500 mg per day in people whose fruit and vegetable intake is high (92). The flavonoid can also be taken as a dietary supplement at a dose between 200 and 1200 mg per day or as a nutraceutical through functional foods at a dose between 10 and 125 mg per portion (91). The Spanish Agency for Food Safety and Nutrition (AESAN) proposed the daily intake of quercetin to be 75 mg in dietary supplements, with the warning not to be used in pregnant women due to the fact that its security has not been guaranteed (92).

1.2.1. Pharmacokinetic properties of quercetin

In humans, the oral bioavailability of quercetin is around 1%, in dogs 4%, and less than 10% in rats (90). This is due to the fact that the flavonoid has very low water solubility and undergoes degradation in gastrointestinal media. This leads to a very low oral bioavailability, being the glucuronide and the sulphate derivatives the most abundant compounds present in plasma (90,93).

When quercetin is orally administered, in the mouth the flavonoid can interact with salivary proteins to form soluble quercetin-protein binary aggregates. In the stomach, quercetin is degraded to phenolic acids, and these acids could also be absorbed in this organ (84). A minor proportion of the flavonoid is absorbed in the stomach, being the primary site of absorption the small intestine (94).

In fruits and vegetables, quercetin is present as quercetin glycoside, that is, quercetin aglycone conjugated to sugar moieties. To make possible the absorption, previously to entering the enterocyte in the small intestine, attached chemical groups are removed by deglycosilation to the aglycone form of quercetin (Figure 6A) (86,94). For quercetin monoglucosides (such as quercetin-3-O-glucoside or quercetin-4'-O-glucoside), two enzymes act as β-glucosidase. One is the brush border enzyme lactase-phlorizin hydrolase (LPH), that hydrolyses lactose to glucose and galactose. The other one is cytosolic β-glucosidase (CBG), which is located in the enterocytes and presents broad specificity. Previously to the hydrolysis by CBG, quercetin glucosides are taken up into the cell (using for example, the sodium-glucose co-transporter type 1 (SGLT1) used for quercetin 4'-O-glucoside). For non-monoglucosidic glycosides (such as rutin), intestinal β-glucosidades cannot hydrolyse the sugar moiety, so microbiota produces quercetin aglycone in the cecum and large intestine. This aglycone is absorbed via the large intestine (95).

Due to the hydrophobic character of quercetin, when it reaches the small intestine, the aglycone can pass through the cellular membranes of the enterocytes, being absorbed primarily by simple diffusion pathway and secondarily by organic anion transporting polypeptide (OATP) (Figure 6A) (96–98). Once in the enterocyte (Figure 6B), quercetin suffers glucuronidation (by the uridine 5'-diphospho-glucuronyltransferase (UGT)), methylation (by the catechol-O-methyltransferase (COMT)), and sulphation (by the sulphotransferase (SULT)), forming quercetin monoglucuronides (such as quercetin-3-O-glucuronide), quercetin diglucuronides, methylquercetins (such as isorhamnetin and tamaraxetin), and quercetin sulphates (84,97). Part of the quercetin is also transported via the lymphatic pathway (99).

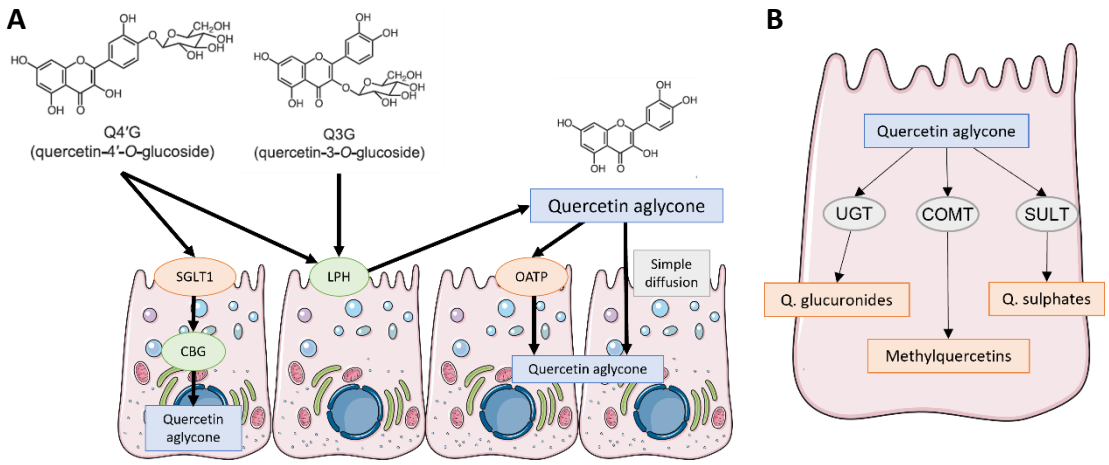

Figure 6. Presystemic metabolism of quercetin. Based on Murota *et al.* (95) and Luca *et al.* (97). **A**: deglycosilation and absorption pathways of quercetin through the enterocytes. **B**: quercetin metabolism inside the enterocyte. SGLT1: sodium-glucose co-transporter type 1; CBG: cytosolic β-glucosidase; LPH: lactase-phlorizin hydrolase; OATP: organic anion transporting polypeptide; UGT: uridine 5'-diphospho-glucuronyltransferase; COMT: catechol-O-methyltransferase; SULT: sulfotrasnferase.

These quercetin and quercetin derivatives are secreted to hepatic portal vein circulation and reach the liver, where quercetin is further metabolized by glucuronidation, methylation, and sulphation. The quercetin and formed derivatives are released to blood circulation via the portal vein or secreted into the bile. Methylation can also be performed in kidneys (84,97). Quercetin and its metabolites can cross the blood-brain barrier (84,99).

Quercetin and rutin that have not been absorbed can be metabolized by colon microflora. First, rutin is hydrolysed by gut microbiota-derived β-glucosidase to quercetin that can be absorbed (97). Quercetin acts as a substrate for several gut bacteria, that can produce C-ring fissions and dehydroxylations, forming low molecular weight phenolic compounds that can be absorbed, such as 3,4-Dihydroxyphenylacetic acid (DOPAC) or 3.4-dihydroxybenzoic acid (PCA) (97,99). These metabolites are absorbed and transported via the portal vein to the liver and undergo more conjugation reactions (84).

Finally, quercetin is eliminated by faeces (1.6 – 4.6% of an oral dose (98)) and urine, being 3-hydroxyphenylacetic acid (3-OPAC), benzoic acid, and hippuric acid the most present metabolites (97). The whole process is summarized in Figure 7.

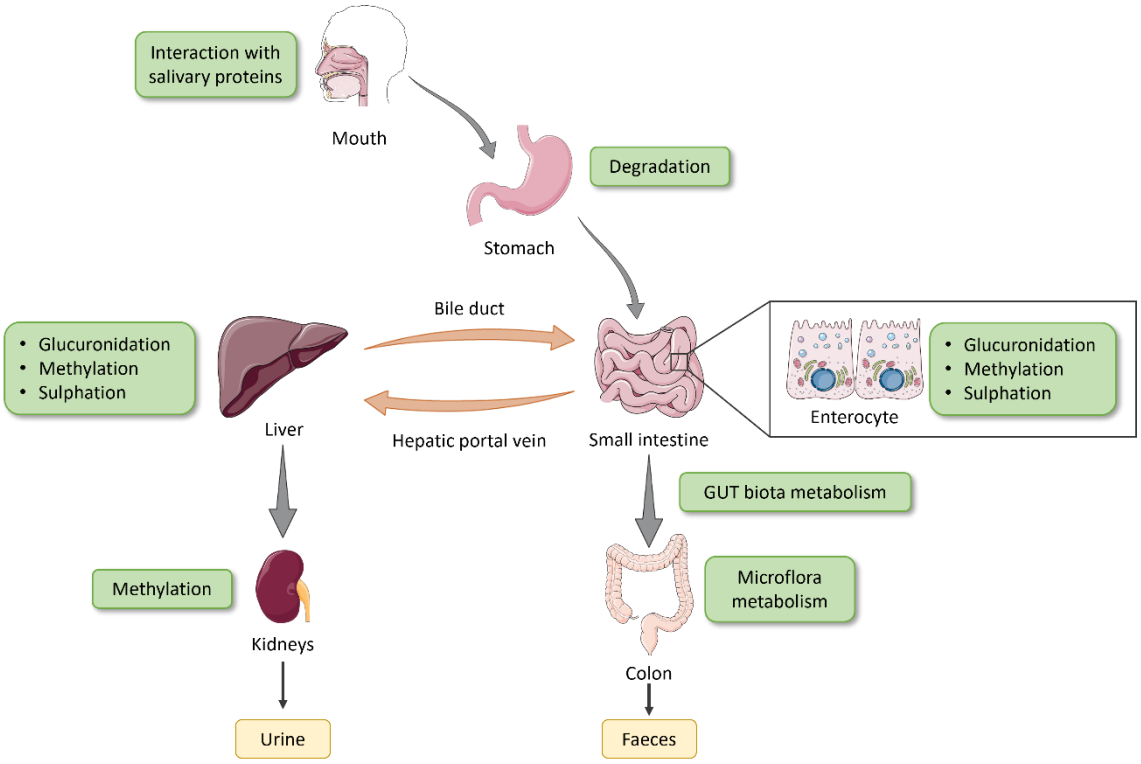

Figure 7. Schematic representation of the adsorption, metabolism, and excretion of quercetin. Based on Wang *et al.* (84) and Luca *et al.* (97).

1.2.2. Pharmacological properties of quercetin

Quercetin has demonstrated to have antioxidant (100), anti-inflammatory (101), anti-cancer (102), anti-obesity (87), or anti-diabetic (86) properties (Table 1), and decreases the risk of coronary heart disease, cancer, diabetes, and neurodegenerative disorders (84,90). Nevertheless, the dietary form of quercetin (quercetin glycoside) and the supplementary form (quercetin aglycone) are different, so it is not clear if both compounds have the same biological effects (99).

1.2.2.1. Antioxidant properties of quercetin

Some reactive oxygen species (ROS) and some reactive nitrogen species (RNS), such as $O_2^{\cdot -}$, $NO^{\cdot}$, and $ONOO^-$, induce oxidative damage, causing harmful effects on cells and tissues and causing some illnesses (84,99). Quercetin can stop this peroxidation reacting with the radicals formed, because is a powerful scavenger of reactive oxygen species (84). In this process, quercetin oxidizes and produces reactive products known as o-quinone/quinone methides (99). This antioxidant capacity is due to the catechol group in the B ring, a 2,3-double bond conjugated with a 4-oxo function in the C ring, and two hydroxyl groups in the heterocyclic ring (positions 3 and 5) (84). Also, in some cells, quercetin has a protective effect against oxidative stress caused by oxidation of lipids,

lipoprotein fragments, and other factors, and as it acts as a chelator for iron, it protects cells against oxidative damage caused by iron overloading (99).

Quercetin demonstrated to inhibit strong oxidant species in mice with endotoxic shock, including $O_2\cdot^-$ and possibly $ONOO^-$ (103), and oral pretreatment with quercetin showed a significant protection against oxidative stress and lipid peroxidation in a model of paracetamol-induced rat liver injury (104). Quercetin demonstrated to have hepatoprotective effect in a model of hepatic damaged mice due to its antioxidant capacity, free radical scavenging effect, inhibition of lipid peroxidation, and increased antioxidant activity (105).

1.2.2.2. Anti-inflammatory properties of quercetin

There are different opinions among scientists about the anti-inflammatory effect of quercetin. Some of them suggest that is related to the antioxidant activity and free radical scavenging properties, because reactive oxygen species are also present in the inflammatory response, by the activation of different transfer factors such as nuclear factor-κ-gene binding, that could induce the production of TNF-α cytokines. This way, quercetin could stop inflammation and prevent oxidation at the same time. Other scientists suggest that quercetin could suppress lipopolysaccharide (LPS)-induced cytokine production in different cells (84). The anti-inflammatory effect has been demonstrated in different animal models, such as carrageenan-induced inflammation in rats (106), chronic rat adjuvant-induced arthritis (107), or LPS-induced endotoxic shock in mice (108).

1.2.2.3. Anti-cancer properties of quercetin

Quercetin has also been demonstrated to have anti-cancer properties *in vitro* in different types of cells. The flavonoid can prevent cancer induced by oxidative stress because of its antioxidant activity and its capacity to suppress many kinases involved in the growth of cancer cells, proliferation, and metastasis (84). Quercetin has anticarcinogenic activity by stimulating apoptosis, inhibiting the cell cycle, promoting the release of matrix metalloproteinase, suppressing the growth, stimulating cell aging and death, and telomerase and antiproliferative effects. It also reduces tumour cell adhesion, metastasis, and angiogenesis. It is also associated with the inactivation of oncogenes that affect in the beginning of the cancer development and activation of tumour suppressor genes (99). This anti-cancer activity has also demonstrated in *in vivo* animal models (109,110).

1.2.2.4. Effects of quercetin on the cardiovascular system

Quercetin is associated with a low risk of cardiovascular disease (84,99). It has effects on the cardiovascular system, such as the reduction of inflammatory responses

(modifying the biosynthesis of eicosanoids), the decrease of the oxidation of low-density lipoproteins (preventing the formation of atherosclerotic plaque), the obstruction of the aggregation of platelets (avoiding the formation of thrombi), and the relaxation of smooth muscles (decreasing hypertension and heart arrhythmias) (93). It is thought that quercetin decreases blood pressure decreasing oxidative stress and improving the renin-angiotensin-aldosterone system and vascular function (99).

1.2.3. Quercetin, obesity, and comorbidities

Flavonols have been demonstrated to protect rodents from high-fat diet-induced obesity in several studies, by reducing body weight gain and lipid accumulation in white adipose tissue via reducing inflammation, modifying lipid metabolism, increasing energy expenditure, inducing browning of white adipose tissue, and activating brown adipose tissue. However, the effectiveness of quercetin is shown to be specie dependent. Studies in rats usually showed more effects than in mice. In humans, results are still unclear, but quercetin levels reached after its administration are lower than in rodents (80).

The anti-obesity effect of quercetin has been demonstrated in obesity models in Wistar rats (111,112), Zucker rats (113), C57BL/6J mice (114,115), or ICR mice (116). Some studies suggest that quercetin improves obesity by different molecular pathways, but limited studies in humans have been performed (87). Some scientists suggest that quercetin binds the glucose transporter GLUT4, that mediates insulin-stimulated glucose uptake in adipocytes and muscles and its up-regulation is associated with obesity (87,117). Different assays have been performed in mice and rats, suggesting, for example, that quercetin reduces body weight by its anti-inflammatory effects on adipose tissue, by improving the expression of oxidative stress and inflammation markers, such as nuclear factor-related factor-2 (Nrf2), heme oxygenase-1 (HO-1), and nuclear factor kappa B (NF-κB) (87,118). Cell studies suggest that protective effects of quercetin against obesity are related to the anti-inflammatory and/or antioxidant effects of the flavonoid, but other mechanisms have been presented too. Some studies have been performed in humans, indicating that quercetin helps in the improvement of obesity (87).

In addition, several studies were performed on the antidiabetic effect of quercetin (86,119,120). This flavonoid improves liver and pancreatic functions by inhibiting cyclin-dependent kinase inhibitor p21 (WAFl/Cipl) (Cdknla) gene expression and improving cell proliferation. In type 1 diabetes, an increase in CYP2E1 protein is considered the main cause of stress-induced liver injury, and quercetin has shown the ability to decrease the activity of this protein and improve pro-oxidant-antioxidant balance in rats. Quercetin can also prevent diabetic retinopathy, by inhibiting oxidative stress and having neuroprotective effects (99).

In type 2 diabetes, this flavonoid inhibits carbohydrate absorption by inhibiting digestive enzymes that are responsible for carbohydrate hydrolysis and glucose carriers

in vitro and *ex vivo*. It also decreases numbness and pain in type 2 diabetes patients. Quercetin effect in skeletal muscle cells in type 2 diabetes was demonstrated to be via the adenosine monophosphate kinase (AMPK) pathway. An increase in intracellular calcium was also seen. As a result, quercetin protects normal blood sugar with such mechanisms as an increase of AMPK, GLUT4 activation and insulin receptor count in muscle cells, pancreatic b cell regeneration, repair of pancreatic oxidative damage, an increased glucokinase activity in the liver, and reduced absorption of glucose in the small intestine (99).

Quercetin has also been demonstrated to have beneficial effects in early stages of NAFLD development, and it improves hepatic insulin sensitivity, reduced liver fat content, and ameliorated hepatic steatosis (80).

Table 1. Main pharmacological properties of quercetin *in vivo*. Q: quercetin; TNF-α: tumour necrosis factor-α; HOMA-IR: homeostasis model of insulin resistance.

Effect	Study model	Dose and duration	Results	Ref.
Antioxidant	ICR mice with lipopolysaccharide (LPS)-induced endotoxemia	Protective regimen: 50 or 100 mg/kg intragastrically, 3 h before LPS administration Therapeutic regimen: 50 or 100 mg/kg intragastrically, 12 h after LPS administration	Q demonstrated to inhibit strong oxidant species, including $O_2^{\cdot -}$ and possibly $ONOO^-$.	(103)
	Sprague Dawley rats with phenylhydrazine-induced vascular dysfunction and oxidative stress	25 or 50 mg/kg intragastrically for 6 days	Q improved parameters related to body oxidative status: it increased blood glutathione (GSH) levels, decreased plasma malondialdehyde (MDA) and NO_x levels, and normalized $O_2^{\cdot -}$ production to near basal rates.	(121)
	Swiss albino mice with tert-butyl hydroperoxide (t-BHP)-induced acute liver damage	20 mg/kg for 5 days (t-BHP was intraperitoneally injected on the 5^{th} day)	Pretreatment with Q showed liver protection against t-BHP induced hepatic injury, by a significant decrease in serum enzymes marker, sleeping time, and MDA, and an increase in the GSH, superoxide dismutase (SOD) and catalase (CAT) activities confirmed by pathology tests.	(105)

Table 1. (continued)

Effect	Study model	Dose and duration	Results	Ref.
Anti-inflammatory	Wistar rats with carrageenan-induced inflammation	10 mg/kg locally 1 h before carrageenan injection (in a subcutaneous air pouch)	The contents of prostaglandin E_2 (PGE_2), TNF-α, RANTES, and the mRNA for cyclooxygenase-2 were suppressed in rats. The histological examination displayed the suppression of the inflammatory response in the pouch tissues from Q treated rats.	(106)
	Lewis rats with chronic adjuvant-induced arthritis	30 mg/rat orally every 2 days for 10 days 5 or 10 mg/rat by intra-cutaneous injection every 2 days for 10 days 5 mg/rat by intra-cutaneous injection every 2 days for 10 days, simultaneously with their immunization	Arthritis severity significantly decreased after oral treatment of Q. Arthritis scores were reduced in a more significant manner in rats treated with 10 mg by intra-cutaneous injection, compared to those treated with 5 mg Q. Injection of relatively low Q doses prior to arthritis induction significantly reduced arthritis signs. Q (intra-cutaneous) improved macrophage inflammatory markers: levels of TNF-α, nitrites, and NO metabolites were decreased following both preventive and therapeutic Q injections.	(107)
Anti-cancer	BALB/c mice with CT-26 or MCF-7 cells subcutaneously injected	50, 100, or 200 mg/kg intraperitoneally	Q significantly reduced the tumour volume and increased animal survival in both CT-26 and MCF-7 tumours.	(109)
	Severe combined immunodeficiency (SCID) mice with implanted tumours from GFP-MDA-MB-231 BC cells	15 mg/kg or 45 mg/kg intraperitoneally 3 times per week for 13 weeks	The administration of Q resulted in a ~70% reduction in tumour growth.	(110)

Table 1. (continued)

Effect	Study model	Dose and duration	Results	Ref.
Cardiovascular effect	Conventional and hypertensive rats	5 mg/kg (as a solid dispersion) intravenously	Q reduced the arterial blood pressure in conventional rats. In hypertensive rats, Q caused a decrease in systolic blood pressure 1h post-administration and continued for 4 h, reaching a 30% reduction of the initial blood pressure.	(122)
Anti-obesity	Wistar rats fed with high fat/high sucrose diet	50 mg/kg orally for 6 weeks	Q decreased serum total cholesterol, triglycerides, and insulin, and hepatic triglycerides.	(111)
	Wistar rats fed with high fat/high sucrose diet	Diet supplemented with 30 mg/kg for 6 weeks	Q decreased serum glucose, serum insulin, and HOMA-IR.	(112)
	Obese Zucker rats	2 or 10 mg/kg by oral gavage for 10 weeks	Q decreased body weight gain, plasma triglycerides, total cholesterol, insulin, and HOMA-IR.	(113)
	C57BL/6J mice fed with high-fat diet	Diet supplemented with 0.1% (w/w) for 12 weeks	Q decreased plasma triglycerides and plasma total cholesterol.	(114)
	C57BL/6J mice fed with a high-fat, high-cholesterol, and high-sucrose Western diet	Diet supplemented with 0.05% for 20 weeks	Q decreased visceral fat, body weight, blood glucose, plasma insulin, total cholesterol, and triglycerides, hepatic steatosis, and hepatic triglycerides.	(115)
	ICR mice fed with high-fat diet	Diet supplemented with 25, 50, or 100 mg/kg for 10 weeks	Q decreased epididymal fat weight and adipocyte size, and plasma triglycerides and total cholesterol, in a dose-dependent manner.	(116)

Table 1. (continued)

Effect	Study model	Dose and duration	Results	Ref.
Anti-diabetic	Alloxan-induced diabetic Wistar rats	0.02 mmol/kg orally for 4 weeks (alloxan was intraperitoneally injected on the 21st day)	Q reduced the serum glycaemia of diabetic rats in a 62%, the total cholesterol in a 30%, the triglycerides in a 62%, and increased HDL-cholesterol in a 26%.	(120)
	Streptozotocin (STZ)-induced diabetic albino Wistar rats	25, 50, or 75 mg/kg orally for 28 days	After 7 days of treatment, Q administered at a dose of 75 mg/kg produced the maximum decrease of 15% in blood glucose levels. At day 28, this decrease was 67%. Q doses of 50 and 75 mg/kg significantly improved the profiles of serum triglycerides, high density lipoprotein, very low density lipoprotein, low density lipoprotein, and total cholesterol at the end of the study. The administration of Q (25, 50, and 75 mg/kg) daily for 28 days resulted in a significant decrease in blood glucose and urine sugar levels, with a considerable rise in plasma insulin and hemoglobin levels.	(123)

1.3. Nutraceuticals

The first definition of the term *nutraceutical* was given by Stephen DeFelice in the 1980s, as a variety of non-pharmaceutical compounds that can have an effect on health and disease (124,125). He proposed the term combining *nutrition* and *pharmaceutical*, so nutraceutical is a food or a part of it with health benefits or that prevents diseases (126).

The term has not a clear definition or legislation, and sometimes nutraceutical and *functional food* are used interchangeably (126,127). In that way, nutraceutical compounds are a combination of nutrients and substances present in food, without nutritional value but with positive effects on human health (126). On the other hand, a functional food is any food with health-promoting and/or disease-preventing properties in addition to the basic nutritional function of supplying nutrients (126). Actually, the term nutraceutical encompasses a lot of terms (Figure 8) (127).

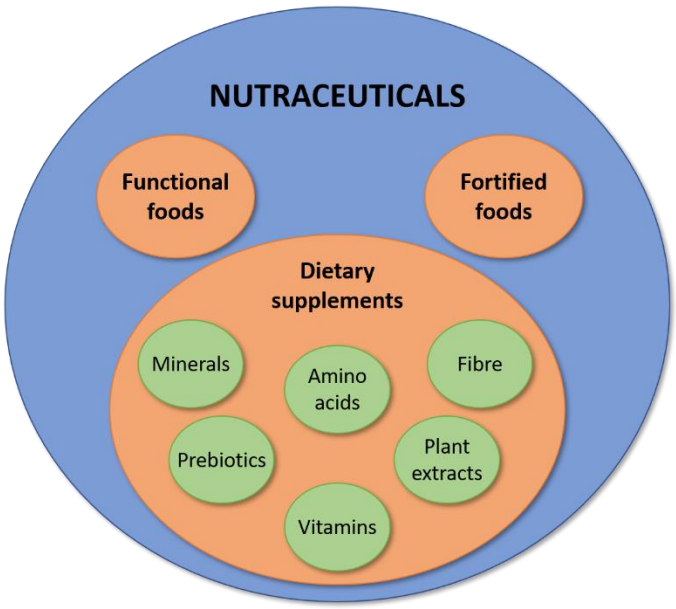

Figure 8. Different concepts comprehended by nutraceuticals. Based on Williamson *et al.* (127).

In that way, some concepts must be defined:

- Nutraceutical: a substance that is not traditionally recognized nutrient but which has positive physiological effects on the human body. It can modify the natural physiological functions of the body and is supported by scientific opinion (128).
- Functional food: besides the basic nutritional requirements, food with health benefits, due to the physiologically active compounds it contains (128).
- Fortified food: food that has been added one or more essential nutrients, regardless of whether the nutrient is normally contained in the food or not, with

the objective to prevent or correct a deficiency of one or more nutrients in the population. It is not the same as enriched food, in which the nutrients removed during the production or refinement are restored (129).

- Dietary supplement: substance to supplement the diet by increasing the total dietary intake. They do not have the objective to prevent, diagnose, treat or cure any disease. Some examples of dietary supplements are vitamins, minerals, herbs, amino acids, or enzymes, usually presented as tablets, capsules, softgels, gelcaps, powders, or liquids (130).
- Medicinal product: A substance or combination of substances that is intended to treat, prevent or diagnose a disease, or to restore, correct, or modify physiological functions by exerting a pharmacological, immunological, or metabolic action (131).

Ingredients contained in nutraceuticals are usually considered as Qualified Presumption of Safety (QPS) in the European Union and Generally Recognized as Safe (GRAS) in the United States. Even so, there is a lack of regulation in the global market, and the regulation of these products can vary depending on the region and tradition (a lot of them are legislated as herbal products), and different terminologies are used to name them (127). For example, FDA regulates dietary supplements, but the term "nutraceutical" is not used (132,133). In the EU, the term "food supplements" is used, and they are regulated as foods (134).

The nutraceutical industry has expanded during the last two decades, and by 2026, the global nutraceutical market should reach $438.9 billion, $149.1 billion more than in 2021 (128,135). Functional beverages as products of the nutraceutical market should grow to $162.4 billion by 2026 ($58.1 billion more than in 2021) and for functional foods, it should grow to $144.9 billion by 2026 ($50.7 billion more than in 2021) (135). The most attractive targets for nutraceuticals are cholesterol reduction, cardiovascular disease, and osteoporosis, followed by high blood pressure, diabetes, gastrointestinal disorders, menopause, and lactose intolerance (135). Also, products that contain polyphenols have especially high sales in the market (127). Nevertheless, the global nutraceutical market has to deal with some barriers, such as the expensive price of nutraceutical products and the lack of awareness regarding nutraceuticals (135).

Nutraceuticals have a high consumer demand by the general public and they are seen more favourably than pharmaceuticals, because they are considered more natural, with fewer side effects (which is not always true), easier to obtain (they are available in supermarkets, food shops, and pharmacies) and they do not have the same level of examination at a regulatory level before commercialization (125).

In human studies, the design and conducting of the methodology are similar to pharmaceutical trials, but some aspects have to be considered, as the fact that nutraceuticals are usually taken as "self-medication". Thus, the target population is heterogeneous and not well characterized, leading to variability in the effects of nutraceuticals (125).

1.3.1. Nanoparticles in functional foods

Nanotechnology is a field of research and innovation that involves the design, characterization, production, and application of materials, devices, and systems with a dimension between 1 and 100 nm (136). These materials, devices, and systems have unique properties due to their high surface-to-volume ratio and other innovative physicochemical characteristics such as colour, solubility, strength, diffusivity, toxicity, and magnetic, optical, or thermodynamic properties, among others. Because of that, nanotechnology offers a wide range of opportunities for the development and application of structures, materials, and systems with new properties in some areas such as agriculture, food, or medicine (137).

The use of nanomaterials in the food industry has increased due to their stability to high temperatures and pressures, their content in essential elements, and that they are non-toxic. They provide food better quality, safety, and health benefits. That's why new methods, techniques, and products are developing in food science (137). Nanomaterials used can be inorganic (metal and metal oxide nanoparticles), organic (mainly natural product nanoparticles), and combined (138). In the food sector, nanotechnology can be applicated in two areas: food processing and food packaging (137,139).

Nanoparticles can encapsulate nutrients and be added to food, increasing its absorption (139). They can mask odours or tastes, can control the interactions between the active ingredient and the food matrix, can control the release of these molecules, ensure availability at a target time and specific rate, and protect them from moisture, heat, chemical or biological degradation during processing, storage, or utilization (137). Nanotechnology can help in the development of functional foods, in order to deliver the nutrients more efficiently, and nanoencapsulation prevents the degradation and/or the inactivation of bioactive compounds, extending the shelf-life of these products (137,139).

A functional food is a food (or its components) that exerts beneficial health effects. Functional foods have components, nutrients, and non-nutrients that can affect some body functions, can help well-being and health, and reduce the risk of diseases. Many fruits, vegetables, grains, and fish are functional foods. Functional components can be enhanced by special growing conditions or breeding techniques, and others are specially formulated with specific components, such as bacteria in yogurt. When a component is removed from food in order to reduce adverse effects (such as reduction of saturated fatty acids), is also considered a functional food (140).

"Bioactive compound" is the name given to the compounds present in food that have beneficial health effects. They are usually present in small quantities, so the intake of functional foods needs to be high in order to be in enough quantity, a fact that is not always possible (140). Because of that, the food industry fortifies food with bioactive compounds, like vitamins, minerals, essential fatty acids, carotenoids, antioxidants, phytosterol, and fibres. Nevertheless, these bioactive compounds suffer reactions with other components during processing, storage, and transport, or are poorly soluble in

water, or sensitive to oxygen, light, temperature, or moisture (140,141). Some of them have also bad aroma and flavour. Bioavailability is low in some cases, due to poor solubility, chemical instability, and interaction with other food components (141). For that reason, nanotechnology has provided solutions, by encapsulating nutrients, bioactive ingredients, and phytochemicals (140). Among the bioactive compounds nano-encapsulated for functional foods, some are the following (141):

- Essential oils:

  Essential oils are volatile aromatic liquids obtained from plants. They have antimicrobial and anti-inflammatory properties, but they have peculiar aroma and flavour, and are sensitive to light, oxygen, and heat, which can degrade the oils. They are poorly soluble in water and present high volatility. The encapsulation of essential oils decreases the interaction with food, preserves its biological activity, and minimizes possible adverse effects on the sensory properties of food (141). It has been encapsulated tea tree oil in nanocapsules (142) or basil oil in nanoemulsions (143).

- Vitamins:

  Vitamins are organic compounds that are required in small amounts for maintaining metabolic integrity. They are needed for the growth and development in humans, and they need to be supplied by the diet because they cannot be synthesized in the body, but they are sensitive biomolecules and have to be protected during processing and storage (141,144). As an example, vitamin C has encapsulated in liposomes (145), and vitamin B2 in alginate and chitosan nanoparticles (146).

- Flavour and aroma compounds:

  Flavours are volatile compounds that can degrade or be lost during the processing and storage of foods. They are related to the quality of food and are important in consumer acceptability. Its encapsulation allows an increase in the stability and permits to be added to food and beverages (141). Menthol has been encapsulated in a nano-emulsion using gum arabic and maltodextrin (147), and vanillin has been nanoencapsulated in polyvinyl alcohol nanofibers (148).

- Polyphenols:

  Polyphenols are secondary plant metabolites with several beneficial effects, such as antioxidant, anti-inflammatory, antibacterial, or antiviral ones. However, they have got low solubility and permeability, added to instability due to the pH and enzymes of the gastrointestinal tract, what results in a low bioavailability. Also, they have an astringent taste. Its encapsulation permits overcoming these drawbacks (141). As some examples, luteolin has been encapsulated in nanostructured lipid carriers and microemulsions (149), or genistein in nano-emulsions (150).

- Carotenoids:

  Carotenoids are tetraterpene molecules, and the most widely distributed pigments in nature, present in some bacteria, archaea, fungi, algae, plants, and animals (151). They have antioxidant properties and are used as natural food colourants. They are poorly soluble in water and oil and are susceptible to oxygen and light, what makes them to be unstable in foods. The encapsulation of these molecules allows the rise of the solubility and prevents degradation during processing (141). For example, beta carotene was nano-encapsulated using casein and dextran (152), and curcumin was encapsulated in an oil-in-water nano-emulsion (153).

- Fatty acids:

  Fatty acids are hydrocarbon chains of variable length, and can be saturated (without double bonds in the chain) or unsaturated (one or more double bonds) (154). Polyunsaturated fatty acids have the ability to decrease blood triacylglycerol and cholesterol levels, they help in the appropriate function of the brain, they have retina immune-modulating properties, help in the prevention of cardiovascular diseases, and reduce the risk of cancer and autoimmune disorders. Nevertheless, these fatty acids are oxidized during the processing and storage of food and have strong odours in the final product. Nanoencapsulation is a good way to prevent these drawbacks in the use of functional foods (141). As examples, β-lactoglobulin and pectin were used to prepare omega 3 fatty acid-loaded nanocapsules (155), and nanoliposomes of fish oil were prepared and fortified into yogurt (156).

- Minerals:

  Minerals are micronutrients that are needed in small quantities in the body. Its nano-encapsulation for food fortification protects minerals from interaction with other components, masks bad flavours and colours, and provides a controlled release. The nano-encapsulation of minerals for mineral fortification can be done with Fe (e.g. $FeSO_4$), Ca (e.g. $Ca_3(PO_4)_2$), or I (e.g. KI) salts. For example, Fe-encapsulated forms used as core materials in fortifying dietary products are electrolytic-Fe or $FeSO_4$ (141).

Materials used to prepare the systems must be food grade, GRAS, or listed by the appropriate regulatory authority, and need to be biodegradable in nature (140,141). Organic or inorganic nanomaterials can be used for food applications. Among the organic used materials for the formation of delivery systems, the most used ones are carbohydrates (alginate, starch, dextrin, chitosan, guar gum, xanthan gum, pectin, galactomannan, cellulose, and their derivatives), lipids (egg yolk phospholipid, phosphatidylcholine, cholesterol, medium- and low-chain triglyceride, lecithin, soybean oil, corn oil, and olive oil), and proteins (gelatine, whey proteins, sodium caseinate, zein, and soy proteins) (141,157). Regarding inorganic materials, a limited number are used in food, such as iron, calcium, or silicates. A combination of organic and inorganic nanomaterials is also used (157).

These delivery systems at the nanoscale have higher surface area and improve solubility, enhance bioavailability, improve the controlled release and facilitate better precision targeting of the encapsulated bioactive compounds, apart from protecting them against degradation in the gastrointestinal tract (140,141). They must be compatible with food matrix and they must not negatively affect the appearance, taste, flavour, texture, and shelf life of the product. Different nano-structured systems can be used for the delivery of nutrients, such as nano-emulsions, solid lipid nanoparticles, liposomes, micelles, or protein nanoparticles (140).

- Liposomes:

  Liposomes are small artificial spherical vesicles formed by the self-assembly of amphiphilic molecules, usually phospholipids. They contain an aqueous core surrounded by one or more phospholipid bilayers, where polar head groups are oriented in the pathway of the interior and exterior aqueous phases. Their sizes are between 30 nm to some microns, and they can encapsulate hydrophilic and hydrophobic compounds (158). Liposomes can encapsulate vitamins, antioxidants, proteins, peptides, minerals, or fatty acids. Nevertheless, the use of liposomes in the food industry is limited due to the high cost of phospholipids, the problems in the scalable process, and the lack of information about the bioavailability of liposome-encapsulated bioactive compounds (140).

- Nano-emulsions:

  Nano-emulsions are dispersions of one immiscible liquid in another, forming transparent or translucid droplets of 20 to 200 nm. There are two types of nano-emulsions: oil-in-water (o/w) and water-in-oil (w/o). Nano-emulsions are thermodynamically unstable systems, which can be stabilized using emulsifiers (159). Its use in the food sector is limited due to the high cost of the production and problems to find food-grade surfactants (140).

- Solid lipid nanoparticles:

  Solid lipid nanoparticles are spherical delivery systems, with a size in the range between 50 and 1000 nm. They are made of lipids, that are solid at room temperature, and emulsifiers (160). They can increase the stability of labile hydrophobic compounds and provide a controlled release (140,160). Solid-lipid nanoparticles have been used to encapsulate fat-soluble vitamins, but their use in food is limited due to a possible loss of the bioactivity of bioactive compounds during the heating step (compounds are solubilized in melted lipid during the formation of nanoparticles). The *in vivo* digestibility has also to be evaluated (140).

- Protein nanoparticles:

  Protein nanoparticles and hydrogels can be formed by a controlled assembly of proteins (140). These nanoparticles can be prepared using animal proteins (such as gelatin, casein, or silk fibroin) or using plant proteins (like zein, gliadin, or soy proteins), and hydrophilic and hydrophobic compounds can be encapsulated

(161,162). They can be added to food also to modify texture. In some cases, heat treatment is needed to produce protein nanoparticles, and limits its application in heat-sensitive molecules (140).

- Protein-polysaccharide composite systems:

  These composite systems are based on a covalent conjugation or electrostatic complexation between proteins and polysaccharides, and hydrophobic and hydrophilic compounds can be encapsulated. Proteins present positive charges at pH values below their isoelectric points, and can complex with anionic polysaccharides, forming soluble and insoluble complexes. Depending on the type and concentrations of the biopolymers, pH, and ionic strength, complexes will have different characteristics (140).

The use of nanomaterials in the food sector is growing, but research and development activities are being performed in order to investigate the benefits and risks of the use of nanomaterials in changing food characteristics (163). In the European Union, EFSA provides independent scientific advice in risk evaluation for food and food contact materials, in order to determine if risks have to be taken into account previous to the commercialization, and the risk managers have to evaluate the current legislation according to this advice. Then, the approval for the use of nano sized substances in food products is responsibility of the European Commission and Member States, which stablish the usage conditions and requirements for labelling (163,164). At present, there are some regulations in the European Union about nanomaterials in the food sector (163). For example, the European Commission published in 2008 the regulatory aspects of nanomaterials (164,165).

Nowadays, some functional foods containing nano-encapsulated bioactive compounds are on the market (140,141,166). For example, Canola Active Oil (Shemen Industries, Israel) uses nano-sized self-assembled structured liquids to carry phytosterols (166,167), Nanotea (Shenzhen Become Industry & Trade Co., Ltd., China) uses selenium nanoparticles as a supplement of the compound as well as antimicrobial protection (166,168) and Nanoceuticals™ Slim Shake Chocolate (RBC Life Sciences®, USA) used nanoclusters to enhance cocoa taste and increase the absorption of nutrients (166,169). In the European Union, all ingredients present as synthetic nanoparticles in food must be labelled on the packaging with the term *nano* in parentheses (170).

1.4. Nanoparticles for the oral administration of quercetin

Quercetin is a highly hydrophobic molecule and degrades in the stomach, what makes the reduction of the bioavailability and efficacy in the body. Because of that, its consumption in enriched foods or as supplements is not enough to achieve the effective concentration to be pharmacologically active. To overcome these drawbacks, two different strategies can be carried out: chemical modification or the inclusion in delivery systems, such as nanoparticles (93).

Thus, different types of quercetin-loaded nanoparticles for oral delivery have been prepared; polymeric (Table 2), polysaccharide (Table 3), lipid (Table 4), and protein (Table 5) nanoparticles. During the last 20 years, the number of patents involving the preparation and/or the application of polyphenol nano-formulations has increased from 0 to 30 approximately (136). However, only a few dietary supplements involving nanoformulations of quercetin are commercialized. Some examples (Figure 9) are *Nano Quercetin* (171), presented as quercetin nanoparticles, *Liposomal Quercetin* (172), present as liposomes, or *Quercetin LipoMicel.Matrix* (173), present as a matrix of micelles (174).

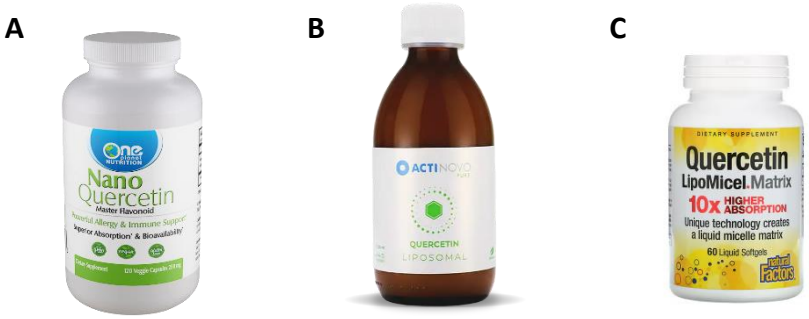

Figure 9. Commercialized quercetin in nanoformulations. **A**: *Nano Quercetin* (One Planet Nutrition, Naples, FL, USA) (171); **B**: *Liposomal Quercetin* (ActiNovo, Hamburg, Germany) (172); **C**: *Quercetin LipoMicel.Matrix* (Natural Factors, Coquitlam, Canada) (173).

1.4.1. Polymeric nanoparticles

Poly(lactic-co-glycolic acid) (PLGA) is a synthetic biodegradable polymer that has been used to prepare quercetin-loaded nanoparticles. It is biocompatible, protects from chemical instability, is sustainable, and approved by the FDA and EMA (175). Anwer *et al.* worked with PLGA nanoparticles developed by single emulsion-solvent evaporation method, obtaining an enhancement in the *in vitro* antioxidant capacity of quercetin when encapsulated in nanoparticles and a rise in the diuretic activity of quercetin-loaded PLGA nanoparticles *in vivo* compared with free quercetin (175). Arasoğlu *et al.* used three different methods of synthesis to produce PLGA nanoparticles, obtaining the best characterization results with single emulsion-solvent evaporation, and analysed the antibacterial activity against four foodborne microorganisms by three different

methods. They showed that quercetin and quercetin-loaded PLGA nanoparticles had antimicrobial activity only against gram-positive bacteria, and this effect was dependent on the drug/polymer ratio (176). Chitkara *et al.* developed PLGA nanoparticles that presented quercetin plasma levels for 6 days *in vivo*, and decreased blood glucose levels in diabetic rats (177).

Some commercial polymers have also been used to prepare quercetin-loaded nanoparticles, such as Eudragit® polymers. Eudragit® L30-D55 was used to prepare nanoparticles by solvent displacement (178). The antioxidant activity of quercetin was not affected by its encapsulation, and they showed that quercetin was not delivered from the nanoparticles in the acidic pH of the stomach and was released under neutral conditions of the intestine (178). On the other hand, Eudragit® S100 is the most suitable Eudragit® polymer for colon targeting, and Sunoqrot *et al.* prepared nanoparticles by nanoprecipitation. They did not detect any quercetin released at pH 1.2 and 4.5, but quercetin was released almost completely at pH 7.2. Nanoparticles also showed higher potency in CT26 colon cancer cells compared to free quercetin (179).

Other polymers have also been used for the preparation of quercetin-loaded nanoparticles, as polycaprolactone (180,181), hydroxypropyl methylcellulose (182), or poly(n-butylcyanoacrylate) (183).

1.4.2. Polysaccharide nanoparticles

Chitosan is the second most abundant polysaccharide and cationic polyelectrolyte present in nature (is the deacetylated form of chitin), and has been used to prepare quercetin-loaded nanoparticles due to its biodegradability, low toxicity, and good biocompatibility (184). Zhang *et al.* prepared chitosan nanoparticles by ionic gelation, concluding that quercetin was present in an amorphous state inside the nanoparticles and the *in vitro* antioxidant activity of the flavonoid was preserved (184). Chitosan has also been combined with other compounds to prepare nanoparticles. Aluani *et al.* prepared chitosan/alginate nanoparticles, demonstrating that particles were not cytotoxic *in vitro* and did not present toxicity *in vivo* (185). A similar formulation was proved in paracetamol-induced rat liver injury, concluding that quercetin provided protection against oxidative stress and lipid peroxidation (104). Fucoidan/chitosan nanoparticles were prepared by Barbosa *et al.*, showing that by increasing the fucoidan ratio nanoparticles were resistant to gastrointestinal pH, preserving the *in vitro* antioxidant activity of quercetin (186). Chitosan and gum arabic nanoparticles have been prepared, showing that they had higher *in vitro* mucin and intestinal cell adhesion compared to free quercetin (187). Chitosan derivatives have also been used to prepare nanoparticles, using carboxymethyl chitosan or chitosan hydrochloride (188).

Quercetin-loaded alginate nanoparticles have also been developed. Alginate is a biopolymer obtained from brown algae, that exerts biocompatible properties, mucoadhesive nature, non-immunogenicity, and low production cost. Selvaraj *et al.* prepared quercetin-loaded nanoparticles by ice cold precipitation method. Particles

showed a sustained release of quercetin, the antioxidant effect of the flavonoid was increased when it was encapsulated and they showed better *in vitro* anticancer activity in human leukemic cells compared to free quercetin (189).

The natural occurring polysaccharide polymer starch has also been used to prepare nanoparticles, due to its biocompatibility, biodegradability, and bio-adhesion properties (190). Farrag *et al.* prepared starch nanoparticles by nanoprecipitation method. They demonstrated that the size, loading capacity, release profile, and antioxidant activity of the quercetin-loaded nanoparticles changed depending on the origin of the starch (190). On the other hand, Wang *et al.* prepared quercetin-loaded starch nanoparticles, that reduced the release of quercetin and presented a better performance on cell inhibitory activity in five types of cancer cells, compared to free quercetin (191).

1.4.3. Lipid nanoparticles

Solid lipid nanoparticles (SLN) have also been prepared for the oral administration of quercetin. Li *et al.* prepared soya lecithin and glyceryl monostearate nanoparticles, and performed gastrointestinal absorption in situ assays in rats (192). They observed that the stomach was not a good absorption site for quercetin-loaded SLNs, being the intestine the major absorption segment. They demonstrated that the nanoparticles improved the relative oral bioavailability five times compared to quercetin aqueous suspension. Ahmad *et al.* used glycerol monostearate, hydrogenated soya PC, and soya PC to prepare SLN, that increased three times the oral bioavailability compared to quercetin aqueous suspension (193). They demonstrated that nanoparticles alleviate the loss of bone mass induced by estrogen deficiency, and the effect of loss preventing in bone was significantly higher for quercetin-loaded SNL than for free quercetin.

1.4.4. Protein nanoparticles

Zein is the major protein of maize, biodegradable, biocompatible, and GRAS considered (108,194). Different methods can be used to prepare quercetin-loaded zein nanoparticles, such as desolvation (108,195) or electrospraying (194). Penalva *et al.* developed quercetin-loaded zein nanoparticles by desolvation method, obtaining an increase in the oral bioavailability of the flavonoid in rats more than ten times compared to quercetin aqueous suspension (close to 35%, 60% when cyclodextrins were added to the nanoparticles), and demonstrating that particles can attenuate the severity of endotoxic shock in mice (108). Moreno *et al.* prepared zein nanoparticles containing cyclodextrins, and showed the improvement of cognition and memory impairments and reduced astrogliosis in a mouse model of Alzheimer's disease (195). On the other hand, the electrospraying method can also be used to prepare zein nanoparticles. Rodríguez-Félix *et al*. showed that the main interactions between zein and quercetin were by hydrogen bonds, and the nanoparticles provided stability to quercetin during gastrointestinal digestion (194).

Table 2. Examples of quercetin-loaded polymeric nanoparticles for oral administration, the methods used to prepare them, characteristics, and effects. Q: quercetin; Q-NP: corresponding quercetin-loaded nanoparticles; EE: encapsulation efficiency; QL: quercetin loading (% w/w).

Polymeric nanoparticles				
Material	**Preparative method**	**Characteristics**	**Bioavailability and/or effect**	**Ref.**
PLGA	Single emulsion-solvent evaporation	180 – 279 nm QL: 13 – 24%	Bioavailability: $AUC_{Q\text{-}NP}$ was 5.2 times higher than $AUC_{Control}$ in male Sprague Dawley rats by oral gavage at 150 mg/kg. Decrease in blood glucose level was observed in streptozotocin-induced diabetic Sprague Dawley rats treated with a Q suspension (150 mg/kg daily) or Q-NP (150 mg/kg given every fifth day) as compared to diabetic control group.	(177)
PLGA	Single emulsion-solvent evaporation	118 – 279 nm EE: 74 – 86%	Diuretic activity of the Q-NP was better than pure quercetin in Swiss albino rats at 10 mg/kg.	(175)
PLGA	Single emulsion-solvent evaporation	244 – 263 nm EE: 93 – 98%	Q-NP increased the duration and effectiveness of antimicrobial activity *in vitro* only against gram-positive bacteria.	(176)
PLGA	Electrospraying	385 nm	*In vitro* release for 59 days in PBS at pH 7.2, 96% of quercetin released.	(196)
PLGA/D-a-tocopherol polyethylene glycol 1000 succinate	Nanoprecipitation	198 nm QL: 8.1%	Q-NPs had stronger inhibition *in vitro* than free Q on human breast (MDA-MB231) and mouse breast (4T1) cancer cells at low concentrations (10 mM). After oral gavage for 10 days (30 mg/kg once daily), Q-NPs significantly inhibited tumour growth with much lower tumour weight and smaller tumour volume compared with saline treatment in a triple-negative 4T1 mammary carcinoma in female Balb/c mice.	(197)

Table 2. (continued)

Material	Preparative method	Characteristics	Bioavailability and/or effect	Ref.
Eudragit® L30-D55	Solvent displacement	369 nm EE: 68%	Antioxidant activity (by the evaluation of the inhibition of lipid peroxidation of phospholipid liposomes) of Q was maintained after its encapsulation.	(178)
Eudragit® S100	Nanoprecipitation	67 nm QL: 2.2%	80-fold increase in *in vitro* cytotoxic activity was observed for Q-NP in CT26 murine colon cancer cells, compared to free Q.	(179)
Polycaprolactone	Nanoprecipitation	-	Bioavailability: $AUC_{Q\text{-}NP}$ was 5.4 times higher than $AUC_{Control}$ in male Sprague Dawley rats at 25 mg/kg.	(180)
Polycaprolactone	Nanoprecipitation	162 – 259 nm EE: 36.5 – 78.0%	*In vitro* release in a mixture of PBS (pH 7.4) and methanol (80:20, v/v) suggested that quercetin remained entrapped in nanoparticles and control release from polymer matrix for more than 48 h.	(181)
Hydroxypropyl methylcellulose	Desolvation	520 – 750 nm	Q-NPs administration (30 mg/kg per day) preserved the structure and function of hippocampal neurons in $AlCl_3$-induced Alzheimer's disease in Sprague Dawley male rats. They could also minimize the degenerative changes in affected hippocampus.	(182)
Poly(n-butylcyanoacrylate)	Anionic emulsion polymerization	161 – 166 nm EE: 74.6 – 79.8%	Bioavailability: $AUC_{Q\text{-}NP}$ was 2.4 and 3 times higher than $AUC_{Control}$ in male Wistar albino rats at 50 mg/kg orally administered. A biodistribution study in rats showed that a higher concentration of Q was found in the brain when NPs were coated with Polysorbate 80.	(183)

Table 3. Examples of quercetin-loaded polysaccharide nanoparticles for oral administration, the methods used to prepare them, characteristics, and effects. Q: quercetin; Q-NP: corresponding quercetin-loaded nanoparticles; EE: encapsulation efficiency; QL: quercetin loading (% w/w).

Polysaccharide nanoparticles				
Material	**Preparative method**	**Characteristics**	**Bioavailability and/or effect**	**Ref.**
Chitosan	Ionic gelation	68 nm	Antioxidant activity (by DPPH) and reducing power was increased by Q-NPs.	(184)
Chitosan/alginate	Electrostatic gelation	300 – 600 nm	Q-NPs were not cytotoxic *in vitro* in human hepatocellular carcinoma cells HepG2 and rat hepatocytes after 24 h exposure. Q-NPs significantly stimulated *in vitro* the proliferation of murine spleen lymphocytes and peritoneal macrophage in two types of murine cells, isolated spleen lymphocytes, and peritoneal macrophages. In a toxicity study, administration of Q-NPs in male Wistar albino rats by oral gavage (0.5 ml/100 g b.w.) for 14 days did not change body weight, the relative weight of rat livers, liver histology and haematology and biochemical parameters.	(185)
Chitosan/alginate	Electrostatic gelation	350 – 550 nm	*In vitro* experiments revealed lack of toxicity in human hepatocellular carcinoma HepG2 cells, and higher protective activity of encapsulated vs free Q in H_2O_2-induced oxidative damage in HepG2 cells. Oral pretreatment with free or encapsulated Q (0.18 mg/kg for 7 days) showed a significant protection against oxidative stress and lipid peroxidation in a model of paracetamol-induced rat liver injury in male Wistar rats.	(104)
Fucoidan/chitosan	Polyelectrolyte self-assembly	335 – 356 nm QL: 14.5 – 14.9%	*In vitro* release in fasted-state simulated gastric fluid (pH 1.6) followed by fasted-state simulated intestinal fluid (pH 6.5) was modified depending on fucoidan/chitosan ratio in Q-NPs. Antioxidant activity (by ABTS) was maintained by Q-NPs at high concentrations.	(186)

Table 3. (continued)

Material	Preparative method	Characteristics	Bioavailability and/or effect	Ref.
Chitosan/Gum Arabic	Ionic gelation	267 – 493 nm QL: 0.7 – 1.3%	Q-NPs showed significantly higher *in vitro* mucin (in a mucin solution) and intestinal cell adhesion (Caco-2 and HT-29 cocultured monolayer) compared with free Q. The *in vitro* cellular antioxidant activity of free Q was significantly increased in Caco-2 cells by its encapsulation in Q-NPs. *In vivo* ferric reducing ability of plasma (FRAP) values were higher for Q-NPs than for free Q in Sprague Dawley rats 2 h post-administration at a dose of 26 mg/kg.	(187)
Carboxymethyl chitosan/ chitosan hydrochloride	Modified ionic gelation	386 – 2083 nm EE: 31 – 70%	The loading of Q into Q-NPs increased its chemical stability and solubility and had relatively higher biological activity in 50% ethanol, water-oil (50:50) simulants or whisky systems (the release rate of Q from Q-NPs increased in whisky during 10 days), and protected Q in the SGF.	(188)
Alginate	Cold precipitation-sonication	180 – 259 nm QL: 0.1 – 0.7%	Q-NPs improved antioxidant potential (by DPPH) of Q. Q-NPs improved the anticancer effect *in vitro* in human leukemic cancer U937 cells.	(189)
Starch	Nanoprecipitation	500 nm fibers QL: 20 – 49%	Loading capacity, release profile, and antioxidant activity (by DDPH) of Q-NPs changed by changing the starch origin.	(190)
Starch	Nanoprecipitation	212 nm 1140 µg Q/mg NP	Compared with free Q, Q-NPs had some degree of increased inhibition effectiveness *in vitro* in five cancer cells (A549, HEPG-2, BGC-823, MCF-7, HTC116).	(191)

Table 4. Examples of quercetin-loaded solid lipid nanoparticles for oral administration, the methods used to prepare them, characteristics, and effects. Q: quercetin; Q-NP: corresponding quercetin-loaded nanoparticles; QL: quercetin loading (% w/w).

Solid lipid nanoparticles				
Material	**Preparative method**	**Characteristics**	**Bioavailability and/or effect**	**Ref.**
Soya lecithin, glyceryl monostearate	Emulsification and low-temperature solidification	155 nm QL: 13%	Bioavailability: $AUC_{Q\text{-}NP}$ was 5.7 times higher than $AUC_{Control}$ in male Wistar rats at 50 mg/kg.	(192)
Glycerol monostearate, hydrogenated soya PC, soya PC	Emulsion solvent evaporation followed by high pressure homogenization	173 nm QL: 8.4%	Bioavailability: $AUC_{Q\text{-}NP}$ was 3.5 times higher than $AUC_{Control}$ in male Sprague Dawley rats at 25 mg/kg. Osteoprotective activity: Q-NPs alleviated the estrogen deficiency induced loss of bone mass, bone strength and the microarchitecture of long bones and vertebrae, eliminating any possibility of endometrial hyperplasic effects in bilaterally ovariectomized female Sprague Dawley rats, at 5 mg/kg/day by oral gavage for 12 weeks. The bone loss preventing effect of Q-NPs was significantly better than Q.	(193)

Table 5. Examples of quercetin-loaded protein nanoparticles for oral administration, the methods used to prepare them, characteristics, and effects. Q: quercetin; Q-NP: corresponding quercetin-loaded nanoparticles; Fr: relative oral bioavailability; EE: encapsulation efficiency; QL: quercetin loading (% w/w).

Protein nanoparticles				
Material	**Preparative method**	**Characteristics**	**Bioavailability and/or effect**	**Ref.**
Zein	Desolvation	294 – 358 nm 62 – 69 µg Q/mg NP	Bioavailability: Fr was 35 – 57% in male Wistar rats at 25 mg/kg (8.4 and 13.9 times higher than the Fr of a Q solution). Q-NP administration (25 mg/kg every 2 days for one week) decreased endotoxemia symptoms and TNF-α serum levels in lipopolysaccharide-induced endotoxic shock model in female C57BL/6J mice, compared to Q oral solution.	(108)
Zein	Electrospraying	70 – 100 nm EE: 88 – 93%	Bioavailability of Q-NP in the gastrointestinal simulation was 5.9%, 3 times higher than for free Q.	(194)
Zein + HP-β-CD	Desolvation	260 nm 70 µg Q/mg NP	Q-NPs administration (25 mg/kg every 2 days for 2 months) improved the cognition and memory impairments and reduced the astrogliosis in a model of Alzheimer's disease in mice (male senescence-accelerated mouse prone 8 (SAMP8) mice).	(195)
Zein with soluble soybean polysaccharide coating	Desolvation	80 – 212 nm EE: 42 – 83%	Q-NPs increased the photochemical stability and antioxidant activity (by ABTS) of Q.	(198)

Table 5. (continued)

Material	Preparative method	Characteristics	Bioavailability and/or effect	Ref.
Zein with caseinate and caseinate-chitosan coating	Desolvation	198 – 1011 nm QL: 1.6 – 2.9 %	Faeces excretion of Q was significantly decreased after the intragastrical administration of Q-NPs in female Sprague Dawley rats at a dose of 10 mg/kg, compared to free Q. After intragastrical administration of Q-NPs in ICR mice at a dose of 15 mg/kg, the presence of Q in caseinate-Q-NP group was significantly higher than Q-Susp and caseinate/chitosan-Q-NP groups in the small intestine at 3 and 6 h. Bioavailability: $AUC_{Q\text{-}NP}$ was 2.3 and 1.9 times higher than $AUC_{Control}$ in female Sprague Dawley rats at 10 mg/kg, administered intragastrically.	(199)
Casein + HP-β-CD	Desolvation	171 – 251 nm 22.3 – 31.5 µg Q/ mg NP	Bioavailability: Fr was 12 – 37% in male Wistar rats at 25 mg/kg (2.9 and 9 times higher than the Fr of a Q solution).	(90)
β-lactoglobulin	Modified desolvation	180 – 300 nm QL: 13.9%	The release rate in PBS/Polysorbate 80 for Q-NPs with low quercetin loading was higher than the other case with high quercetin loading. At the end of a two-step digestion (SGF and SIF), about 80% of quercetin was recovered from the two buffers.	(200)

Chapter 2

Objectives

2. Objectives

The flavonoid quercetin as a nutraceutical compound presents interesting properties against the symptomatology of obesity-related comorbidities. However, its use is hampered by its low oral bioavailability, so strategies to overcome this drawback are required. Thus, the general objective of this work was the encapsulation of quercetin in zein-based nanoparticles, in order to improve the oral bioavailability and hence, the effect, which was assessed in *in vivo* models of obesity.

More concretely, four partial objectives were proposed:

1. Development and characterization of zein-based nanoparticles (as nanospheres, nanocapsules, and coated nanospheres) and loading of the flavonoid quercetin.
2. Evaluation of the effect of the nanoparticles on the fat accumulation of the nematode *Caenorhabditis elegans*.
3. Evaluation of the biodistribution and pharmacokinetic profile of quercetin when encapsulated in the nanoparticles in Wistar rats.
4. Evaluation of the effect of the nanoparticles in a diet-induced obesity (DIO) model in Wistar male rats.

Chapter 3

Materials and Methods

3. Materials and methods

3.1. Materials

Quercetin, zein, L-lysine, polyethylene glycol 35,000 (PEG), 2-hydroxypropyl-β-cyclodextrin (HP-β-CD), trifluoroacetic acid, Rose Bengal, sodium chloride, dipotassium hydrogen phosphate, magnesium chloride, sodium phosphate dibasic heptahydrate, Orlistat, glucose, sterile DMSO, Nile Red, Kollisolv® PEG E 400, and sulfadimetoxine were purchased from Sigma-Aldrich (Saint Louis, MO, USA). Wheat germ oil and mannitol were obtained from Guinama (La Pobla de Vallbona, Spain). Absolute ethanol, isopropanol, and chloroform were from Scharlab (Sentmenat, Spain). Acetonitrile (ACN, HPLC grade), methanol (HPLC grade), calcium chloride, and EMPLURA® Sodium hypochlorite solution (6-14% active chlorine) were purchased from Merck (Darmstadt, Germany). Lumogen® Red 305 was provided by BASF (Ludwigshafen am Rhein, Germany). Hydrochloric acid 37%, formaldehyde 3.7-4.0 % w/v buffered to pH=7 and stabilized with methanol, and UHPLC grade ACN were acquired from Panreac AppliChem (Castellar del Vallès, Spain). Phosphate Buffered Saline (PBS) was obtained from Gibco (Thermo Fisher Scientific, Waltham, MA, USA). Magnesium sulphate heptahydrate and formic acid were purchased from VWR Chemicals (Radnor, PA, USA). Potassium phosphate monobasic was from Acorfarma (Madrid, Spain), and sodium hydroxide from Honeywell (Charlotte, NC, USA). European bacteriological agar, peptone, LB Broth, and agarose were provided by Condalab (Torrejón de Ardoz, Spain). Isoflurane (IsoVet®) was acquired from B. Braun Vetcare (Rubí, Spain). Tissue-Tek® O.C.T. Compound was purchased from Sakura Finetek Europe (Alphen aan den Rijn, The Netherlands), and commercial rat plasma was obtained from Envigo (Indianapolis, IN, USA). Type I water was used for all the experiments, produced by a Wasserlab water purification system (Barbatáin, Spain).

3.2. Preparation of nanoparticles

In this work, two kinds of nanoparticles were developed. In the former, zein nanospheres were prepared. These nanospheres were also coated with polyethylene glycol (PEG) 35,000 to obtain a hydrophilic surface and improve their mucus-permeating properties. In the latter, zein nanocapsules, characterized by an oily core of wheat germ oil, were prepared. In all cases, quercetin was encapsulated in zein-based nanospheres and nanocapsules.

3.2.1. Zein nanospheres

Zein nanospheres (NS) were prepared by a previously reported desolvation method with some modifications (108). Thus, 200 mg zein and 30 mg L-lysine were mixed in 20 mL of a hydroalcoholic solution (ethanol 70% v/v) with magnetic stirring. Then, 20 mL

water were added to induce the formation of the nanospheres. Eventually, 2 mL of an aqueous solution of mannitol (200 mg/mL) were added as protectant. Nanospheres were dried in a Büchi mini Spray Dryer B-290 (Büchi Labortechnik AG, Flawil, Switzerland), with the following conditions: inlet temperature: 90 °C; outlet temperature: 45-50 °C; air pressure: 4-6 bar; pumping rate: 5 mL/min; aspirator: 80 % and air flow: 400-500 L/h.

For the preparation of quercetin-loaded nanospheres (Q-NS), nanoparticles were prepared as described above after the addition of 20 mg quercetin in the initial hydroalcoholic solution of zein and lysine. The resulting nanospheres were dried as described above.

3.2.2. Zein nanocapsules

Zein nanocapsules (NC) were obtained in a similar way as described for the preparation of nanospheres, with the difference of the incorporation of an oily compound. Briefly, 200 mg zein and 30 mg L-lysine were mixed in 17 mL of a hydroalcoholic solution (ethanol 65% v/v) with magnetic stirring. In parallel, 22 µL of wheat germ oil were dissolved in 3 mL ethanol and added to the initial solution of zein and lysine. Then, 20 mL water were added to induce the formation of the nanocapsules. Eventually, a solution of mannitol was added (400 mg in 2 mL of water). Nanocapsules were dried in a Büchi mini Spray Dryer B-290 (Büchi Labortechnik AG, Flawil, Switzerland), using the same conditions described in section 3.2.1.

For the preparation of quercetin-loaded nanocapsules (Q-NC), 20 mg quercetin were added to the initial mixture of zein and lysine before the formation of nanocapsules. Then, the nanocapsules were dried as described above.

3.2.3. PEG-coated zein nanospheres

Nanospheres were coated by simple incubation between the nanospheres and PEG 35,000, as previously described (201). Two different PEG-to-zein ratios were used (0.25 and 0.50, w/w). For this purpose, freshly prepared zein nanospheres (as described in 3.2.1) were incubated with 1 mL of a solution of PEG in water (50 or 100 mg/mL) before the drying step. The solution of mannitol was added occasionally and dried in a Büchi mini Spray Dryer B-290 (Büchi Labortechnik AG, Flawil, Switzerland) using the same conditions previously described (section 3.2.1). These formulations were named as NS-PEG25 and NS-PEG50.

For the preparation of PEG-coated quercetin-loaded zein nanospheres (Q-NS-PEG25 and Q-NS-PEG50), 20 mg quercetin were added to the initial hydroalcoholic solution of zein and lysine, before the formation of nanospheres. The coating of nanospheres with PEG and the drying in the Spray Dryer apparatus was performed as described above.

3.2.4. Lumogen® Red-loaded nanoparticles

For some experiments, Lumogen® Red was loaded in zein nanospheres and nanocapsules. For this purpose, 2.7 mL of a solution of Lumogen® Red in ethanol was added to the initial mixture of zein and lysine, before the addition of water to form the nanoparticles. Different Lumogen® concentrations were used depending on the assay: (i) 0.04 mg/mL for multiple particle tracking assays, (ii) 0.4 mg/mL for *C. elegans* intake assay and, (iii) 0.1 mg/mL (NS and NS-PEG) and 0.05 mg/mL (NC) for biodistribution studies in Wistar rats. Lumogen® was added to the initial solution of zein and lysine in ethanol 65% (v/v) in the case of nanospheres, and 60% (v/v) in the case of nanocapsules. Then, nanoparticles were formed and dried as described above.

3.3. Characterization of nanoparticles

3.3.1. Size, zeta potential and morphology

The size and zeta potential of the nanoparticles was measured in a ZetaPlus Analyzer (Brookhaven Instrument Corporation, Holtsville, NY, USA), by dynamic light scattering (DLS) and electrophoretic light scattering (ELS), using a dispersion of the formulation in water.

The morphology of nanoparticles was analysed by scanning electron microscopy (SEM) in a FE-SEM Sigma 500 (Zeiss Microscopy, Jena, Germany). For the preparation of the samples, 0.5 mg of mannitol-free nanospheres were redispersed in 1 mL water. Then 3.5 µL drops were put in SEM grids, dried overnight, and coated with a gold layer using an Emitech K550 sputter coater (Quorum Technologies, Laughton, UK). In the case of nanocapsules, 1.5 mg of the formulation were redispersed in 1 mL water and centrifuged at 5,000 rpm for 5 minutes, in order to eliminate the mannitol. Supernatant was discarded and the particles were dispersed again, dried, mounted in SEM grids, and coated with gold as described above.

3.3.2. Zein quantification

The content of zein in the nanoparticles was quantified using a MicroBCA Protein Assay Kit (Thermo Fisher Scientific, Waltham, MA, USA), following the instructions of the manufacturer. Briefly, the calibration curve was prepared with serial dilutions of zein in water from a stock solution (2 mg/mL) in ethanol 75% (v/v). Samples were prepared by dissolving 6 mg of the formulation powder in 1 mL ethanol 75% (v/v) to break the nanoparticles, and diluting with water afterwards. Then, 150 µL of each standard or sample and 150 µL of the Working Reagent from the MicroBCA Protein Assay Kit were mixed in a 96-well plate, shaken for 30 seconds, and incubated at room temperature for

2 hours. The absorbance was measured at 562 nm in a BioTek PowerWave XS microplate spectrophotometer (BioTek Instruments Inc, Winooski, VT, USA).

3.3.3. Quercetin content

The payload of quercetin in the nanoparticles was quantified in an Agilent 1200 Series HPLC System with an UV-Vis detector (Agilent Technologies, Santa Clara, CA, USA), using a Kinetex C18 column (5 µm, 100 Å, 100 x 4.6 mm) and a C18 SecurityGuard™ ULTRA Cartridge precolumn for 4.6 mm ID columns (Phenomenex, Torrance, CA, USA). An isocratic mobile phase of 0.1% trifluoroacetic acid (TFA) in water and 0.1% TFA in acetonitrile (ACN) (60:40) was used, with a flow rate of 0.7 mL/min, an injection volume of 10 µL, and a column temperature of 40 °C. Quercetin was detected at a wavelength of 370 nm, and the retention time (RT) was 2.3 minutes. Calibration curves were prepared from 2 to 100 µg/mL in ethanol ($R^2 \geq 0.9997$). The limit of detection was calculated to be 0.5 µg/mL and the limit of quantification was 1.6 µg/mL.

For the preparation of the samples, 5 mg of each formulation were dissolved in ethanol 75% (v/v) and vortexed for 1.5 minutes to break the nanoparticles. A dilution with absolute ethanol (0.4 mL to 2 mL) was made before injecting the samples in the chromatograph. Samples were prepared in triplicate and data were expressed as µg of quercetin loaded by milligram nanoparticles. The encapsulation efficiency (expressed in percentage) was calculated as the quotient between the payload of quercetin in the nanoparticles and the quantity initially added, as shown in Equation 2.

$$EE\ (\%) = \frac{Quercetin\ loading}{Initial\ quercetin} \times 100 \qquad \text{[Eq. 2]}$$

3.3.4. Hydrophobicity assay

The hydrophobicity of the nanoparticles was analysed using the Rose Bengal method with minor modifications (202). For each formulation, five serial dilutions were prepared from a dispersion of 9.5 mg in 1.5 mL water, in triplicate. Afterwards, 500 µL of each dilution were incubated with 1 mL of an aqueous solution of Rose Bengal (100 µg/mL) for 30 minutes, at 25 °C and 300 rpm in a Labnet Vortemp 56 EVC incubator (Labnet International Inc, Edison, NJ, USA). Then, samples were centrifuged for 30 minutes (13500 g at 4 °C) in a Mikro 220R Hettich centrifuge (Hettich, Tuttlingen, Germany). Finally, 200 µL of the supernatants were placed in a 96 round bottom well plate and the absorbance was measured at 548 nm in a BioTek PowerWave XS microplate spectrophotometer (BioTek Instruments Inc, Winooski, VT, USA). Also, a triplicate of 200 µL of the Rose Bengal solution was measured.

The hydrophobicity of the nanoparticles was calculated as the slope of the linear regression obtained by plotting the partitioning quotient (PQ) versus the total surface

area (TSA, in m^2/mL). The greater the slope, the greater the hydrophobicity. To calculate the PQ, the following equation (Equation 3) was employed:

$$PQ = \frac{Abs_{RB\ bound}}{Abs_{RB\ unbound}} \quad \text{[Eq. 3]}$$

where $Abs_{RB\ bound}$ is the absorbance of the fraction of Rose Bengal bound to the nanoparticles (as the subtraction of the absorbance of the Rose Bengal alone and the absorbance of each supernatant) and $Abs_{RB\ unbound}$ is the absorbance of the fraction present in the supernatant for each concentration. At the same time, the TSA was calculated using the total area of all the nanoparticles in the sample (Equation 4).

$$TSA = A_{NP} \cdot N_{NP} \quad \text{[Eq. 4]}$$

in which A_{NP} is the area of a single nanoparticle ($4\pi r^2$) and N_{NP} the number of nanoparticles dispersed in water calculated as in Equation 5, assuming that the nanoparticles are spherical and monodisperse. The radius of the nanoparticles was obtained from the measurement by DLS previously obtained.

$$N_{NP} = \frac{TM_{NP}}{M_{NP}} \quad \text{[Eq. 5]}$$

being TM_{NP} the total mass of nanoparticles and M_{NP} the mass of a single nanoparticle, calculated as in Equation 6:

$$M_{NP} = V_{NP} \cdot \rho_{zein} \quad \text{[Eq. 6]}$$

where V_{NP} is the volume of a single nanoparticle ($4/3\pi r^3$) and ρ_{zein} the density of zein (1.41 g/mL) previously calculated by pycnometry (203).

3.3.5. Fourier Transform Infrared spectroscopy (FTIR) analysis

The presence of the wheat germ oil inside the nanocapsules was analysed by FTIR spectroscopy. Dry powder of nanoparticles was placed in the diamond crystal of a Fourier Transform spectrophotometer IR Affinity-1S (Shimadzu, Kyoto, Japan) equipped with a MKII Golden-Gate single reflection ATR system (Specac, Orpington, UK), and spectra were collected from 600 to 4,000 cm^{-1} with a resolution of 2 cm^{-1} and 50 scans per spectrum. Data were then analysed with Labsolution IR software (Shimadzu, Kyoto, Japan).

3.4. *In vitro* release studies

In vitro release studies of quercetin from nanoparticles were carried out in simulated gastric (SGF, pH 1.2) and intestinal fluids (SIF, pH 6.8) containing 1% (w/v) of 2-hydroxypropyl-β-cyclodextrin (HP-β-CD) as a solubilizing agent in order to offer sink conditions. Experiments were carried out at 37 °C in an Unitronic 320 OR bath (P Selecta, Barcelona, Spain) with stirring (300 rpm) using a Cimarec™ i Telesystem Multipoint

Stirrer (Thermo Fisher Scientific, Waltham, MA, USA). Thus, amount of nanoparticles equivalent to 250-300 µg quercetin (12.1 mg of each formulation approximately) was dispersed in 5 mL water and introduced in a Float-A-Lyzer®G2 Dialysis Device with a molecular weight cut-off of 300 kD (Spectrum Laboratories, Inc., Rancho Dominguez, CA, USA). Immediately, the devices were immersed in 47 mL of SGF and after 2 h, changed to 47 mL of SIF. At different timepoints, 500 µL of external media was taken, replacing the extracted volume with new media, and immediately analysed by HPLC. Quercetin was quantified using the chromatographic method previously described (see section 3.3.3). In this case, calibration curves were prepared in ethanol ranging from 0.3 µg/mL to 12 µg/mL ($R^2 \geq 0.998$). The limit of detection was calculated to be 0.3 µg/mL and the limit of quantification 0.9 µg/mL.

3.5. Diffusion of nanoparticles in pig intestinal mucus by multiple particle tracking (MPT)

Fluorescently labelled nanoparticles with Lumogen® Red were used to analyse the diffusion of nanoparticles through pig intestinal mucus, based on the multiple particle tracking technique described by Abdulkarim *et al.* (204). For this purpose, 4 mg of formulation powder were dispersed in 1 mL water, and 25 µL of this suspension was incorporated in approximately 0.5 mL pig intestinal mucus.

To obtain the mucus, the small intestine from pigs were collected from a slaughterhouse and kept in ice for 2 h maximum. Then, the intestine was cut in portions of approximately 10 cm and opened to expose the lumen. After washing with PBS, mucus was collected using a spatula, scraping gently to avoid dragging the epithelial tissue. The recovered mucus was mixed and, from this pool, aliquots of approximately 0.5 mL were frozen and stored in microtubes at -80 °C until use.

Once the nanoparticles were incorporated in the mucus, the sample was incubated for 2h in a Labnet Vortemp 56 EVC incubator (Labnet International Inc., Edison, NJ, USA) at 37 °C and 300 rpm. Then, the mucus was placed in a 35 mm Petri dish with a 14 mm microwell and visualized in a Confocal Microscope Cell Observer Z1 (Zeiss Microscopy, Jena, Germany) equipped with a Plan-Apochromat 63x/1.4 Oil objective and using the rhodamine filter. Two-dimensional videos were captured, with a duration of 15 s and a total of 378 frames. More than 300 nanoparticles were analysed for each type of nanoparticles. Videos were analysed using Fiji ImageJ (205). Only particles present in the X-Y plane for more than 30 sequential frames were evaluated, whose trajectories were converted into numeric pixel data and then into metric distance. The distance was expressed as squared displacement (SD) in a time interval (Δt), and the mean square displacement (MSD) of each particle was calculated, which represents the geometric mean of particle's squared displacements along its 30-frame trajectory. MSD was calculated as shown in Equation 7.

$$MSD = (X_{\Delta t})^2 + (Y_{\Delta t})^2 \qquad \text{[Eq. 7]}$$

For each kind of nanoparticle, the “ensemble mean square displacement” (<MSD>) was determined by calculating the MSD of 100 individual trajectories. The Effective Diffusion Coefficient (<Deff>) was calculated by Equation 8.

$$< Deff >= \frac{< MSD >}{4 \cdot \Delta t} \quad \text{[Eq. 8]}$$

where *4* is a constant related to the 2-dimensional mode of video capture.

Moreover, the diffusion coefficient (D°) of the nanoparticles in water was calculated by the Stokes-Einstein equation (Equation 9) at a temperature of 37 °C:

$$D° = \frac{kT}{6\pi\eta r} \quad \text{[Eq. 9]}$$

where *k* is the Boltzmann constant, *T* is absolute temperature, *η* is water viscosity and *r* is the radius of the nanoparticle.

The diffusion of the particles was also expressed as the ratio <Deff>/D° (%). This ratio provides a measure of the relative diffusion of the nanoparticles in intestinal mucus when considering their Brownian motion in water.

3.6. *In vivo* studies in *Caenorhabditis elegans*

3.6.1. *C. elegans* strains and maintenance

Wild-type N2 Bristol strain was obtained from the *Caenorhabditis Genetics Center* (CGC, University of Minnesota, MN, USA) and grown in Nematode Growth Medium (NGM) at 20 °C, using *Escherichia coli* OP50 as normal diet, as previously described (206,207). For the following experiments, the nematodes were age-synchronized by standard sodium hypochlorite treatment. Finally, eggs were incubated in M9 medium for at least 18 hours to promote the hatching.

3.6.2. Intake of nanoparticles

To evaluate the ingestion of nanoparticles by the worms, L1/L2 larvae were grown to L4 larvae in NGM. Treatment plates were prepared as a mixture of NGM and Lumogen® Red-loaded nanospheres, adding *E. Coli* on the surface of the dry media. At L4 stage, worms were put in these plates and two hours later, they were collected with PBST (0.01% Triton X-100 in Phosphate Buffered Saline) and placed in a 2% agarose pad with 1% of sodium azide (w/v). Samples were visualized using an Automated Microscope Zeiss Axio Imager M1 with an Axiocam MRm camera (Zeiss Microscopy, Jena, Germany), using the rhodamine filter to visualize the Lumogen® Red-loaded nanospheres and the DAPI filter to see the autofluorescence of the worms. The photographs were taken with ZEN software (Zeiss Microscopy, Jena, Germany) and processed with ImageJ (205).

3.6.3. Evaluation of fat accumulation

The evaluation of the accumulation of fat in the body of the nematode *C. elegans* was performed by the Nile Red method, as previously described (208). First, the effect of free quercetin was evaluated. For that purpose, different quercetin concentrations were analysed (10 µM, 50 µM, and 100 µM), by mixing the adequate volume of quercetin stock solutions in dimethyl sulfoxide (DMSO) with 4 mL NGM in 6-well plates (only 4 wells were used). Orlistat was used as a positive control of fat reduction (6 µg/mL in DMSO), and an equivalent volume of DMSO was added to the control NGM plates as a negative control.

Once the plates were prepared, dried, and *E. Coli* was added, between 300 and 500 L1/L2 larvae per well were transferred. After 46 h, L4 worms were collected in 1 mL PBST for each well, centrifuged for 4 minutes at 263 g in a Microfuge® 16 centrifuge (Beckman coulter, Brea, CA, USA), and the supernatant was eliminated. Worms were redispersed in PBST and put in ice for 15 minutes. After the supernatant was removed, 200 µL isopropanol 40% (v/v) were added to the pellet, and after 3 minutes of incubation, the samples were centrifuged. The supernatant was eliminated, 150 µL of Nile Red staining (3 µg/mL in isopropanol 40% vol.) was added to the pellet, and the mixture was incubated at 20 °C for 25-30 minutes in an orbital shaker at 60 rpm. Then, samples were centrifuged, the supernatant was again removed, and the obtained pellet was washed with PBST, by the addition of 1 mL of PBST, centrifugation, and elimination of the supernatant. Finally, worms present in the pellet were mounted in 2% (w/v) agarose pad to be visualized afterwards in a fluorescent microscope. Images were taken at 100x magnification in a Nikon SMZ18 stereomicroscope equipped with an epi-fluorescence system with a DS-FI1C refrigerated color digital camera (Nikon Instruments Inc., Tokyo, Japan), using a GFP filter (Ex 480-500; DM 505; BA 535-550), and fat was quantified using the software ImageJ (205).

On the other hand, the possible effect of the components of nanoparticles (zein and mannitol) on the nematode was evaluated. With this aim, free zein, mannitol, and a mixture of both, as well as empty nanospheres with and without mannitol were analysed. Treatments were added as described, mixing the nanoparticles with the NGM, letting dry, and adding *E. Coli* as a normal nematode diet. Then, worms were collected, dyed, and mounted as described above.

Finally, glucose-supplemented NGM was used to evaluate the effect of the quercetin nanoparticles on the accumulation of fat, at a concentration equivalent to 50 µM quercetin. For that purpose, 0.5% (w/v) glucose was added to NGM in order to have an increased fat accumulation. Treatments were added as previously described, and normal NGM was used as a control of the rise of fat accumulation.

3.7. Biodistribution studies in Wistar rats

3.7.1. *In vivo* gastrointestinal transit of Technetium labelled nanoparticles

In order to evaluate the biodistribution through the gastrointestinal tract of the nanoparticles, they were radiolabelled with technetium-99m (^{99m}Tc). The radiolabelling was performed in a direct way by reduction and reaction of a solution of ^{99m}Tc with the nanoparticles. For that purpose, 2.5 mg nanoparticles were dispersed in 100 µL water, and 50 µL of a solution of $SnCl_2 \cdot 2H_2O$ (0.05 mg/mL) were added, purging afterwards the dispersion with N_2 for 5 minutes. Then, 111 ± 11 MBq of a solution of $[^{99m}Tc]TcO_4^-$ was added, obtained from a ^{99}Mo/^{99m}Tc generator (8,6 GBq Drytec, General Electric, Boston, MA, USA), in a volume lower than 200 µL. After incubation for 10 minutes, the radiolabelling was verified by radio-TLC, using iTLC-SG paper (Agilent Technologies, Santa Clara, CA, USA) as stationary phase and 2-butanone as mobile phase, where nanoparticles remain in the origin and $[^{99m}Tc]TcO_4^-$ moved forward. Finally, the sample was mixed with 7.5 mg of non-modified nanoparticles.

All the experiments were approved by the Ethical and Biosafety Committee for Research on Animals of the University of Navarra (protocol number 066-16). Female Wistar rats (weight 250 g) were slightly anesthetized with 2% isoflurane gas, radiolabelled nanoparticles were administered dispersed in 1 mL water by oral gavage, and then the animals were quickly awakened.

Animals were scanned by single photon emission computed tomography (SPECT) in a U-SPECT6/E-class (MILabs, Houten, The Netherlands) using a UHR-RM-1 mm multi-pinhole collimator. After 1 h, 2 h, 4 h, and 8 h of the administration, rats were placed prone on the scanner bed under continuous anaesthesia with isoflurane (2% in 100% O_2 gas) to acquire a whole body scan over 15 min. Following the SPECT acquisition, CT scans were performed to obtain anatomical information using a tube setting of 55 kV and 0.33 mA. The SPECT images were reconstructed using the ^{99m}Tc photopeak centered at 140 keV with a 20% energy window width and using a calibration factor to obtain the activity information (MBq/mL). Finally, attenuation correction was applied using the CT attenuation map. Studies were visualized using PMOD software (PMOD Technologies Ltd., Adliswil, Switzerland).

3.7.2. *In vivo* biodistribution on the gastrointestinal mucosa of Lumogen® Red-loaded nanoparticles

For the evaluation of the *in vivo* biodistribution of nanoparticles in the gastrointestinal tract, Lumogen® Red-loaded nanoparticles were administered to Wistar rats by the oral route, as previously described with minor modifications (209). Wistar male rats were provided by Envigo (Indianapolis, IN, USA). They were acclimated at least for a week, in 12 hours dark/light cycles at 23 ± 2 °C, with free access to food and water.

All the experiments were approved by the Ethical and Biosafety Committee for Research on Animals of the University of Navarra (protocol number 045-18).

Animals were fasted overnight, nanoparticles were dispersed in water and administered by oral gavage at a dose of 20 mg nanoparticles per rat. After 4 hours, animals were sacrificed and different parts of the gastrointestinal tract were extracted (portions of around 1 cm), washed with PBS, collected in Tissue-Tek® O.C.T. Compound and immediately frozen at -80 °C until analysis. Free Lumogen® Red was used as a control, as a suspension in water (0.07 mg/mL) with 0.35% (v/v) Polysorbate 80 as dispersing agent.

Frozen samples were cut in 5 µm slices with a Microm HM550 cryostat (Thermo Fisher Scientific, Waltham, MA, USA), placed in a slide, and dried for 1h. Samples were fixed with formaldehyde (3.7-4.0 % w/v buffered to pH=7 and stabilized with methanol) for 5 minutes, washed with tap water and then with Tris-buffered saline with 0.05% Tween 20 (TBS-T). Samples were covered with a solution of DAPI (2.5 µg/mL) for 15 minutes, washed with TBS-T and a cover slip was put with PBS/glycerol gelatin (1:1).

Pictures were taken in an Automated Microscope Zeiss Axio Imager M1 with an Axiocam MRm camera (Zeiss Microscopy, Jena, Germany) using the DAPI filter to see the cellular nuclei of the enterocytes and Rhodamine filter to see Lumogen® Red-loaded nanoparticles. Images were taken using ZEN software (Zeiss Microscopy, Jena, Germany) and posterior analysis was carried out with the ImageJ software (205).

3.8. Pharmacokinetic study

For the pharmacokinetic assay, Wistar rats were purchased from Envigo (Indianapolis, IN, USA) and acclimated at least for a week, in 12 hours dark/light cycles at 23 ± 2 °C, with free access to food and water. All the experiments were approved by the Ethical and Biosafety Committee for Research on Animals of the University of Navarra (protocol number 056-19).

Rats were fasted overnight and an oral single dose of quercetin (15 mg/kg), either as an aqueous suspension (Q-Susp) or loaded in nanoparticles dispersed in water, was administered by oral gavage. Q-Susp was formed by incorporating 6.25 mg/mL quercetin and 30.2 mg/mL HP-β-CD in water, as previously described (108). At different times, animals were anesthetized with inhaled isoflurane and blood samples were extracted from the tail vein and added to EDTA tubes. An intravenous administration of quercetin was also performed. For this purpose, 62.5 mg quercetin were dissolved in 10 mL of a PEG 400:water mixture (6:4 v/v) (108). All blood samples were centrifuged for 10 minutes at 2,500 g and 4 °C, and supernatants were collected and frozen at -80 °C for further quantification.

For quercetin extraction, plasma samples were defrosted and 100 µL of each sample was mixed with 600 µL of cold 0.95% (v/v) HCl in methanol. Samples were vortexed at 2,500 rpm in a DXV-2500 Multi-Tube Vortexer (VWR International, Radnor, PA, USA) for

15 minutes to induce the precipitation of proteins and centrifuged at 10,000 rpm for 10 minutes in a Mikro 220R Hettich centrifuge (Hettich, Tuttlingen, Germany). Supernatants were collected and dried under nitrogen atmosphere using a TurboVap® LV Evaporator (Caliper Life Sciences, Waltham, MA, USA) at 45 °C for 1 hour. Once the samples were dried, 200 µL methanol were added to redissolve the quercetin, samples were shaken in the multivortex for 5 minutes and centrifuged. Supernatants were collected, dried again under nitrogen for 10 minutes and frozen until the quantification.

Samples were quantified by UHPLC-Q Exactive Orbitrap High-Resolution Mass Spectrometry (Thermo Fisher Scientific, Waltham, MA, USA), using a Thermo Hypersil GOLD column (1.9 µm, 100 x 2.1 mm, Thermo Fisher Scientific, Waltham, MA, USA). The mobile phase (gradient conditions shown in Table 6) was constituted by 0.1% of formic acid in water (mobile phase A) and 0.1% of formic acid in ACN (mobile phase B), at a flow rate of 0.25 mL/min. The injection volume was 2 µL, the column temperature 30 °C, and the samples were maintained at 10 °C. A negative ionization mode was used, with the following conditions: sheath gas flow rate: 40 (arbitrary units); auxiliary flow rate: 10 (arbitrary units); sweep gas flow rate: 1 (arbitrary units); spray voltage: 2.5 kV; capillary temperature: 320 °C; S-lens RF level: 55%; aux gas heater temperature: 320 °C.

Table 6. Gradient conditions used for the quantification of plasma quercetin by UHPLC mass spectrometry. A: 0.1% of formic acid in water; B: 0.1% of formic acid in ACN.

Time (min)	A (%)	B (%)
0	99	1
1	99	1
5	92	8
15	60	40
17	4	96
19	4	96
20	99	1
22	99	1

For the quantification of the quercetin extracted, samples were redissolved in 160 µL of mobile phase (0.1% formic acid in water and 0.1% formic acid in ACN, 50:50 v/v) with 1 µg/mL of sulfadimethoxine, centrifuged at 15,000 rpm for 10 minutes, and supernatants were injected in the UHPLC. To prepare the calibration curve, standard solutions were prepared in a range from 0.25 to 1 µg/mL of quercetin in methanol. Different volumes of these standards were mixed with 100 µL of commercial rat plasma to form the calibration curve (R^2 > 0.99; LOQ: 0.25 µg/mL), and the same extraction procedure was followed.

Finally, pharmacokinetic parameters (T_{max}, C_{max}, $t_{1/2}$, AUC, and MRT) were calculated using the Excel complement PKSolver (210), and the relative oral bioavailability was calculated using Equation 10.

$$Fr\ (\%) = \frac{AUC_{oral}}{AUC_{i.v.}} \times 100 \qquad \text{[Eq. 10]}$$

where AUC_{oral} and $AUC_{i.v.}$ are the Area Under the Curve of the oral treatment and the intravenous treatment, respectively.

3.9. Efficacy study

3.9.1. Experimental design

For the efficacy study, 72 Wistar male rats were obtained from Envigo (Indianapolis, IN, USA). Animals were received with a weight of 80 g, and acclimated for two weeks with 12 hours dark/light inverted cycle, with free access to food and water. Then, 60 animals were fed with a high fat/high sucrose diet (HFS, D12451, Research Diets Inc., New Brunswick, NJ, USA) for 23 weeks, while 12 animals were followed feeding with standard diet (2014, Teklad Global 14% Protein Rodent Maintenance Diet, Teklad Diets Envigo, Madison, WI, USA). All the experiments were approved by the Ethical and Biosafety Committee for Research on Animals of the University of Navarra (protocol number 016-21).

At week 18, HFS-fed rats were divided into five experimental groups (n = 12): (i) HFS control, (ii) quercetin-loaded nanospheres (Q-NS), (iii) quercetin-loaded nanocapsules (Q-NC), (iv) PEG-coated quercetin-loaded nanospheres coated with a PEG-to-zein ratio of 0.25 (Q-NS-PEG) and (v) free quercetin as an aqueous suspension of quercetin (Q-Susp) prepared as previously described (see section 3.8). Rats were fasted overnight every day, and water dispersed nanoparticles were administered daily by oral gavage at a dose of 15 mg/kg quercetin for 5 weeks. All the formulations were prepared in the absence of mannitol. An equivalent volume of water was administered to standard and HFS controls.

Body weight was measured every week. At week 22, an oral glucose tolerance test (OGTT) was performed. Also, the measurement of the proportion of body fat and lean was carried out in duplicate for each rat, by magnetic resonance spectroscopy using the EchoMRI™ system (Echo Medical Systems, Houston, TX, USA). Rats were sacrificed at week 23, and blood, fat depots, liver, kidneys, spleen, and the gastrocnemius muscle were extracted, weighted, and immediately frozen at -80 °C for further experiments. Figure 10 summarizes the experimental design of the efficacy study.

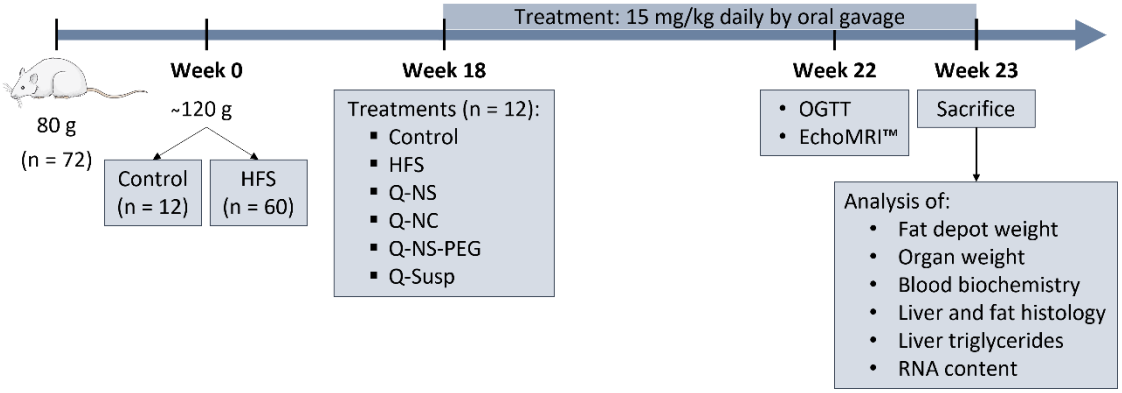

Figure 10. Summary of the efficacy experiment. Control: animals fed with standard diet; HFS: animals fed with high fat/high sucrose (HFS) diet; Q-NS: animals fed with HFS diet and treated with quercetin-loaded nanospheres; Q-NC: animals fed with HFS diet and treated with quercetin-loaded nanocapsules; Q-NS-PEG: animals fed with HFS diet and treated with quercetin-loaded PEG-coated nanospheres; Q-Susp: animals fed with HFS diet and treated with quercetin suspension; OGTT: oral glucose tolerance test; EchoMRI™: magnetic resonance spectroscopy.

3.9.2. Oral glucose tolerance test

At week 22, an oral glucose tolerance test (OGGT) was carried out. For that purpose, 2 g glucose per kg of body weight were administered dissolved in water, by oral gavage. Glucose levels were measured at 0, 15, 30, 60, 120, and 150 minutes by venous tail puncture using an Accu-Check® Aviva glucometer with Accu-Chek Aviva test strips (Roche Diagnostics, Basel, Switzerland). The area under the curve (AUC) was calculated using the trapezoid method (Equation 11). In addition, blood glucose levels were quantified at week 17, previously to the treatment.

$$AUC_{0-150} = \left(\frac{BG+G15'}{2} \times 15\right) + \left(\frac{G15'+G30'}{2} \times 15\right) + \left(\frac{G30'+G60'}{2} \times 30\right) + \left(\frac{G60'+G120'}{2} \times 60\right) + \left(\frac{G120'+G150'}{2} \times 30\right) \quad \text{[Eq. 11]}$$

in which *BG* is the basal glycaemia and G_i the glycaemia at different times.

3.9.3. Biochemical analysis

Some serum parameters were measured after the sacrifice using the HK-CP kit (ABX Pentra, Montpelier, France) adapted for the Pentra C200 analyser (HORIBA ABX, Montpelier, France). Triglycerides (TAG), total cholesterol, HDL-cholesterol, glucose, aspartate transaminase (AST), and alanine transaminase (ALT) were quantified. Plasma insulin and monocyte chemoattractant protein-1 (MCP-1) levels were determined using specific rat ELISA kits (Mercodia, Uppsala, Sweden and Thermo Fisher Scientific, Waltham, MA, USA, respectively). The atherogenic index of plasma (AIP) was calculated using de following equation (Equation 12) (211):

$$AIP = \log\left(\frac{TAG}{HDL}\right) \quad \text{[Eq. 12]}$$

in which *TAG* is the value obtained in serum for the triglycerides and *HDL* the value obtained for the HDL-cholesterol.

The insulin resistance was evaluated using the homeostasis model of insulin resistance (HOMA-IR), calculated using Equation 13 (212–214).

$$HOMA - IR = \frac{serum\ glucose\ levels\ \left(\frac{mmol}{L}\right) \times plasma\ insulin\ levels\ \left(\frac{mU}{L}\right)}{22.5} \quad \text{[Eq. 13]}$$

3.9.4. Histological analyses

Samples from liver, epididymal fat, and retroperitoneal fat were collected and fixed in formaldehyde (3.7-4.0 % w/v buffered to pH=7 and stabilized with methanol for clinical diagnosis), and 48 hours later, they were transferred to absolute ethanol. Samples were included in paraffin, cut, and dyed with haematoxylin-eosin.

Liver samples (6 samples per treatment) were analysed at 20x using a Histological Slide Scanner Leica Aperio CS2 (Leica Biosystems, Wetzlar, Germany), to see any differences at the histological level.

Furthermore, the size of the adipocytes for epididymal and retroperitoneal fat was analysed using a Nikon SMZ18 stereomicroscope equipped with an epi-fluorescence system and a DS-FI1C refrigerated color digital camera, using a GFP filter (Ex 480/40; DM 505; BA 535/50). For these experiments 6 rats per treatment were analysed. Pictures were processed using the software ImageJ and a macro modified from Navarro-Herrera *et al.* (215). Once the diameter of the adipocytes was determined, the adipocytes of the standard control diet were classified in four groups (quartiles); small, medium, large, and extra-large. Later, the adipocytes of the HFS groups were classified using these intervals.

3.9.5. Hepatic determination of the triglyceride content

For the extraction of triglycerides from the liver, a modification of the method performed by Cui *et al.* was used (216). For the extraction, 100 mg of tissue were added to 1 mL PBS and broken using a Mini-Beadbeater (Biospec products, Bartlesville, OK, USA). Then, 5 mL of a mixture between chloroform and methanol (2:1 v/v) were added, vortexed for 10 minutes at 2,100 rpm in a DXV-2500 Multi-Tube Vortexer (VWR International, Radnor, PA, USA), and incubated at 4 °C overnight. Samples were centrifuged for 10 minutes at 1,650 g and 4 °C in a 5804R centrifuge (Eppendorf, Hamburg, Germany), and the bottom layer was extracted and added to a new tube. Then, 600 µL $MgCl_2$ and 1.5 mL chloroform were added to the remaining phase, vortexed, and left in ice for 30 minutes. Samples were centrifuged, and the bottom layer

was added to the previous one. Afterwards, 4 mL of the sample were added to a new tube, and 600 µL of 1% Triton X-100 in chloroform were added. Samples were evaporated to dryness under vacuum at 40 °C in a LABCONCO vortex vacuum dry evaporator (Hucoa-Erlöss, Madrid, Spain). The pellet was dispersed in 600 µL water, vortexed, and frozen at -80 °C until analysis. Finally, liver triglyceride content was quantified using a Triglyceride Quantification Kit (Sigma-Aldrich, Steinheim, Germany).

3.9.6. RNA content and gene expression analyses

Total RNA was extracted from 500 mg of the retroperitoneal fat and liver of animals from Control, HFS, and Q-NS-PEG groups, using a TRIzol® RNA isolation reagent (Invitrogen Life Technologies, Paisley, UK). The concentration and purity of RNA were determined by a NanoDrop ND-1000 spectrophotometer (Thermo Fisher Scientific, Waltham, MA, USA) at 260/280 nm. Then, 500 ng of RNA were treated with DNAse I (DNase I-RNase free, Invitrogen Life Technologies, Paisley, UK) and reverse transcribed into cDNA using 200 IU of M-MLV-RT (Invitrogen Life Technologies, Paisley, UK) in the presence of 40 IU of a recombinant RNAsin® Ribonuclease inhibitor (Promega, Madison, WI, USA), with an incubation of 10 min at 25 °C, 50 min at 37 °C, and 15 min at 70 °C.

Gene expression analyses were performed by quantitative-real time PCR (qPCR) using TaqMan Universal PCR master mix and specific probes (TaqMan™ Gene Expression Assays, Thermo Fisher Scientific, Waltham, MA, USA) in triplicate using a CFX384 Touch™ Real-Time PCR Detection System (BioRad Laboratories, Hercules, CA, USA). Gene expression levels were normalized compared to TATA box binding protein (Tbp) gene expression as a housekeeping control. Differences in gene expression between Control, HFS, and Q-NS-PEG groups were estimated using the relative quantification $2^{-\Delta\Delta Ct}$ method (217).

In the liver, genes that encode proteins involved in lipid metabolism (*Acot8*, *Acox1*, *Cpt2*) and synthesis (*Fasn*) were evaluated, and genes encoding transcription factors related to adipogenesis (*Pparg*, *Srebp1*). In the retroperitoneal fat, genes encoding proteins involved in lipid metabolism (*Acot8*, *Acox1*, *Hsd17b4*) and synthesis (*Fasn*, *Scp2*) were analysed. Also, genes encoding two adipokines (*AdipoQ*, *Lep*) and a gene related to the browning of fat (*Ucp1*) were evaluated. Genes encoding transcription factors related to adipogenesis (*Pparg*, *Srebp1*) were also quantified.

3.10. Statistical analysis

For the statistical analysis, a one-way ANOVA was used when samples fulfilled normality and homoscedasticity. Then, Dunnett's multiple comparison test was performed, but in the case of the analysis of fat accumulation in *C. elegans*, Tukey's multiple comparison test was applied.

In the case of the efficacy study, a t-Student test was used to compare the HFS diet control with the standard diet control (when normality and homoscedasticity complied), to verify the validity of the *in vivo* DIO model (Figure 11). In the cases where samples respected the normality but did not respect the homoscedasticity, the t-test with Welch's correction was used. On the other hand, when the normality was not complied, the Mann-Whitney test was used. A one-way ANOVA followed by a Dunnett's multiple comparison test was used to compare the treatments to HFS control when normality and homoscedasticity complied (Figure 11). If the normality or/and homoscedasticity of the samples were not respected, the Kruskal-Wallis test was used, followed by Dunn's multiple comparison test. Also, the adipocyte distribution was analysed by a contingency assay using the Bonferroni correction. The gene analysis was performed by ANOVA/Kruskal Wallis for the three selected groups.

All tests were done with GrapPad Prism v9.4 (San Diego, CA, USA) and data was plotted using Origin 8.6 (OriginLab, Northampton, USA).

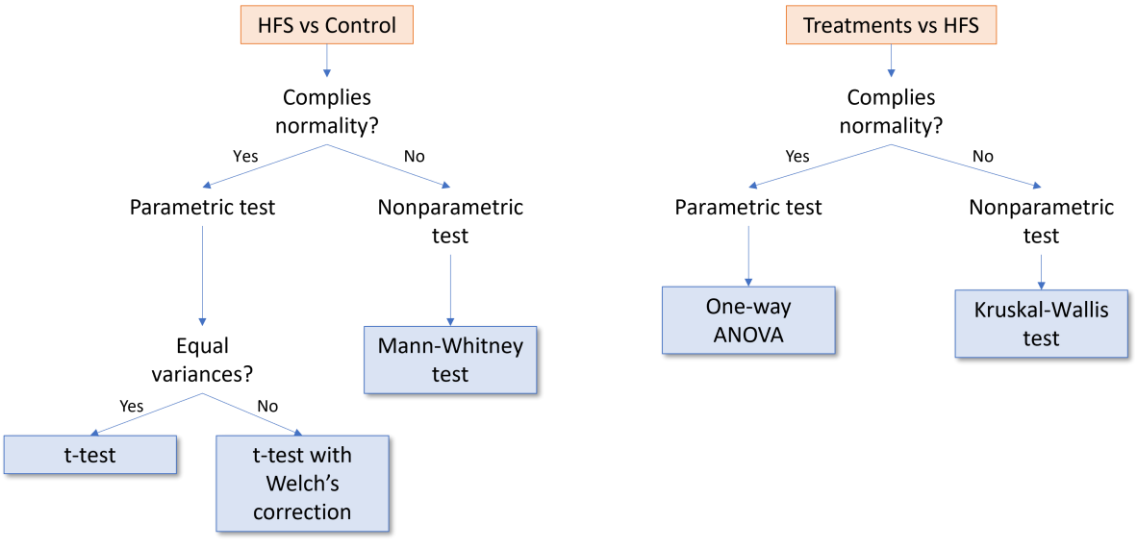

Figure 11. Statistical analysis of the efficacy study. HFS: high fat/high sucrose diet; Control: standard diet control.

Chapter 4

Results

4. Results

4.1. Empty zein nanoparticles

4.1.1. Size, zeta potential and morphology

In this work, three different types of zein-based nanoparticles were designed, optimized, and evaluated: nanospheres (NS), PEG-coated nanospheres (NS-PEG), and nanocapsules (NC). Both nanospheres and nanocapsules were prepared by a desolvation procedure after the addition of water to a hydroalcoholic solution of zein. The resulting nanospheres (NS) were incubated with PEG 35,000 to produce PEG-coated NS. For the preparation of nanocapsules, the hydroalcoholic solution of zein also included wheat germ oil. In all cases, the resulting nanoparticles were always dried by spray drying.

Table 7 compiles the main physico-chemical characteristics of the different nanoparticulate devices employed as drug carriers in this work. NS displayed a mean size close to 230 nm and a negative zeta potential of -40 mV. The coating of NS with PEG induced a slight decrease of the mean size of resulting nanoparticles (between 210 and 220 nm) as well as a moderate increase of the negative zeta potential (about -45 mV). NS-PEG were prepared at two different PEG-to-zein ratios (0.25 and 0.50). Both NS-PEG25 and NS-PEG50 displayed similar sizes and zeta potential values. On the other hand, the incorporation of wheat germ oil in the matrix of zein-based nanoparticles (NC) produced a significant increase of the mean size (about 10%; $p < 0.01$), compared with plain NS, without apparent modification of the negative zeta potential. Another important aspect to highlight was that, in all cases, the polydispersity index of the different types of nanoparticles was always below 0.2, evidencing a high homogeneity of the formulations. The mean yield of the process obtained in the Spray Dryer ranged from 58% to 64%.

Table 7. Physico-chemical characteristics of zein nanospheres (NS, NS-PEG25, NS-PEG50) and nanocapsules (NC). The formulations were dried by spray drying using mannitol as protectant. Data are expressed as mean ± SD (n = 3, *p < 0.05, **p < 0.01, compared to NS). PDI: polydispersity index.

	Size (nm)	PDI	Zeta potential (mV)
NS	228 ± 6	0.08 ± 0.05	-40.6 ± 1.6
NC	247 ± 5**	0.11 ± 0.02	-42.1 ± 0.9
NS-PEG25	209 ± 3**	0.06 ± 0.03	-43.7 ± 1.4*
NS-PEG50	218 ± 4	0.10 ± 0.02	-44.9 ± 0.7**

Figure 12 shows the morphology and shape of NS and NC. In both cases, nanoparticles were characterized by a spherical shape, with an apparent diameter similar to that determined by dynamic light scattering (Table 7). Furthermore, NC displayed a structure with a continuous inner medium surrounded by a corona of about 37 nanometres. This structure would be compatible with an oil nucleus covered by zein.

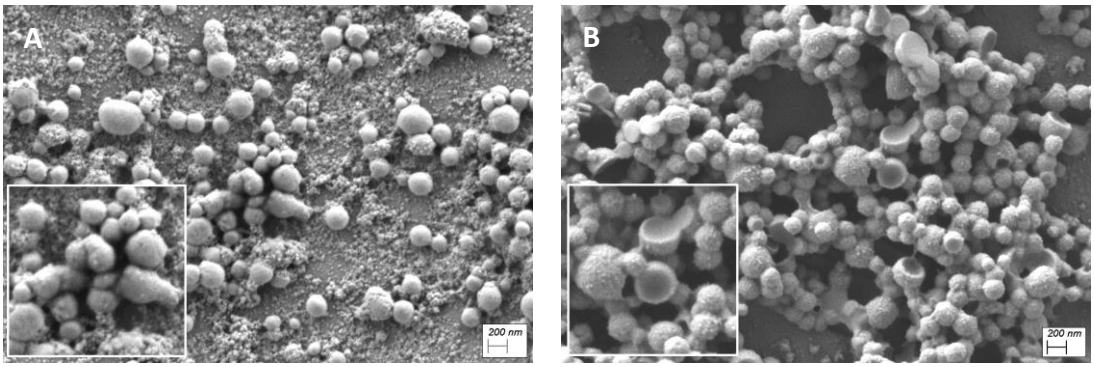

Figure 12. Scanning electron microscopy (SEM) of zein nanospheres (NS; **A**) and nanocapsules (NC; **B**).

4.1.2. Zein quantification

In order to quantify the amount of zein present in the preparation of nanoparticles, the samples were broken using ethanol 75% and the zein content was quantified by MicroBCA Protein Assay Kit.

Data were expressed in percentage as the proportion of weight of nanoparticles in the total weight formulation (Table 8). These experimental values were similar to theoretical ones (all data were only between 6 and 10% higher than the theoretic zein content). NS presented an amount of zein of 33.7%. The coating of NS with PEG decreased the total proportion of zein. Thus, the zein content was calculated to be 32.1% for NS-PEG25 and 30.5% for NS-PEG50. NS and NC presented similar zein percentages (33.3% for NC), since the only difference between them was the small amount of oil in the formulation (20 mg of oil in 650 mg of formulation).

Table 8. Zein content in nanospheres (NS, NS-PEG25, and NS-PEG50) and nanocapsules (NC). The formulations were dried by spray drying using mannitol as protectant. Data are expressed as mean ± SD (n = 3).

	Zein content (%)	Theoretic zein content (%)
NS	33.7 ± 0.4	31.7
NC	33.3 ± 0.3	30.8
NS-PEG25	32.1 ± 1.0	29.4
NS-PEG50	30.5 ± 2.2	27.4

4.1.3. Hydrophobicity assay

The hydrophobicity of the surface of the nanoparticles was analysed by the Rose Bengal method. For this purpose, a solution of Rose Bengal was incubated with serial dilutions of the nanoparticles in water before the measurement of the absorbance by spectrophotometry. Hydrophobicity was calculated as the slope of the linear regression for the representation of the partitioning quotient (PQ) versus the total surface area (TSA) of the nanoparticles (Equations 3 and 4 in section 3.3.4). When increasing the slope, the higher the hydrophobicity.

Figure 13 shows the hydrophobicity of nanoparticles employed in this study. Interestingly, NS and NC displayed a similar value of hydrophobicity, so the presence of the oil in NC did not affect the hydrophobicity of the surface compared to NS, suggesting that the wheat germ oil would be inside the nanoparticles. On the other hand, when nanospheres were coated with PEG, the hydrophobicity of the resulting nanocarriers significantly decreased ($p < 0.001$), confirming that the PEG-coating confers hydrophilic properties to the nanoparticles.

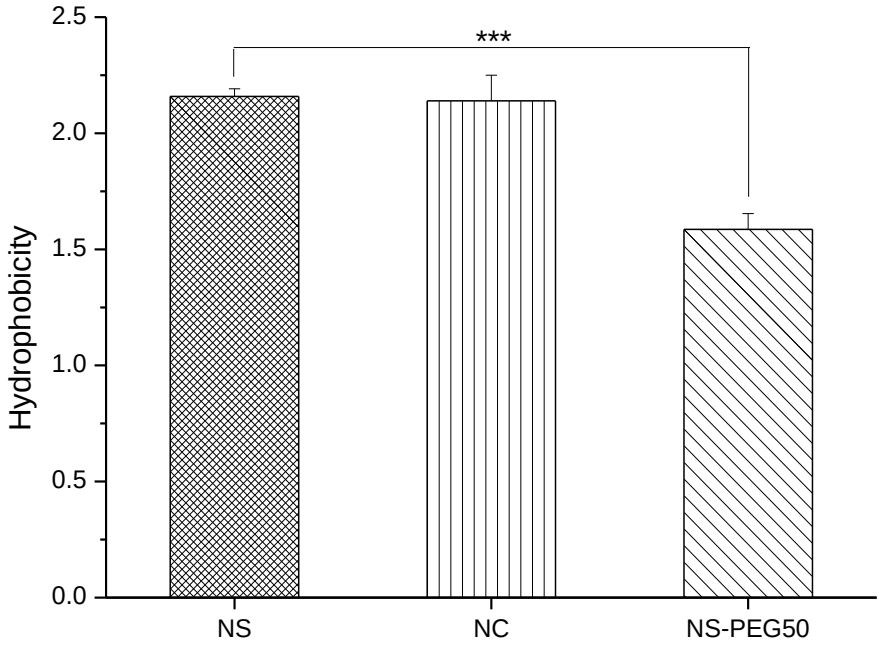

Figure 13. Hydrophobicity values obtained in the Rose Bengal assay. The formulations were dried by spray drying using mannitol as protectant. Data are expressed as mean ± SD (n = 3, ***p < 0.001). NS: nanospheres; NC: nanocapsules; NS-PEG50: PEG-coated nanospheres (PEG-to-zein ratio 0.5 (w/w)).

4.1.4. Fourier Transform Infrared spectroscopy (FTIR) analysis

Figure 14 shows the FTIR spectra of zein nanoparticles in the presence of mannitol, as well as some raw materials employed in the preparation (mannitol and wheat germ

oil). Both NS and NC, displayed the characteristic absorption vibrations corresponding to the amide groups of zein: 1653, 1531, and 1448 cm^{-1}, for C=O stretching vibration of amide I, N-bending coupled to -C-N stretching vibration of amide II, and N-H in plane bending and C-N vibration of amide III, respectively. In addition, the double signal at 3248 and 3190 cm^{-1} corresponds to N-H vibration.

Regarding the wheat germ oil, the stretching vibrations associated to $-CH_3$ and $-CH_2$ appeared at 2950-2920 and 2850 cm^{-1}, respectively, whereas the signal observed at 3007 cm^{-1} could be attributed to the presence of linoleic acid. One of the most characteristic absorption peaks appeared at 1741 cm^{-1} which is associated to -C=O stretching vibration of fatty acids. It is noticeable that in the IR spectrum of NC, the presence of the oil is detected since a weak intensity signal appears at 1743 cm^{-1} with a shoulder associated at 1726 cm^{-1} that can be attributed to carbonyl group (-C=O) of wheat germ oil interacting with the zein. The low intensity of this signal is due to the small amount of oil (20 mg) with respect to the rest of components present in nanocapsules (about 650 mg).

Finally, mannitol, which was used as protectant in the preparation of nanoparticles, displayed a broad band around 3400 cm^{-1} (OH) and two intense peaks at 1076 and 1016 cm^{-1} corresponding to OH stretching vibrations of alcoholic groups. In the case of the nanoparticles, both showed the two strongest mannitol peaks corresponding to OH stretching vibrations slightly shifted to a higher frequency (1082 and 1022 cm^{-1}).

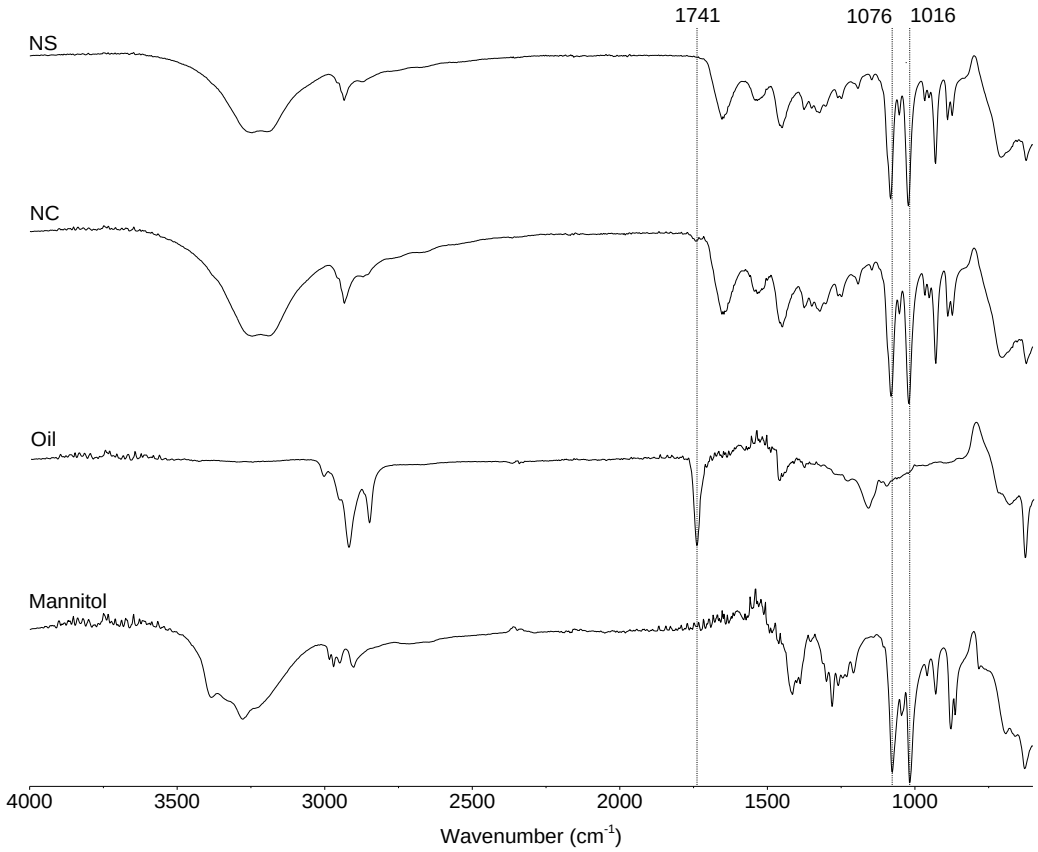

Figure 14. FTIR spectra of zein nanospheres (NS), zein nanocapsules (NC), wheat germ oil, and mannitol. Dashed lines correspond to wheat germ oil (1741 cm^{-1}) and mannitol bands (1076 and 1016 cm^{-1}).

4.2. Quercetin-loaded zein nanoparticles

4.2.1. Size, zeta potential, quercetin content and morphology

Once the three types of nanoparticles were developed and characterized, the flavonoid quercetin was nanoencapsulated, resulting in quercetin-loaded nanospheres (Q-NS), PEG-coated quercetin-loaded nanospheres (Q-NS-PEG25 and Q-NS-PEG50) and quercetin-loaded nanocapsules (NC). These nanoparticles were also prepared by the desolvation method, and quercetin was quantified by HPLC.

Table 9 summarizes the main physico-chemical characteristics of quercetin-loaded nanoparticles. Q-NS displayed a mean size and zeta potential similar to NS (around 230 nm and a negative zeta potential of -42 mV). When these nanoparticles were coated with PEG, no significant effect on the size of the resulting nanoparticles was observed; although, the zeta potential slightly decreased (about -45 mV). On the contrary, for Q-NC, their size was significantly higher than for Q-NS (254 nm; $p < 0.0001$), showing a zeta potential of -45 mV. In all cases, the PDI was below 0.2, suggesting that the

encapsulation of quercetin did not affect the homogeneity of the formulations. The mean yield of the process obtained in the Spray Dryer was between 56% and 65%.

The quercetin loading in the nanoparticles ranged from 70 to 76 µg per milligram nanoparticles. The lowest quercetin payload was found for Q-NS-PEG50. In a similar way, the encapsulation efficiency was, for all the formulations, around 80%.

Table 9. Physico-chemical characteristics of quercetin-loaded nanospheres (Q-NS, Q-NS-PEG25, and Q-NS-PEG50) and nanocapsules (Q-NC). The formulations were dried by spray drying using mannitol as protectant. Data are expressed as mean ± SD (n = 3, *p < 0.0001, compared to Q-NS). PDI: polydispersity index; EE: encapsulation efficiency.

	Size (nm)	PDI	Zeta potential (mV)	Quercetin loading (µg/mg NP)	EE (%)
Q-NS	226 ± 2	0.08 ± 0.04	-41.8 ± 4.0	74.8 ± 0.8	82.3 ± 0.5
Q-NC	254 ± 5*	0.12 ± 0.01	-44.5 ± 2.1	74.1 ± 7.8	82.3 ± 8.3
Q-NS-PEG25	224 ± 1	0.07 ± 0.03	-45.1 ± 2.1	76.0 ± 2.1	84.3 ± 3.3
Q-NS-PEG50	228 ± 2	0.08 ± 0.03	-44.4 ± 1.3	69.5 ± 2.0	79.5 ± 2.3

In order to compare empty nanoparticles with quercetin-loaded ones, Tukey's multiple comparison test was performed. Comparing the size of NS, NC, and NS-PEG50 with their quercetin-loaded homologues, no significant differences were found, except for NS-PEG25 and Q-NS-PEG25 ($p < 0.01$), in which the presence of quercetin seemed to increase the size of the nanospheres. No significant differences were found regarding the zeta potential.

SEM images were taken for quercetin-loaded nanospheres and nanocapsules (Figure 15). In all cases, the different quercetin-loaded nanocarriers displayed a spherical shape and a size similar to that determined by DLS (Table 9). Besides, some sponginess could be appreciated for PEG-coated nanospheres.

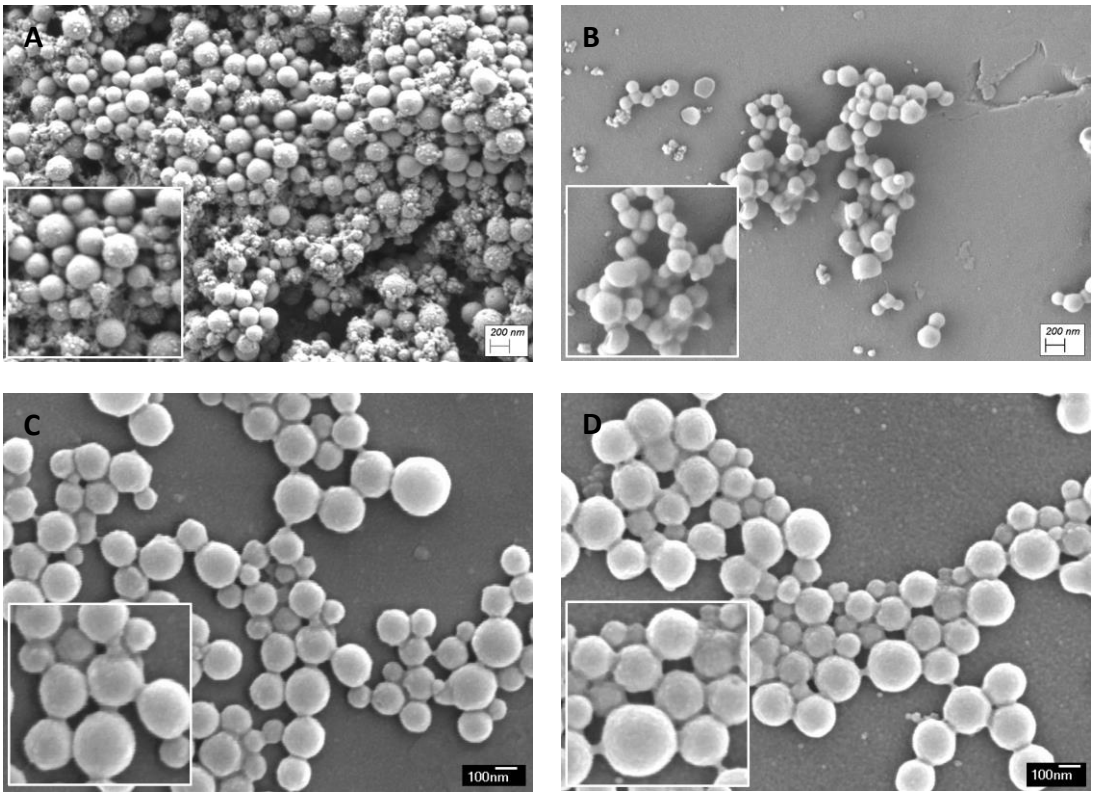

Figure 15. Scanning electron microscopy of quercetin-loaded nanoparticles. **A**: quercetin-loaded nanospheres (Q-NS), **B**: quercetin-loaded nanocapsules (Q-NC); **C**: PEG-coated quercetin-loaded nanospheres, PEG-to-zein ratio 0.25 (Q-NS-PEG25), **D**: PEG-coated quercetin-loaded nanospheres, PEG-to-zein ratio 0.5 (Q-NS-PEG50).

4.3. *In vitro* release studies

The *in vitro* release of quercetin from the nanoparticles was evaluated in simulated gastric fluid (SGF) for 2 h and, then, in simulated intestinal fluid (SIF) for 8 supplementary hours (Figure 16). Samples were taken, quantified by HPLC, and replaced with new media.

Profiles presented a similar shape for the three types of nanoparticles, and all of them were capable of releasing a similar amount of quercetin (about 70% of total content). In SGF, one-third of the flavonoid content was released in 2 h from the three types of nanoparticles. In SIF, the amount of quercetin released was also similar for the three formulations (about 35-40% of the total content); although at the end of the experiment the amount of quercetin released was slightly lower for Q-NS than for Q-NC and Q-NS-PEG50. These results suggest that the release of quercetin from zein-based nanoparticles was independent of the pH conditions and the structure of nanoparticles.

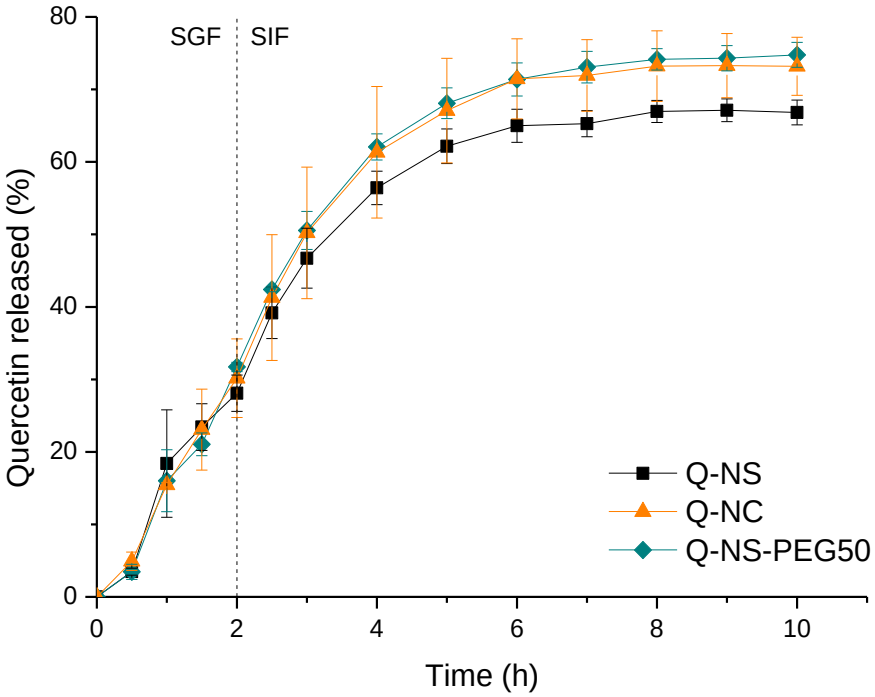

Figure 16. *In vitro* release profile of quercetin-loaded nanospheres (Q-NS and Q-NS-PEG50) and quercetin-loaded nanocapsules (Q-NC). The formulations were dried by spray drying using mannitol as protectant. Data are expressed as mean ± SD (n = 3).

4.4. Diffusion of nanoparticles in pig intestinal mucus by multiple particle tracking (MPT)

In order to analyse the diffusion of the nanoparticles through the intestinal mucus, the multiple particle tracking technique was carried out. For this purpose, the diffusion of Lumogen® Red-loaded nanoparticles in pig intestinal mucus was quantified.

Results obtained for this technique are shown in Table 10. Some examples of the movement of nanoparticles in pig intestinal mucus can be observed in Figure 17. Effective Diffusion Coefficient (<Deff>) values obtained for NS and NC were similar (0.063 and 0.046 x 10^{-9} cm^2/s, respectively), but when nanospheres were coated with PEG at a PEG-to-zein ratio of 0.5 (w/w), this value increased significantly to 0.108 x 10^{-9} cm^2/s ($p < 0.05$). When the <Deff>/D° ratio was calculated (being D° the diffusion coefficient in water), PEG-coated nanospheres displayed two times higher ratio than NS ($p < 0.05$), while NC showed similar values compared to NS (Table 10). These results denote that PEG-coated nanospheres displayed a higher ability to move and diffuse through the mucus than both plain NS and NC.

Table 10. Diffusion of nanoparticles in pig intestinal mucus obtained by the MPT technique. The formulations were dried by spray drying using mannitol as protectant. Data are expressed as mean ± SD (n = 3, *p < 0.05 compared to NS). NS: nanospheres; NC: nanocapsules; NS-PEG50: PEG-coated nanospheres; <Deff>: Effective Diffusion Coefficient; D° (water): diffusion coefficient in water; <Deff>/D°: quotient between the diffusion coefficients of nanoparticles in mucus and water (expressed in percentage); R: ratio between <Deff>/D° of NC or NS-PEG50, and the value for NS.

	<Deff> · 10^{-9} ($cm^2 \cdot s^{-1}$)	D° (water) · 10^{-9} ($cm^2 \cdot s^{-1}$)	<Deff>/D° (%)	R
NS	0.063 ± 0.036	18.1	0.35 ± 0.12	1.00
NC	0.046 ± 0.028	18.0	0.26 ± 0.10	0.74
NS-PEG50	0.108 ± 0.055*	15.8	0.69 ± 0.06*	1.97

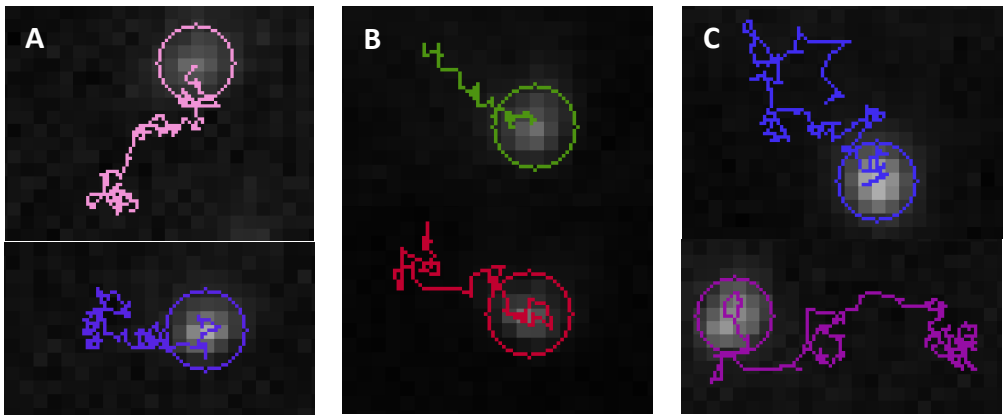

Figure 17. Some examples of trajectories of nanoparticles through intestinal mucus. **A**: nanospheres (NS); **B**: nanocapsules (NC); **C**: PEG-coated nanospheres at a PEG-to-zein ratio of 0.5 (w/w) (NS-PEG50).

4.5. *In vivo* studies in *Caenorhabditis elegans*

4.5.1. Intake of nanoparticles

Previously to the evaluation of the effect of zein nanoparticles in the fat accumulation of the nematode *C. elegans*, their intake by the worms was assessed. For this purpose, L4 larvae were put in contact with Lumogen® Red-loaded nanospheres and pictures were taken. In Figure 18 fluorescent images of worms (taken 2 h after the addition of fluorescently labelled nanoparticles to the NGM) are shown. Figure 18A shows the autofluorescence of the worm, and in Figure 18B the nanoparticles through the gastrointestinal lumen of *C. elegans* can be observed, evidencing that nanoparticles enter the worm by the oral route.

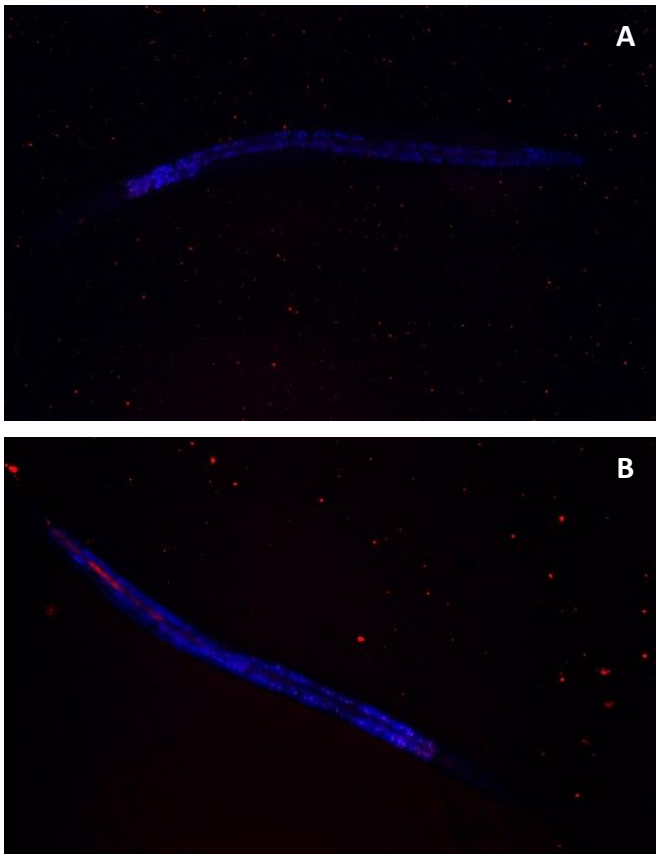

Figure 18. Fluorescent images of *C. elegans* 2 hours post-administration. **A**: self-fluorescence of *C. elegans*. **B**: worm fed with Lumogen® Red-loaded nanospheres.

4.5.2. Evaluation of fat accumulation

The effect of free and encapsulated quercetin on the accumulation of fat by *C. elegans* was evaluated. Worms were age-synchronized in L1/L2 larval stage and grown in a NGM supplemented with either free quercetin or quercetin-loaded nanoparticles. The fat content was always quantified when worms achieved L4 stage. First, the effective quercetin concentration was evaluated, by dissolving the flavonoid in DMSO and mixing it with the NGM.

4.5.2.1. Effect of free quercetin in the fat content of *C. elegans*

Three quercetin concentrations were evaluated (10 µM, 50 µM, and 100 µM) as shown in Figure 19. The positive control Orlistat decreased the fat accumulation in a 40.2% ($p < 0.0001$) compared to NGM. On the other hand, the concentration of 10 µM of quercetin significantly decreased the fat accumulation in *C. elegans* in a 5.7% compared to NGM ($p < 0.001$). This reduction was two times higher for the concentrations of 50 µM and 100 µM, achieving a decrease of 11.7% and 12.6% ($p < 0.0001$), respectively, compared to NGM. The effect for both concentrations was similar

and significantly different to 10 µM ($p < 0.0001$). In view of these results, the concentration of 50 µM of quercetin was chosen for further experiments.

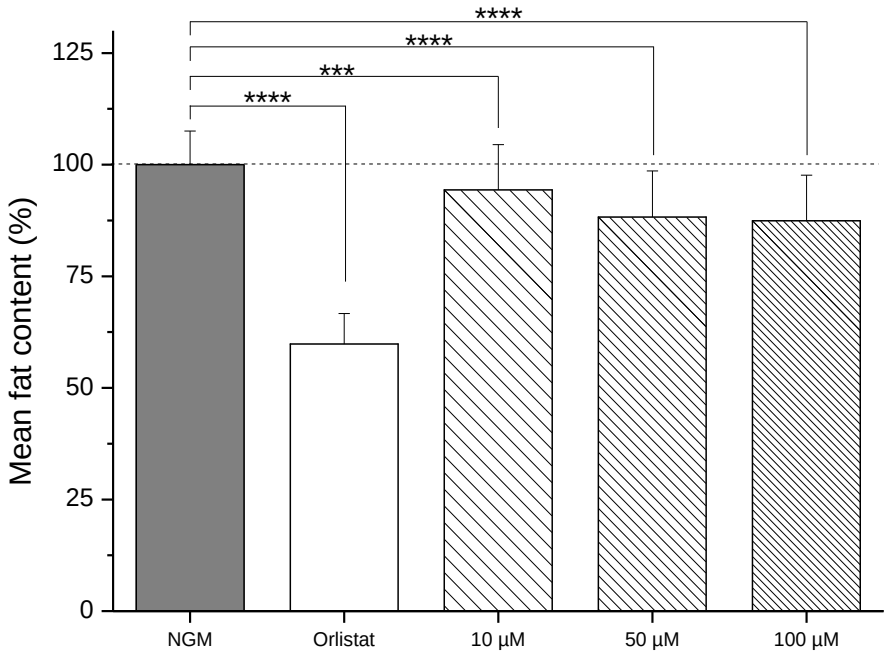

Figure 19. Evaluation of the effect of free quercetin in the fat accumulation of *C. elegans*, represented as the mean fat content normalized to NGM. Worms were cultured on NGM containing *E. Coli* OP50. Orlistat was employed as a positive control. Data are expressed as mean ± SD ($n \geq 76$, ***$p < 0.001$, ****$p < 0.0001$).

4.5.2.2. Effect of zein nanospheres in the fat content of *C. elegans* grown in NGM

Once the quercetin concentration was evaluated and the working concentration was established, a preliminary study was performed to analyse the effect of the formulation components (zein and mannitol) in the accumulation of fat by *C. elegans* (Figure 20). Free zein had no effect on the fat accumulation of *C. elegans* at a concentration equivalent to that employed when nanoparticles were evaluated. On the contrary, mannitol (at the concentration present in the nanoparticles) increased the accumulation of fat in a 11.7% ($p < 0.0001$) compared to NGM.

When worms were treated with a mixture of zein and mannitol, the amount of fat was increased in a 13.7% ($p < 0.0001$). When nanospheres containing mannitol were evaluated, the amount of fat increased in a 31.6% ($p < 0.0001$) compared to NGM. However, for NS prepared in the absence of mannitol, the amount of fat accumulated in the body of *C. elegans* was similar to that quantified in control animals (NGM). Thus, NS with mannitol presented 30.8% higher fat accumulation than NS ($p < 0.0001$), being the latter similar to free zein. The positive control Orlistat decreased the fat accumulation in a 40.0% compared to NGM ($p < 0.0001$).

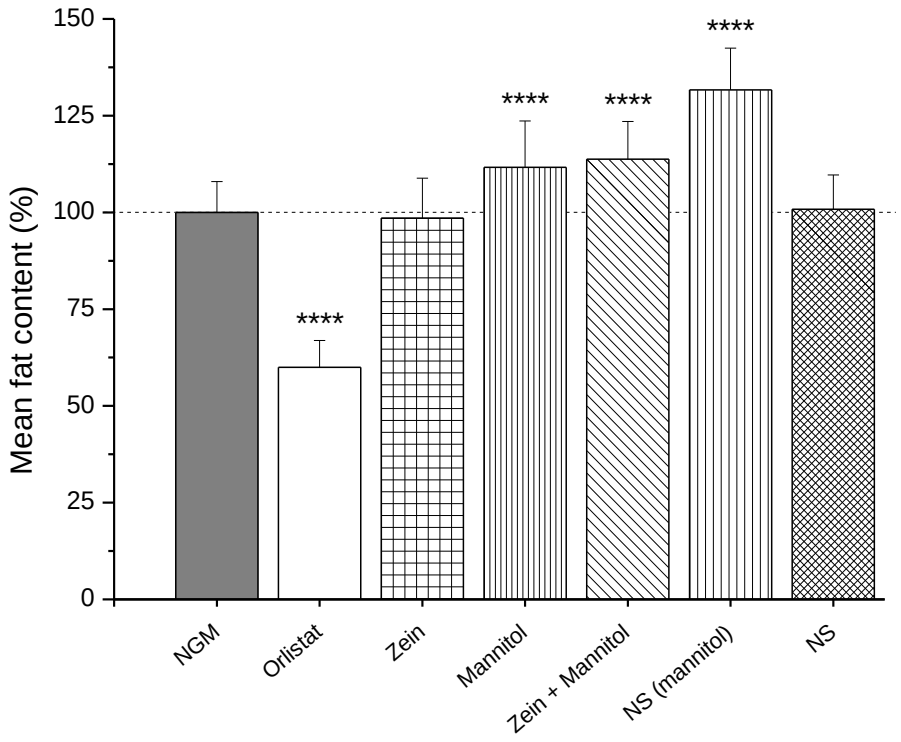

Figure 20. Fat accumulation of *C. elegans*, represented as the mean fat content normalized to NGM. Worms were cultured on NGM containing *E. Coli* OP50. Data are expressed as mean ± SD (n ≥ 112, ****p < 0.0001 compared to NGM). NS: empty nanospheres, with and without mannitol.

4.5.2.3. Effect of quercetin-loaded nanospheres on the accumulation of fat by *C. elegans* in a glucose-supplemented NGM

The effect of nanoencapsulated quercetin in NS and NS-PEG50 was analysed in a glucose-supplemented NGM (Figure 21). To assess the effect of glucose, a control in NGM without glucose was added, obtaining that glucose increased the amount of fat in a 19.2% ($p < 0.0001$, data not shown). Also, the positive control Orlistat decreased the fat accumulation in a 31.5% ($p < 0.0001$) compared to NGM.

Free zein (at the concentration present in NS) was also analysed in this glucose-supplemented media, obtaining an increase of 5.4% ($p < 0.0001$), compared to NGM. On the other hand, free quercetin decreased the accumulation of fat significantly compared to NGM by 5.7% ($p < 0.0001$). The administration of Q-NS significantly decreased the accumulation of fat, achieving a decrease of 12.4% ($p < 0.0001$) compared to NGM. When these nanospheres were coated with PEG at a PEG-to-zein ratio of 0.5 (w/w) (Q-NS-PEG50), the fat accumulation decreased by 9.1% ($p < 0.0001$) compared to NGM. Q-NS achieved a slightly higher decrease in the accumulation of fat compared to Q-NS-PEG50 (3.3%; $p < 0.05$). When these nanospheres (NS and NS-PEG50) were analysed without quercetin, the accumulation of fat increased by 3.8% and 4.2% ($p < 0.0001$) compared to NGM, respectively. Comparing empty and loaded nanospheres, Q-NS significantly decreased the accumulation of fat compared to NS by 16.2% ($p < 0.0001$).

A similar phenomenon was observed when PEG-coated nanospheres were evaluated. In this case, Q-NS-PEG50 decreased the accumulation of fat value by 13.3% compared to NS-PEG50 ($p < 0.0001$).

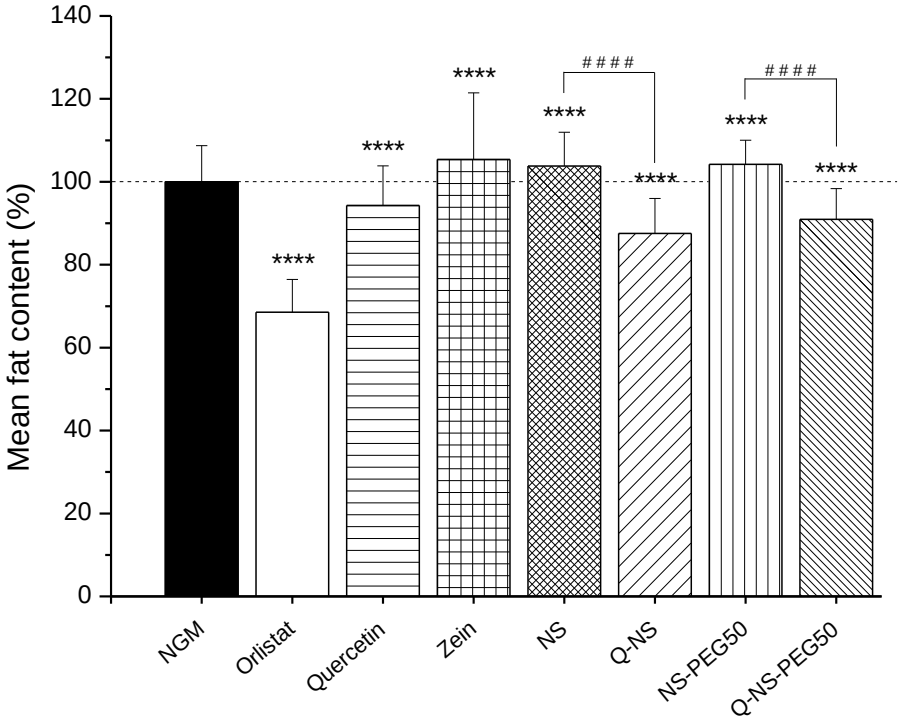

Figure 21. Fat accumulation of *C. elegans*, represented as the mean fat content normalized to NGM. Worms were cultured on a glucose-supplemented (0.5% w/v) NGM containing *E. Coli* OP50. Quercetin dose: 50 µM. Data are expressed as mean ± SD ($n \geq 129$, ****$p < 0.0001$ compared to NGM, $^{\#\#\#\#}p < 0.0001$). NS, Q-NS: empty and quercetin-loaded nanospheres; NS-PEG50, Q-NS-PEG50: empty and quercetin-loaded PEG-coated nanospheres. Nanoparticles were prepared without mannitol. All the significances are not shown.

4.5.2.4. Effect of quercetin-loaded nanocapsules on the accumulation of fat by *C. elegans* in a glucose-supplemented NGM

The effect of quercetin loaded in nanocapsules was also evaluated (Figure 22). The same controls as for nanospheres were employed (NGM, Orlistat, and quercetin). When wheat germ oil was incorporated in the growth medium of worms at the same concentration present in NC, the amount of fat accumulated by these animals significantly increased (10.5%; $p < 0.0001$) compared to NGM group. In the same way, the addition of a mixture of oil and free zein also increased the accumulation of fat by 12.6% ($p < 0.0001$).

When nanocapsules (NC) were analysed, they increased the fat accumulation again by 12.6% ($p < 0.0001$) compared to NGM. On the contrary, when quercetin was encapsulated (Q-NC), the fat accumulation in the worms was similar to the control. In

any case, Q-NC significantly decreased the amount of fat in a 12.3% compared to NC ($p < 0.0001$), demonstrating again that quercetin decreases the fat accumulation in *C. elegans*.

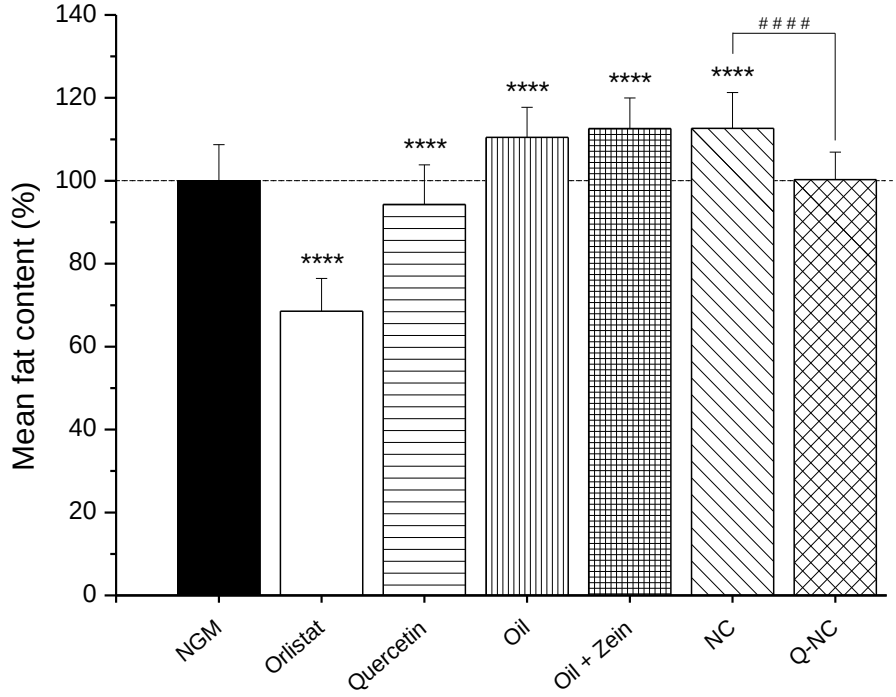

Figure 22. Fat accumulation of *C. elegans*, represented as the mean fat content normalized to NGM. Worms were cultured on a glucose-supplemented (0.5% w/v) NGM containing *E. Coli* OP50. Quercetin dose: 50 µM. Data are expressed as mean ± SD ($n \geq 92$, ****$p < 0.0001$ compared to NGM, $^{\#\#\#\#}p < 0.0001$). NC, Q-NC: empty and quercetin-loaded nanocapsules. Nanoparticles were prepared without mannitol. All the significances are not shown.

4.6. Biodistribution studies in Wistar rats

4.6.1. *In vivo* gastrointestinal transit of Technetium labelled nanoparticles

The fate of nanoparticles in the gut, radiolabelled with ^{99m}Tc, was evaluated in Wistar rats. It was observed that the radioactivity was only present in the gastrointestinal tract, indicating that nanoparticles (at least during the experimental period of time) were not absorbed or translocated to other regions of the body. In that way, nanoparticles ensured the gastrointestinal release of the entrapped bioactive, reducing the possible toxicity that could be developed in other regions.

The gastrointestinal profile of nanoparticles was similar in all cases, where particles moved towards the distal zones of the small intestine. During the overall experiment, a high intensity of radioactivity was observed in the stomach of animals. This observation may be explained by the release of a fraction of the radioactive tag bound to the surface of nanoparticles inside the stomach and/or by the high binding affinity of pertechnetate for the stomach mucosa (218).

For NS (Figure 23), 1 h and 2 h post-administration, radioactivity was visualized in the stomach and small intestine. At 4 h post-administration, nanospheres continued moving forward, arriving to the latest portion of the small intestine and cecum, with presence in the stomach. At 8 h post-administration, the quantity of NS in cecum seemed to be increased.

In case of NC (Figure 24), radioactivity was present in the stomach and in the small intestine at 1 h and 2 h post-administration, similarly to NS. At 4 h post-administration, nanoparticles were localized in the cecum and ascending colon (apart from the stomach). At 8 h, NC arrived to the descending colon, being present in the stomach, cecum, and ascending colon too. Also, NC seemed to be forming aggregates, due to the presence of red colour in the longitudinal sections, and seemed to move faster than NS.

PEG-coated nanospheres were also analysed (Figures 25 and 26). For NS-PEG25 (Figure 25), at 1 h and 2 h post-administration nanospheres were localized in the stomach and more modestly in small intestine. At 4 h after administration, nanospheres were present more considerably and reached the cecum. At the end of the experiment, 8 h post-administration, coated nanospheres achieved notably the cecum, and were still present in stomach and small intestine. NS-PEG25 seem to move in a similar way than NS.

Similarly to the rest of the nanoparticles, NS-PEG50 were present in stomach and small intestine at 1 h and 2 h post-administration (Figure 26). At 4 hours, particles were localized in cecum too, and at 8 h, also in ascending colon, so it seemed to be faster than NS during the journey through the gastrointestinal tract, due to the lower hydrophobicity and higher diffusivity in intestinal mucus, as seen in sections 4.1.3 and 4.4.

Thus, considering the regions of the gastrointestinal tract that nanoparticles achieved at 4 and 8 h post-administration, NC seemed to be the fastest ones, followed by NS-PEG50, then NS-PEG25, and finally NS. In addition, spots of radioactivity were present in the gastrointestinal tract of rats administered with NS and NC, while for PEG-coated nanospheres (NS-PEG25 and NS-PEG50) rests covering the mucosa could be observed. These rests could be related to the permeability of the nanoparticles through the intestinal mucus, obtaining a higher residence time inside the intestine.

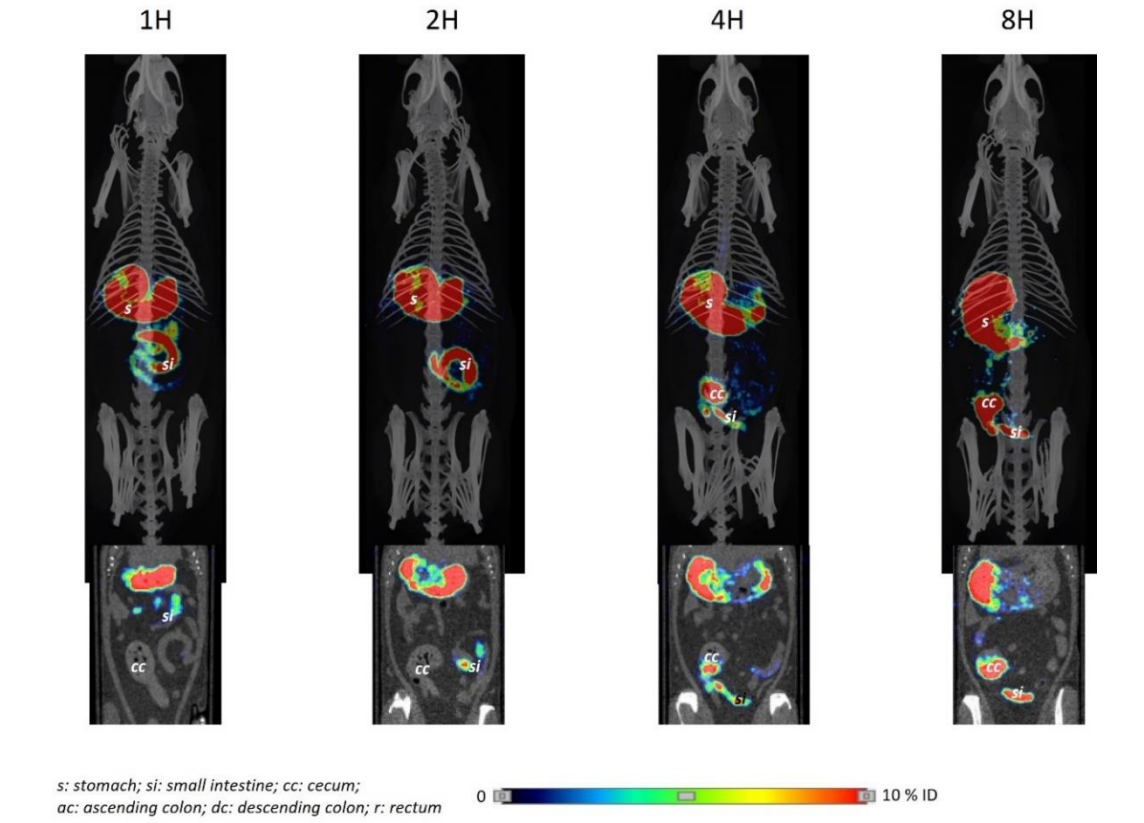

Figure 23. Gastrointestinal transit of Technetium-labelled nanospheres (NS) at different times. Longitudinal slices are also shown. *s*: stomach; *si*: small intestine; *cc*: cecum.

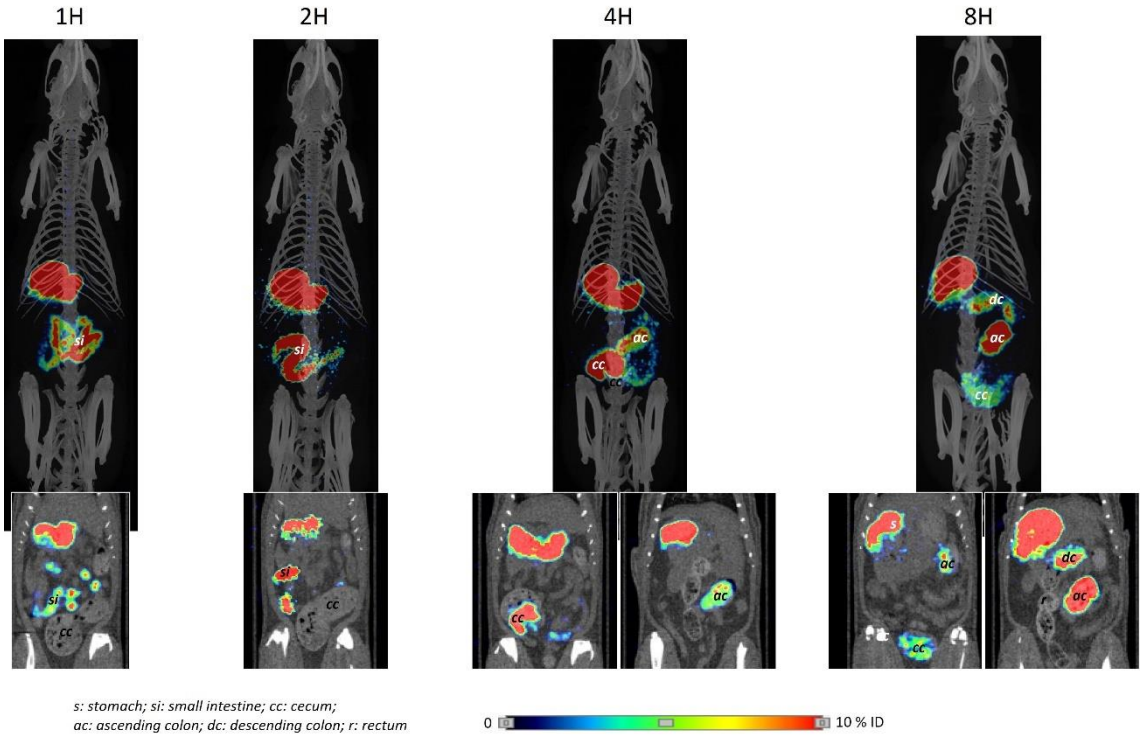

Figure 24. Gastrointestinal transit of Technetium-labelled nanocapsules (NC) at different times. Longitudinal slices are also shown. *si*: small intestine; *cc*: cecum; *ac*: ascending colon; *dc*: descending colon.

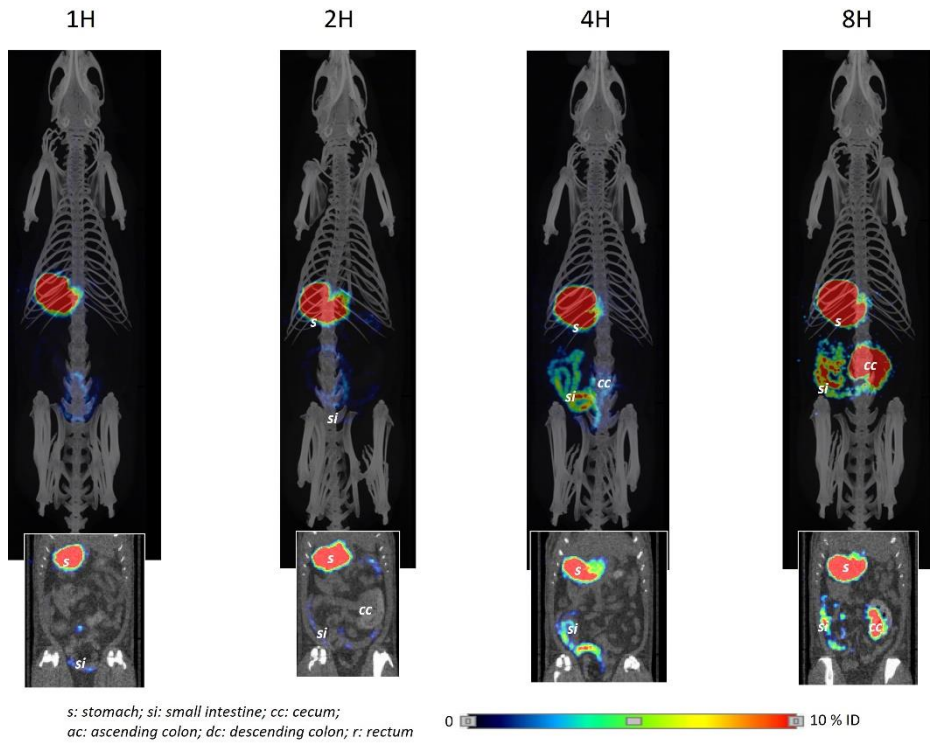

Figure 25. Gastrointestinal transit of Technetium-labelled PEG-coated nanospheres (PEG-to-zein ratio 0.25, NS-PEG25) at different times. Longitudinal slices are also shown. *s*: stomach; *si*: small intestine; *cc*: cecum.

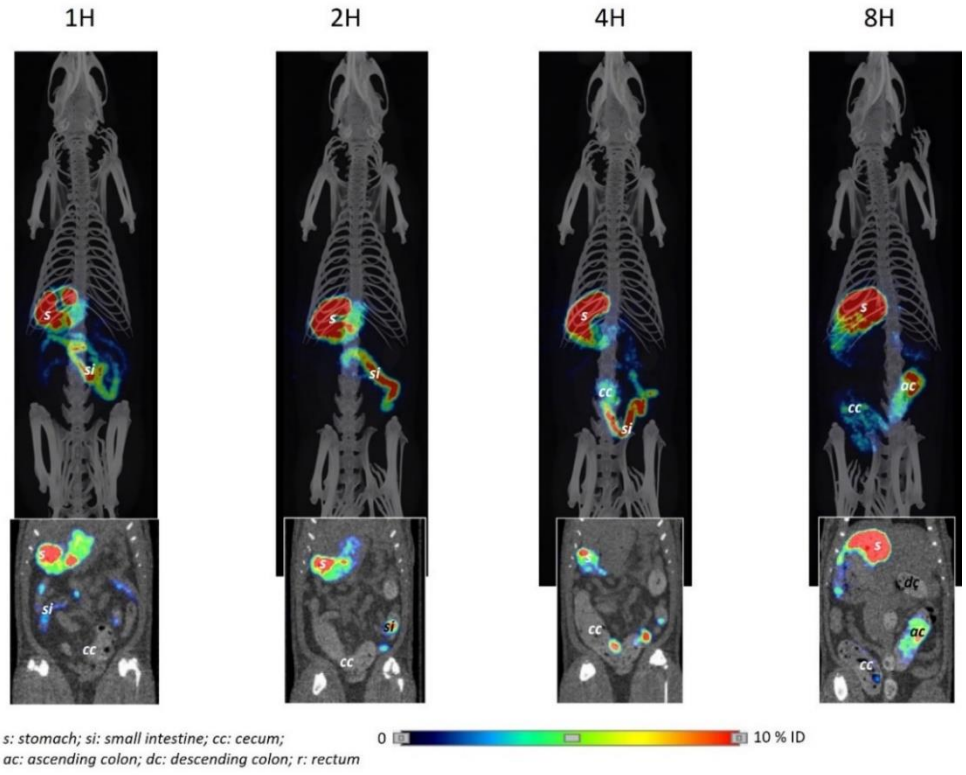

Figure 26. Gastrointestinal transit of Technetium-labelled PEG-coated nanospheres (PEG-to-zein ratio 0.50, NS-PEG50) at different times. Longitudinal slices are also shown. *s*: stomach; *si*: small intestine; *cc*: cecum; *ac*: ascending colon; *dc*: descending colon.

4.6.2. *In vivo* biodistribution on the gastrointestinal mucosa of Lumogen® Red-loaded nanoparticles

In order to evaluate the biodistribution of zein-based nanoparticles at the microscopic level, the different nanocarriers were labelled with Lumogen® Red and orally administered to Wistar rats (dose of 20 mg). The animals were sacrificed 4 h post-administration, and different parts of the gastrointestinal tract were extracted and visualized by fluorescent imaging.

The biodistribution of the fluorescent marker Lumogen® Red was performed as control (Figure 27). Almost all the Lumogen® was present in the stomach at 4 h, forming large aggregates. A small quantity was found in the duodenum and cecum, probably due to the presence of Polysorbate 80 used to prepare the aqueous suspension, which made Lumogen® not only to achieve the microvilli but also to move forward through the gastrointestinal tract.

In Figure 28 the biodistribution of NS and NC is shown. At 4 h, NS could be found in the stomach, small intestine, and cecum, confirming the results obtained in the previous section (4.6.1). No particles were found in the duodenum, while some were localized in the jejunum and ileum. In the ileum, nanoparticles appeared to be attached to the mucus layer. In case of NC, particles were particularly present in the stomach and cecum at 4 h post-administration, while very little quantity seemed to be in the small intestine. This could be because probably NC already arrived ascending colon, as previously shown in the *in vivo* gastrointestinal transit assay (Figure 23, section 4.6.1).

On the other hand, the distribution of PEG-coated nanospheres can be observed in Figure 29. NS-PEG25 were found all along the tract (stomach, small intestine, and cecum). In duodenum, nanoparticles appeared to be attached to the microvilli, while in the jejunum, where the highest amount of particles was observed, some of them were in the microvilli and others in the intestinal lumen. It seemed that a little quantity of particles was localized in the ileum and cecum. In case of NS-PEG50, similar results were obtained. Particles were found in every segment, being the ileum the one that seemed to have the highest quantity. This also would prove the movement of the particles through the intestinal mucus, not only to reach the microvilli but also through the gastrointestinal tract, because NS-PEG25 seemed to concentrate in jejunum and NS-PEG50 in ileum. NS-PEG50 in close contact with the microvilli could be seen in duodenum and jejunum. A very low quantity of nanospheres was found in cecum, confirming the previously obtained results in section 4.6.1 (Figure 23).

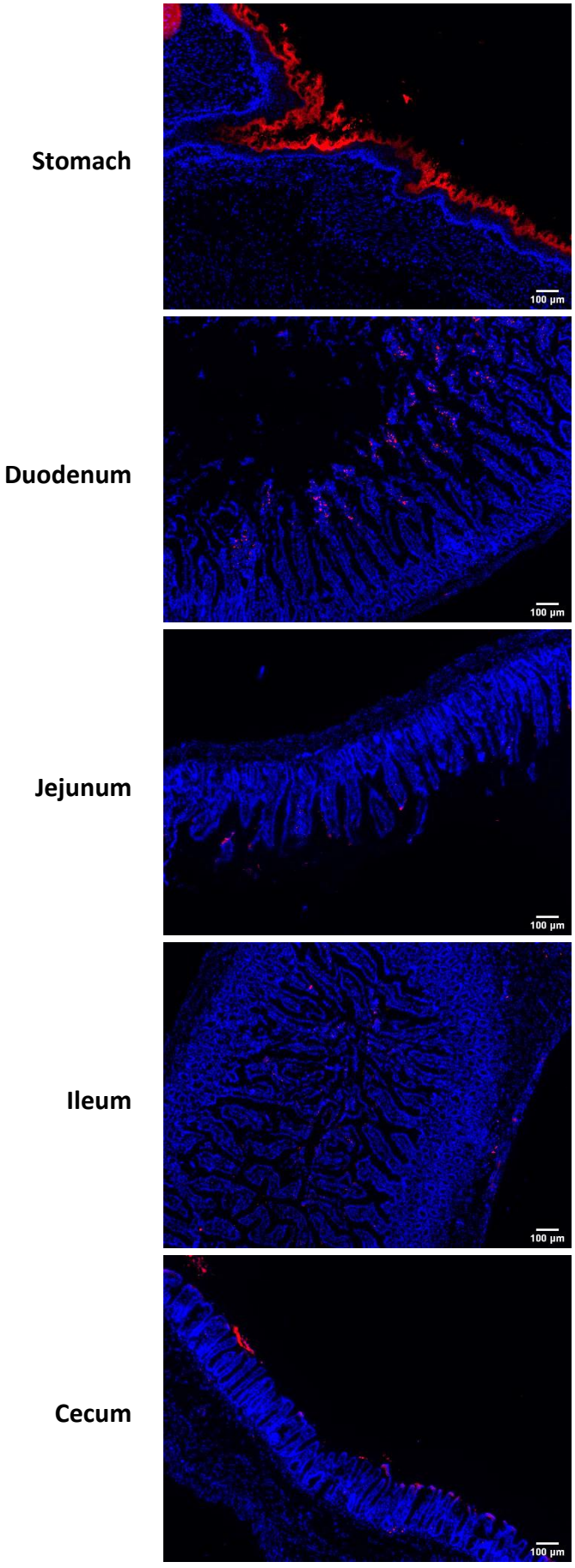

Figure 27. Biodistribution of free Lumogen® Red through the gastrointestinal tract of Wistar rats 4 h post-administration.

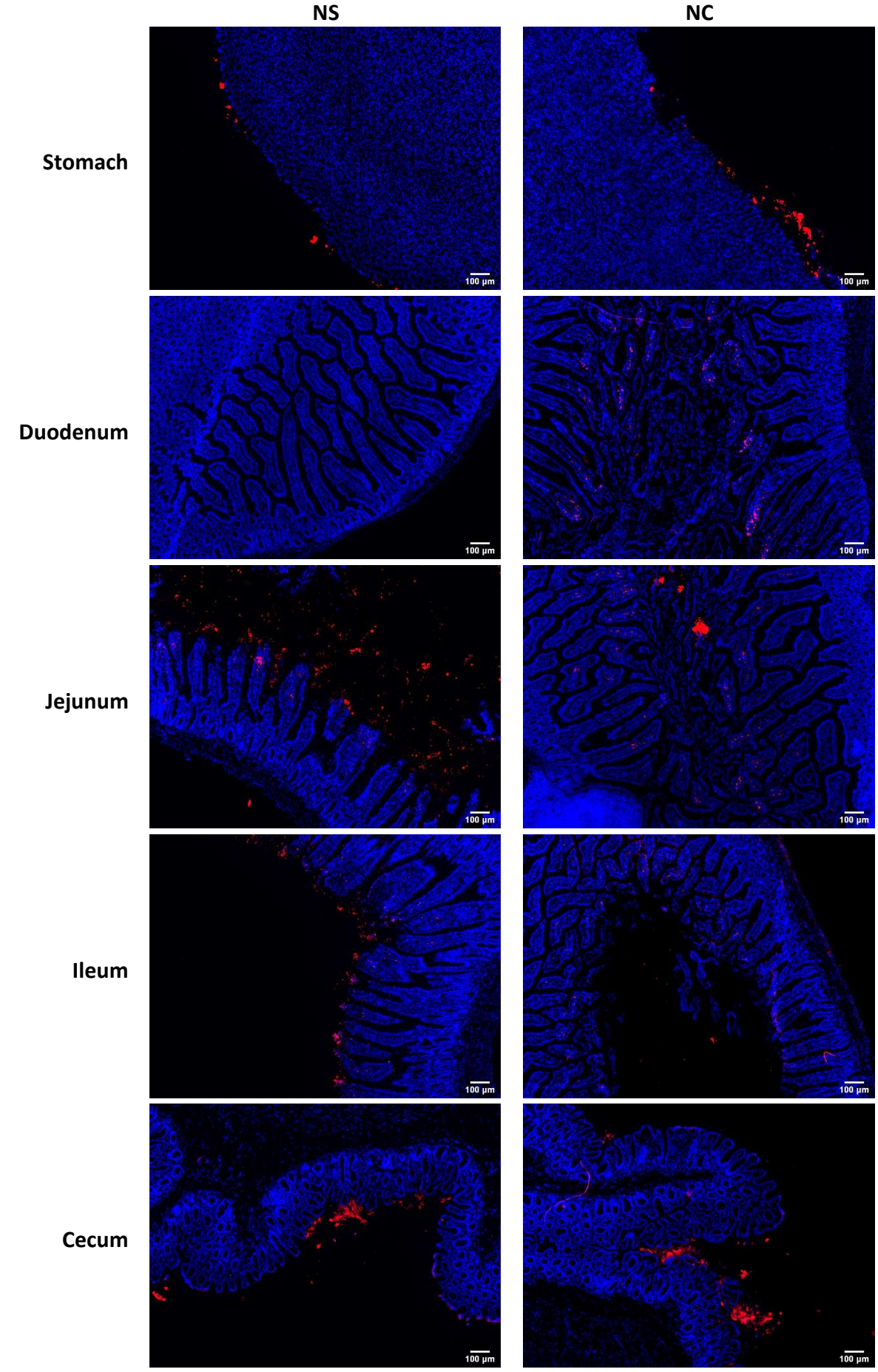

Figure 28. Biodistribution of nanospheres (NS) and nanocapsules (NC) (containing mannitol) through the gastrointestinal tract of Wistar rats 4 h post-administration.

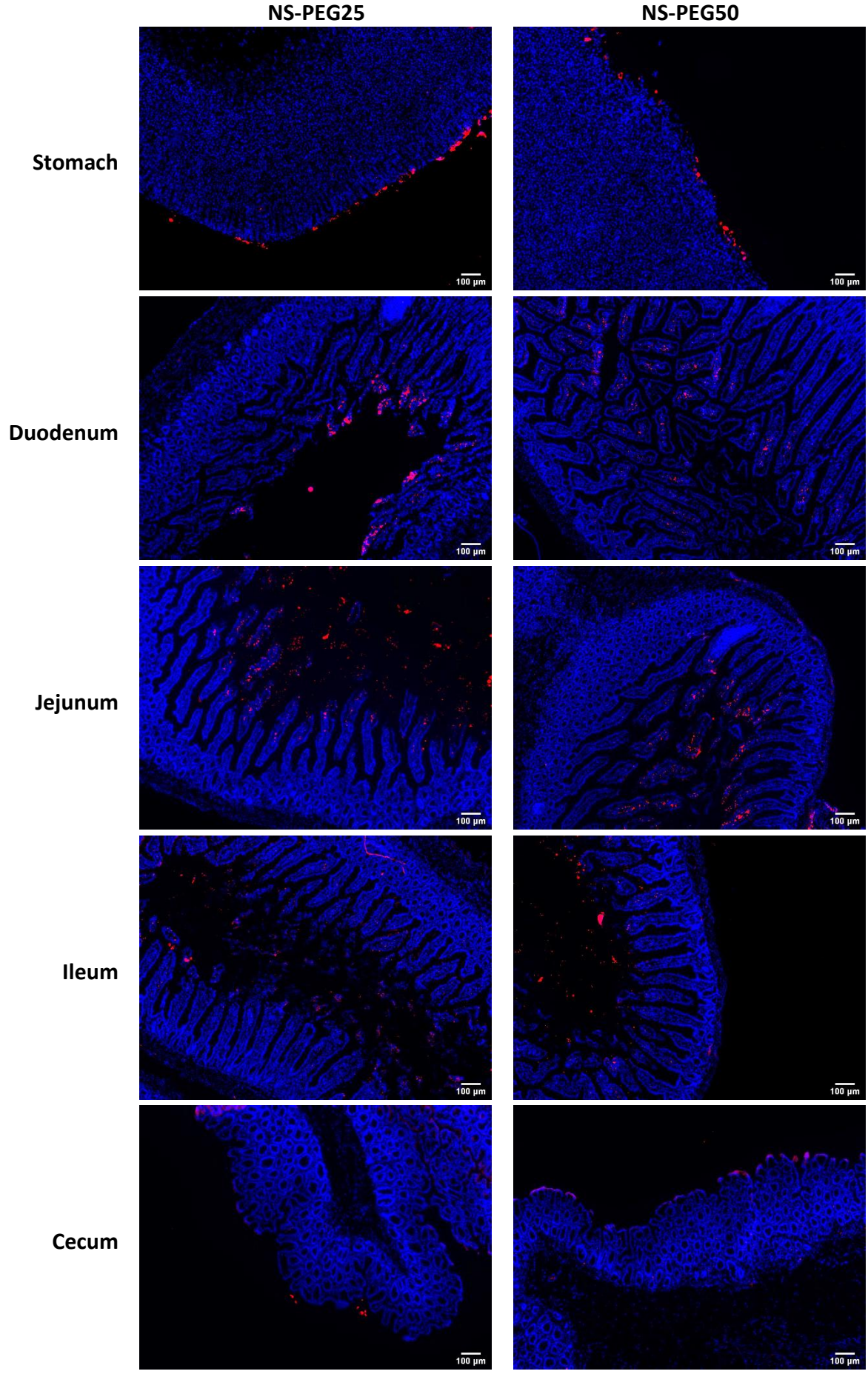

Figure 29. Biodistribution of PEG-coated nanospheres (NS-PEG25 and NS-PEG50) (containing mannitol) through the gastrointestinal tract of Wistar rats 4 h post-administration.

4.7. Pharmacokinetic assay

The pharmacokinetic profile of quercetin-loaded nanoparticles and the relative oral bioavailability of the flavonoid when formulated in zein-based nanoparticles was evaluated in Wistar rats. In all cases, the dose of quercetin was 15 mg/kg, either as a quercetin suspension or as loaded in the developed zein-based nanoparticles. As intravenous control, a solution of quercetin in a mixture of PEG 400 and water was used.

Figure 30 shows the pharmacokinetic profile of the intravenous administration of quercetin formulated as a solution in a mixture of PEG 400 and water (6:4 v/v). The maximum quercetin concentration reached in plasma (C_{max}) was about 70 µg/mL at time 0 (T_{max}), and, then, the concentration decreased (as in a typical intravenous bolus administration) until 8h, where the concentration was 2,350 ng/mL. The pharmacokinetic parameters are summarized in Tables 11 and 12. The half-life ($t_{1/2}$) was calculated to be 4.0 h, and the mean residence time (MRT) was 3.5 h.

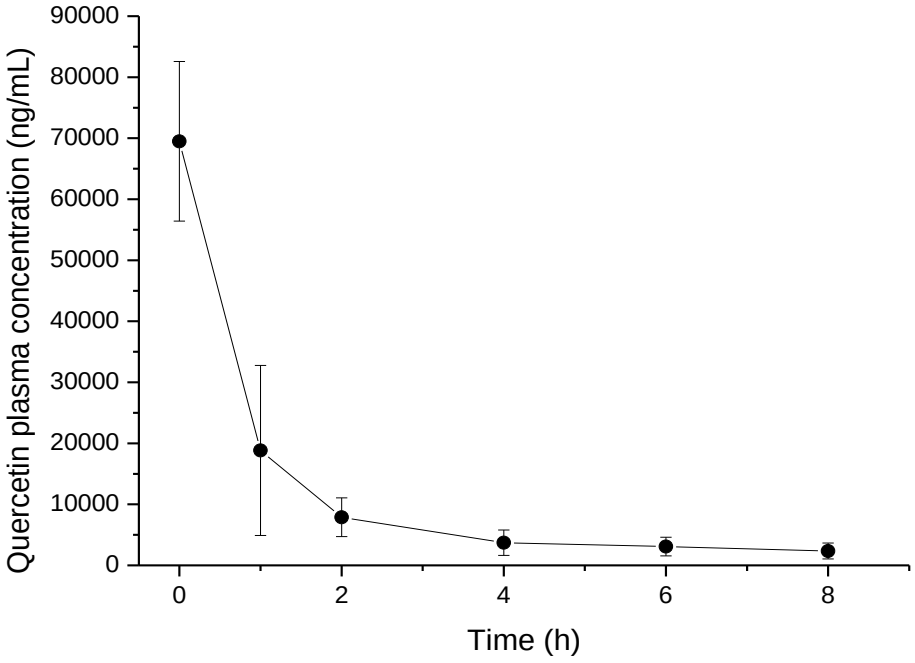

Figure 30. Pharmacokinetic profile of intravenously administered quercetin after a single dose of 15 mg/kg, as a quercetin solution in PEG400 and water. Data are expressed as mean ± SD (n = 5).

The pharmacokinetic profiles of quercetin formulations are shown in Figure 31. For all the formulations tested (aqueous suspension and nanoparticles) a similar pattern was observed. This profile was characterized by an initial rapid increase of quercetin plasma levels, followed by a plateau up to 8 h post-administration, and finally a slow decrease during the following hours. Overall, the encapsulation of quercetin in nanoparticles increased the amount of the flavonoid quantified in plasma.

The pharmacokinetic parameters, calculated from the plasma quercetin levels vs time curve, are summarized in Table 11. The quercetin control formulation (Q-Susp) displayed the lowest plasma profile, with a C_{max} of 358 ng/mL of quercetin in plasma. On the contrary, Q-NS offered the highest C_{max}, achieving a five times higher concentration, 1,925 ng/mL. In all cases, T_{max} were between 0.5 and 1 hour post-administration. Nevertheless, regarding the $t_{1/2}$ and MRT the results were different. Whereas Q-Susp showed a $t_{1/2}$ of 8.2 h, Q-NS-PEG25 had the highest half-life, 48.9 h, that is, six times higher ($p < 0.001$). Regarding the MRT, the same phenomenon was observed. Q-Susp had a mean residence time of 12.3 h, which was significantly increased to 70.4 h in case of Q-NS-PEG25 ($p < 0.01$).

Moreover, the area under the curve (AUC) for each treatment was calculated, from time 0 to infinity (Table 12). Q-NS showed an AUC of 56,019 ng·h/mL, significantly higher than for Q-Susp (4,790 ng·h/mL; $p < 0.01$). These AUC values were compared to the intravenous ones, to obtain the relative oral bioavailability (Table 12). Q-Susp displayed a quercetin oral bioavailability close to 5%, while all nanoparticles increased this value. Q-NS increased the Fr to 57.4%, twelve times higher than Q-Susp, being the formulation that obtained the highest Fr, followed by Q-NS-PEG25 (37.3%), Q-NC (25.6%), and Q-NS-PEG50 (20.0%), that increased the Fr seven, five and four times compared to Q-Susp, respectively.

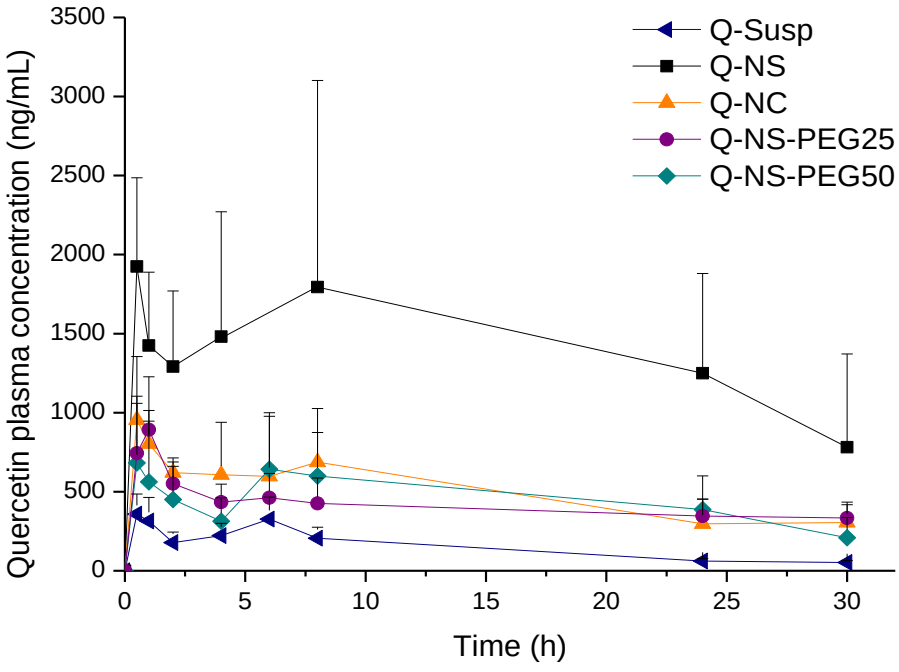

Figure 31. Pharmacokinetic profile of oral administered free quercetin or quercetin-loaded nanoparticles after a single dose of 15 mg/kg. The formulations were dried by spray dryer without mannitol. Data are expressed as mean ± SD ($n \geq 5$). Q-Susp: quercetin suspension; Q-NS: quercetin-loaded nanospheres; Q-NC: quercetin-loaded nanocapsules; Q-NS-PEG25 and Q-NS-PEG50: PEG-coated quercetin-loaded nanospheres.

Table 11. Pharmacokinetic parameters obtained for the administration of free and encapsulated quercetin at 15 mg/kg. Data are expressed as mean ± SD (n ≥ 5, **p < 0.01, ***p < 0.001, ****p < 0.0001, nanoparticles compared to Q-Susp). i.v.: intravenous administration of quercetin; Q-Susp: quercetin suspension; Q-NS: quercetin-loaded nanospheres; Q-NC: quercetin-loaded nanocapsules; Q-NS-PEG25 and Q-NS-PEG50: PEG-coated quercetin-loaded nanospheres. T_{max}: time to reach maximum plasma concentration; C_{max}: maximum plasma concentration; $t_{1/2}$: half-life; MRT: mean residence time.

	T_{max} (h)	C_{max} (ng/mL)	$t_{1/2}$ (h)	MRT (h)
i.v.	0	69,494 ± 13,067	4.0 ± 2.1	3.5 ± 2.0
Q-Susp	0.5	358 ± 128	8.2 ± 1.7	12.3 ± 2.3
Q-NS	0.5	1,925 ± 561****	11.5 ± 4.2	16.7 ± 6.4
Q-NC	0.5	955 ± 400	20.1 ± 4.8	30.5 ± 7.1
Q-NS-PEG25	1	893 ± 334	48.9 ± 31.8***	70.4 ± 47.6**
Q-NS-PEG50	0.5	683 ± 376	16.6 ± 10.5	25.3 ± 14.7

Table 12. Area under the curve (AUC) and relative oral bioavailability (Fr) obtained for the administration of free and encapsulated quercetin at 15 mg/kg. Data are expressed as mean ± SD (n ≥ 5, **p < 0.01, nanoparticles compared to Q-Susp). i.v.: intravenous administration of quercetin; Q-Susp: quercetin suspension; Q-NS: quercetin-loaded nanospheres; Q-NC: quercetin-loaded nanocapsules; Q-NS-PEG25 and Q-NS-PEG50: PEG-coated quercetin-loaded nanospheres.

	$AUC_{0-\infty}$ (ng h/mL)	Fr (%)
i.v.	97,524 ± 34,067	100
Q-Susp	4,790 ± 1,478	4.9
Q-NS	56,019 ± 44,131**	57.4
Q-NC	24,986 ± 8,860	25.6
Q-NS-PEG25	36,380 ± 23,554	37.3
Q-NS-PEG50	19,525 ± 7,921	20.0

4.8. Efficacy study

4.8.1. Diet induced obesity (DIO) model

For the efficacy study, 72 Wistar male rats were divided in two groups depending on the diet: 12 rats were fed with standard diet (Control) and 60 rats were fed with a high fat/high sucrose diet (HFS) for 23 weeks. Before starting the treatments, animals were weighed every week (Figure 32). The initial body weight was similar for both groups, around 120 g per animal, and it increased in a similar way in both groups until week 5. Significant differences were not found between groups until week 6, with a weight of

344 g for Control and 363 g for HFS on average, indicating a higher body weight for HFS-fed rats than for Control animals ($p < 0.05$). The difference between the weight of animals fed with HFS and the standard diet increased with time. Thus, just before the beginning of the treatments (week 17), the weight of the animals fed with HFS was about 16% higher ($p < 0.0001$) than that of animals fed with the standard diet (Figure 31).

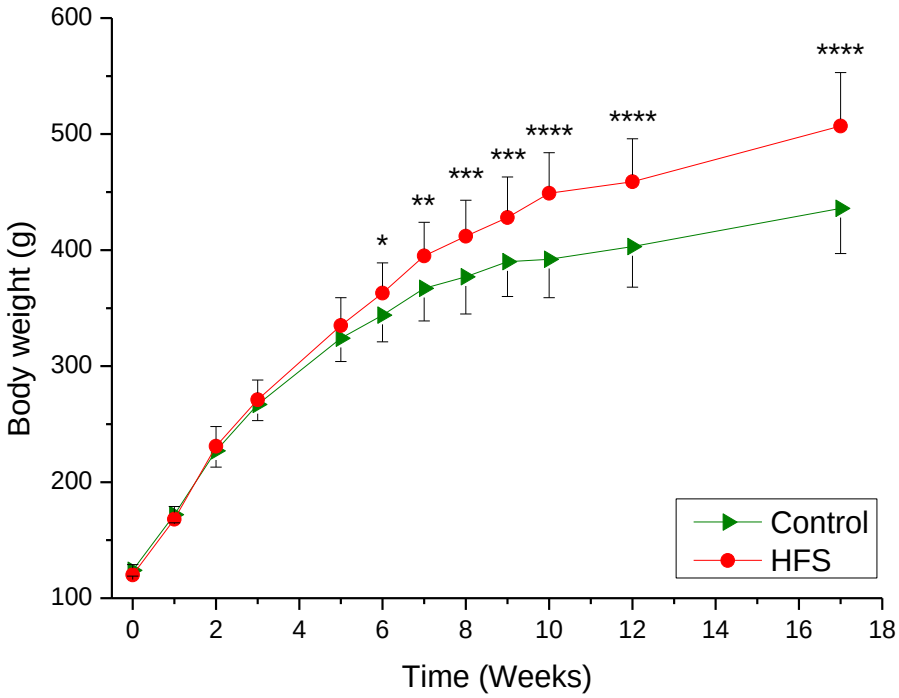

Figure 32. Weight gain before the administration of the treatments in the efficacy study. Data are expressed as mean ± SD (n = 12 for Control and n = 60 for HFS, *p < 0.05, **p < 0.01, ***p < 0.001, ****p < 0.0001). Control: standard diet; HFS: high fat/high sucrose diet.

4.8.2. Body composition

In the efficacy study, DIO model Wistar rats were daily treated with the equivalent to 15 mg/kg of quercetin for 5 weeks. The different treatments were as follows: (i) quercetin-loaded nanospheres (Q-NS), (ii) quercetin-loaded nanocapsules (Q-NC), (iii) PEG-coated quercetin-loaded nanospheres at a PEG-to-zein ratio of 0.25 (w/w) (Q-NS-PEG), and (iv) quercetin suspension (Q-Susp). The formulations of quercetin encapsulated in nanoparticles (Q-NS, Q-NC, and Q-NS-PEG) were, in all cases, prepared without mannitol.

The body weight gain during the treatment was calculated as the subtraction of the weight at the end of the experiment (week 23) and the weight before the start of the treatments (week 17). Figure 33 presents the body weight gain for each treatment. Control rats increased their weight by 30 g, while for HFS rats this gain was of 36 g. A slight tendency of Q-NS and Q-NS-PEG to reduce the body weight gain was observed (24

and 28 g of weight gain, respectively); although no differences were found between treatments and HFS in the a posteriori test, even if ANOVA was significant ($p < 0.05$).

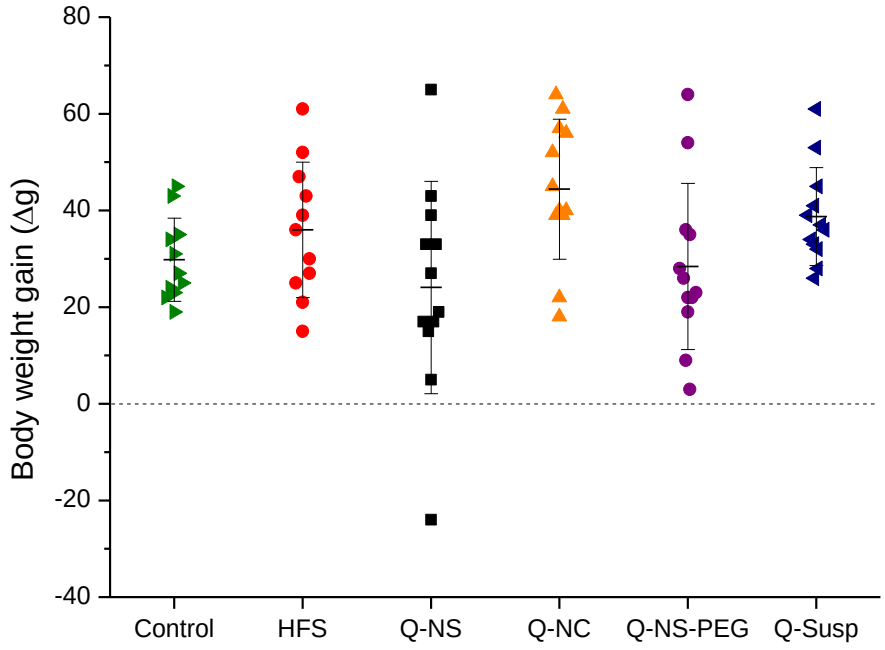

Figure 33. Body weight gain during the period of the treatments (from week 18 until week 23). Data are expressed as mean ± SD ($n \geq 11$). Control: standard diet; HFS: high fat/high sucrose diet; Q-NS; quercetin-loaded nanospheres; Q-NC: quercetin-loaded nanocapsules; Q-NS-PEG: PEG-coated quercetin-loaded nanospheres; Q-Susp: quercetin suspension.

The previous week to the sacrifice of the animals (week 22), the amount of both body fat and lean was measured by magnetic resonance spectroscopy (by EchoMRI) and the proportion to the body weight calculated (Figure 34). Control rats displayed a proportion of fat of 13% of the total body weight (Figure 34A), while HFS rats presented a double amount of fat (26%; $p < 0.0001$). Quercetin slightly decreased the fat content in comparison to HFS, being Q-NS-PEG the treatment that significantly decreased the fat content up to 20% ($p < 0.01$).

Regarding the lean mass (Figure 34B), Control presented a 59% of lean mass in the total body weight, while this value was significantly lower for HFS (52%; $p < 0.01$). All treatments displayed similar results to HFS (between 54 and 55%), indicating that none of the treatments was capable of reverting the HFS effect on the lean content during the experiment period.

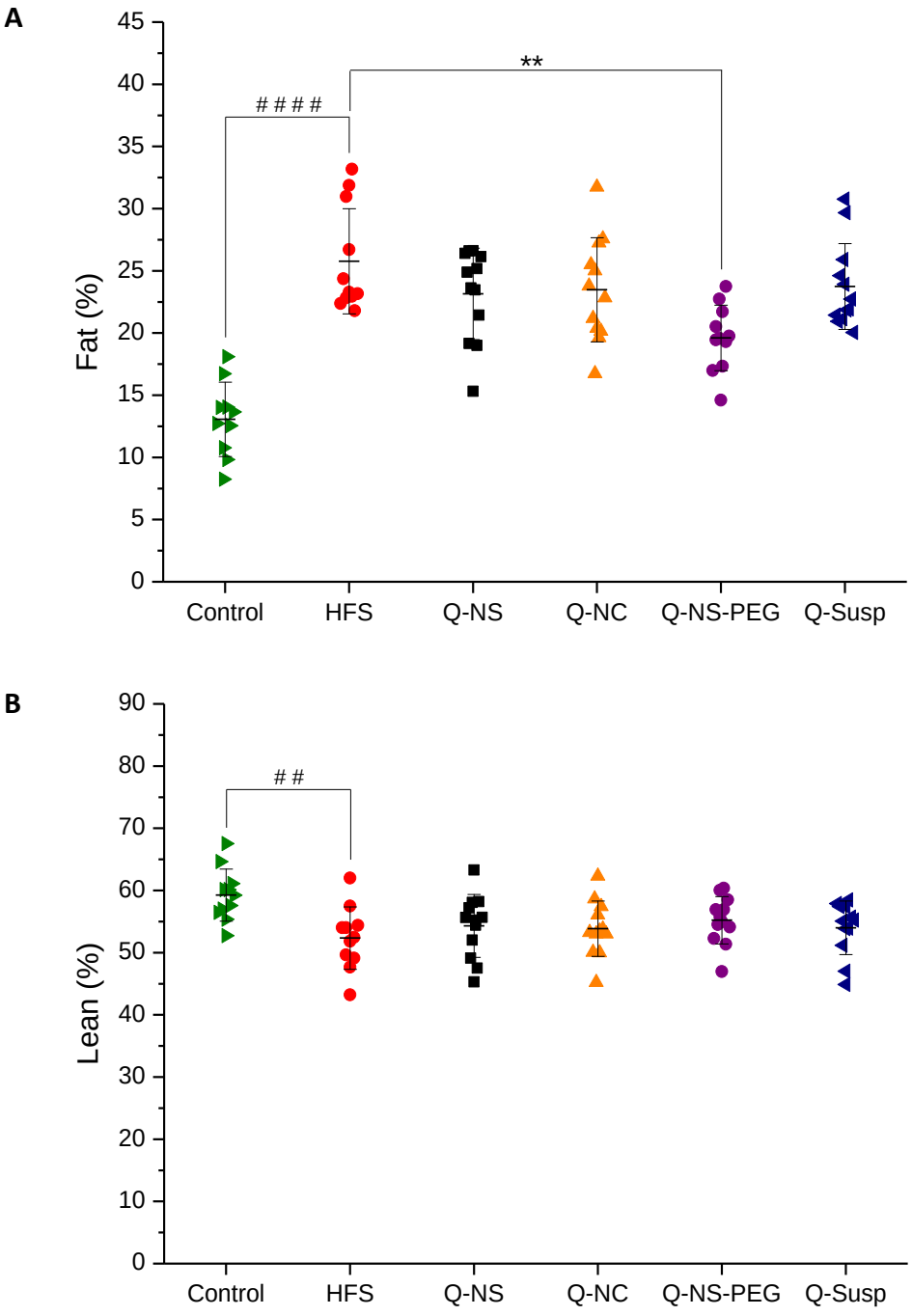

Figure 34. Fat (**A**) and lean (**B**) content (in percentage) obtained by magnetic resonance spectroscopy (EchoMRI) at week 22. Data are expressed as mean ± SD (n ≥ 10). $^{\#\#}p < 0.01$, $^{\#\#\#\#}p < 0.0001$, HFS compared to Control. $^{**}p < 0.01$, treatments compared to HFS. Control: standard diet; HFS: high fat/high sucrose diet; Q-NS; quercetin-loaded nanospheres; Q-NC: quercetin-loaded nanocapsules; Q-NS-PEG: PEG-coated quercetin-loaded nanospheres; Q-Susp: quercetin suspension.

The effect of quercetin treatment on the Fat-to-Lean ratio is shown in Figure 35. Control rats displayed a ratio of 0.22, whereas for HFS rats the ratio was 0.5 (two times higher; $p < 0.0001$). Similarly to the fat content (Figure 34A), quercetin slightly decreased the fat-to-lean ratio (between 0.43 and 0.45). For Q-NS-PEG, this decrease (0.35) was significant ($p < 0.01$).

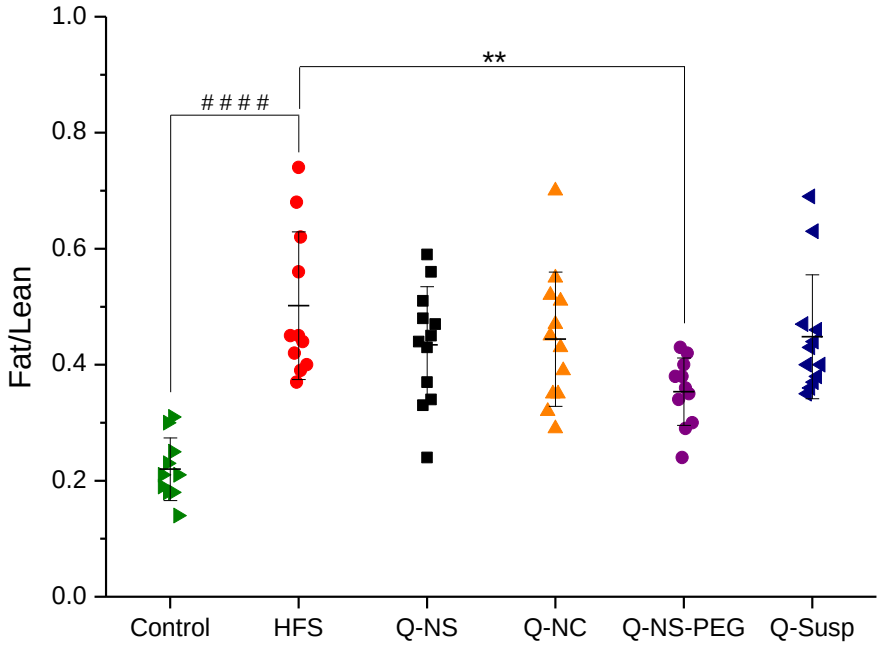

Figure 35. Relationship between fat and lean obtained by magnetic resonance spectroscopy (EchoMRI) at week 22. Data are expressed as mean ± SD ($n \geq 10$). $^{\#\#\#\#}p < 0.0001$, HFS compared to Control. $^{**}p < 0.01$, treatments compared to HFS. Control: standard diet; HFS: high fat/high sucrose diet; Q-NS; quercetin-loaded nanospheres; Q-NC: quercetin-loaded nanocapsules; Q-NS-PEG: PEG-coated quercetin-loaded nanospheres; Q-Susp: quercetin suspension.

After 5 weeks of treatment (week 23), rats were sacrificed and different fat depots and organs were extracted and weighted (Figures from 36 to 39). The content of epididymal fat (expressed as percentage to the total body weight), localized in the perigonadal region (219), is shown in Figure 35A. Control rats displayed an amount of epididymal fat of 2.33%, while this value was two times higher for HFS rats (4.38%; $p < 0.0001$). Quercetin treatments decreased the amount of this kind of fat (between 12 and 17% compared to HFS), but only Q-NS-PEG and Q-Susp did it in a significant way ($p < 0.05$), up to 3.66% and 3.64%, respectively.

Retroperitoneal fat, the fat located on the kidneys (219), was also extracted (Figure 36B). Control rats presented a percentage of 2.51% of retroperitoneal fat, while for HFS this value was 5.11% ($p < 0.0001$). As for epididymal fat, all the treatments slightly decreased the fat proportion compared to HFS. Again, only Q-NS-PEG displayed a significant decrease compared to the animals of the HFS group (up to 3.90%; $p < 0.01$).

Mesenteric fat (the fat located alongside the intestinal tract (219)) was also extracted after the sacrifice, as shown in Figure 37A. Control rats exhibited an amount of 0.56% of mesenteric fat in the total body weight, while for HFS rats this value rose to 1.33%, more than two times higher than Control rats ($p < 0.0001$). Quercetin was able to decrease the amount of mesenteric fat with percentages between 1.09% and 1.28%, but no significant differences were found compared to HFS, being Q-NS-PEG the treatment that showed the highest tendency to decrease mesenteric fat.

Percentages of subcutaneous fat, which is the fat present between the skin and the abdominal wall (220), are shown in Figure 37B. Control rats displayed an amount of 1.64% of subcutaneous fat, while for HFS the percentages to total body weight increased more than two times (3.56%; $p < 0.0001$). Quercetin decreased subcutaneous fat and, as with epididymal fat, Q-NS-PEG and Q-Susp significantly reduced the subcutaneous fat proportion up to 2.72% and 2.76% compared to HFS ($p < 0.05$), respectively.

On the other hand, interscapular brown fat (219,221) was also extracted and weighted (Figure 38A). The amount of this kind of fat was 0.16% for Control and 0.23% for HFS, significantly higher ($p < 0.001$). All treatments reduced brown fat, but only Q-Susp decreased it in a significant way (0.17%; $p < 0.01$).

Finally, visceral white adipose tissue (WAT) was calculated as the sum of epididymal, retroperitoneal, and mesenteric fats, as shown in Figure 38B. Control presented a percentage of visceral WAT of 5.6% of the total body weight, while this value was increased almost twice for HFS, up to 10.8%. In this case, three treatments decreased significantly visceral WAT: Q-NC (9.2%; $p < 0.05$), Q-NS-PEG (8.6%; $p < 0.01$), and Q-Susp (9.1%; $p < 0.05$).

After the sacrifice at week 23, some organs were extracted and weighted (Figure 39). For the liver (Figure 39A) and kidneys (Figure 39B), all controls and treatments had a similar percentage to total body weight, and quercetin did not have an effect on the weight of these organs compared to HFS, even though the Kruskal-Wallis' test was significant for the liver ($p < 0.05$). In case of the spleen (Figure 39C), Control displayed a percentage of 0.14% while the value for HFS was significantly lower, 0.12% ($p < 0.01$). In case of the gastrocnemius muscle (Figure 39D), one of the muscles present in the hind limb (222), Control presented an amount of 0.59% and HFS 0.47%, that is, rats fed with standard diet displayed higher percentage of muscle than HFS-fed rats ($p < 0.0001$). All treatments had similar values compared to HFS regarding the spleen and the gastrocnemius muscle.

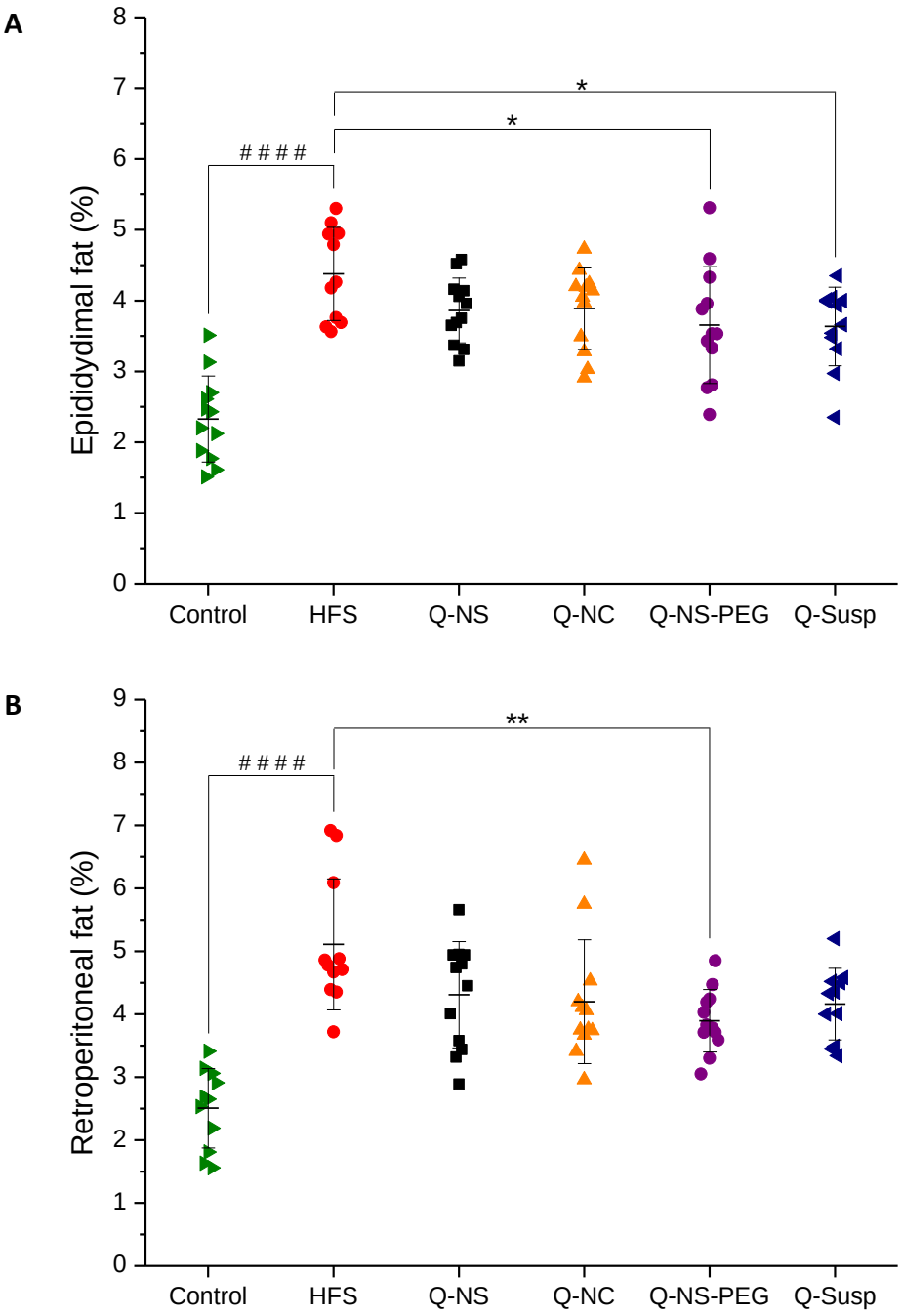

Figure 36. Fat depots extracted at week 23: epididymal (**A**) and retroperitoneal (**B**) fats (percentage to total body weight). Data are expressed as mean ± SD (n ≥ 11). $^{\#\#\#\#}p < 0.0001$, HFS compared to Control. *p < 0.05, **p < 0.01, treatments compared to HFS. Control: standard diet; HFS: high fat/high sucrose diet; Q-NS; quercetin-loaded nanospheres; Q-NC: quercetin-loaded nanocapsules; Q-NS-PEG: PEG-coated quercetin-loaded nanospheres; Q-Susp: quercetin suspension.

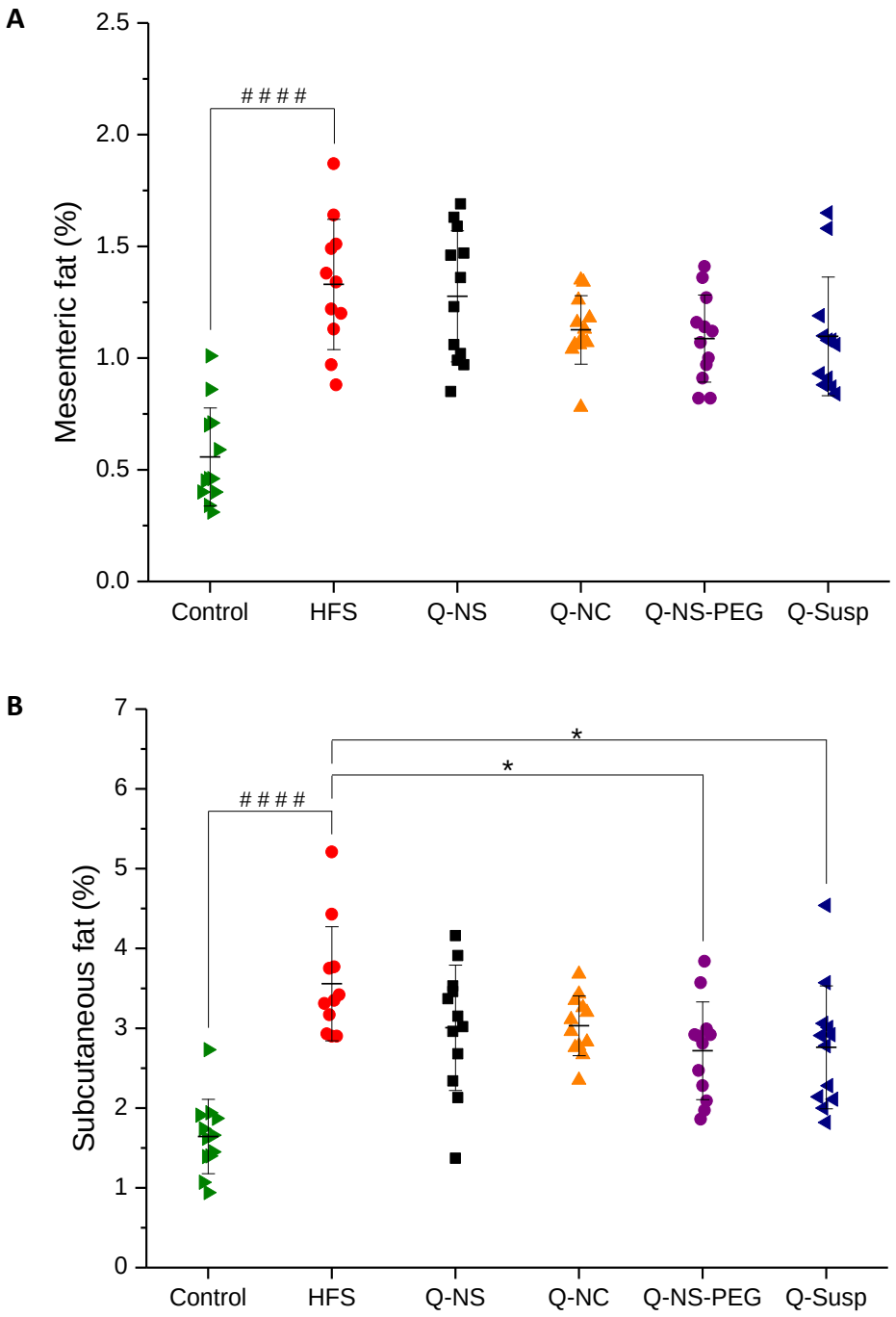

Figure 37. Fat depots extracted at week 23: mesenteric (**A**) and subcutaneous (**B**) fats (percentage to total body weight). Data are expressed as mean ± SD (n ≥ 11). $^{####}p < 0.0001$, HFS compared to Control. *$p < 0.05$, treatments compared to HFS. Control: standard diet; HFS: high fat/high sucrose diet; Q-NS; quercetin-loaded nanospheres; Q-NC: quercetin-loaded nanocapsules; Q-NS-PEG: PEG-coated quercetin-loaded nanospheres; Q-Susp: quercetin suspension.

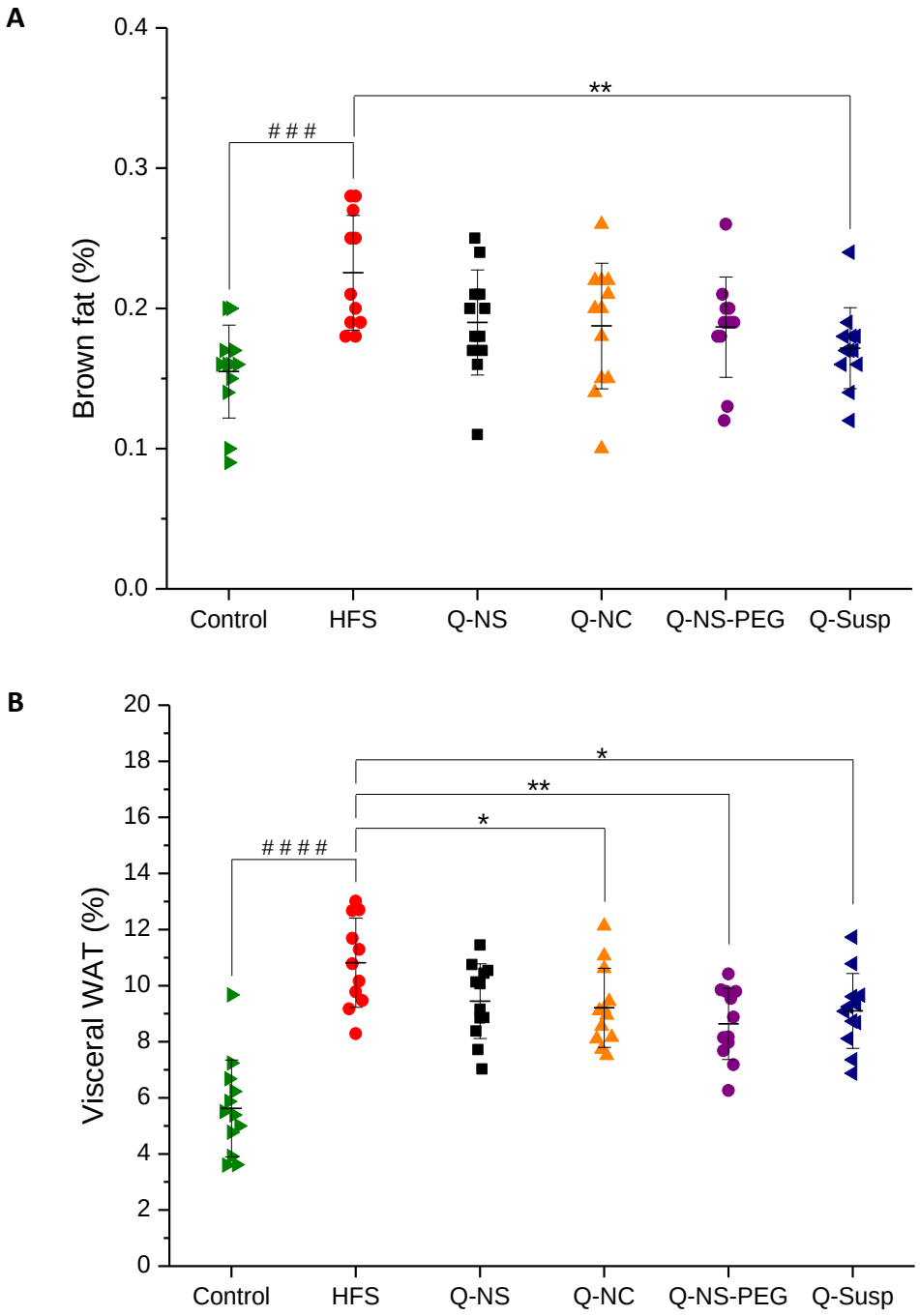

Figure 38. Fat depots extracted at week 23: brown fat (**A**) and visceral WAT (**B**) (percentage to total body weight). Visceral WAT (white adipose tissue) corresponds to the sum of epididymal, retroperitoneal and mesenteric fat. Data are expressed as mean ± SD (n ≥ 11). $^{###}p < 0.001$, $^{####}p < 0.0001$, HFS compared to Control. *p < 0.05, **p < 0.01, treatments compared to HFS. Control: standard diet; HFS: high fat/high sucrose diet; Q-NS; quercetin-loaded nanospheres; Q-NC: quercetin-loaded nanocapsules; Q-NS-PEG: PEG-coated quercetin-loaded nanospheres; Q-Susp: quercetin suspension.

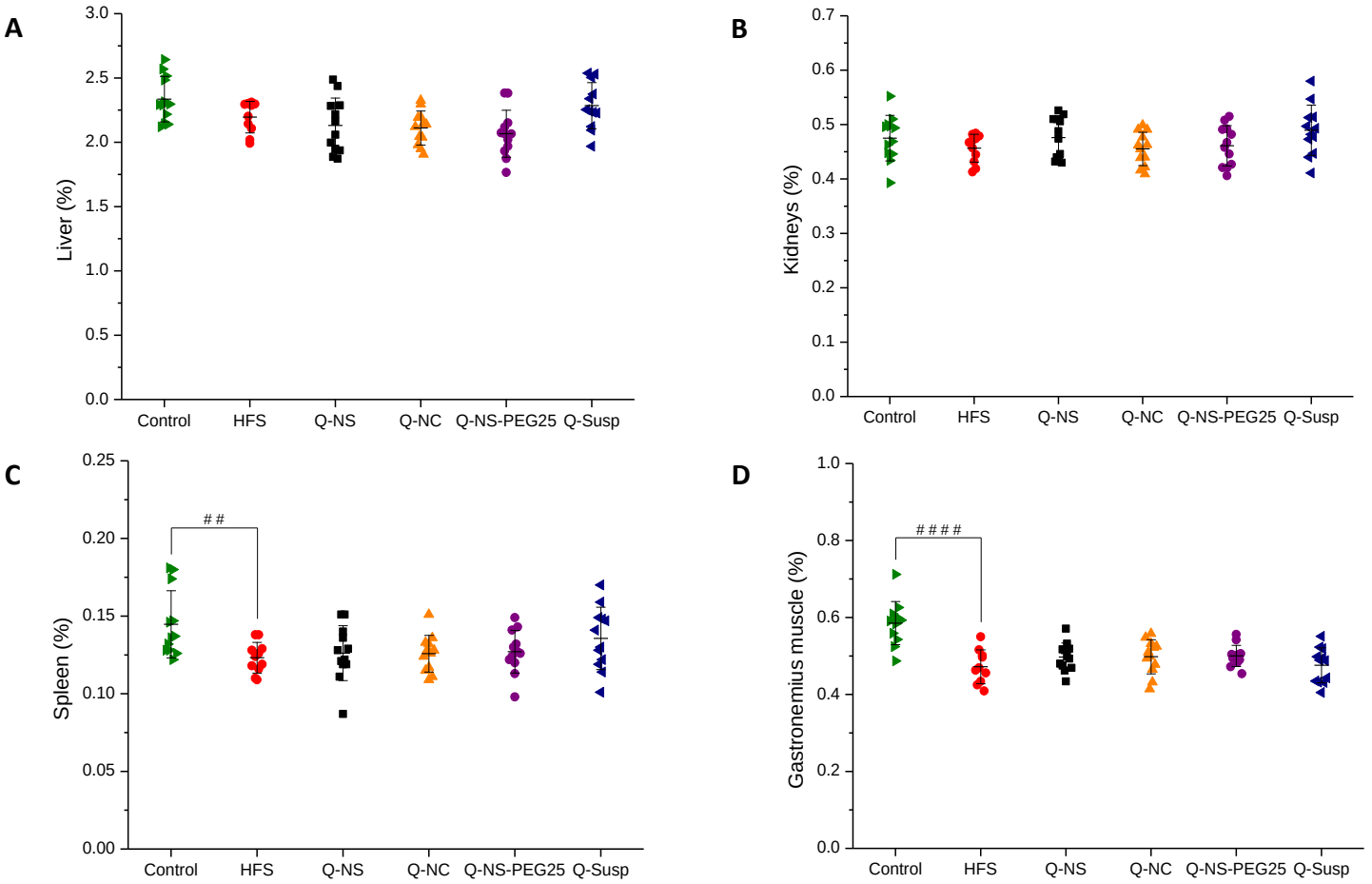

Figure 39. Organs extracted at week 23: liver (**A**), kidneys (**B**), spleen (**C**), and gastrocnemius muscle (**D**) (percentage to total body weight). Data are expressed as mean ± SD ($n \geq 10$). $^{\#\#}p < 0.01$, $^{\#\#\#\#}p < 0.0001$, HFS compared to Control. Control: standard diet; HFS: high fat/high sucrose diet; Q-NS; quercetin-loaded nanospheres; Q-NC: quercetin-loaded nanocapsules; Q-NS-PEG: PEG-coated quercetin-loaded nanospheres; Q-Susp: quercetin suspension.

4.8.3. Oral glucose tolerance test

At week 22, an oral glucose tolerance test (OGTT) was performed. For this purpose, glucose was orally administered to rats and blood levels were measured along the time using a glucometer. In addition, before the start of the treatment (week 17), blood glucose levels were also measured.

Table 13 compares blood glucose levels at weeks 17 and 22. At week 17, Control rats displayed a blood glucose of 103 mg/dL, while in HFS rats this value was significantly increased up to 117 mg/dL ($p < 0.001$). At week 22 (time 0 of the OGTT), Control presented an amount of 108 mg/dL of glucose, while HFS showed significantly higher levels (120 mg/dL; $p < 0.001$), and quercetin treatments slightly decreased these glucose levels compared to HFS.

Table 13. Blood glucose levels of animals before the treatment (week 17) and at the end of the treatment (week 22, time 0 of the OGTT). Data are expressed as mean ± SD ($^{\#\#\#}p < 0.001$, HFS compared to Control). Control: standard control; HFS: high fat/high sucrose diet; Q-NS: quercetin-loaded nanospheres; Q-NC: quercetin-loaded nanocapsules; Q-NS-PEG: PEG-coated quercetin-loaded nanospheres; Q-Susp: quercetin suspension.

	Week 17 (mg/dL)
Control (n = 12)	103 ± 12
HFS (n = 59)	117 ± 10$^{\#\#\#}$

n ≥ 11	**Week 22 (mg/dL)**
Control	108 ± 7
HFS	120 ± 9$^{\#\#\#}$
Q-NS	114 ± 10
Q-NC	113 ± 5
Q-NS-PEG	112 ± 12
Q-Susp	118 ± 12

In the OGTT, the blood glucose concentration profile across time showed a similar shape for all treatments (Figure 40). Control rats started with a lower glycaemia than HFS rats ($p < 0.001$, see also Table 13). Statistics were performed for each timepoint, obtaining that in all of them (except 15 min), blood glucose concentrations were significantly lower for Control than for HFS. Comparing HFS with treatments, ANOVA was statistically significant ($p < 0.05$) for 30 and 60 minutes, but Dunnet's test did not find any differences between HFS and treatments. At the end of the OGTT (150 min), Q-NC and Q-NS-PEG showed lower glucose levels compared to HFS ($p < 0.05$, not shown in the figure, ANOVA $p < 0.01$).

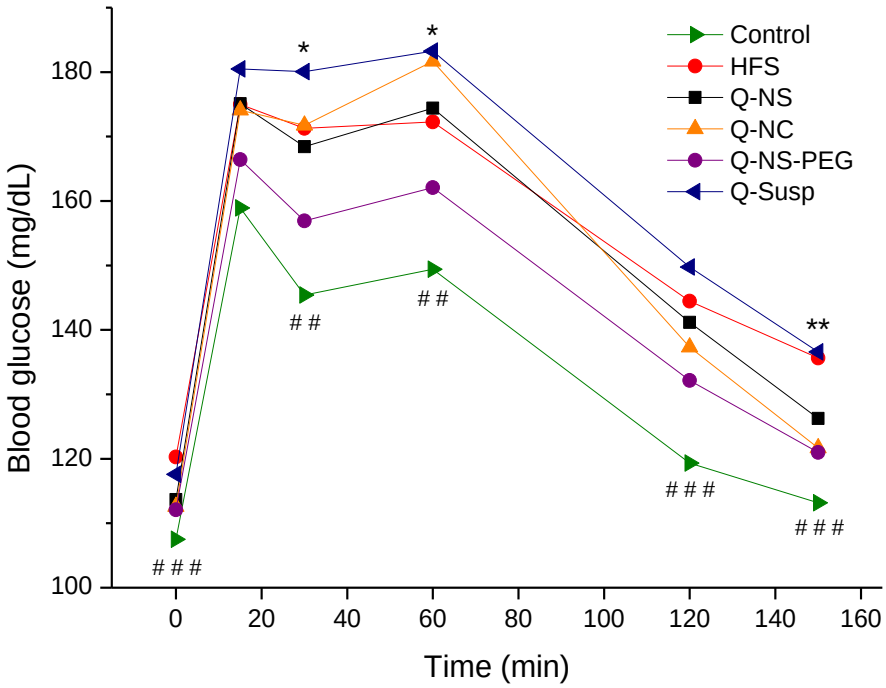

Figure 40. Blood glucose levels across the time in the OGTT. Data are expressed as mean ($n \geq 11$; $^{\#\#}p < 0.01$, $^{\#\#\#}p < 0.001$, HFS compared to Control; ANOVA $*p < 0.05$, $**p < 0.01$, treatments compared to HFS). Control: standard control; HFS: high fat/high sucrose diet; Q-NS: quercetin-loaded nanospheres; Q-NC: quercetin-loaded nanocapsules; Q-NS-PEG: PEG-coated quercetin-loaded nanospheres; Q-Susp: quercetin suspension.

Table 14 summarizes the maximum glucose concentration obtained for the OGTT as a function of the treatment. Control, HFS, Q-NS, and Q-NS-PEG achieved the maximum glucose concentration 15 minutes after the administration, while Q-NC and Q-Susp reached this maximum one hour post-administration. Maximum concentrations obtained ranged from 160 to 180 mg/dL. Even if no statistical differences were found, Control achieved a lower C_{max} (159 mg/dL) compared to HFS. In a similar way, animals treated with Q-NS-PEG presented a slightly lower glucose C_{max} than the other HFS-fed animals.

In addition, the areas under the curve (AUC) of the OGTT profiles were calculated (Figure 41). As expected, HFS presented a significantly higher AUC than Control (14%; $p < 0.0001$). Any differences were found in the AUC between HFS and the rest of the treatments by Dunnett's test, even if ANOVA was significant ($p < 0.01$), meaning that free or encapsulated quercetin did not improve the AUC of the OGTT study compared to HFS. In any case, the tendency observed was that Q-NS-PEG decreased the AUC by 8% compared to HFS group.

Table 14. Maximum glucose concentration (C_{max}) and the time when this concentration was reached (T_{max}) obtained for the OGTT. Control: standard control; HFS: high fat/high sucrose diet; Q-NS: quercetin-loaded nanospheres; Q-NC: quercetin-loaded nanocapsules; Q-NS-PEG: PEG-coated quercetin-loaded nanospheres; Q-Susp: quercetin suspension.

	T_{max} (min)	C_{max} (mg/dL)
Control	15	159 ± 20
HFS	15	175 ± 23
Q-NS	15	175 ± 23
Q-NC	60	182 ± 15
Q-NS-PEG	15	166 ± 15
Q-Susp	60	183 ± 14

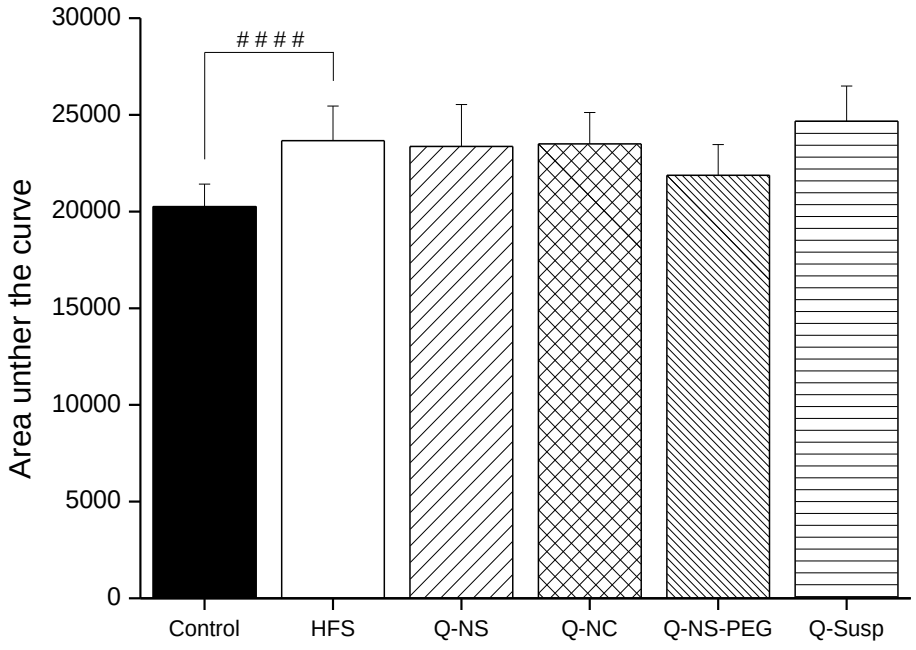

Figure 41. Area under the curve for each treatment obtained for the OGTT. Data are expressed as mean ± SD (n ≥ 11; $^{####}p < 0.0001$, HFS compared to Control). Control: standard control; HFS: high fat/high sucrose diet; Q-NS: quercetin-loaded nanospheres; Q-NC: quercetin-loaded nanocapsules; Q-NS-PEG: PEG-coated quercetin-loaded nanospheres; Q-Susp: quercetin suspension.

4.8.4. Biochemical analysis

After the sacrifice of the animals (week 23), blood samples were collected, and some biochemical parameters were quantified (Figures from 42 to 48). The biochemical parameters were: serum total cholesterol, HDL-cholesterol, triglycerides (TAG), alanine

transaminase (ALT), aspartate transaminase (AST), and glucose, and also plasma insulin and monocyte chemoattractant protein-1 (MCP-1).

Control rats displayed a total serum cholesterol of 90 mg/dL, while HFS control and treatments ranged from 97 to 106 mg/dL, but no significant differences were found, neither between HFS and Control nor between treatments and HFS (Figure 42A). Consequently, HFS diet did not have any effect on the serum total cholesterol levels, during the evaluated period of time.

Regarding HDL-cholesterol (Figure 42B), Control rats presented 28 mg/dL of HDL-cholesterol in serum. This value was significantly lower for animals of the HFS group (up to 26 mg/dL; $p < 0.05$). On the other hand, quercetin treatments did not significantly modify the HDL-cholesterol levels of animals fed with HFS, except for animals treated with Q-Susp ($p < 0.05$).

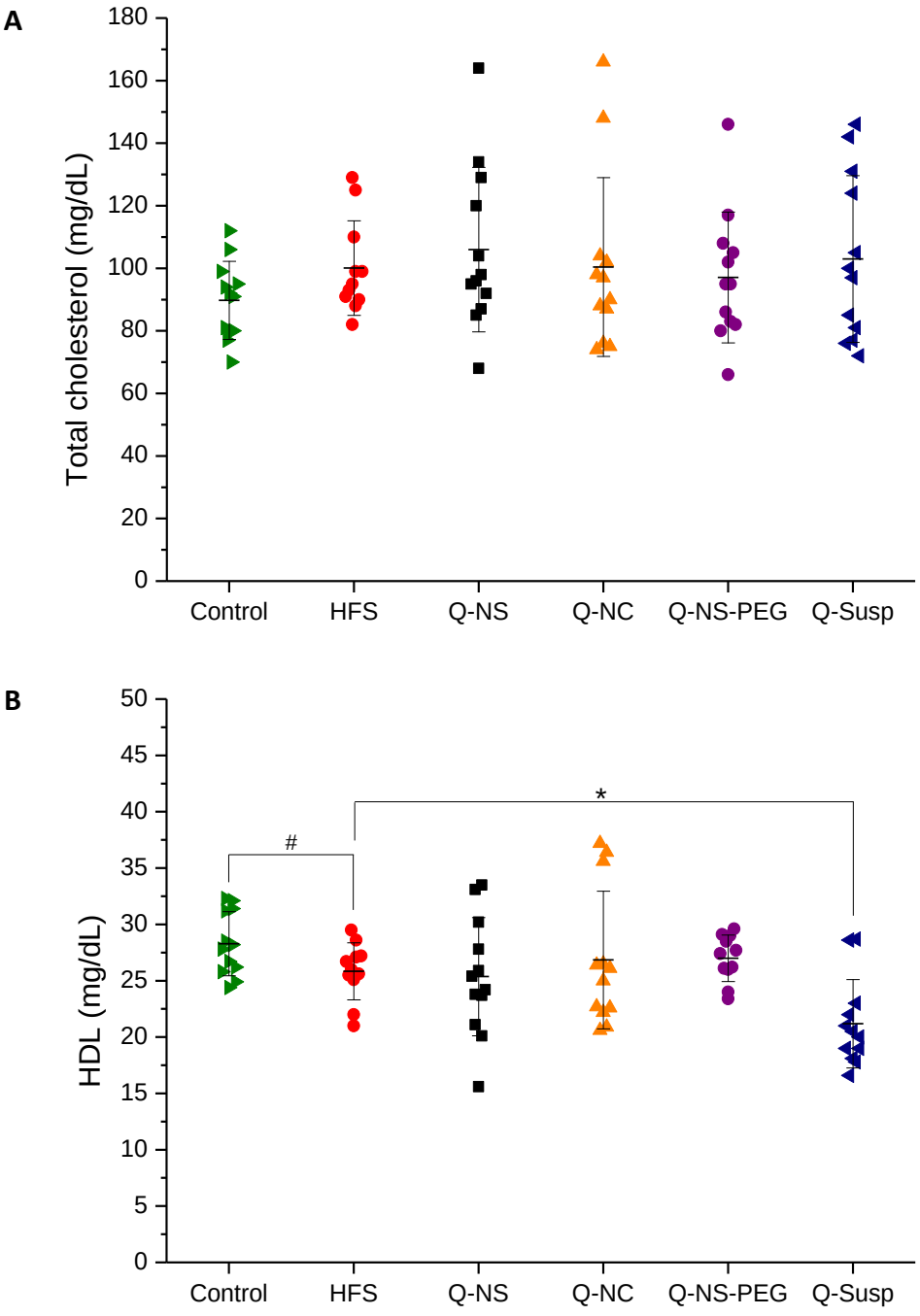

Figure 42. Biochemical parameters obtained in serum at week 23: total cholesterol (**A**) and HDL-cholesterol (**B**). Data are expressed as mean ± SD (n ≥ 11). $^{\#}p < 0.05$, HFS compared to Control. $^{*}p < 0.05$, treatments compared to HFS. Control: standard control; HFS: high fat/high sucrose diet; Q-NS: quercetin-loaded nanospheres; Q-NC: quercetin-loaded nanocapsules; Q-NS-PEG: PEG-coated quercetin-loaded nanospheres; Q-Susp: quercetin suspension.

The ratio between HDL-cholesterol and total cholesterol was also calculated (Figure 43). Control displayed a ratio of 0.32, while for HFS this value was calculated to be 0.26 ($p < 0.01$). Treatments with nanoencapsulated quercetin presented similar HDL/total cholesterol ratio than HFS (between 0.24 and 0.28), and only Q-Susp significantly decreased this ratio (0.22; $p < 0.05$).

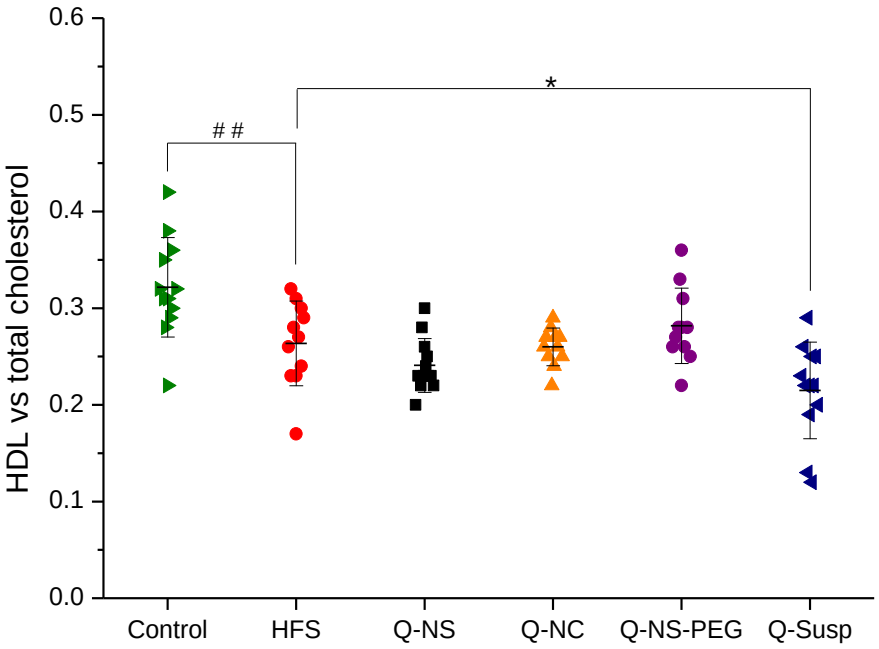

Figure 43. Biochemical parameters obtained in serum at week 23: HDL vs total cholesterol. Data are expressed as mean ± SD ($n \geq 11$). $^{\#\#}p < 0.01$, HFS compared to Control. $^{*}p < 0.05$, treatments compared to HFS. Control: standard control; HFS: high fat/high sucrose diet; Q-NS: quercetin-loaded nanospheres; Q-NC: quercetin-loaded nanocapsules; Q-NS-PEG: PEG-coated quercetin-loaded nanospheres; Q-Susp: quercetin suspension.

Triglycerides (TAG) were also quantified in the serum of animals (Figure 44A). Control rats exhibited 64 mg/dL of triglycerides, value significantly increased in HFS group by 35%, up to 100 mg/dL ($p < 0.0001$). The three kinds of nanoparticles reduced serum triglyceride levels compared to HFS. Animals treated daily with either Q-NS or Q-NC displayed levels of about 57 mg/dL ($p < 0.01$). On the other hand, animals treated with Q-NS-PEG presented the lowest triglyceride values: 49 mg/dL ($p < 0.0001$). These values seemed to be similar to Control.

Using the TAG and HDL-cholesterol data, the atherogenic index of plasma (AIP) was calculated using Equation 12, as shown in Figure 44B. Control rats presented an AIP of 0.35, while this index was significantly higher for HFS (0.58; $p < 0.0001$). These results are in accordance with TAG and HDL results (for HFS, higher values of TAG and lower values of HDL, increased the AIP). All the treatments of nanoencapsulated quercetin

decreased the AIP in a significant way compared to HFS. Thus, the animals treated with Q-NS presented an AIP of 0.34 ($p < 0.001$), for those treated with Q-NC the AIP was 0.36 ($p < 0.001$) and the index for animals receiving Q-NS-PEG offered an AIP of 0.27 ($p < 0.0001$).

Alanine transaminase (ALT) and aspartate transaminase (AST) were also quantified in serum (Figure 45). For ALT (Figure 45A), Control and HFS displayed similar levels; Control presented 51.4 U/L and HFS 48.3 U/L of ALT. All treatments showed slightly lower values, between 44 and 50 U/L. A similar effect was seen for AST (Figure 45B), where Control presented 179.6 U/L and HFS 155.7 U/L of AST, and treatments exhibited slightly higher values compared to HFS, being in a range from 174 to 221 U/L. In any case, no statistical differences were found between HFS and Control, or between treatments and HFS, neither for ALT nor AST, indicating that diet and treatments did not have a significant effect on transaminases.

Figure 46 presents the glycaemia and insulin plasma levels of animals as a function of the treatment. For Control animals, the glucose level in serum was of about 120 mg/dL (Figure 46A), whereas for animals fed with HFS, the glycaemia was of about 150 mg/dL ($p < 0.0001$). The animals treated with quercetin formulations, presented glucose levels slightly lower than for animals of the HFS group. However, the animals treated with Q-NS-PEG presented glucose levels in serum significantly lower than HFS (123 mg/dL; $p < 0.01$). These results are in accordance with the OGTT (section 4.8.3), in which the rise of glucose levels by HFS compared to Control was seen, and showing Q-NS-PEG the highest effect at 150 min.

Regarding insulin levels (Figure 46B), Control presented 1.34 µg/L of plasma insulin, while HFS exhibited a significantly higher level (35% more), 2.05 µg/L ($p < 0.001$). Nanoparticles displayed values from 1.7 to 2 µg/L, and Q-Susp presented even a higher value (3.39 µg/L). In the comparison of HFS and treatments, even if the Kruskal-Wallis test was significant ($p < 0.05$), statistical differences were not found between groups.

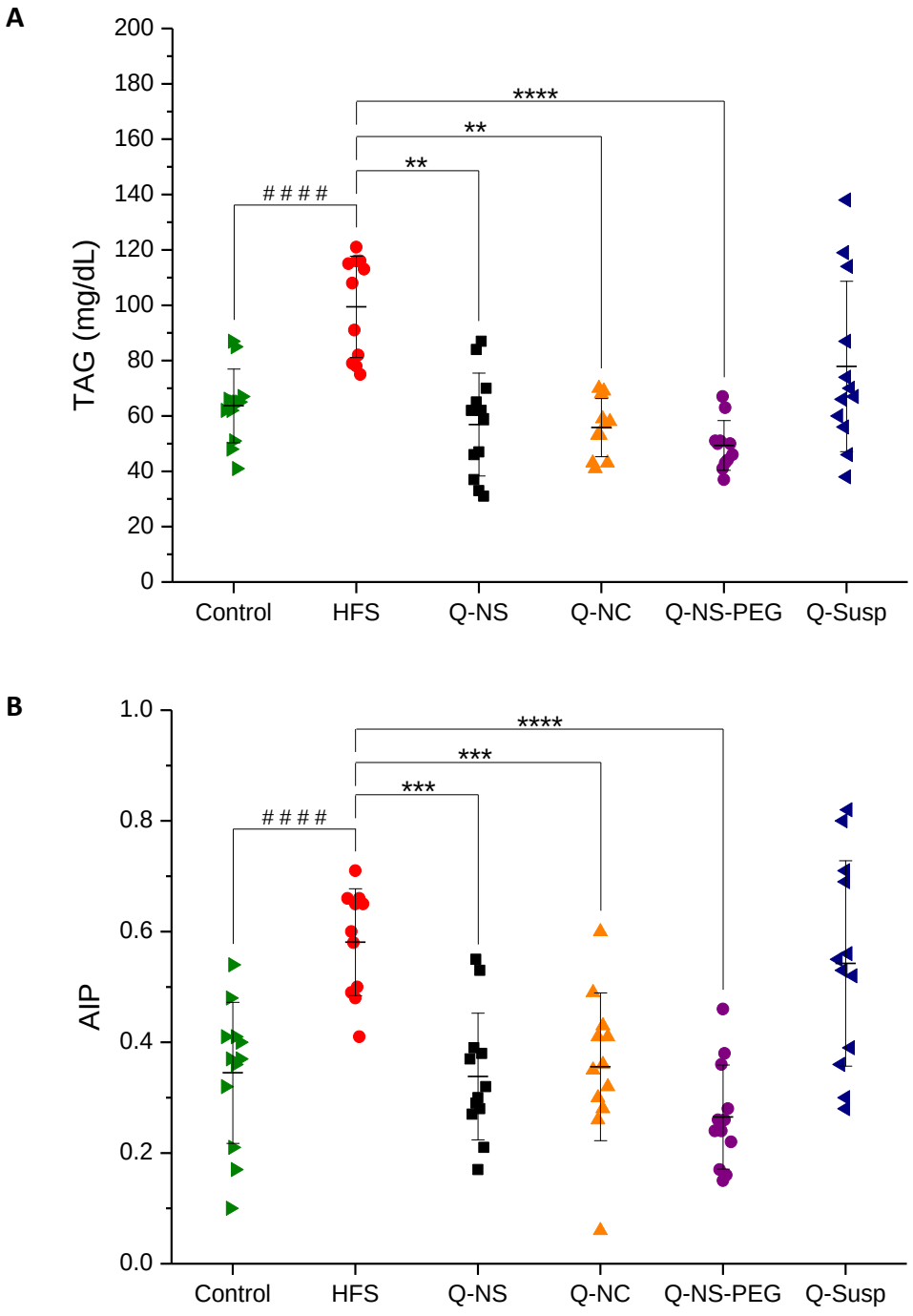

Figure 44. Biochemical parameters obtained in serum at week 23: triglycerides (TAG) (**A**) and atherogenic index of plasma (AIP) (**B**). Data are expressed as mean ± SD (n ≥ 11). ####p < 0.0001, HFS compared to Control. **p < 0.01, ***p < 0.001, ****p < 0.0001, treatments compared to HFS. Control: standard control; HFS: high fat/high sucrose diet; Q-NS: quercetin-loaded nanospheres; Q-NC: quercetin-loaded nanocapsules; Q-NS-PEG: PEG-coated quercetin-loaded nanospheres; Q-Susp: quercetin suspension.

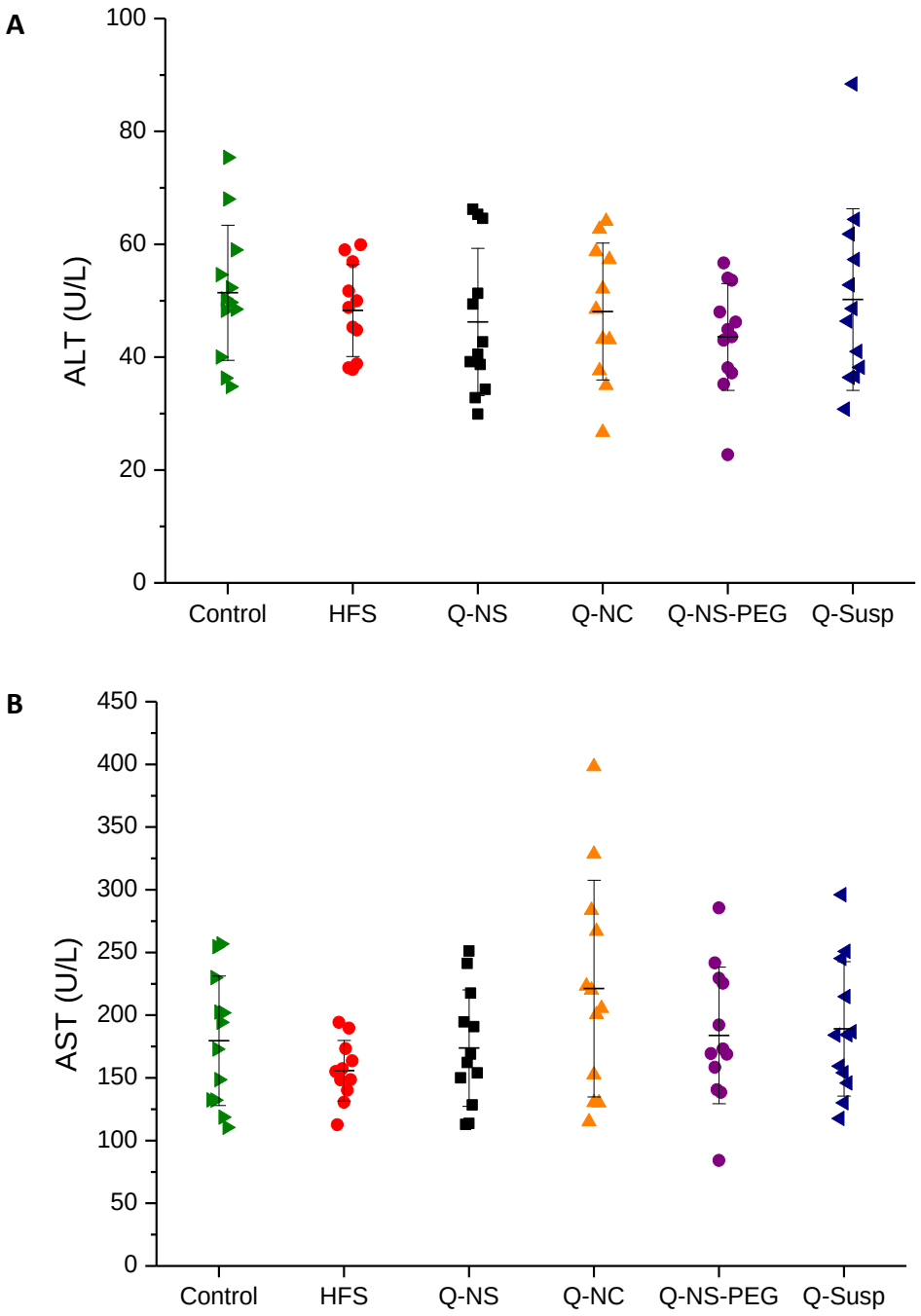

Figure 45. Biochemical parameters obtained in serum at week 23: alanine transaminase (ALT) (**A**) and aspartate transaminase (AST) (**B**). Data are expressed as mean ± SD (n ≥ 11). Control: standard control; HFS: high fat/high sucrose diet; Q-NS: quercetin-loaded nanospheres; Q-NC: quercetin-loaded nanocapsules; Q-NS-PEG: PEG-coated quercetin-loaded nanospheres; Q-Susp: quercetin suspension.

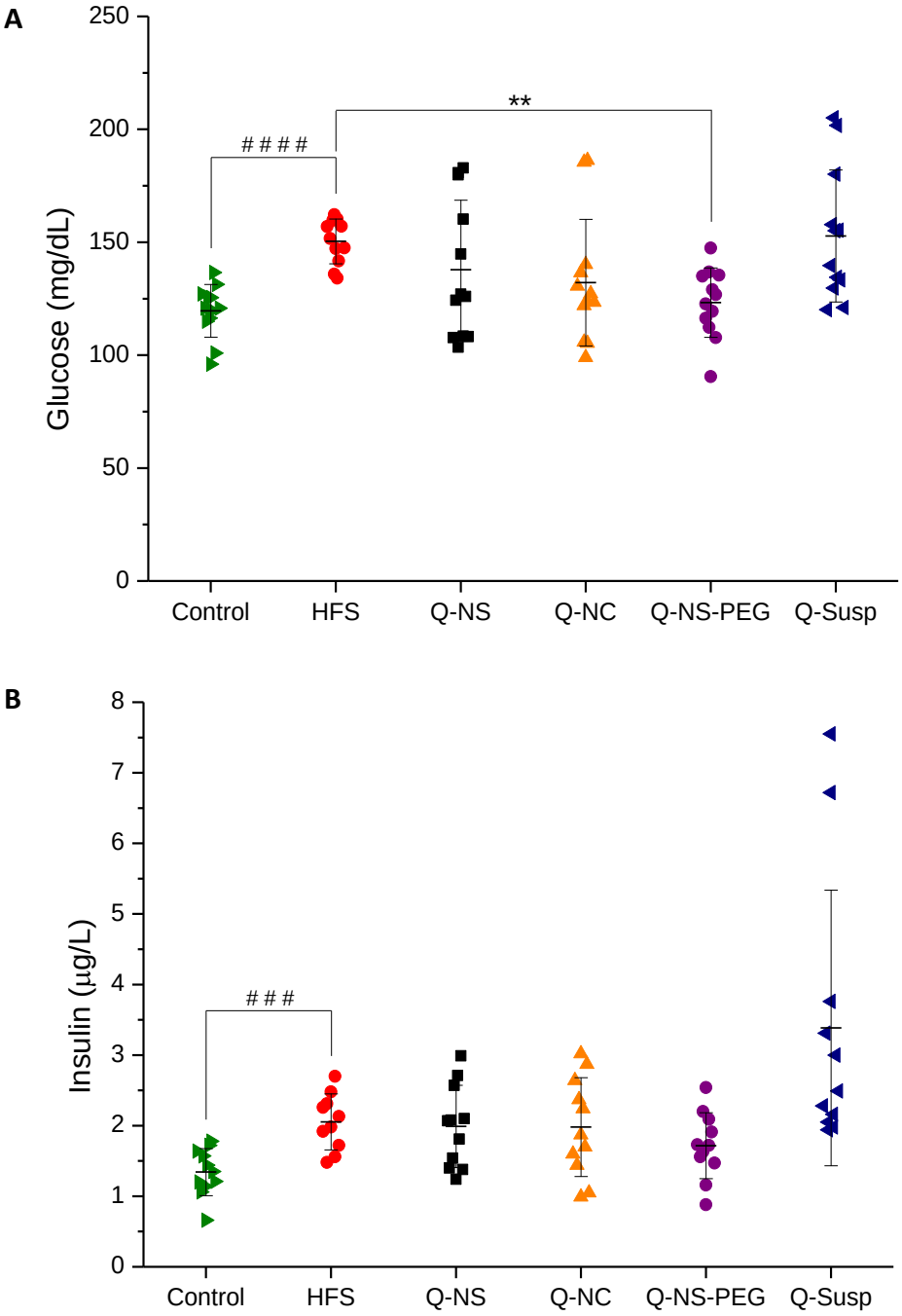

Figure 46. Biochemical parameters obtained in serum and plasma at week 23: glucose (**A**) and insulin (**B**). Data are expressed as mean ± SD (n ≥ 10). $^{\#\#\#}p < 0.001$, $^{\#\#\#\#}p < 0.0001$, HFS compared to Control. **p < 0.01, treatments compared to HFS. Control: standard control; HFS: high fat/high sucrose diet; Q-NS: quercetin-loaded nanospheres; Q-NC: quercetin-loaded nanocapsules; Q-NS-PEG: PEG-coated quercetin-loaded nanospheres; Q-Susp: quercetin suspension.

Linking glucose and insulin levels, the homeostasis model of insulin resistance (HOMA-IR) was calculated using Equation 13. The results are shown in Figure 47. Control animals presented a HOMA-IR of 10.0, while the value for HFS was significantly higher, 18.7 ($p < 0.0001$). All nanoparticles presented a slight decrease compared to HFS. Q-NS and Q-NC presented a HOMA-IR around 16, while Q-NS-PEG exhibited the lowest value, 13.3. Nevertheless, no statistical differences were found between HFS and each treatment, even the Kruskal-Wallis test was significant ($p < 0.001$).

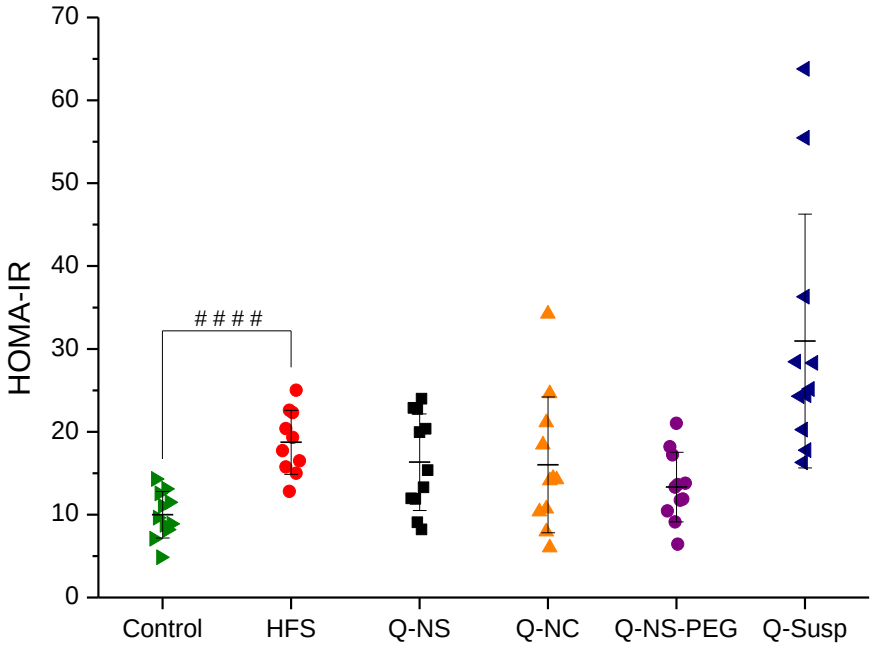

Figure 47. Biochemical parameters obtained in serum at week 23: homeostasis model of insulin resistance (HOMA-IR). Data are expressed as mean ± SD ($n \geq 10$). $^{####}p < 0.0001$, HFS compared to Control. Control: standard control; HFS: high fat/high sucrose diet; Q-NS: quercetin-loaded nanospheres; Q-NC: quercetin-loaded nanocapsules; Q-NS-PEG: PEG-coated quercetin-loaded nanospheres; Q-Susp: quercetin suspension.

Finally, the monocyte chemoattractant protein-1 (MCP-1) in plasma was quantified by ELISA (Figure 48). Control rats exhibited protein levels of 4,832 pg/mL, and this value was significantly increased by HFS diet to 6,843 pg/mL ($p < 0.01$). Al treatments decreased plasma MCP-1 values compared to HFS, three of them in a significant way; Q-NS displayed MCP-1 levels of 4,696 pg/mL ($p < 0.05$), Q-NS-PEG 4,642 pg/mL ($p < 0.05$) and Q-Susp 3,930 pg/mL ($p < 0.0001$). These results seem to be similar to the Control ones.

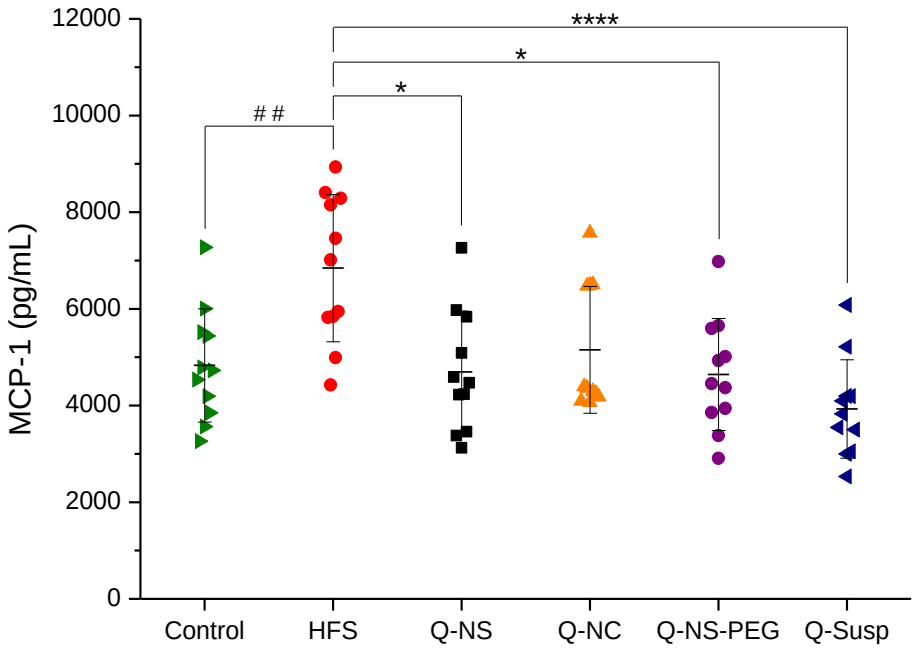

Figure 48. Biochemical parameters obtained in plasma at week 23: monocyte chemoattractant protein-1 (MCP-1). Data are expressed as mean ± SD (n = 11). $^{\#\#}p < 0.01$, HFS compared to Control. *$p < 0.05$, ****$p < 0.0001$, treatments compared to HFS. Control: standard control; HFS: high fat/high sucrose diet; Q-NS: quercetin-loaded nanospheres; Q-NC: quercetin-loaded nanocapsules; Q-NS-PEG: PEG-coated quercetin-loaded nanospheres; Q-Susp: quercetin suspension.

4.8.5. Histological analyses

When livers were extracted at week 23, colour differences were observed at a glance between the Control diet and PEG-coated nanospheres with other high fat/high sucrose diet treatments. Control and Q-NS-PEG presented a reddish bright colour while the livers of the rest of the treatments had a paler colour, with marron dots. An example of the extracted livers is shown in Figure 49.

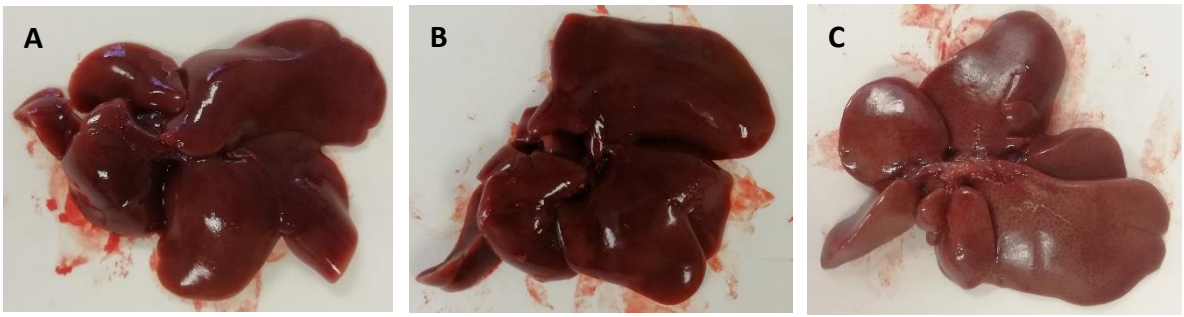

Figure 49. Example of extracted livers. Standard diet (Control, **A**) and two treatments are shown. **B**: PEG-coated quercetin-loaded nanospheres (Q-NS-PEG); **C**: quercetin suspension (Q-Susp).

These observations were confirmed by histological images presented in Figure 50. For that purpose, liver sections were fixed, dyed with haematoxylin-eosin, and images were taken. In Control livers, healthy hepatocytes were seen, but in HFS rats, hepatic steatosis was observed, as white lines among cells. Steatosis is characterized as the accumulation of small or big lipid inclusions, being the bigger ones more usual in alcoholic hepatic steatosis (223). Therefore, our model presents hepatic steatosis due to obesity, and quercetin decreased this steatosis, especially in those animals treated with either Q-NC or Q-NS-PEG.

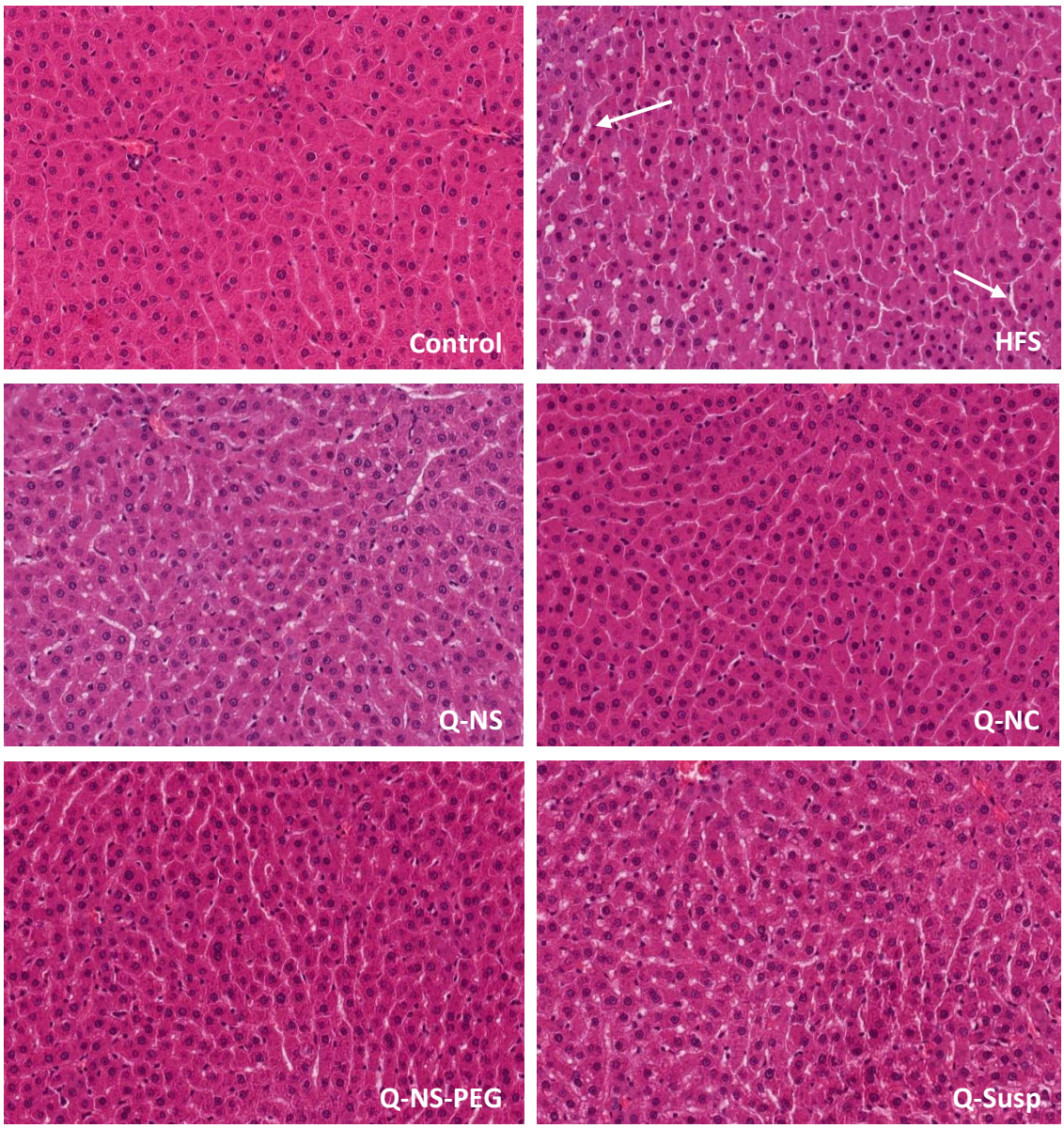

Figure 50. Example of histological analysis of the liver. White arrows indicate steatosis. Control: standard control; HFS: high fat/high sucrose diet; Q-NS: quercetin-loaded nanospheres; Q-NC: quercetin-loaded nanocapsules; Q-NS-PEG: PEG-coated quercetin-loaded nanospheres; Q-Susp: quercetin suspension.

On the other hand, the size of the adipocytes present in the epididymal and retroperitoneal fats was analysed. The size distribution of adipocytes was calculated and, then, the obtained data evaluated by a contingency assay.

In Figure 51 the distribution of the adipocytes in the epididymal and retroperitoneal fat can be observed, classified as extra large, large, medium, and small. This classification was obtained by calculating quartiles for Control and using the values for classifying the rest of the groups in consequence.

In case of the epididymal fat (Figure 51A), HFS presented 42% of extra large adipocytes, while treatments ranged from 32 to 37%. The proportion of large adipocytes was similar in all controls and treatments. Regarding small and medium adipocytes, HFS had an amount of 17% each, while samples were between 20 and 22% for medium, and between 19 and 22% for small adipocytes. All treatments showed an effect, specially on the size of the extra large adipocytes, being Q-NC the ones that have less effect ($p < 0.01$). All this data can be visualized in the pictures of Figure 52. Together with the previous data of fat percentage (Figure 36A) we can obtain that Q-NS and Q-NC decreased the size of the epididymal adipocytes but not the amount of fat, while Q-NS-PEG had the ability to decrease both parameters.

In case of the retroperitoneal fat (Figure 51B), the extra large proportion of adipocytes was similar in HFS and all treatments (39% for HFS and 35-41% for treatments). In the case of large adipocytes, HFS showed 22% of adipocytes and treatments had 20-23%, for medium adipocytes 20% for HFS and 19-21% for treatments, and for small adipocytes 19% for HFS and 18-23% for treatments. Only Q-NS-PEG had a significant effect on the size of the adipocytes of the retroperitoneal fat ($p < 0.0002$), so this formulation not only decreased retroperitoneal fat as shown in Figure 36B, but also the size of the adipocytes of this tissue.

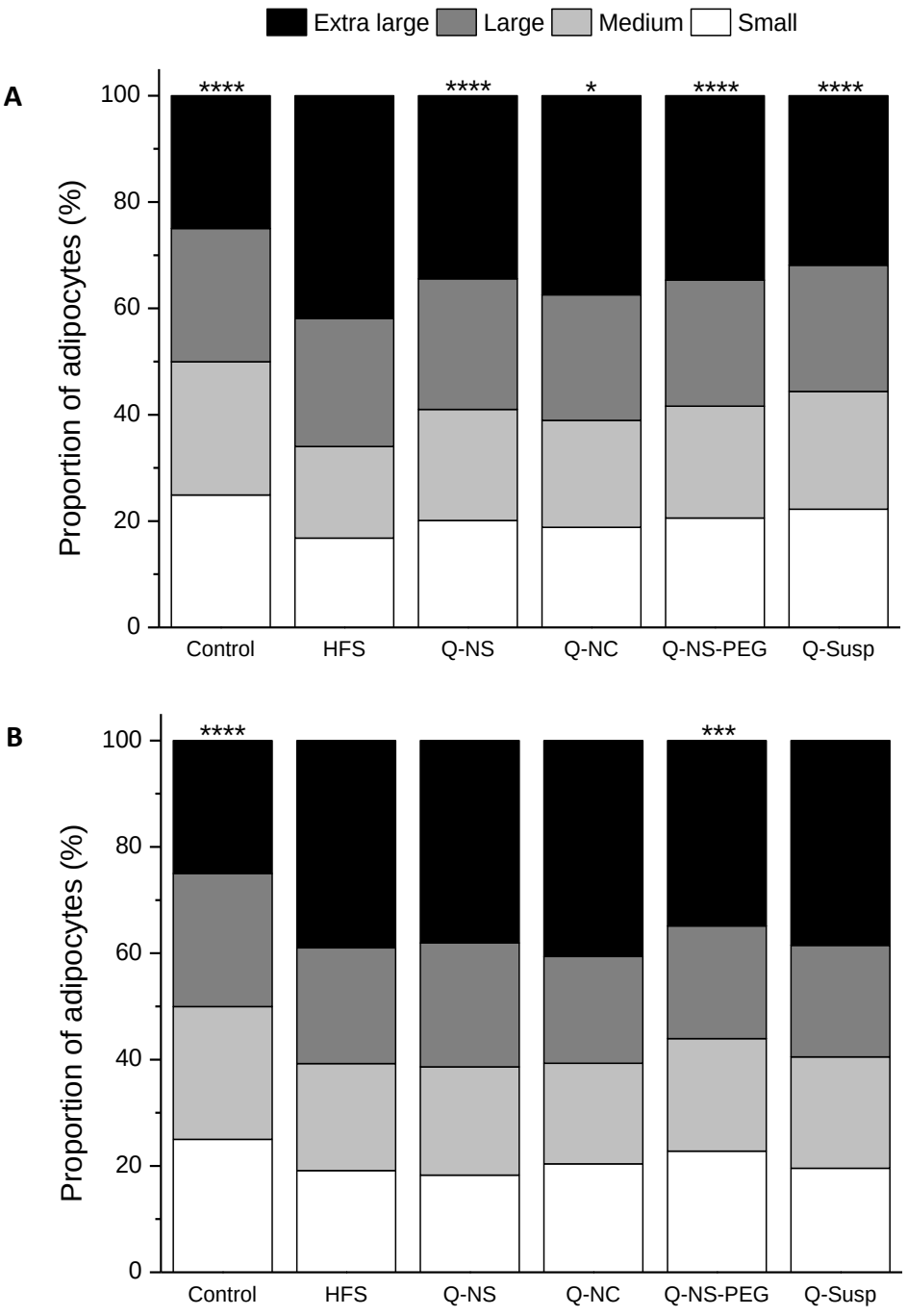

Figure 51. Adipocyte distribution for epididymal (**A**) and retroperitoneal (**B**) fats, classified according to the quartiles obtained for the standard control (Control). Data are expressed as the proportion of the adipocytes for each treatment. Asterisks represent the differences with the HFS group (*p < 0.05/k; **p < 0.01/k; ***p < 0.001/k; ****p < 0.0001/k, where k = 5 is the number of comparisons). HFS: high fat/high sucrose diet; Q-NS: quercetin-loaded nanospheres; Q-NC: quercetin-loaded nanocapsules; Q-NS-PEG: PEG-coated quercetin-loaded nanospheres; Q-Susp: quercetin suspension.

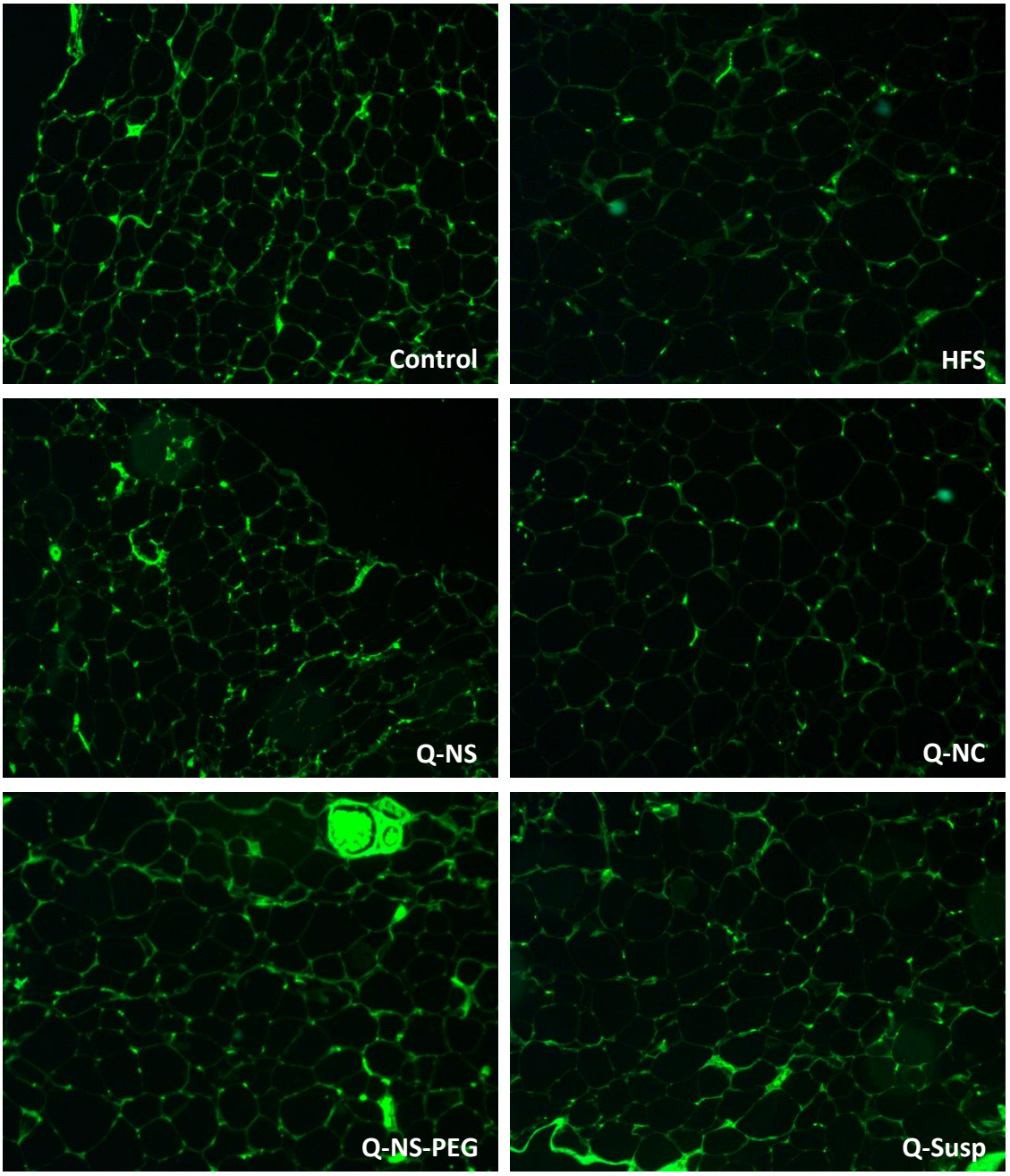

Figure 52. Example of the fluorescent images of the adipocytes from the epididymal fat. Control: standard control; HFS: high fat/high sucrose diet; Q-NS: quercetin-loaded nanospheres; Q-NC: quercetin-loaded nanocapsules; Q-NS-PEG: PEG-coated quercetin-loaded nanospheres; Q-Susp: quercetin suspension.

4.8.6. Hepatic determination of the triglyceride content

At week 23, livers were extracted and frozen until use. Afterwards, organs were defrosted and a portion was cut. These liver sections were broken mechanically, hepatic triglycerides were extracted using chloroform and methanol, and quantified using a commercial Triglyceride Quantification Kit. Data from hepatic triglycerides are presented in Figure 53.

Control livers displayed an amount of 5.0 µg of triglycerides by mg of tissue, while HFS had an amount of 16.3 µg/mg tissue, that is, HFS diet increased the hepatic triglycerides more than three times compared to Control ($p < 0.0001$). These results are consistent with the previous histological analysis of the liver (Figure 50). On the other hand, quercetin showed a slight decrease of this amount compared to HFS, but only Q-NS-PEG decreased significantly hepatic triglycerides ($p < 0.01$), reaching an amount of 10.6 µg triglyceride/mg tissue.

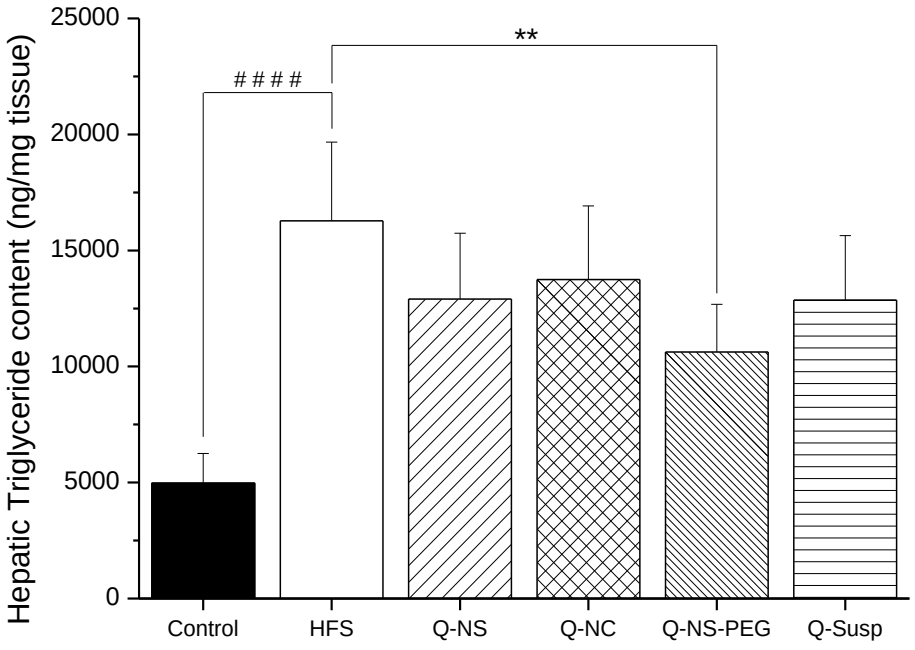

Figure 53. Hepatic triglyceride content, given as ng of triglyceride per mg of liver analysed. Data are expressed as mean ± SD (n = 10). $^{####}p < 0.0001$, HFS compared to Control. $^{**}p < 0.01$, treatments compared to HFS. Control: standard control diet; HFS: high fat/high sucrose diet; Q-NS: quercetin-loaded nanospheres; Q-NC: quercetin-loaded nanocapsules; Q-NS-PEG: PEG-coated quercetin-loaded nanospheres; Q-Susp: quercetin suspension.

4.8.7. Gene expression analyses

With the aim of evaluating the effects of HFS diet and the treatment with Q-NS-PEG in DIO rats, some obesity-related genes were analysed in the liver and retroperitoneal fat of Control, HFS, and Q-NS-PEG groups, by quantitative-real time PCR (qPCR), and evaluated by $2^{-\Delta\Delta Ct}$ method. Different genes were evaluated, such as genes that encode proteins involved in lipid metabolism (*Acot8*, *Acox1*, *Cpt2*, *Hsd17b4*) and synthesis (*Fasn*, *Scp2*), genes encoding adipokines (*AdipoQ*, *Lep*), a gene related to the browning of fat (*Ucp1*), and genes encoding transcription factors related to adipogenesis (*Pparg*, *Srebp1*).

In the liver, slight differences were found regarding the genes that codify proteins involved in lipid metabolism (Figure 54). In this context, *Acot8* gene, which encodes an enzyme present in the peroxisome (Acyl-CoA thioestherase 8, ACOT8) (224), is significantly downregulated in HFS group compared to Control ($p < 0.001$), while Q-NS-PEG slightly upregulated it. In case of *Acox1*, a gene encoding an enzyme involved in the peroxisomal β-oxidation (Acyl-CoA oxidase 1, ACOX1) (225), any significant differences were found among groups, even if slight differences were found (a slight downregulation by HFS and upregulation by Q-NS-PEG). The gene *Cpt2*, which encodes an enzyme (Carnitine palmitoyltransferase-2, CPT2) involved in the mitochondrial β-oxidation (226), was downregulated in HFS and Q-NS-PEG groups compared to Control, but only in the case of the nanospheres this downregulation was significantly lower than Control ($p < 0.05$), although no differences were found with respect to HFS.

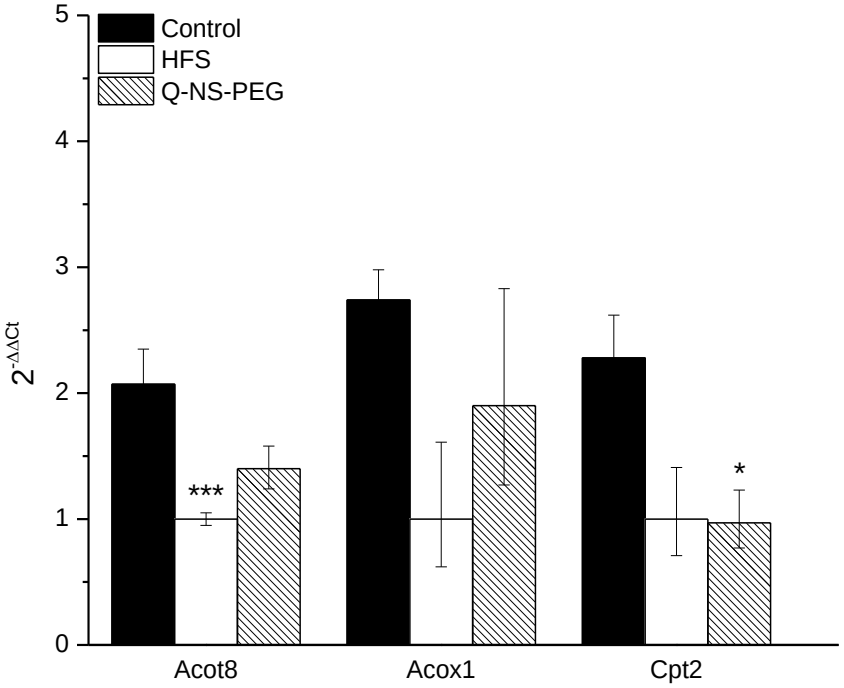

Figure 54. Expression levels of genes encoding proteins involved in the lipid metabolism in the liver: *Acot8*, *Acox1*, and *Cpt2*. Data are expressed as $2^{-\Delta\Delta Ct}$ with respect to HFS, and error bars are expressed as $2^{-(\Delta\Delta Ct-s)}$ and $2^{-(\Delta\Delta Ct+s)}$ ($n \geq 8$). *$p < 0.05$, ***$p < 0.001$, compared to Control. Control: standard control diet; HFS: high fat/high sucrose diet; Q-NS-PEG: PEG-coated quercetin-loaded nanospheres.

Regarding the gene *Fasn* (Figure 55), which encodes the enzyme fatty acid synthase (FASN), involved in lipid de novo synthesis (227), significant differences were found. This gene was significantly underexpressed in both the liver of HFS and Q-NS-PEG treated rats compared to Control ($p < 0.01$ and $p < 0.0001$, respectively). No differences were found between HFS and Q-NS-PEG groups.

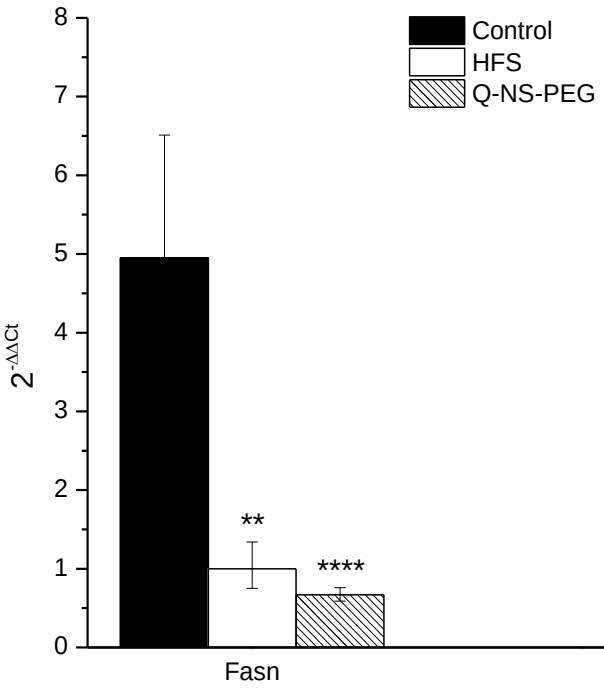

Figure 55. Expression levels of a gene encoding an enzyme involved in the lipid synthesis in the liver: *Fasn*. Data are expressed as $2^{-\Delta\Delta Ct}$ with respect to HFS, and error bars are expressed as $2^{-(\Delta\Delta Ct-s)}$ and $2^{-(\Delta\Delta Ct+s)}$ ($n \geq 8$). **$p < 0.01$, ****$p < 0.0001$, compared to Control. Control: standard control diet; HFS: high fat/high sucrose diet; Q-NS-PEG: PEG-coated quercetin-loaded nanospheres.

Finally, genes encoding two adipogenesis transcription factors were also analysed in the liver, *Pparg* and *Srebp1* (Figure 56), which encode the peroxisome proliferator-activated receptor γ (PPARγ) and the sterol regulatory element-binding protein-1 (SREBP-1), respectively (228,229). Both are transcription factors that activate genes, in the case of PPARγ, for white adipogenesis, and in the case of SREBP-1, for the synthesis of cholesterol and unsaturated fatty acids. In this case, any differences were observed between groups. However, a slight overexpression was observed in *Pparg* in HFS-fed rats, while the treatment with Q-NS-PEG decreased it. Similarly, a slight underexpression was obtained in *Srebp1* in the liver of HFS and Q-NS-PEG groups, compared to Control livers.

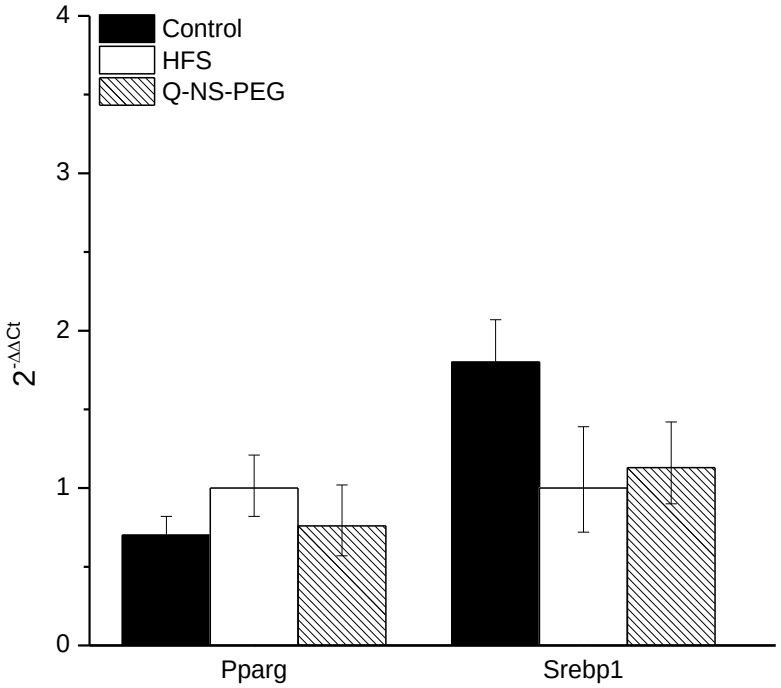

Figure 56. Expression levels of genes encoding transcription factors related to adipogenesis in the liver: *Pparg* and *Srebp1*. Data are expressed as $2^{-\Delta\Delta Ct}$ with respect to HFS, and error bars are expressed as $2^{-(\Delta\Delta Ct-s)}$ and $2^{-(\Delta\Delta Ct+s)}$ ($n \geq 8$). Control: standard control diet; HFS: high fat/high sucrose diet; Q-NS-PEG: PEG-coated quercetin-loaded nanospheres.

Different genes were also evaluated in the retroperitoneal fat of Control, HFS, and Q-NS-PEG groups, and significant differences were found for all the analysed genes (Figures 57 to 61). For genes involved in the lipid metabolism (Figure 57), *Acot8* was significantly downregulated in HFS-fed rats compared to Control rats ($p < 0.05$), while the treatment with Q-NS-PEG increased its overexpression six times compared to HFS ($p < 0.0001$) and three times compared to Control ($p < 0.001$). For *Acox1*, a slight underexpression was obtained in HFS compared to Control, and this gene was significantly overexpressed in the retroperitoneal fat of the rats treated with Q-NS-PEG ($p < 0.001$), compared to HFS rats. The gene *Hsd17b4* was also analysed. This gene encodes the multifunctional enzyme 2 (MFE-2), involved in the peroxisomal β-oxidation (225). It was significantly overexpressed in the retroperitoneal fat of rats treated with the formulation Q-NS-PEG compared to HFS ($p < 0.0001$) and Control ($p < 0.0001$).

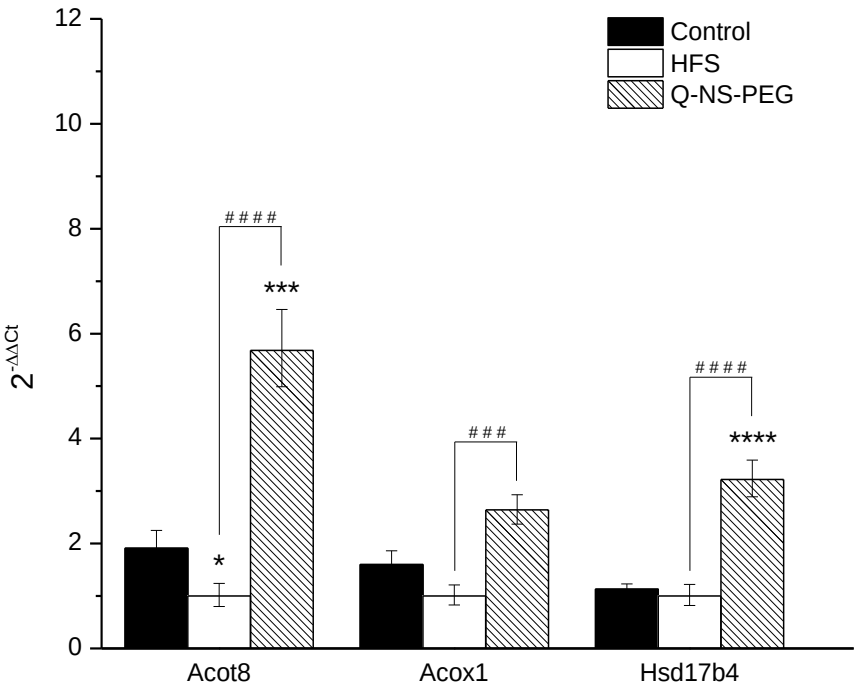

Figure 57. Expression levels of genes encoding proteins involved in the lipid metabolism in retroperitoneal fat: *Acot8*, *Acox1*, and *Hsd17b4*. Data are expressed as $2^{-\Delta\Delta Ct}$ with respect to HFS, and error bars are expressed as $2^{-(\Delta\Delta Ct-s)}$ and $2^{-(\Delta\Delta Ct+s)}$ ($n \geq 7$). *$p < 0.05$, ***$p < 0.001$, ****$p < 0.0001$, compared to Control. $^{\#\#\#}p < 0.001$, $^{\#\#\#\#}p < 0.0001$, Q-NS-PEG compared to HFS. Control: standard control diet; HFS: high fat/high sucrose diet; Q-NS-PEG: PEG-coated quercetin-loaded nanospheres.

Genes related to the lipid synthesis were also quantified in retroperitoneal fat (Figure 58). *Fasn* was significantly downregulated in HFS rats compared to Control ($p < 0.0001$), and the treatment with Q-NS-PEG significantly increased the expression of this gene when comparing to HFS ($p < 0.05$). The gene *Scp2* was also analysed, which encodes the sterol carrier protein-2 (SCP-2), involved in the transport of cholesterol and other lipids (230). No differences were found between HFS and Control expression levels, but the retroperitoneal fat of Q-NS-PEG rats significantly overexpressed this gene, both compared to HFS ($p < 0.05$) and Control ($p < 0.01$).

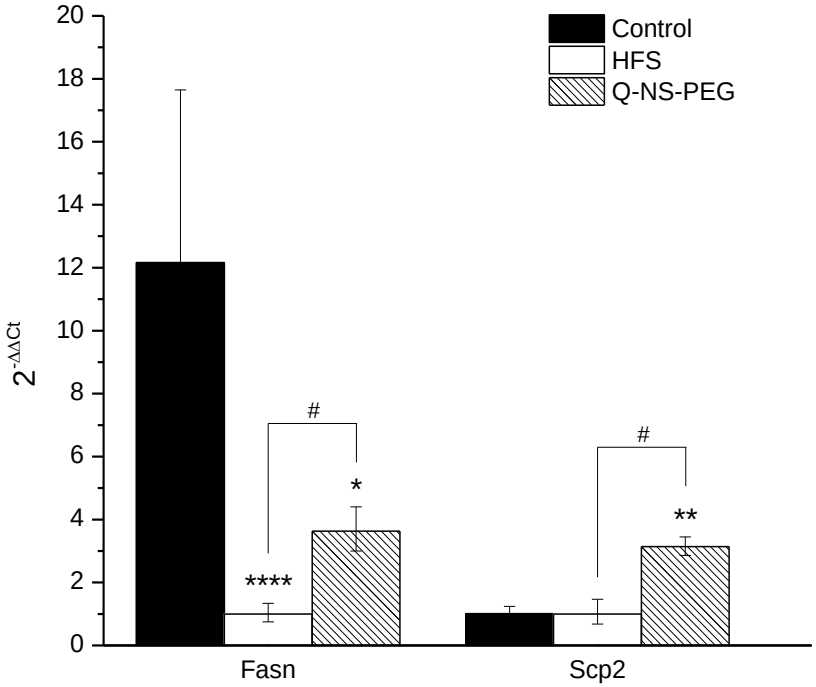

Figure 58. Expression levels of genes encoding proteins involved in the lipid synthesis in retroperitoneal fat: *Fasn* and *Scp2*. Data are expressed as $2^{-\Delta\Delta Ct}$ with respect to HFS, and error bars are expressed as $2^{-(\Delta\Delta Ct-s)}$ and $2^{-(\Delta\Delta Ct+s)}$ ($n \geq 7$). *$p < 0.05$, **$p < 0.01$, ****$p < 0.0001$, compared to Control. $^{\#}p < 0.05$, Q-NS-PEG compared to HFS. Control: standard control diet; HFS: high fat/high sucrose diet; Q-NS-PEG: PEG-coated quercetin-loaded nanospheres.

Two genes encoding adipokines (molecules secreted by adipocytes) were also evaluated in the retroperitoneal fat of Control, HFS, and Q-NS-PEG groups (Figure 59). *AdipoQ*, encoding adiponectin, and *Lep*, encoding leptin (231) were analysed. For *AdipoQ*, the gene was significantly downregulated by the HFS diet compared to Control ($p < 0.01$), and significantly upregulated by the treatment with Q-NS-PEG, both compared to HFS ($p < 0.0001$) and Control ($p < 0.01$). *Lep* was slightly upregulated in HFS rats, and significantly upregulated by Q-NS-PEG, obtaining levels six times higher than for HFS ($p < 0.05$).

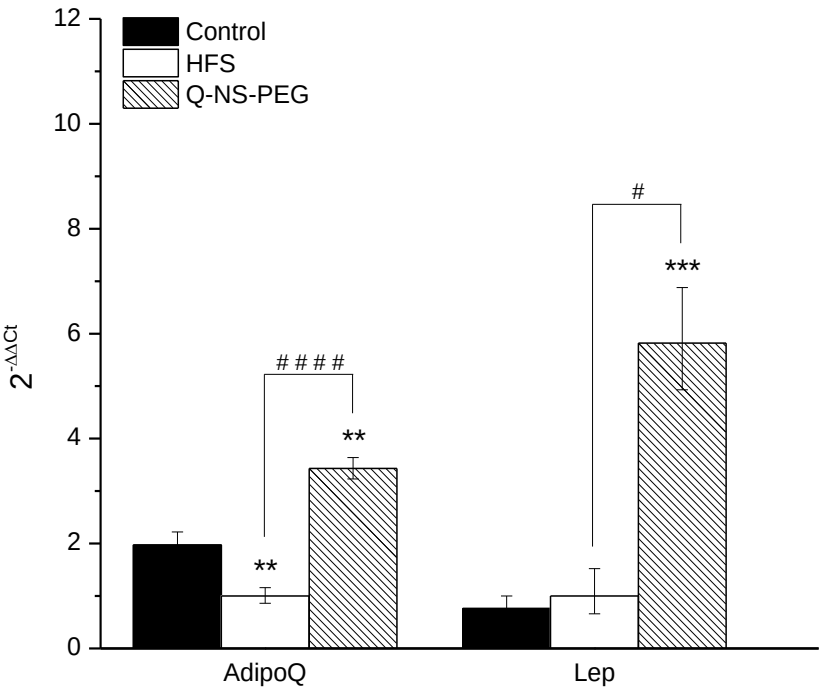

Figure 59. Expression levels of genes encoding adipokines in retroperitoneal fat: *AdipoQ* and *Lep*. Data are expressed as $2^{-\Delta\Delta Ct}$ with respect to HFS, and error bars are expressed as $2^{-(\Delta\Delta Ct-s)}$ and $2^{-(\Delta\Delta Ct+s)}$ (n ≥ 7). *p < 0.05, **p < 0.01, ***p < 0.001, ****p < 0.0001, compared to Control. $^{\#}$p < 0.05, $^{\#\#\#\#}$p < 0.0001, Q-NS-PEG compared to HFS. Control: standard control diet; HFS: high fat/high sucrose diet; Q-NS-PEG: PEG-coated quercetin-loaded nanospheres.

In the retroperitoneal fat, the *Ucp1* gene was also analysed (Figure 60), which encodes the uncoupling protein 1 (UCP1), a proton channel involved in the browning of the adipose tissue (232). In this case, Q-NS-PEG group presented an overexpression of *Ucp1* of almost 170 times higher than in HFS group (p < 0.001), being the most remarkable result of gene expression analysis, and indicating that white adipose tissue was suffering the process of browning due to the treatment with Q-NS-PEG.

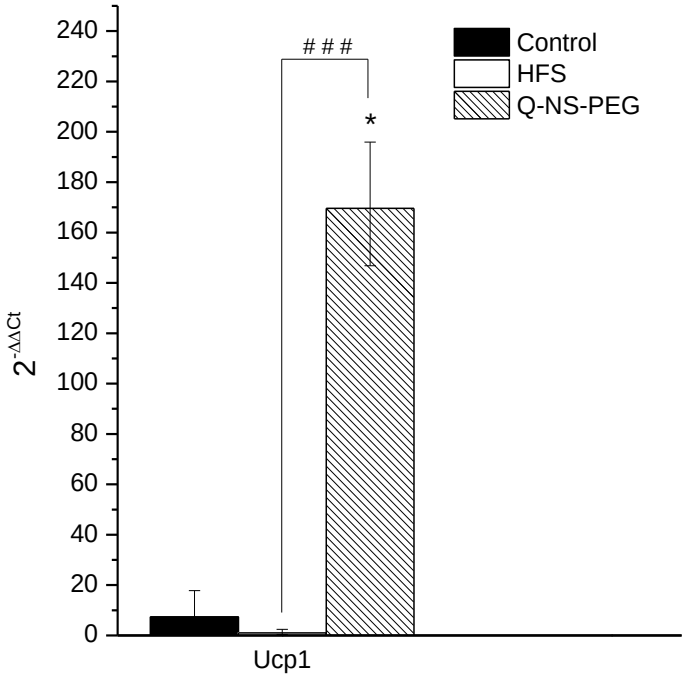

Figure 60. Expression levels of a gene related to the browning of fat in retroperitoneal fat: *Ucp1*. Data are expressed as $2^{-\Delta\Delta Ct}$ with respect to HFS, and error bars are expressed as $2^{-(\Delta\Delta Ct-s)}$ and $2^{-(\Delta\Delta Ct+s)}$ ($n \geq 8$). *$p < 0.05$, ***$p < 0.001$, compared to Control. $^{\#\#\#}p < 0.001$, Q-NS-PEG compared to HFS. Control: standard control diet; HFS: high fat/high sucrose diet; Q-NS-PEG: PEG-coated quercetin-loaded nanospheres.

Finally, genes encoding adipogenesis transcription factors (*Pparg* and *Srebp1*) were evaluated in the retroperitoneal fat of rats (Figure 61). *Pparg* was significantly underexpressed in HFS rats compared to Control rats ($p < 0.001$), while the treatment with the formulation Q-NS-PEG significantly overexpressed this gene, both compared to HFS (five times higher, $p < 0.0001$) and Control ($p < 0.0001$). Similar results were obtained for *Srebp1*, where the gene was significantly decreased in the retroperitoneal fat of HFS rats compared to Control ones ($p < 0.001$), and the treatment with Q-NS-PEG significantly overexpressed this gene, compared to HFS ($p < 0.0001$) and Control ($p < 0.05$).

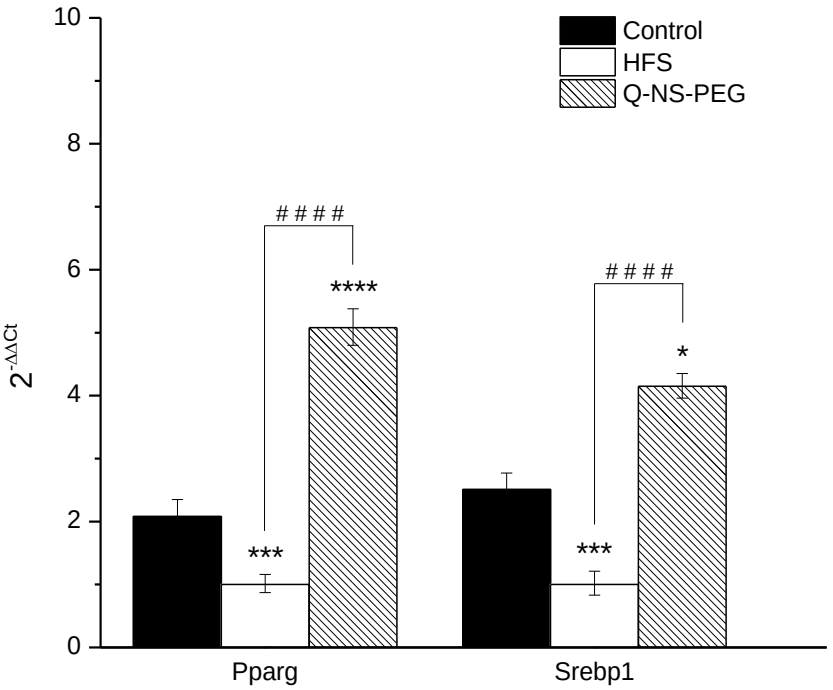

Figure 61. Expression levels of genes encoding transcription factors related to adipogenesis in retroperitoneal fat: *Pparg* and *Srebp1*. Data are expressed as $2^{-\Delta\Delta Ct}$ with respect to HFS, and error bars are expressed as $2^{-(\Delta\Delta Ct-s)}$ and $2^{-(\Delta\Delta Ct+s)}$ ($n \geq 9$). *$p < 0.05$, ***$p < 0.001$, ****$p < 0.0001$, compared to Control. $^{\#\#\#\#}p < 0.0001$, Q-NS-PEG compared to HFS. Control: standard control diet; HFS: high fat/high sucrose diet; Q-NS-PEG: PEG-coated quercetin-loaded nanospheres.

Chapter 5

Discussion

5. Discussion

5.1. Why zein nanoparticles were selected as vehicles for quercetin administration?

Zein is the major storage protein of corn (233). Its origin from renewable sources, its biodegradability, price, and GRAS (Generally Recognized as Safe) regulatory status by FDA justify its choice for pharmaceutical, cosmetic, food, or nutraceutical applications, such as coating for tablets, as an excipient, food coating, or packaging, or to manufacture biodegradable plastics, adhesives, or textile fibers (233,234). Zein is not considered a human food product because of its insolubility and poor nutritional value (it lacks some essential amino acids) (234). Because of all these reasons, zein is a good choice to prepare nanoparticles for the oral delivery of bioactives. This protein can be easily transformed into nanoparticles by desolvation or coacervation methods, starting from a hydroalcoholic solution and adding water to form fractal-like nanoparticles, without using toxic reagents (161,233).

Zein-based nanoparticles have previously been studied for the oral administration of hydrophilic (235) and hydrophobic (236) compounds. Among the hydrophobic compounds, quercetin was previously encapsulated in zein nanoparticles using the desolvation method (108,195,198,199). The average sizes described in previous works are similar to those obtained in this work (Table 15), with differences probably owing to slight changes in the methodology or the presence of coatings. Regarding the quercetin loading, the payload of the flavonoid obtained in this work was similar to that described by Penalva *et al.* (108) or Moreno *et al.* (195) (around 70 μg quercetin/mg nanoparticles). Those payload levels are significantly higher than that obtained by Zhou *et al.* (199) (between 1.6 and 2.9% of quercetin loading, equivalent to 16-29 μg quercetin/mg nanoparticles).

Table 15. Quercetin-loaded zein-based nanoparticles developed by desolvation method present in the literature. NP: nanoparticles. PW: present work.

Formulation	Size (nm)	Payload	Reference
Nanospheres, nanocapsules	225 - 254	69.5 – 76 μg/mg NP	PW
NP	358	62.4 μg/mg NP	(108)
NP with HP-β-CD	294	68.7 μg/mg NP	
NP with HP-β-CD	260	70 μg/mg NP	(195)
NP with caseinate coating	198	1.6%	(199)
NP with caseinate-chitosan coating	1011	2.9%	

5.2. What were the expected advantages from the formulation of zein-based nanocapsules?

Two strategies were followed to improve the characteristics of the zein nanospheres (NS). The first strategy was based on the addition of an oil to form zein nanocapsules (NC), in order to improve the quercetin loading, modify the *in vitro* release, and promote the quercetin absorption by the lymphatic system (96), minimizing its pre-systemic metabolism. For this purpose, wheat germ oil was chosen. Wheat germ oil is used for formulation purposes (in the medicine or cosmetic industry) and as a dietary supplement (237,238).

Wheat germ oil was successfully entrapped in zein nanocapsules, as confirmed by FTIR assay (4.1.4 section). However, any differences were found in the quercetin loading (Table 9) or in the *in vitro* release profile of the flavonoid (Figure 16) when compared with quercetin-loaded nanospheres (Q-NS). This could mean that quercetin was only partly dissolved in the oil, due to a similar payload but a slightly higher amount released at 10 h in the *in vitro* release, or that the oil-to-zein ratio (0.10 w/w) was not high enough to dissolve the flavonoid and modify the characteristics of nanoparticles. Furthermore, the relative oral bioavailability (Fr) was not improved (Table 12), indicating that quercetin absorption by the lymphatic system was not promoted, probably due to the mentioned reasons. Besides, a faster transit into the gastrointestinal tract probably caused a higher difficulty to release all the loaded quercetin, giving a lower relative oral bioavailability compared to Q-NS.

5.3. What were the expected advantages from the coating of nanospheres with PEG?

The intestinal epithelium is covered with a mucus layer, which is secreted by Goblet cells. When nanoparticles are orally administered, they must pass through the mucus in order to reach the surface of the enterocytes. Their passage through this mucus layer depends on their physico-chemical characteristics, particularly size, shape, and surface properties (141,239). Regarding the size, nanocarriers decrease their ability to diffuse through the mucus when the size increases (240). Regarding surface characteristics, neutral nanoparticles larger than 50-55 nm are not able to cross the mucus layer. Cationic particles would remain trapped in the negatively charged mucus, while anionic nanoparticles could cross the mucus layer (Figure 62) (141,239). In addition, mucus-permeating systems can be developed, classified as active and passive systems. Active systems interact with the mucus layer and can partially break down the three-dimensional structure of the mucus. Passive systems, however, minimize the development of adhesive interactions of nanoparticles with the mucus (240).

Among the passive systems, one strategy is the modification of the surface by PEGylation (240,241). It has been demonstrated that nanoparticles can cross the intestinal mucus layer when they are coated with polyethylene glycol (PEG) (Figure 62)

(209,235,239). In this context, the second strategy for our zein-based nanospheres consisted in the coating of the nanospheres with PEG 35,000, to confer them mucus-permeating properties. PEG is a GRAS considered polymer used as an excipient (241,242) that can be adsorbed into the surface of zein-based nanoparticles, with the advantage of simple operation and the lack of new chemical entities (201,243).

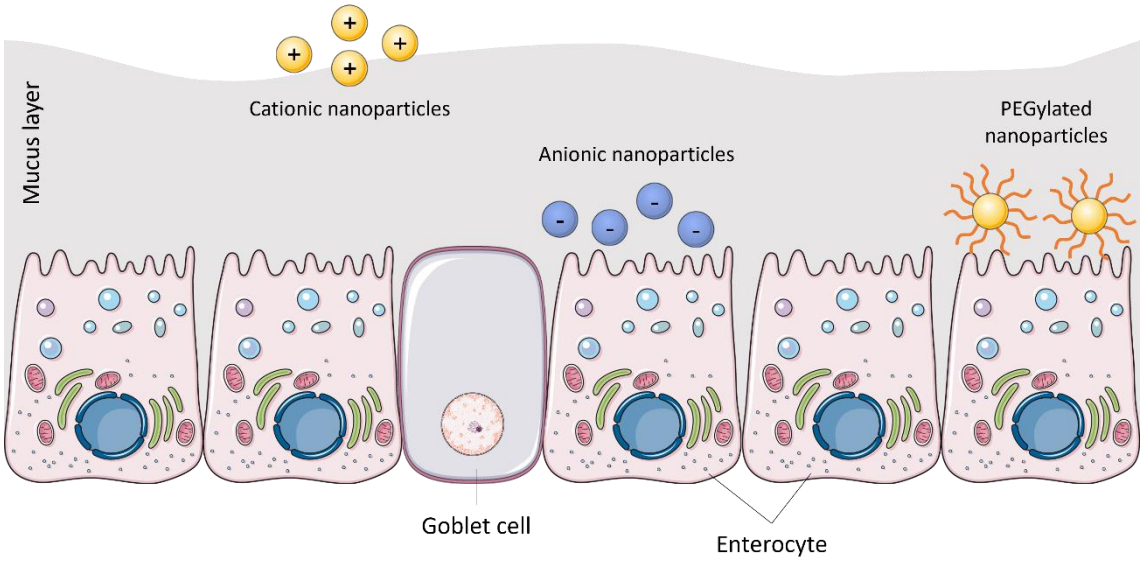

Figure 62. Schematic representation of the behaviour of mucoadhesive and mucus-permeating nanoparticles in the gastrointestinal tract.

Recently, Reboredo *et al.* reported the production of PEG-coated zein nanoparticles, demonstrating the presence of PEG in the nanoparticles by FTIR (201). In this work, the surface modification was confirmed by the hydrophobicity assay (section 4.1.3), where PEG conferred hydrophilic properties to the hydrophobic surface of zein nanospheres. The diffusive properties of these nanoparticles (NS-PEG) through the pig intestinal mucus were higher than for bare nanospheres (NS) (section 4.4). This observation is in line with the hydrophobic characteristics obtained by the Rose Bengal method. Coated nanospheres were less hydrophobic than NS, which is related to the higher penetration capability in intestinal mucus. Thus, these coated nanospheres showed an improved capability to diffuse through the mucus. These results are in accordance with previously reported ones, in which PEG demonstrated to improve mucus permeating properties of different kinds of nanoparticles (201,209,244).

5.4. Why evaluate the developed formulations in *Caenorhabditis elegans*?

Caenorhabditis elegans is a transparent nematode that lives in soil, being an adult worm approximately 1 mm long. It presents a short life cycle; this nematode develops from an egg into a fertile adult in 3 days at 25 °C. It is a multicellular organism with an invariant number of somatic cells, with different organs and tissues, including muscle,

hypoderm, intestine, reproductive system, secretory-excretory system, and glands (245,246). This nematode has widely been used in research due to its small size, ease of cultivation, short life cycle, low cost of the maintenance, long-term cryopreservation, transparency, invariant cell number, and development. They also have a high progeny (around 300 self-progeny) and are benign to humans (246). Moreover, its complete genome sequence is available and between the 60 and 80% of human genes have an ortholog in *C. elegans* genome (246), allowing gene expression studies.

Furthermore, the gastrointestinal tract of the nematode, even if it comprises only a simple pharynx (oesophagus), intestine, and hindgut (rectum) (247), presents similarities to the mammalian tract, like an acid lumen, microvilli forming a brush border, secretion of digestive enzymes, uptake of digested components, and peristalsis (248). Also, this nematode stores fat in lipid droplets in its intestinal and hypodermal cells (249), and they can be dyed and quantified (208).

Thus, *C. elegans* has become a useful model to evaluate different diseases, including obesity (250), and it has been previously used to study the effect of bioactives on fat accumulation, both in glucose-supplemented (251–254) and non-supplemented (208,211,215,254–256) nematode growth medium (NGM). Moreover, this nematode has also been used to analyse these effects in the accumulation of fat when using such bioactives encapsulated in zein-based nanoparticles (203,235,257–259), poly(anhydride) nanoparticles (260,261), or nanoemulsion-based delivery systems (262). For all the mentioned reasons, *C. elegans* is a good *in vivo* model for the screening of the developed formulations.

5.5. What was the effect of quercetin formulations on the fat content of *C. elegans*?

It was previously reported that some phenolic compounds such as curcumin or resveratrol decreased the fat accumulation in *C. elegans* at a concentration between 10 and 500 µM (255). Nevertheless, to our knowledge, only one study has analysed the effect of quercetin on the *C. elegans* fat accumulation. Lin *et al.* observed a reduction in the fat accumulation of N2 strain at 50 and 100 µM (about 20% and 35%, respectively), but any effect was seen at 25 µM (249).

In this work, it has been demonstrated that quercetin decreases the accumulation of fat in the nematode in a range of concentrations from 10 to 100 µM (Figure 19). When *C. elegans* was grown in a glucose-supplemented NGM, quercetin still maintained its fat reduction effect at a concentration of 50 µM; particularly when nanoencapsulated in zein nanospheres (both bare or PEG-coated, Figure 21). However, the fat reduction was lower in normal NGM compared to the previous work (249), even if a reduction was also observed at 10 µM. These differences between studies could be related to the differences in the methodology. Lin and co-workers fed the nematode with dead *E. coli* OP50 (to exclude the influence of the bacterial metabolism), left the worms with the treatment for 44h (while we did for 46h), and used Oil Red O Staining for the

quantification of the fat accumulation (Nile Red allows for the quantification of total lipid levels, while Oil Red O facilitates the evaluation of lipid distribution among tissues (263)).

Table 16 summarizes the effect of free and encapsulated quercetin (50 µM) in the fat accumulation of *C. elegans* grown in a glucose-supplemented NGM. Nanospheres (plain or PEG-coated) induced a decrease between 9 and 12% compared to NGM, and the decrease in the fat accumulation for Q-NS was 2.2-fold higher than free quercetin, while for Q-NS-PEG50 was 1.6-fold. Nanospheres would protect quercetin against the environment (NGM and *E. Coli*) and allow it to achieve the *C. elegans* intestine, improving the bioavailability of the flavonoid and consequently its effect on the nematode.

Table 16. Fat accumulation decrease in *C. elegans* in a glucose-supplemented NGM. Q-NS: quercetin-loaded nanospheres; Q-NS-PEG50: quercetin-loaded PEG-coated nanospheres; Q-NC: quercetin-loaded nanocapsules.

	Decrease of fat accumulation (%)
Free quercetin 50 µM	5.7
Q-NS	12.4
Q-NS-PEG50	9.1
Q-NC	0.3

On the other hand, Q-NC did not show any differences compared to NGM (Figure 22), where the effect of quercetin was inhibited when administered with the wheat germ oil, because free oil increased fat accumulation in *C. elegans* at the concentration present in NC. Table 17 summarizes the composition of the wheat germ oil used in this work. Navarro-Herrera *et al.* analysed the effect of different fatty acids in the fat accumulation of *C. elegans*, obtaining that linoleic acid increased fat accumulation at 10 µM, and oleic acid did not modify the accumulation of fat compared to NGM; although, a slight increase was observed (208). These results would be in line with our results, due to the fact that linoleic and oleic acids were the main components of the wheat germ oil used to prepare zein nanocapsules.

Table 17. Composition of wheat germ oil used for the preparation of nanocapsules, obtained from Guinama (La Pobla de Vallbona, Spain).

Common name	Percentage (%)
Linoleic acid (18:2)	57.2
Palmitic acid (16:0)	16.8
Oleic acid (18:1)	16.7
Linolenic acid (18:3)	5
Stearic acid (18:0)	1.2

It is worth mentioning that the three kinds of nanoparticles decreased the accumulation of fat when quercetin was encapsulated (Figures 21 and 22), compared to each type of empty nanoparticles. These findings evidence the fat-lowering effect of quercetin in *C. elegans*.

Empty zein-based nanoparticles were also evaluated in the nematode, in order to verify that the effect of quercetin-loaded nanoparticles was attributed to the flavonoid (Figure 20). Free zein did not have an effect at the same concentration as in nanospheres; although mannitol and the mixture of zein and mannitol increased the fat accumulation by 13%. When NS with mannitol were administered, this effect increased more than two times (32%), what may suggest that NS are more accessible than free zein. Zein nanospheres were previously evaluated in *C. elegans* by Lucio *et al.*, and, similarly to our work, they demonstrated that mannitol containing empty zein nanospheres increased the accumulation of fat by more than 10% compared to the NGM (258). In both works, the fat accumulation was increased due to the presence of mannitol, because NS free of mannitol were similar to NGM. The difference in the percentage between works could be due to the dose of nanospheres given to the worms, because of the different loading of the active in the nanoparticles and the differences in the effective concentration in NGM.

Empty vehicles were also evaluated in a glucose-supplemented NGM (Figures 21 and 22). In all cases, empty nanoparticles increased the fat accumulation, as well as zein, wheat germ oil, and a mixture of wheat germ oil and zein. Reboredo *et al.* evaluated the effect of these nanospheres in a glucose-supplemented NGM, obtaining a decrease by 11% compared to control (235). In our work, free mannitol empty nanospheres increased the fat accumulation by 4%. A similar fact was observed for PEG-coated nanospheres (PEG-to-zein ratio 0.50), which increased the amount of fat in the nematode by 4%, compared to the decrease of 14% previously described. These differences could be attributed to the concentration of nanoparticles added to the NGM.

5.6. How the morphology of nanoparticles influences their biodistribution and gastrointestinal transit?

The intestinal transit study in Wistar rats showed that all the formulations tested were capable to reach the small intestine in less than 1 h, the cecum in about 4 hours, and the colon in less than 8 hours (Figures 23-26). The transit of these nanoparticles along the gut seemed to be faster for NC than for NS and PEG-coated NS. Eliminating the radioactivity observed in the stomach, certain differences between bare and PEG-coated NS may be observed. Thus, plain NS and NC mainly appeared as large and intense spots along the gut, suggesting the presence of a large amount of radioactivity in the lumen of animals, whereas PEG-coated nanoparticles displayed a more diffuse presence, outlining (in some areas) the wall of the digestive tract.

At a microscopic level, the distribution of the nanoparticles (fluorescently labeled) in the gut presented a different behaviour than that observed for the control formulation (dispersion of the marker in water) (Figures 27-29). Again, the fate of bare and PEG-coated nanoparticles appeared to be different. Plain nanoparticles appeared in the mucus layer covering the surface of the epithelium, whereas PEG-coated nanospheres were mainly observed on the surface of cells that form the mucosa. This different behaviour is in line with the capability of these nanoparticles to diffuse in intestinal pig mucus (Figure 17), evidencing the importance of the surface characteristics of the nanoparticles for their distribution *in vivo*.

5.7. What was the effect of the encapsulation of quercetin on its pharmacokinetic properties?

Quercetin was orally administered as a single dose of 15 mg/kg to Wistar rats as an aqueous suspension (Q-Susp) or nanoencapsulated in zein-based nanoparticles (Figure 31). The pharmacokinetic plasma profile was similar for all the formulations tested; although higher levels of the flavonoid were observed for the nanoencapsulated quercetin than for the control formulation, particularly for Q-NS. For Q-NS, both the maximum plasma concentration (C_{max}) and the AUC were significantly higher than for the other formulations tested (Tables 11 and 12). Interestingly, the half-life ($t_{1/2}$) and the mean residence time (MRT) of quercetin in plasma were significantly longer for Q-NS-PEG25 than for bare nanoparticles (up to four times for $t_{1/2}$ and three times for MRT when compared with Q-NS). This slow elimination for quercetin when nanoencapsulated in PEG-coated nanoparticles would be related to their mucus-permeating properties (Figure 17, Figure 29) and their slow gastrointestinal transit (Figure 25).

The relative oral bioavailability of quercetin when formulated as aqueous suspension was calculated to be close to 5%. This result is in line with previously published data in which quercetin was formulated in conventional oral formulations (solutions or suspensions), including the works from Chen and co-workers (5.3%) (264), Penalva and

collaborators (4.1%) (108), or Li *et al.* (3.6%) (265). For nanoencapsulated quercetin, Q-NS displayed the highest relative oral bioavailability (about 57%), followed by Q-NS-PEG25 (37%) and Q-NC (26%). In any case, the nanoencapsulation of quercetin in zein-based nanoparticles dramatically improved the oral bioavailability of quercetin. This observation is in agreement with Penalva and collaborators, who performed a pharmacokinetic study in Wistar rats using quercetin-loaded zein-based nanoparticles at an oral single dose of 25 mg/kg (108).

5.8. Validity and robustness of the rat model of obesity fed with a high fat/high sucrose diet.

Obesity is defined as a complex multifactorial disease characterized by an excess of adiposity that can be risky to health (1). In this context, rodents are the most used pre-clinical human obesity model. For example, mesenteric fat is considered the most analogous to human intra-abdominal adipose tissue because of its biology and location (it has access to the portal vein), even if it is not well studied in rodents (219). In our efficacy study, male Wistar rats were fed with a high fat/high sucrose (HFS) diet for 18 weeks previously to the treatment, with the objective of achieving a diet-induced obesity (DIO) model. Following the definition of obesity, this objective was successfully achieved. It was demonstrated that the HFS diet increased body weight (Figure 32) and the proportion of epididymal, retroperitoneal, and mesenteric fats, that is, visceral white adipose tissue (WAT), compared to the standard diet (Figures from 36 to 38). Subcutaneous and brown fats were also increased (Figures 37B and 38A). All the effects caused by the HFS diet are summarized in Table 18.

In obesity, adipocytes suffer hypertrophy (increased size of adipocytes) and hyperplasia (higher number of adipocytes), what result in the release of fatty acids, because they lose the ability to buffer circulating fatty acids. These fatty acids are deposited in non-adipose tissues, such as the liver (31). Here, this fact is confirmed; rats fed with HFS diet presented a higher size of epididymal and retroperitoneal fat adipocytes compared to rats fed with standard diet (Control) (Figure 51). In addition, HFS-fed rats presented an important accumulation of fat in the liver, compared to Control rats (Figure 50).

Some biochemical parameters were also disrupted in HFS-fed animals compared to those receiving the standard diet (Figures 42-47). Patients with obesity commonly present increased triglyceride (TAG) levels (8,266–268) and low HDL-cholesterol levels (8,269), a tendency that was also observed in our results. Total cholesterol levels (266,267,269,270), alanine transaminase (ALT), and aspartate transaminase (AST) (266,270) are commonly in the normal range, as happened with the DIO rat model. However, glucose levels can be elevated (267,271) or be in the normal range (268,269) in obese patients. So, taking into account all the presented data, we consider that the DIO model was successfully achieved in Wistar male rats, induced by the HFS diet.

Table 18. Summary of the effects of HFS diet compared to Control in the efficacy study. WAT: white adipose tissue; TAG: triglycerides; AIP: atherogenic index of plasma; ALT: alanine transaminase; AST: aspartate transaminase; HOMA-IR: homeostasis model of insulin resistance; MCP-1: monocyte chemoattractant protein-1; ↑: HFS increased the proportion or amount. ↓: HFS decreased the proportion or amount; -: any effect was seen.

Fat (%)	↑	Serum total cholesterol	-
Lean (%)	↓	Serum HDL-cholesterol	↓
Fat/Lean	↑	HDL vs total cholesterol	↓
Epididymal fat (%)	↑	Serum TAG	↑
Epidydimal adipocyte size	↑	AIP	↑
Retroperitoneal fat (%)	↑	Serum ALT	-
Retroperitoneal adipocyte size	↑	Serum AST	-
Mesenteric fat (%)	↑	Serum glucose	↑
Subcutaneous fat (%)	↑	Plasma insulin	↑
Brown fat (%)	↑	HOMA-IR	↑
Visceral WAT (%)	↑	Plasma MCP-1	↑
Liver (%)	-	Hepatic TAG	↑
Spleen (%)	↓		
Kidneys (%)	-		
Gastrocnemius muscle (%)	↓		

In addition to obtaining an obesity model, we have managed to mimic some associated comorbidities. DIO rats presented not only a higher weight and fat content, but they also had altered biochemical values in blood, and hepatic steatosis. We could consider that a model of metabolic syndrome was also achieved, due to the fact that apart from obesity, HFS-fed rats also presented increased TAG and glucose levels, and decreased HDL-cholesterol values, fulfilling three of the four criteria to consider that metabolic syndrome is present (29).

Peripheral insulin resistance can cause fatty liver by increasing fatty acid, glucose, and insulin plasma levels, which stimulates hepatic lipid synthesis and impairs hepatic β-oxidation (111). Animals also presented hepatic steatosis, which could be observed in the histology of the liver (Figure 50) and in the triglyceride quantification in the organ (Figure 53). Thus, it could be considered that a model of non-alcoholic fatty liver disease (NAFLD) was also achieved, characterized by the accumulation of fat in the hepatocytes (35). However, ALT and AST were not altered (Figure 45). ALT and AST are enzymes found mainly in the liver. They can also be found in red blood cells, heart cells, muscle tissue, or in some organs (like the pancreas and kidneys). These enzyme levels are used in the diagnosis of liver disease. If a body tissue like the liver is damaged or has a disease, additional ALT and AST are released into the bloodstream, causing an increase in the levels of these enzymes. Also, ALT and AST amount is directly related to the extent of the tissue damaged (272). Therefore, in NAFLD there is a rise in ALT and AST (273–275). In this work, serum ALT and AST levels were not modified by the HFS diet compared to

standard diet, so we could conclude that even if obese rats presented hepatic steatosis and high levels of TAG in the liver, probably there was not a serious damage. Furthermore, we have confirmed that NAFLD was reversible (quercetin-loaded nanoparticles decreased the hepatic steatosis and liver TAG levels).

Diabetes is another obesity-induced comorbidity (33). In Wistar rats, animals are usually considered as diabetic when fasting glucose levels are higher than 200 mg/dL (276,277) or 250 mg/dL (235,259,278,279). In our case, fasting glucose levels were always lower than 120 mg/dL in mean (Table 13), so we could conclude that HFS diet did not induce diabetes in Wistar rats after 23 weeks of feeding. However, the homeostasis model of insulin resistance (HOMA-IR) was increased (Figure 47), indicating that insulin resistance was probable. Insulin resistance is defined as a reduced biological action of insulin (280). It increases the incidence of metabolic syndrome and is a major pathophysiological factor in the development and progression of diabetes. HOMA-IR is a key index for the assessment of insulin resistance, but cut-off values are different between races, ages, genders, etc.

Other authors have previously worked with rodent obesity models. Aranaz *et al.* (211,281) and Navarro-Herrera *et al.* (215) previously performed similar efficacy studies, with Wistar male rats fed with standard diet for 6 weeks and then with HFS diet for 10 weeks. Similar results were obtained regarding the fat depots and organs percentage to total body weight, being our results of fat percentage by magnetic resonance spectroscopy slightly higher. Regarding the biochemical analysis, some of the levels obtained in this work were higher than previously obtained ones, such as cholesterol, HDL-cholesterol, glucose, or insulin levels. However, unlike in this work, they observed an increase in the body weight gain in HFS compared to standard diet, and they did not observe an effect in the brown fat proportion, spleen weight, TAG, or glucose levels (211,215,281). They also saw a reduction in kidney weight (211,281) and any effect in gastrocnemius muscle (215). Nevertheless, all these dissimilarities could be ascribed to the differences in the experimental design (10 weeks fed with HFS compared to 23 weeks). Ragab *et al.* also fed Wistar rats with HFS diet for 12 weeks, but they did not obtain any significant change in the body weight compared to standard diet group (111). However, similarly to our results, they found an increase in serum TAG and insulin, a decrease in HDL-cholesterol levels, accompanied by hepatic steatosis and increased hepatic TAG levels, but they found an increase in serum total cholesterol too.

Other types of rodents have also been used. Rivera *et al.* worked with obese Zucker rats (113). Similarly to our results, they obtained that obese rats displayed higher body weight, plasma TAG levels, insulin, and HOMA-IR compared to lean controls. However, they observed increased plasma levels of total cholesterol and body weight gain, with any change in glucose levels. On the other side, Kobori *et al.* fed C57BL/6J mice with a high-fat, high-cholesterol and high-sucrose Western diet for 20 weeks (115). They observed that these Western diet-fed mice exhibited higher visceral fat and body weight compared to control diet, with increased blood glucose, plasma insulin, TAG, and hepatic TAG, as happened in our work. However, plasma total cholesterol was increased too.

Seo *et al.* used ICR mice fed with a high-fat diet for 10 weeks. Similarly to our results, they obtained that obese mice presented higher amount of epididymal fat, with increased levels of plasma TAG, HOMA-IR, and the presence of hepatic steatosis compared to a normal diet (116). However, they also observed an increase in the liver weight and plasma total cholesterol levels, without differences in HDL-cholesterol levels.

Therefore, different obesity models can be used in research. We used the diet HFS to obtain a DIO model in rats, which was successfully achieved, in order to evaluate the effect of quercetin and quercetin-loaded zein-based nanoparticles in this pathology. As can be observed, several similarities are present among obesity models in rodents, but slight differences also appear in some parameters, such as in cholesterol levels, which in this work was only slightly increased in HFS rats. These differences could be attributed to differences in experimental designs, diets, species, and/or age of the animals.

5.9. What was the effect of quercetin on the weight of animals fed with HFS diet?

After 5 weeks of the treatment with free or nanoencapsulated quercetin, none of the treatments had a significant effect on the body weight gain of HFS-fed rats. However, a trend toward gradual weight reduction in animals treated with quercetin was observed; particularly in those groups of animals that received Q-NS or Q-NS-PEG (see Figure 33).

Different results have previously been obtained on quercetin treatment and body weight. Ragab *et al.* did not find any differences in body weight between quercetin treatment (daily 50 mg/kg for 6 weeks) in HFS-fed Wistar rats and obese controls (111), as well as Arias *et al.* (male Wistar rats fed with HFS diet supplemented with quercetin at 30 mg/kg for 6 weeks) (112). However, Rivera and co-workers observed a reduction in the final body weight of Zucker obese rats when administered 10 mg/kg of daily quercetin by oral gavage for 10 weeks, but not when the dose was 2 mg/kg (113). They also found a reduction in the body weight gain at 10 mg/kg. In another interesting work, Kuipers *et al.* observed that supplementation of high-fat diet with quercetin (0.1% w/w) in C57BL/6J mice for 12 weeks did not affect the body weight (114), whereas Kobori *et al.* reported that quercetin supplementation (0.05%) to a high-fat, high-cholesterol and high-sucrose Western diet decreased body weight at 20 weeks compared to Western diet (115). A dose-dependent reduction of body weight due to quercetin supplementation for 10 weeks (25, 50, and 100 mg/kg) was also observed in high fat-fed ICR mice by Seo and co-workers (116).

All these differences among studies could be due to the use of different species, doses, type of treatment administration (for example, supplementation on the diet (114,115) or oral gavage (113)) and/or length of the treatment. In the present study, quercetin did not have an effect on body weight gain after 5 weeks of treatment at a daily dose of 15 mg/kg, like similarly described by Ragab *et al.* in Wistar rats (50 mg/kg for 6 weeks) (111). If the treatment had continued, changes in weight gain of the animals

would probably have been seen, maybe with Q-NS and Q-NS-PEG decreasing the body weight gain significantly.

5.10. What was the effect of quercetin formulations on the fat content of animals fed with HFS diet?

After the treatment with quercetin for 5 weeks, a tendency to decrease the weight of fat depots of obese rats was observed (Figures 36-38). PEG-coated nanospheres decreased almost all kinds of fat significantly after five weeks of administration. Surprisingly, Q-NC did not have any effect on fat depots, but when visceral white adipose tissue was calculated, an effect was seen, probably attributed to the sum of the slight reductions observed in epididymal, retroperitoneal, and mesenteric fats. On the other hand, an increased body fat and/or reduced lean mass have higher risk of cardiometabolic diseases and mortality (282). Here, lean mass was decreased by HFS diet, but it was not modified by quercetin. All the effects of free or encapsulated quercetin in HFS-fed rats are summarized in Table 19.

Obesity is also defined as a result of expansion in both the number and size of adipocytes (283). In this work, it was confirmed that HFS diet increased the size of the adipocytes, and quercetin (free or encapsulated in zein-based nanoparticles) decreased adipocyte size in epididymal fat. However, this effect was less noticeable in retroperitoneal fat, in which only PEG-coated nanospheres decreased the adipocyte size in a significant way (Figure 51), result that is in accordance with the fact that it was the only treatment decreasing retroperitoneal fat significantly (Figure 36B).

Table 19. Summary of the effects of the nanoparticles in fat proportion and adipocyte size compared to HFS in the efficacy study. Q-NS; quercetin-loaded nanospheres; Q-NC: quercetin-loaded nanocapsules; Q-NS-PEG: PEG-coated quercetin-loaded nanospheres; Q-Susp: quercetin suspension; WAT: white adipose tissue. ↓: treatment decreased the proportion or amount; **-**: any effect was seen.

	Q-NS	Q-NC	Q-NS-PEG	Q-Susp
Fat (%)	-	-	↓	-
Lean (%)	-	-	-	-
Fat/Lean	-	-	↓	-
Epididymal fat (%)	-	-	↓	↓
Epidydimal adipocyte size	↓	↓	↓	↓
Retroperitoneal fat (%)	-	-	↓	-
Retroperit. adipocyte size	-	-	↓	-
Mesenteric fat (%)	-	-	-	-
Subcutaneous fat (%)	-	-	↓	↓
Brown fat (%)	-	-	-	↓
Visceral WAT (%)	-	↓	↓	↓

These results are partially in accordance with the ones obtained for *C. elegans* fat accumulation assay. As happened with the worms, Q-NS-PEG decreased the fat content, and Q-NC did not have an effect. On the other hand, the effect of Q-NS was less marked in rats, where a decrease was observed, but it was not statistically significant.

Our results are in line with the ones obtained by Kobori *et al.* in C57BL/6J mice (quercetin-supplemented high-fat, high-cholesterol and high-sucrose Western diet-fed mice for 20 weeks), who saw a decrease of the visceral fat weight (115). However, using the same mice but a different diet, Kuipers *et al.* did not see an effect of quercetin (supplemented high-fat diet for 12 weeks) in the fat and lean composition (114), as well as Arias *et al.*, who observed a decrease in the sum of epididymal, perirenal, mesenteric and subcutaneous fat of Wistar obese rats in a non-significative way after supplementation with quercetin for 6 weeks (112). Seo *et al.* also saw a decrease in the epididymal weight and adipocyte size in ICR mice after 10 weeks of quercetin supplementation (116).

5.11. What was the effect of quercetin formulations on the lipid profile of animals fed with HFS diet?

In the efficacy study, the lipid profile of the animals was evaluated after 5 weeks of treatment with free or encapsulated quercetin. The serum total cholesterol was not modified compared to the HFS group (Figure 42A), while all kinds of zein-based nanoparticles decreased serum TAG levels (Figure 44A). The complete lipid profile is summarized in Table 20.

Table 20. Summary of the effects of the nanoparticles in the serum lipidic profile compared to HFS in the efficacy study. Q-NS; quercetin-loaded nanospheres; Q-NC: quercetin-loaded nanocapsules; Q-NS-PEG: PEG-coated quercetin-loaded nanospheres; Q-Susp: quercetin suspension; TAG: triglycerides; AIP: atherogenic index of plasma; ↓, ↓: treatment decreased the proportion or amount; -: any effect was seen.

	Q-NS	Q-NC	Q-NS-PEG	Q-Susp
Total cholesterol	-	-	-	-
HDL-cholesterol	-	-	-	↓
HDL vs total cholesterol	-	-	-	↓
TAG	↓	↓	↓	-
AIP	↓	↓	↓	-

Our results are in accordance with previously obtained ones. Thus, Ragab *et al.* fed Wistar rats with HFS diet for 6 weeks, and then they were treated with 50 mg/kg oral quercetin daily for 6 weeks more (111). Quercetin treatment decreased TAG levels, maintaining HDL-cholesterol levels compared to HFS diet. In another interesting study with obese Zucker rats, animals were fed with 2 or 10 mg/kg quercetin (in 1% of

methylcellulose) by gavage for 10 weeks, achieving lower TAG levels compared to obese rats (113). However, both studies observed a decrease in total cholesterol levels.

Similarly, the plasma TAG levels of C57BL/6J mice, fed with a high-fat diet, decreased by quercetin supplementation (0.1% in high-fat diet for 12 weeks), without affecting plasma glucose, but increasing plasma total cholesterol (114). Using the same mice, Kobori *et al.* fed the animals with a high-fat, high-cholesterol and high-sucrose Western diet supplemented with quercetin for 20 weeks, observing a lowering effect of the diet in plasma TAG and cholesterol levels compared to non-supplemented Western diet (115). Seo *et al.* used ICR mice fed with high-fat diet supplemented with quercetin for 10 weeks, obtaining a decrease in TAG and total cholesterol plasma levels (116).

To sum up, all the studies observed a decrease in TAG levels by quercetin, what is in accordance with the obtained results. However, almost all of them found an effect of quercetin in decreasing total cholesterol levels, because obese animals presented increased levels of cholesterol compared to lean ones. In our case, HFS diet did not have a significant effect increasing the serum total cholesterol of obese rats, so quercetin did not have an effect on improving this value.

5.12. What was the effect of quercetin formulations on the glycaemic profile of animals fed with HFS diet?

Serum glucose and plasma insulin levels were quantified at the end of the efficacy study (Figure 46). Quercetin slightly decreased glucose levels, but only when encapsulated in PEG-coated nanospheres was able to decrease these levels significantly. However, insulin levels were not modified by quercetin treatment. A slight decrease was observed in the HOMA-IR (Figure 47), which means that quercetin was not able to decrease significantly the insulin resistance caused by the HFS diet. A summary of these effects can be observed in Table 21.

In addition, blood glucose levels were measured before the treatments by a glucometer, indicating again an increase in glucose levels of HFS compared to the standard diet (Table 13). An oral glucose tolerance test was performed, in which the area under the curve was slightly modified by quercetin, and at the end of the test, Q-NC and Q-NS-PEG presented lower glucose levels compared to HFS. On the other hand, serum glucose levels (measured by Pentra C200 analyser) were slightly higher than blood glucose levels (measured by a glucometer), because red blood cells have higher protein concentration, while serum has higher water content and higher quantity of glucose dissolved in it (284).

Table 21. Summary of the effects of the nanoparticles in the glycaemic profile compared to HFS in the efficacy study. Q-NS; quercetin-loaded nanospheres; Q-NC: quercetin-loaded nanocapsules; Q-NS-PEG: PEG-coated quercetin-loaded nanospheres; Q-Susp: quercetin suspension; HOMA-IR: homeostasis model of insulin resistance; ↓: treatment decreased the proportion or amount; -: any effect was seen.

	Q-NS	Q-NC	Q-NS-PEG	Q-Susp
Serum glucose	-	-	↓	-
Plasma insulin	-	-	-	-
HOMA-IR	-	-	-	-

Different results have been reported regarding the glycaemic profile of obese animals. Quercetin treatment in obese rodents has been demonstrated to cause a decrease in insulin levels (111–113,115), but different effects have been found regarding glucose levels. Kobori *et al.* (115) and Arias *et al.* (112) found a glucose decrease in C57BL/6J obese mice (quercetin supplementation for 20 weeks) and Wistar rats (quercetin supplementation for 6 weeks, 30 mg/kg), respectively, by quercetin treatment. However, Rivera *et al.* (113) and Kuipers *et al.* (114) did not find differences in obese Zucker rats (quercetin oral treatment for 10 weeks, 10 mg/kg) and C57BL/6J mice (quercetin supplementation for 12 weeks), respectively, compared to obese control. Some researchers also found a reduction of the HOMA-IR in obese Zucker rats (113), Wistar rats (112), and ICR mice (116). A glucose tolerance test was performed in Wistar obese rats, obtaining that for the supplementation with quercetin for 6 weeks, the glucose levels in the test and the AUC were decreased (112). In this work, glucose and insulin levels were not modified by quercetin, probably due to the dose and duration of the treatment (15 mg/kg, 5 weeks), in view of the mentioned previous results. If the treatment was longer or with a higher dose, it would probably decrease glucose levels, and consequently, insulin and HOMA-IR levels.

5.13. What was the effect of quercetin formulations on the inflammatory markers of animals fed with HFS diet?

Obesity induces a chronic inflammation in the adipose tissue, liver, skeletal muscle, and vascular system, and this chronic inflammation induces the release of proinflammatory cytokines such as tumour necrosis factor-α (TNF-α), monocyte chemoattractant protein-1, and interleukin-6 (IL-6) (285).

Monocyte chemoattractant protein-1 (MCP-1), also known as Chemokine ligand 2 (CCL2), is the first discovered and mostly studied human C-C class chemokine. It is one of the key factors involved in the initialization of inflammation, and its expression is present in different cell types and upregulated by a variety of stimuli (283,286). One of the sources of MCP-1 is the adipocytes (283), and this protein has been found to be increased in the plasma (270) and serum (287) of obese patients. It was also demonstrated that MCP-1 is expressed in murine adipocytes and its expression is

upregulated in white adipose tissue and plasma of obese mice (288). These data confirm our results, where plasma MCP-1 was significantly increased in obese rats (Figure 48).

Obesity also induces systemic oxidative stress, what is related to irregular production of adipokines (white adipose tissue produced cytokines), such as TNF-α, IL-1, or IL-6. These adipokines stimulate the production of reactive oxygen species (ROS) and nitrogen species by macrophages and monocytes (289). Reactive oxygen species may act as signal transduction messengers for some transcription factors, including the pro-inflammatory nuclear factor kappa B (NF-κB). At the same time, MCP-1 expression is regulated at the transcriptional level by stimulatory agents like TNF-α, interferon gamma (INF-γ), platelet-derived growth factor (PDGF), and stress factors. In many of these regulatory responses, NF-κB transcription factor plays a key role (Figure 63) (286).

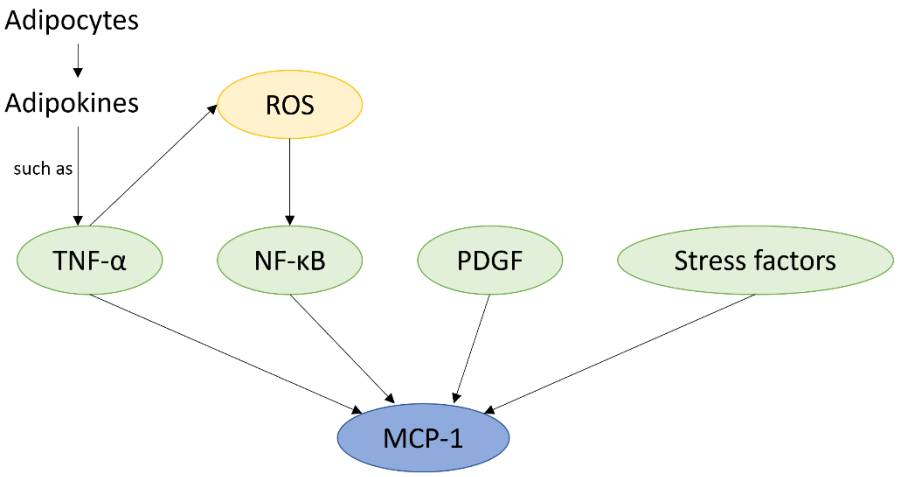

Figure 63. Factors that stimulate MCP-1 transcription. Based on Melgarejo *et al.* (286) and Fernández-Sánchez *et al.* (289). ROS: reactive oxygen species; TNF-α: tumour necrosis factor alpha; NF-κB: nuclear factor kappa B; PDGF: platelet-derived growth factor.

We demonstrated that quercetin decreased plasma MCP-1 levels in obese rats. Quercetin is a powerful scavenger of ROS (84), what could decrease NF-κB activity and hence, induce a reduction of MCP-1. In fact, quercetin has been demonstrated to inhibit the activity of NF-κB and the generation of inflammatory cytokines *in vitro* (290,291) and *in vivo* (118,291). In this work, free and encapsulated quercetin decreased MCP-1 plasma levels, being this decrease significant for Q-NS, Q-NS-PEG, and Q-Susp (Figure 48, summary in Table 22). Therefore, a feasible hypothesis could be that quercetin decreases MCP-1 levels by its antioxidant effect, what indirectly causes an anti-inflammatory effect.

Table 22. Effects of the nanoparticles in the plasma MCP-1 levels compared to HFS in the efficacy study. Q-NS; quercetin-loaded nanospheres; Q-NC: quercetin-loaded nanocapsules; Q-NS-PEG: PEG-coated quercetin-loaded nanospheres; Q-Susp: quercetin suspension; MCP-1: monocyte chemoattractant protein-1; ↓: treatment decreased the proportion or amount; -: any effect was seen

	Q-NS	Q-NC	Q-NS-PEG	Q-Susp
Plasma MCP-1	↓	-	↓	↓

5.14. What was the effect of quercetin formulations on the histology and triglyceride content in the liver of animals?

After 5 weeks of treatment, obese rats were sacrificed and livers were extracted. Differences were visually observed, which were afterwards confirmed by the histological analysis (Figures 49 and 50). Hepatic steatosis was observed in HFS groups compared to standard diet, and it was slightly improved by quercetin treatment, especially after the treatment with Q-NC and Q-NS-PEG. In addition, hepatic TAG levels were decreased by quercetin, particularly when animals were treated daily with Q-NS-PEG ($p < 0.01$; Figure 53), which is in accordance with steatosis images (data are summarized in Table 23).

These results are also in accordance with serum TAG levels (Figure 44A); in both cases, nanoparticles decreased TAG in a higher way than free quercetin. Besides, as previously explained, adipocytes suffer hypertrophy and hyperplasia in obesity, releasing fatty acids that are accumulated in some tissues, such as the liver (31). Here, all treatments decreased the hypertrophy of epididymal fat, probably leading to a reduction of the release of fatty acids and consequently lower deposition in the liver. In the case of Q-NS-PEG, it was the only treatment decreasing retroperitoneal adipocyte size, apart from epididymal fat adipocyte size, what could explain its significant reduction of hepatic TAG and steatosis. Q-NC also appeared to decrease hepatic steatosis, probably due to beneficial effects of the wheat germ oil in the liver (wheat germ oil decreases liver cholesterol (237)).

Table 23. Summary of the effects of the nanoparticles in the liver compared to HFS in the efficacy study. Q-NS; quercetin-loaded nanospheres; Q-NC: quercetin-loaded nanocapsules; Q-NS-PEG: PEG-coated quercetin-loaded nanospheres; Q-Susp: quercetin suspension; TAG: triglycerides; ↓: treatment decreased the proportion or amount; -: any effect was seen.

	Q-NS	Q-NC	Q-NS-PEG	Q-Susp
Hepatic steatosis	-	↓	↓	-
Hepatic TAG	-	-	↓	-

The obtained results are in accordance with previous studies in rodents. Oral daily administration of quercetin for 6 weeks (50 mg/kg) to HFS-fed Wistar rats reduced

hepatic TAG levels compared to HFS-fed rats, but the steatosis was not improved (111). In C57BL/6J mice, the supplementation of a Western diet with quercetin (0.05%) for 20 weeks reduced hepatic TAG and steatosis (115).

When fat is accumulated in the liver, usually there is an increase in reactive oxygen species (ROS), produced because of the mitochondrial dysfunction and impaired fatty acids. This oxidative stress stimulated the production of proinflammatory cytokines through the induction of the NF-κB. ROS can also damage mitochondria, what produces more ROS. Flavonoids can overcome this situation by their antioxidant effect. They scavenge reactive oxygen species and correct mitochondrial dysfunction. Flavonoids are also able to inhibit the enzyme nicotiamide adenine dinucleotide phosphate oxidase (NOX2), what plays a role in the production of ROS, and are transition metal chelators, so they can bind and inhibit hepatic iron, which has a strong oxidative potential (31).

5.15. What was the effect of quercetin formulations on the expression of determined genes in the adipocytes of retroperitoneal fat and liver of animals fed with HFS diet?

In most organisms, fatty acid degradation occurs primarily via the β-oxidation cycle. In mammals, β-oxidation occurs in both mitochondria and peroxisomes (225).

When free fatty acids enter the cell, they are activated by the conversion to fatty-acyl-CoAs (free fatty acid esterified with coenzyme A (CoA), Figure 64) (224). The mitochondrial membrane is impermeable to acyl-CoAs, so they enter the mitochondria using the carnitine shuttle. Once the acyl-CoAs are inside the mitochondria, they are degraded to acetyl-CoA units by β-oxidation (292). These CoA esters are also transported into peroxisomes (293).

Both mitochondrial and peroxisomal β-oxidation catalyse the chain shortening of acyl-CoA esters between carbons 2 and 3, yielding as products chain-shortened acyl-CoA and acetyl-CoA or propionyl-CoA, depending on substrates. Fatty acids and their CoA esters have many roles in cellular processes by serving as components in cellular lipids, carbon storage as triacylglycerols, regulators of enzymes and membrane channels, ligands for nuclear receptors, precursor molecules for hormones, signaling molecules including second messengers, and substrates for α-, β-, and ω- oxidations (225).

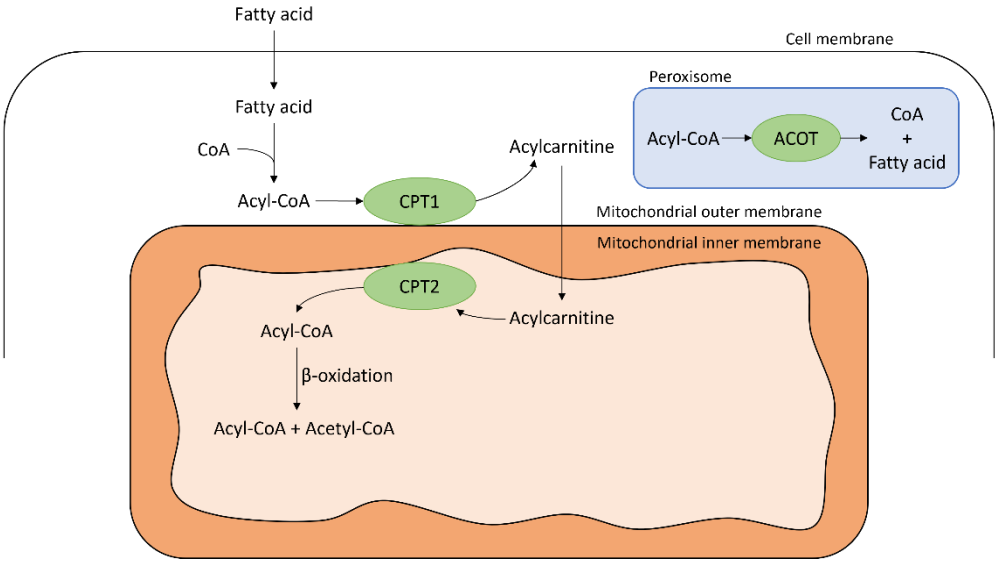

Figure 64. β-oxidation in mammalian cells. CoA: coenzyme A; CPT1 and CPT2: Carnitine palmitoyltranferase-1 and -2; ACOT: Acyl-CoA thioestherase. Based on Houten *et al.* (292) and Hunt *et al.* (294).

The gene *Acot8* encodes an enzyme from the Acyl-CoA thioestherase (ACOT) family, enzymes that within the peroxisome, convert fatty acyl-CoAs into free fatty acids and coenzyme A (Figure 64) (224,294). The protein ACOT8 activity is inhibited by CoA and its expression is upregulated by fasting and PPARα activation. Also, its overexpression leads to peroxisomal proliferation in murine and human cell lines (224). The overexpression was associated with increased PPARγ expression, suggesting that high ACOT8 activity caused lipid accumulation. Thus, strong overexpression of ACOT8 inhibits peroxisomal β-oxidation to such an extent that lipids accumulate in droplets (294). However, it is thought that ACOTs regulate lipid metabolism by maintaining suitable levels of acyl-CoA, CoA, and free fatty acids. During periods of high β-oxidation, and in particular during conditions that decrease cellular carnitine content, ACOTs would have important functions in hydrolysing acyl-CoAs in peroxisomes to release CoA and enable efficient β-oxidation to proceed. The free fatty acids released may be transported out of the peroxisome and reesterified in a futile cycle similar to that proposed for mitochondria (295).

In the present study, *Acot8* is underexpressed in the retroperitoneal fat of HFS rats compared to Control, and this situation is reverted by Q-NS-PEG, who significantly overexpressed the gene compared to HFS (Figure 57). Due to the effects performed by this formulation in the efficacy study, we could think that the peroxisomal β-oxidation was promoted, what could cause an overexpression of *Acot8* in order to release CoA and permit efficient β-oxidation. These results are also in accordance with *Pparg* overexpression in retroperitoneal fat of Q-NS-PEG treated rats (Figure 61). In the liver, a similar tendency was observed (Figure 54) which is in accordance with Aranaz *et al.*, who reported that *Acot8* was downregulated in the liver of HFS-fed rats compared to standard control (211).

Carnitine palmitoyltranferase-2 (CPT2), an enzyme encoded by the gene *Cpt2*, is located in the inside of the mitochondrial membrane, and is necessary for the oxidation of long chain fatty acids (226,296). In the previously mentioned carnitine shutter, CPT1 converts acyl-CoA into acylcarnitine, and once inside the mitochondria, CPT2 reconverts the acylcarnitine to acyl-CoAs (Figure 64) (292). Thus, the dysfunction of CPT2 affects the β-oxidation of long-chain fatty acids in the mitochondrial matrix, and it has been demonstrated that CPT2 deficiency or dysfunction plays important roles in lipid metabolic diseases, like obesity, NAFLD, or diabetes (226). This fact is confirmed in our results, where *Cpt2* was slightly downregulated in the liver of HFS rats, but nanoencapsulated quercetin did not have the ability to increase again the expression of the gene (Figure 54).

The peroxisomal Acyl-CoA oxidase 1 (ACOX1) is an enzyme encoded by the gene *Acox1*. In the peroxisomal β-oxidation, it catalyses the initial and rate-determining reaction using long and medium straight-chain fatty acyl-CoAs as substrates, which donates electrons to molecular oxygen, generating hydrogen peroxide (225,297). Disruption of *Acox1* in mice results in liver abnormalities (225), and *Acox1*-deficient and mutant mice exhibit spontaneous steatosis and steatohepatitis (298,299). It has also demonstrated that NAFLD progression associated with *Acox1* mutation resulted in accelerated and exacerbated hepatocellular damage (300). Here, *Acox1* was similar in HFS and Control rats in retroperitoneal fat, and it was upregulated by Q-NS-PEG (Figure 57). In the liver, *Acox1* was slightly decreased in HFS rats compared to Control (Figure 54), similarly that happened in previous studies, where *Acox1* was downregulated in the liver of HFS-fed Wistar rats (211), and it was slightly upregulated by Q-NS-PEG. These results would confirm the hepatic steatosis present in HFS, which was reduced by PEG-coated nanospheres (Figure 50).

In the peroxisomal β-oxidation, multifunctional enzymes (MFE-1 and MFE-2) catalyse the second and third reactions of the pathway (225). *Hsd17b4* gene encodes the protein 17b-hydroxysteroid dehydrogenase type 4 (HSD17B4), also known as multifunctional protein 2 (MFP-2 or MFE-2) and D-bifunctional protein (DBP) (225,301). It is crucial for fatty acid utilization and lipid metabolism, as contributes to the synthesis of bile acids and docosahexaenoic acid (225). The deficiency of MFP-2 at birth causes neonatal hypotonia, and it has been seen that large fat droplets are present in hepatocytes of several patients, or other less common liver pathologies have also been detected (302). In the present work, obesity did not upregulate or downregulate *Hsd17b4* gene in retroperitoneal fat of HFS rats, but Q-NS-PEG upregulated it (Figure 57), which would indicate that the peroxisomal β-oxidation was activated and fatty acids were degraded.

Adipose tissue is not only an energy storage organ, but also an active endocrine organ, secreting cytokines, chemokines, and hormone-like factors. These molecules are known as adipokines and are produced and secreted by adipocytes. Two examples of adipokines are adiponectin and leptin, encoded by the genes *AdipoQ* and *Lep*, respectively (Figure 65) (231).

Adiponectin is an anti-inflammatory and insulin-sensitizing hormone that promotes lipid oxidation in some tissues, such as the liver. It also produces an antiatherosclerotic effect, as it strongly inhibits the expression of adhesion molecules and growth factors. Adiponectin serum levels are inversely correlated with body fat percentage in obese subjects, and its gene *AdipoQ* has been identified as a susceptibility locus for metabolic syndrome (231). In this work, *AdipoQ* in the retroperitoneal fat of HFS rats was downregulated compared to Control rats, as could be expected, and levels were increased by quercetin-loaded nanoparticles (Figure 59), improving the effects of adiponectin.

Leptin is produced mainly in WAT, it regulates food intake and body mass, and plays important role in proinflammatory immune responses and lipolysis, among others. Leptin levels increase with percentage of body fat. When fat cells increase, leptin levels rise proportionally, then bind to leptin receptors in the brain that send signals to inhibit food intake and increase the energy expenditure. When a positive energy balance (caloric intake is higher than energy expenditure) is sustained in time, weight gain is produced (303). In this work, any differences were observed between HFS and Control rats in the retroperitoneal fat (Figure 59), probably due to the intake of an HFS diet for a long period of time. However, Q-NS-PEG treatment significantly overexpressed *Lep* in retroperitoneal fat of HFS-fed rats, what could be translated in an inhibition of the food intake and a rise in energy expenditure.

Adipocytes are classified as white, brown, and beige (brown-like adipocytes within white adipose tissue) according to their morphophysiological properties (Figure 65) (221,232). White adipocytes are specialized for lipid storage and release, while brown and beige adipocytes are specialized thermogenic cells able to expend nutritional energy in the form of heat (10). Brown adipose tissue is considered a target against obesity, due to the fact that the activation of this tissue increases energy expenditure and reduces adiposity (232).

Brown and beige adipocytes express the uncoupling protein 1 (UCP1) encoded by the gene *Ucp1* (228). When UCP1 is expressed in beige adipocytes, the process is known as WAT browning (Figure 65) (232). UCP1 is a proton channel present in the inner mitochondrial membrane. Its activation allows energy-charged protons to leak across the inner mitochondrial membrane, uncoupling oxidative phosphorylation from ATP synthesis and dissipating chemical energy as heat (228). Thus, UCP1 plays important roles in thermogenesis, regulation of energy expenditure, and decreasing oxidative stress. Thermogenesis in brown adipose tissue has important roles in thermal and energetic balance and, when deficient, may lead to obesity (304). In the present study, *Ucp1* was slightly decreased in the retroperitoneal fat of HFS rats compared to Control (Figure 60), and it was significantly overexpressed in Q-NS-PEG (170 times higher), indicating that UCP1 was working on thermogenesis, regulating energy spending, and decreasing oxidative stress. In addition, *Ucp1* was quantified in white fat (retroperitoneal fat), indicating that the formulation had the ability to promote WAT browning. Adipose tissue browning consists of the induction of thermogenically active

adipocytes in white depots (these adipocytes are called beige, and they express high levels of UCP1), and studies suggest that browning of subcutaneous and visceral white adipose tissue could have a beneficial effect on global energy metabolism (305).

Few studies have been performed in the analysis of the connection between quercetin and UCP1, and our results are in agreement with these previously reported ones. Kuipers and co-workers reported that quercetin administration (as high fat diet supplemented with quercetin 0.1% w/w for 12 weeks) increased *Ucp1* levels in the subcutaneous white adipose tissue of obese C57BL/6J mice, but it did not modify it in the brown adipose tissue, gonadal WAT, and visceral WAT (114). This increase was three times compared to obese control. Choi *et al.* used the same mice and diet, obtaining that quercetin supplementation for 9 weeks (0.05% w/w) increased *Ucp1* levels on inguinal WAT and brown adipose tissue, and also in 3T-L1 adipocytes *in vitro* (306). In the present work, the treatment with Q-NS-PEG overexpressed *Ucp1* more significantly than in the mentioned works, probably due to the formulation of the quercetin in zein-based nanocarriers, which would promote higher bioavailability and effects that quercetin-supplemented diet.

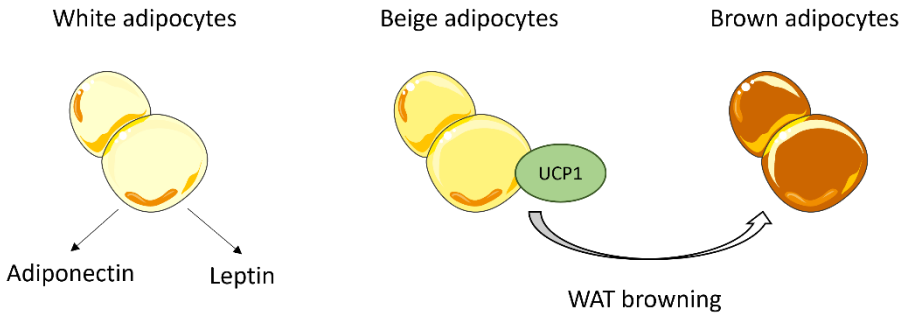

Figure 65. Type of adipocytes and schematic representation of *AdipoQ*, *Lep*, and *Ucp1*.

Peroxisome proliferator-activated receptor γ (PPARγ, encoded by the gene *Pparg*) is a transcription factor needed for white adipogenesis (115,228). It is primarily expressed in adipose tissue (white and brown), but also in the liver, large intestine, spleen, and muscle tissue (307,308). It plays a key role in the regulation of adipogenesis, energy balance, and lipid biosynthesis, participates in lipoprotein metabolism and insulin sensitivity (308). Its ability to stimulate preadipocyte differentiation into either white or brown/beige adipocytes appears to be determined by its associated coactivators (228). PPARγ has an important role in the lipogenesis of adipocytes by promoting the uptake of free fatty acids and increasing the content of triglycerides in the adipocytes and reduction of free fatty acids delivery to the liver (111). Hepatic free fatty acids synthesis is catalysed by acetyl-CoA carboxylase and fatty acid synthase, an enzyme that is complexly regulated by nuclear receptors (PPARα and PPARγ) (111). The dysregulation of *Pparg* is related to the development of obesity, T2DM, atherosclerosis, and other diseases (308). PPARγ regulates high-fat diet-induced fat accumulation in the liver (115),

and its overexpression induces hepatic steatosis (309). In fact, PPARγ is increased in livers with steatosis of both animal models of obesity and NAFLD patients (310).

Thus, in this work a very slight increase of *Pparg* was seen in the liver of HFS rats, which could be related to hepatic steatosis, and the gene expression was slightly decreased by Q-NS-PEG (Figure 56), what could explain the improvement of the steatosis. However, in adipocytes, the activation of PPARγ ensures the adequate and balanced secretion of adipocytokines (adiponectin and leptin) (308). In addition, *Pparg* upregulation improves metabolic indices in T2DM (308). Inflammatory factors decrease the expression of PPARγ and increase free fatty acids in the circulation by promoting lipolysis through inhibiting the insulin signaling pathway in an indirect way (27). In this work, HFS diet produced inflammation (measured by MCP-1), what could explain the underexpression of *Pparg* in the retroperitoneal fat of HFS rats compared to Control, while Q-NS-PEG reverted this situation, overexpressing the gene compared to HFS (Figure 61). This situation is in accordance with the overexpression of *AdipoQ* and *Lep* in the retroperitoneal fat of rats treated with Q-NS-PEG (Figure 59), compared to HFS, and with the serum glucose reduction observed by the formulation (Figure 46A). Our results are only partially in accordance with previously reported ones, in which PPARγ was downregulated in HFS-fed Wistar rats in adipose tissue and in the liver, and quercetin did not revert this situation (111). However, in Western diet-fed C57BL/6J mice, *Pparg* was upregulated in the liver compared to standard diet, while quercetin decreased this value compared to obese mice (115).

Sterol regulatory element-binding proteins (SREBPs) are a family of transcription factors that activate genes that encode enzymes required for the synthesis of cholesterol and unsaturated fatty acids. *Srebp1* gene encodes SREBP-1a and SREBP-1c, that activate transcription of genes required for the synthesis of fatty acids and triglycerides, including acetyl-coenzyme A carboxylase, fatty acid synthase, stearoyl-CoA desaturase, and glycerol 3-phosphate acyltransferase (229). Among the two isoforms, SREBP-1c is weaker transcriptional activator than SREBP-1a, but is the main isoform in animal and human tissues, including liver and adipose tissue (311). SREBP1 activation causes lipid-mediated cellular stress (lipotoxicity) that contributes to metabolic diseases such as obesity, diabetes, or hepatic steatosis (312). However, global SREBP-1 deficiency completely ameliorates hepatic steatosis in mouse models of obesity, while SREBP-1c deficiency partially ameliorates hepatic steatosis (312).

In our case, a slight decrease of *Srebp1* was observed in the livers of HFS compared to Control, while Q-NS-PEG did not modify these values (Figure 56), what could indicate that the effect of SREBP-1 on hepatic steatosis was not significant. This tendency is not in accordance with previously obtained results; *Srebp1* was previously upregulated in the livers of HFS-fed Wistar rats (211) and western diet-fed C57BL/6J mice (115) in previous studies, and quercetin diet supplementation for 20 weeks downregulated it (115). These differences could be attributed to the obesity model (specie, diet) and length of treatment. In the retroperitoneal fat, *Srebp1* was downregulated in HFS rats, and overexpressed in Q-NS-PEG (Figure 61). Oberkofler *et al.* demonstrated that SREBP-

1a mRNA expression levels in intra- and extraperitoneal adipose tissue of obese, never-obese, and post-obese humans were similar, but differences were found in SREBP-1c (311). SREBP-1c mRNA levels on intraperitoneal tissue were as follows: obese < never-obese < post-obese, a fact that would be in accordance with our results, being obese HFS rats, never-obese Control rats, and post-obese Q-NS-PEG-treated rats.

In animal metabolism, fatty acids come from two different sources: the exogenously derived fatty acids (dietary fatty acids) or endogenously synthetized de novo (313). *Fasn* gene encodes the enzyme fatty acid synthase (FASN), that catalyses the endogenous synthesis of fatty acids and plays a key role in the synthesis of short- and medium-chain fatty acids in mammals (227). Under normal physiological conditions, FASN is a housekeeping protein in the liver where controls the hepatic triglyceride mechanism. When a high amount of carbohydrates is present, glucose is converted to fatty acids with the help of FASN. Excess fatty acids are then assembled into triglycerides and stored in the form of lipid droplets or secreted as very low-density lipoproteins (314).

In retroperitoneal fat, *Fasn* was significantly downregulated in HFS rats compared to Control, and was again upregulated by Q-NS-PEG (Figure 58). In the liver, the gene was decreased in HFS-treated rats compared to Control, and, even more with the Q-NS-PEG treatment, but any differences were found between HFS and Q-NS-PEG (Figure 55). These results are not in accordance with previously reported ones, where *Fasn* was upregulated in the liver of HFS-fed Wistar rats in the study performed by Aranaz and co-workers (211), and also in the one performed by Kobori *et al.*, where quercetin downregulated *Fasn* (115). Nevertheless, as previously explained, obesity induces a chronic inflammation in the adipose tissue and liver, and this chronic inflammation induces the release of proinflammatory cytokines such as TNF-α (285). It has been demonstrated that TNF-α decreases the expression of some genes in adipocytes, including *Fasn* (313), what could explain its downregulation in retroperitoneal fat of HFS rats. At the same time, it was demonstrated that quercetin decreases TNF-α (101,315), what could lead to an increase in FASN in retroperitoneal fat.

The sterol carrier protein-2 (SCP-2), encoded by the gene *Scp2* (316), is a multi-purpose lipid binding protein that transports cholesterol and other lipids from the endoplasmatic reticulum (where they are synthesized) to the surface of the cell, or from the outer to the inner mitochondrial membrane. It can bind to different types of lipids, such as fatty acids, fatty acyl CoA derivatives, and phospholipids, facilitating the transfer of those lipids between membranes (230,317). It also promotes the transport of fatty acids, glycosphingolipids, and gangliosides between vesicles (317). Recently, it is been demonstrated that SCP-2 is closely related to the development of metabolic disorders, such as obesity or T2DM, but it has been found to protect against NAFLD by regulating the intracellular transport and metabolism of lipids, such as cholesterol, endocannabinoid, and fatty acid (317). In this work, *Scp2* was not modified in HFS-fed rats, whereas Q-NS-PEG had the ability to upregulate the gene in the retroperitoneal fat (Figure 58), probably protecting against NAFLD, and hence, reducing hepatic steatosis.

Table 24 summarizes the effect of HFS diet compared to standard diet, and the effect of the treatment with Q-NS-PEG compared to HFS group in the expression of all the genes of the efficacy study. As can be observed, Q-NS-PEG upregulated significantly all the analysed genes in retroperitoneal fat, while any significant effect was present in the liver. This would be translated in a high effect on fat lipolysis, β-oxidation, reduction of hepatic steatosis, and WAT browning.

Table 24. Summary of the effects of HFS (compared to Control) and Q-NS-PEG (compared to HFS) in the expression of the analysed genes in retroperitoneal fat and liver. Control: standard diet; HFS: high fat/high sucrose diet; Q-NS-PEG: PEG-coated quercetin-loaded nanospheres; ns: non-significant; ↓: downregulation; ↑: upregulation.

	Liver		**Retroperitoneal fat**	
Gene	**HFS (vs Control)**	**Q-NS-PEG (vs HFS)**	**HFS (vs Control)**	**Q-NS-PEG (vs HFS)**
Acot8	↓	ns	↓	↑
Cpt2	ns	ns	-	-
Acox1	ns	ns	ns	↑
Hsd17b4	-	-	ns	↑
AdipoQ	-	-	↓	↑
Lep	-	-	ns	↑
Ucp1	-	-	ns	↑
Pparg	ns	ns	↓	↑
Srebp1	ns	ns	↓	↑
Fasn	↓	ns	↓	↑
Scp-2	-	-	ns	↑

5.16. Which are the reasons that may explain the apparent lack of correlation between the bioavailability and efficacy results obtained with the Q-NS-PEG formulation?

From the experimental results presented in this work, it may be inferred a certain lack of concordance between the pharmacokinetic data in healthy animals and the efficacy results in the obese rat model. Thus, the formulation capable of achieving the highest oral bioavailability of quercetin (NS) presented mediocre efficacy results, significantly lower than those obtained with Q-NS-PEG25. This lack of concordance may be explained by, at least, two different concepts (or a combination of both).

The former would be related with the slow elimination rate of quercetin when nanoencapsulated in PEG-coated nanospheres. In principle, a long half-life usually means a long duration of the effect (318). In a similar way, a long MRT implies an increase of the average time that molecules of a dosed drug spend in the body (319). This sustained effect that would promote PEG-coated nanoparticles would facilitate a

prolonged and continuous presence of the flavonoid in the body and, thus, maintaining the intensity of the pharmacological effect of quercetin for a long period than with the other nanoformulations. This increased efficacy of sustained-release formulations is widely reported for a number of drugs in the treatment of hypertriglyceridemia (320), diabetes (321), or liver damage (322).

The latter would be related to a greater ability of PEG-coated nanoparticles to conduct the loaded flavonoid and reach the colon than bare nanoparticles. In the human gastrointestinal microbiota, the microbial density increases from the proximal to the distal gut, and bacterial diversity increases in the same axes and manner (311). In the colon, the released quercetin would be metabolized by the microbiota, yielding active metabolites that would later reach the bloodstream. It is well known that colonic microbiota can degrade flavonoids, generating a large number of metabolites that can be absorbed and exert biological effects in the body (95,97). The major microbial metabolite of quercetin is 3,4-dyhydroxyphenylacetic acid (DOPAC) (323,324), which also has potent antioxidant properties (325). In spite of this microbiota-derived metabolite of quercetin has scarcely studied, DOPAC would alleviate hyperglycaemia and decrease insulin resistance of Type-2 diabetes mice (326). Furthermore, DOPAC exhibits a significant anti-inflammatory effect by decreasing the levels of pro-inflammatory cytokines (e.g., IL-6) and increasing that of anti-inflammatory cytokine IL-10 (326).

5.17. Summary of the effects of the efficacy study

To sum up all the effects of quercetin either as free or encapsulated treatments, Figure 67 has been developed. In the study, it was observed that Q-NS decreased the epididymal adipocyte size, and also, serum TAG, AIP, and plasma MCP-1 levels. In the case of Q-NC, similar results have been observed. Effects on the epididymal adipocyte size, serum TAG, and AIP were similar. However, nanocapsules presented the ability to decrease the visceral WAT and also hepatic steatosis, maybe due to the presence of the oil, but they were not able to decrease MCP-1 levels significantly.

Regarding Q-Susp, the formulation was able to decrease epididymal fat and its adipocyte size, but also subcutaneous fat, brown fat, and visceral WAT. Plasma MCP-1 levels were also decreased, but HDL-cholesterol levels too.

On the other hand, PEG-coated nanospheres were the ones that presented a higher amount of positive effects in the DIO model. This formulation was the only one decreasing the percentage of general body fat. It decreased epididymal and retroperitoneal fats and the size of its adipocytes, subcutaneous fat, and visceral WAT. It also exerted beneficial effects on biochemical parameters: Q-NS-PEG decreased serum TAG levels, AIP, and serum glucose levels. It also presented a reduction of plasma MCP-1. In the liver, it improved the steatosis and TAG levels.

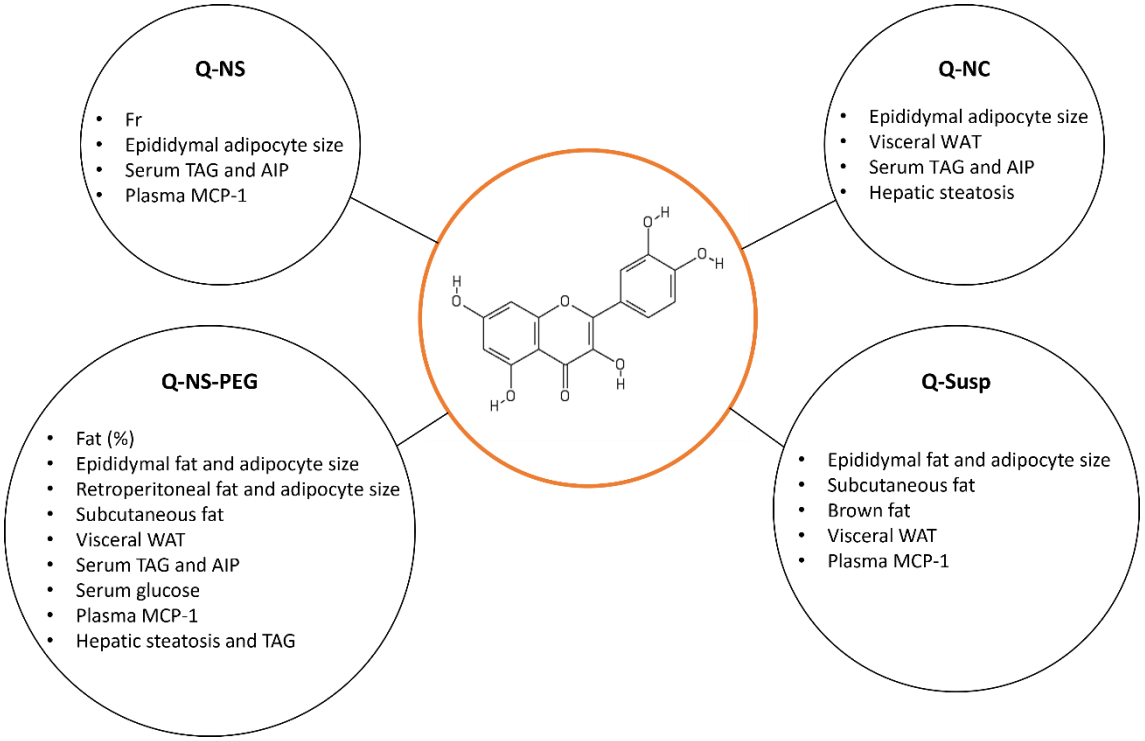

Figure 67. Positive effects of quercetin, as free or encapsulated formulations, in the pharmacokinetic study in Wistar rats and in the efficacy study performed in a DIO model of Wistar rats. Q-NS; quercetin-loaded nanospheres; Q-NC: quercetin-loaded nanocapsules; Q-NS-PEG: PEG-coated quercetin-loaded nanospheres; Q-Susp: quercetin suspension.

Chapter 6

Conclusions

6. Conclusions

1. Zein-based nanoparticles have successfully been prepared by the desolvation method. Three kinds of nanoparticles have been developed: nanospheres, nanocapsules (containing wheat germ oil), and polyethylene glycol 35,000 (PEG)-coated nanospheres. The coating of nanospheres with PEG significantly improved its hydrophilicity and its movement through intestinal mucus.

2. The flavonoid quercetin was successfully loaded in zein-based nanoparticles, without affecting the physico-chemical properties of the nanocarrier. A similar amount of flavonoid was encapsulated in all kinds of nanoparticles (between 70 and 76 μg quercetin/mg). The *in vitro* release profile of quercetin was not affected by the nanoencapsulation of the flavonoid in zein-based nanoparticles.

3. Quercetin decreased the fat accumulation in the nematode *Caenorhabditis elegans*, both in a nematode growth medium (NGM) and in a glucose-supplemented NGM. Under high glucose conditions, the effect of quercetin was significantly increased when encapsulated in zein nanospheres (bare or coated ones). Nevertheless, this effect was inhibited when the flavonoid was formulated in zein nanocapsules.

4. All zein-based nanoparticles displayed similar gastrointestinal transit in rat, being NC and NS-PEG50 the fastest formulations. PEG-coated nanospheres appeared to be more internalized in the intestinal mucus layer.

5. Quercetin-loaded zein nanoparticles improved the relative oral bioavailability and pharmacokinetic parameters after an oral single dose of 15 mg/kg in Wistar rats, compared to an aqueous suspension of the flavonoid. The highest relative oral bioavailability was obtained for Q-NS (about 57%), followed by Q-NS-PEG25 (37%).

6. Diet-induced obesity (DIO) model was achieved when Wistar male rats were fed with a high fat/high sucrose diet for 18 weeks. Animals presented higher weight and amount of fat depots, bigger adipocyte size, altered biochemical parameters, hepatic steatosis, and higher hepatic triglycerides, compared to standard diet-fed rats.

7. Quercetin demonstrated to have an effect in decreasing the proportion of fat depots in the DIO model in Wistar rats after 5 weeks of daily treatment by oral gavage at 15 mg/kg dose. Q-NS-PEG was the formulation that decreased more kinds of fat depots (epididymal, retroperitoneal, subcutaneous, and visceral white adipose tissue), including the decrease in the adipocyte size in epididymal and retroperitoneal fats.

8. All the quercetin-loaded zein-based nanoparticles demonstrated to have an effect in decreasing serum triglyceride levels in the DIO model in Wistar rats after 5 weeks of daily treatment by oral gavage at 15 mg/kg dose. The atherogenic index of plasma (AIP) was also decreased.

9. Only PEG-coated quercetin-loaded zein nanospheres demonstrated to have an effect in decreasing serum glucose levels in the DIO animal model.

10. Both quercetin-loaded bare and coated zein nanospheres (Q-NS and Q-NS-PEG) decreased the amount of the inflammatory cytokine monocyte chemoattractant protein-1 (MCP-1) plasma levels in the DIO model, due, probably, to the anti-inflammatory effect of quercetin.

11. Quercetin slightly decreased the hepatic steatosis and triglycerides present in the DIO model. Q-NS-PEG was the only formulation in decreasing liver triglycerides significantly (35% lower liver triglycerides than obese control).

12. Q-NS-PEG promoted the overexpression of all the analysed genes (genes that encode proteins involved in lipid metabolism (*Acot8*, *Acox1*, *Hsd17b4*) and synthesis (*Fasn*, *Scp2*), genes encoding adipokines (*AdipoQ*, *Lep*), a gene related to the browning of fat (*Ucp1*), and genes encoding transcription factors related to adipogenesis (*Pparg*, *Srebp1*)) in the retroperitoneal fat of DIO model, compared to obese control. In the case of the liver, there were not any changes between treated and obese rats, although a reduction of *Cpt2* and *Fasn* (genes involved in lipid metabolism and synthesis, respectively) was observed, but compared to Control.

References

References

1. WHO Regional Office for Europe. WHO European Regional Obesity Report 2022. Copenhagen; 2022.
2. Noda M. BMI normogram. Clin Nutr. 2008;27(1):168–9.
3. Koliaki C, Liatis S, Kokkinos A. Obesity and cardiovascular disease: revisiting an old relationship. Metabolism. 2019;92:98–107.
4. Lin X, Li H. Obesity: Epidemiology, Pathophysiology, and Therapeutics. Front Endocrinol (Lausanne). 2021;12(September):1–9.
5. Durrer Schutz D, Busetto L, Dicker D, Farpour-Lambert N, Pryke R, Toplak H, et al. European Practical and Patient-Centred Guidelines for Adult Obesity Management in Primary Care. Obes Facts. 2019;12(1):40–66.
6. Ruban A, Stoenchev K, Ashrafian H, Teare J. Current treatments for obesity. Clin Med (Northfield Il). 2019 May;19(3):205–12.
7. Coppock JH, Ridolfi DR, Hayes JF, St. Paul M, Wilfley DE. Current Approaches to the Management of Pediatric Overweight and Obesity. Curr Treat Options Cardiovasc Med. 2014 Nov 11;16(11):343.
8. Sarma S, Sockalingam S, Dash S. Obesity as a multisystem disease: Trends in obesity rates and obesity-related complications. Diabetes, Obes Metab. 2021;23(S1):3–16.
9. Ćurić M, Klobučar Majanović S, Detel D, Ružić A, Štimac D. Obesogens – new global health problem? Period Biol. 2021 Jul 1;123(3–4):49–53.
10. Sakers A, De Siqueira MK, Seale P, Villanueva CJ. Adipose-tissue plasticity in health and disease. Cell. 2022;185(3):419–46.
11. World Health Organization (WHO). Obesity and overweight [Internet]. [cited 2022 Jul 27]. Available from: https://www.who.int/news-room/fact-sheets/detail/obesity-and-overweight
12. Boccellino M, D'Angelo S. Anti-obesity effects of polyphenol intake: Current status and future possibilities. Int J Mol Sci. 2020;21(16):1–24.
13. Abarca-Gómez L, Abdeen ZA, Hamid ZA, Abu-Rmeileh NM, Acosta-Cazares B, Acuin C, et al. Worldwide trends in body-mass index, underweight, overweight, and obesity from 1975 to 2016: a pooled analysis of 2416 population-based measurement studies in 128·9 million children, adolescents, and adults. Lancet. 2017 Dec;390(10113):2627–42.
14. Global Health Observatory. Geneva: World Health Organization. Noncommunicable diseases: risk factors. Overweight/Obesity [Internet]. [cited 2022 Jul 22]. Available from: https://www.who.int/data/gho/data/themes/topics/noncommunicable-diseases-risk-factors

15. Copenhagen: WHO Regional Office for Europe. WHO European Health Equity Status Report initiative (HESRi) - Health Equity Dataset [interactive platform].

16. The United Nations Children's Fund (UNICEF). UNICEF-WHO-World Bank: Joint Child Malnutrition Estimates - 2021 edition interactive dashboard [Internet]. 2021 [cited 2022 Sep 7]. Available from: https://data.unicef.org/resources/joint-child-malnutrition-estimates-interactive-dashboard-2021/

17. Agencia Española de Seguridad Alimentaria y Nutrición (AESAN). Memoria AESAN 2020. 2020.

18. Agencia Española de Seguridad Alimentaria y Nutrición (AESAN). Estudio ALADINO 2019. Estudio sobre la Alimentación, Actividad Física, Desarrollo Infantil y Obesidad en España 2019. 2019.

19. Agencia Española de Seguridad Alimentaria y Nutrición (AESAN). Ministerio de Consumo. Evaluación y seguimiento de la Estrategia NAOS: conjunto mínimo de indicadores [Internet]. Madrid, 2021. [cited 2022 May 17]. Available from: https://www.aesan.gob.es/AECOSAN/web/nutricion/subseccion/indicadores.htm

20. Withrow D, Alter DA. The economic burden of obesity worldwide: A systematic review of the direct costs of obesity. Obes Rev. 2011;12(2):131–41.

21. Health and Environment Alliance (HEAL). Health costs in the European Union - How much is related to EDCS? 2014.

22. Okunogbe A, Nugent R, Spencer G, Ralston J, Wilding J. Economic impacts of overweight and obesity: Current and future estimates for eight countries. BMJ Glob Heal. 2021;6(10).

23. European Parliament. Commetee on the Environment Public Health and Food Safety. Compromise amendments 1 - 10. Brussels; 2020.

24. Kral JG, Kava RA, Catalano PM, Moore BJ. Severe obesity: The neglected epidemic. Obes Facts. 2012;5(2):254–69.

25. Institute for Health Metrics and Evaluation. Deaths by risk factor in WHO European Region, both sexes, all ages, 2019 [Internet]. Viz Hub. [cited 2022 Jul 22]. Available from: http://ihmeuw.org/5o2n

26. Institute for Health Metrics and Evaluation. Deaths by risk factor Globally, both sexes, all ages, 2019 [Internet]. Viz Hub. [cited 2022 Jul 22]. Available from: http://ihmeuw.org/5o2n

27. Tong Y, Xu S, Huang L, Chen C. Obesity and insulin resistance: Pathophysiology and treatment. Drug Discov Today. 2022;27(3):822–30.

28. Castro-Barquero S, Ruiz-León AM, Sierra-Pérez M, Estruch R, Casas R. Dietary strategies for metabolic syndrome: A comprehensive review. Nutrients. 2020;12(10):1–21.

29. Alberti G, Zimmet P, Shaw J, Grundy SM. The IDF consensus worldwide definition of the metabolic syndrome. International Diabetes Federation (IDF). 2006.

30. Scuteri A, Laurent S, Cucca F, Cockcroft J, Cunha PG, Mañas LR, et al. Metabolic syndrome across Europe: Different clusters of risk factors. Eur J Prev Cardiol. 2015;22(4):486–91.

31. Akhlaghi M. Non-alcoholic Fatty Liver Disease: Beneficial Effects of Flavonoids. Phyther Res. 2016;1571(June):1559–71.

32. Care D, Suppl SS. 2. Classification and Diagnosis of Diabetes: Standards of Medical Care in Diabetes—2020. Diabetes Care. 2020 Jan 1;43(Supplement_1):S14–31.

33. Tamayo T, Rosenbauer J, Wild SH, Spijkerman AMW, Baan C, Forouhi NG, et al. Diabetes in Europe: An update. Diabetes Res Clin Pract. 2014;103(2):206–17.

34. Zou B, Yeo YH, Cheung R, Ingelsson E, Nguyen MH. Fatty Liver Index and Development of Cardiovascular Disease: Findings from the UK Biobank. Dig Dis Sci. 2021;66(6):2092–100.

35. Cholongitas E, Pavlopoulou I, Papatheodoridi M, Markakis GE, Bouras E, Haidich AB, et al. Epidemiology of nonalcoholic fatty liver disease in europe: A systematic review and meta-analysis. Ann Gastroenterol. 2021;34(3):404–14.

36. Estes C, Anstee QM, Arias-Loste MT, Bantel H, Bellentani S, Caballeria J, et al. Modeling NAFLD disease burden in China, France, Germany, Italy, Japan, Spain, United Kingdom, and United States for the period 2016–2030. J Hepatol. 2018;69(4):896–904.

37. Powell EE, Wong VWS, Rinella M. Non-alcoholic fatty liver disease. Lancet. 2021;397(10290):2212–24.

38. Cobbina E, Akhlaghi F. Non-alcoholic fatty liver disease (NAFLD)–pathogenesis, classification, and effect on drug metabolizing enzymes and transporters. Drug Metab Rev. 2017;49(2):197–211.

39. Avgerinos KI, Spyrou N, Mantzoros CS, Dalamaga M. Obesity and cancer risk: Emerging biological mechanisms and perspectives. Metabolism. 2019;92:121–35.

40. Townsend N, Kazakiewicz D, Lucy Wright F, Timmis A, Huculeci R, Torbica A, et al. Epidemiology of cardiovascular disease in Europe. Nat Rev Cardiol. 2022;19(2):133–43.

41. Lauby-Secretan B, Scoccianti C, Loomis D, Grosse Y, Bianchini F, Straif K. Body Fatness and Cancer — Viewpoint of the IARC Working Group. N Engl J Med. 2016 Aug 25;375(8):794–8.

42. Dixon AE, Peters U. The effect of obesity on lung function. Expert Rev Respir Med. 2018 Sep 2;12(9):755–67.

43. Quaderi SA, Hurst JR. The unmet global burden of COPD. Glob Heal Epidemiol Genomics. 2018;3:18–20.

44. Narang I, Bush A. Early origins of chronic obstructive pulmonary disease. Semin Fetal Neonatal Med. 2012;17(2):112–8.

45. Brigham EP, Anderson JA, Brook RD, Calverley PMA, Celli BR, Cowans NJ, et al.

Challenging the obesity paradox: Extreme obesity and COPD mortality in the SUMMIT trial. ERJ Open Res. 2021;7(3):1–9.

46. Young T. Risk Factors for Obstructive Sleep Apnea in Adults. JAMA. 2004 Apr 28;291(16):2013.

47. Hermann DM, Bassetti CL. Role of sleep-disordered breathing and sleep-wake disturbances for stroke and stroke recovery. Neurology. 2016 Sep 27;87(13):1407–16.

48. Seetho IW, Wilding JPH. Sleep-disordered breathing, type 2 diabetes and the metabolic syndrome. Chron Respir Dis. 2014;11(4):257–75.

49. Senaratna C V., Perret JL, Lodge CJ, Lowe AJ, Campbell BE, Matheson MC, et al. Prevalence of obstructive sleep apnea in the general population: A systematic review. Sleep Med Rev. 2017;34:70–81.

50. Wearing SC, Hennig EM, Byrne NM, Steele JR, Hills AP. Musculoskeletal disorders associated with obesity: A biomechanical perspective. Obes Rev. 2006;7(3):239–50.

51. Neogi T, Zhang Y. Epidemiology of Osteoarthritis. Rheum Dis Clin North Am. 2013;39(1):1–19.

52. Reyes C, Leyland KM, Peat G, Cooper C, Arden NK, Prieto-Alhambra D. Association Between Overweight and Obesity and Risk of Clinically Diagnosed Knee, Hip, and Hand Osteoarthritis: A Population-Based Cohort Study. Arthritis Rheumatol. 2016;68(8):1869–75.

53. Milaneschi Y, Simmons WK, van Rossum EFC, Penninx BW. Depression and obesity: evidence of shared biological mechanisms. Mol Psychiatry. 2019 Jan 16;24(1):18–33.

54. Peeters A, Barendregt JJ, Willekens F, Mackenbach JP, Al Mamun A, Bonneux L, et al. Obesity in adulthood and its consequences for life expectancy: A life-table analysis. Ann Intern Med. 2003;138(1):24–32.

55. MacMahon S, Baigent C, Duffy S, Rodgers A, Tominaga S, Chambless L, et al. Body-mass index and cause-specific mortality in 900 000 adults: Collaborative analyses of 57 prospective studies. Lancet. 2009;373(9669):1083–96.

56. Institute for Health Metrics and Evaluation. Years lived with disability by risk factor in WHO European Region, both sexes, all ages, 2019 [Internet]. Viz Hub. [cited 2022 Jul 23]. Available from: http://ihmeuw.org/5o2n

57. Aghili SMM, Ebrahimpur M, Arjmand B, Shadman Z, Pejman Sani M, Qorbani M, et al. Obesity in COVID-19 era, implications for mechanisms, comorbidities, and prognosis: a review and meta-analysis. Int J Obes. 2021;45(5):998–1016.

58. Mossink JP. Zinc as nutritional intervention and prevention measure for COVID–19 disease. BMJ Nutr Prev Heal. 2020;3(1):111–7.

59. Zhong Q, Lin R, Nong Q. Adiposity and serum selenium in U.S. adults. Nutrients. 2018;10(6).

60. Sun Y, Sun M, Liu B, Du Y, Rong S, Xu G, et al. Inverse association between serum vitamin B12 concentration and obesity among adults in the United States. Front Endocrinol (Lausanne). 2019;10(JUN):4–10.

61. Kim H, Hwang JY, Kim KN, Ha EH, Park H, Ha M, et al. Relationship between body-mass index and serum folate concentrations in pregnant women. Eur J Clin Nutr. 2012;66(1):136–8.

62. Dewansingh P, Reckman GAR, Mijlius CF, Krijnen WP, van der Schans CP, Jager-Wittenaar H, et al. Protein, Calcium, Vitamin D Intake and 25(OH)D Status in Normal Weight, Overweight, and Obese Older Adults: A Systematic Review and Meta-Analysis. Front Nutr. 2021;8(September):1–15.

63. Barazzoni R, Bischoff S, Boirie Y, Busetto L, Cederholm T, Dicker D, et al. Sarcopenic Obesity: Time to Meet the Challenge. Obes Facts. 2018;11(4):294–305.

64. Devlieger R, Benhalima K, Damm P, Van Assche A, Mathieu C, Mahmood T, et al. Maternal obesity in Europe: where do we stand and how to move forward? Eur J Obstet Gynecol Reprod Biol. 2016 Jun;201:203–8.

65. Poston L, Harthoorn LF, Van Der Beek EM. Obesity in pregnancy: Implications for the mother and lifelong health of the child. A consensus statement. Pediatr Res. 2011;69(2):175–80.

66. Razaz N, Villamor E, Muraca GM, Bonamy A-KE, Cnattingius S. Maternal obesity and risk of cardiovascular diseases in offspring: a population-based cohort and sibling-controlled study. Lancet Diabetes Endocrinol. 2020 Jul;8(7):572–81.

67. Kong L, Nilsson IAK, Brismar K, Gissler M, Lavebratt C. Associations of Different Types of Maternal Diabetes and Body Mass Index with Offspring Psychiatric Disorders. JAMA Netw Open. 2020;3(2):1–15.

68. Wharton S, Lau DCW, Vallis M, Sharma AM, Biertho L, Campbell-Scherer D, et al. Obesity in adults: A clinical practice guideline. Cmaj. 2020;192(31):E875–91.

69. Oppert JM, Bellicha A, van Baak MA, Battista F, Beaulieu K, Blundell JE, et al. Exercise training in the management of overweight and obesity in adults: Synthesis of the evidence and recommendations from the European Association for the Study of Obesity Physical Activity Working Group. Obes Rev. 2021;22(S4):1–12.

70. Hashem A, Khalouf A, Acosta A. Management of Obesity and Nonalcoholic Fatty Liver Disease: A Literature Review. Semin Liver Dis. 2021;41(4):435–47.

71. Mares AC, Chatterjee S, Mukherjee D. Semaglutide for weight loss and cardiometabolic risk reduction in overweight/obesity. Curr Opin Cardiol. 2022;37(4):350–5.

72. Shetty R, Basheer FT, Poojari PG, Thunga G, Chandran VP, Acharya LD. Adverse drug reactions of GLP-1 agonists: A systematic review of case reports. Diabetes Metab Syndr Clin Res Rev. 2022;16(3):102427.

73. Smits MM, Van Raalte DH. Safety of Semaglutide. Front Endocrinol (Lausanne). 2021;12(July).

74. Di Lorenzo N, Antoniou SA, Batterham RL, Busetto L, Godoroja D, Iossa A, et al. Clinical practice guidelines of the European Association for Endoscopic Surgery (EAES) on bariatric surgery: update 2020 endorsed by IFSO-EC, EASO and ESPCOP. Surg Endosc. 2020;34(6):2332–58.

75. World Health Organization (WHO). Guideline: assessing and managing children at primary health-care facilities to prevent overweight and obesity in the context of the double burden of malnutrition. Updates for the Integrated Management of Childhood Illness (IMCI). Geneva; 2017.

76. Baker JL, Farpour-Lambert NJ, Nowicka P, Pietrobelli A, Weiss R. Evaluation of the overweight/obese child - Practical tips for the primary health care provider: Recommendations from the childhood obesity task force of the European association for the study of obesity. Obes Facts. 2010;3(2):131–7.

77. Srivastava G, Fox CK, Kelly AS, Jastreboff AM, Browne AF, Browne NT, et al. Clinical Considerations Regarding the Use of Obesity Pharmacotherapy in Adolescents with Obesity. Obesity. 2019;27(2):190–204.

78. Pratt JSA, Browne A, Browne NT, Bruzoni M, Cohen M, Desai A, et al. ASMBS pediatric metabolic and bariatric surgery guidelines, 2018. Surg Obes Relat Dis. 2018;14(7):882–901.

79. Hosseini A, Razavi BM, Banach M, Hosseinzadeh H. Quercetin and metabolic syndrome: A review. Phyther Res. 2021;35(10):5352–64.

80. Sandoval V, Sanz-Lamora H, Arias G, Marrero PF, Haro D, Relat J. Metabolic impact of flavonoids consumption in obesity: From central to peripheral. Nutrients. 2020;12(8):1–55.

81. Bennick A. Interaction of plant polyphenols with salivary proteins. Crit Rev Oral Biol Med. 2002 Mar 1;13(2):184–96.

82. Rambaran TF. Nanopolyphenols: a review of their encapsulation and anti-diabetic effects. SN Appl Sci. 2020;2(8):1–26.

83. Harwood M, Danielewska-Nikiel B, Borzelleca JF, Flamm GW, Williams GM, Lines TC. A critical review of the data related to the safety of quercetin and lack of evidence of in vivo toxicity, including lack of genotoxic/carcinogenic properties. Food Chem Toxicol. 2007;45(11):2179–205.

84. Wang W, Sun C, Mao L, Ma P, Liu F, Yang J, et al. The biological activities, chemical stability, metabolism and delivery systems of quercetin: A review. Trends Food Sci Technol. 2016;56:21–38.

85. National Library of Medicine. Quercetin in PubChem [Internet]. [cited 2022 Jun 13]. Available from: https://pubchem.ncbi.nlm.nih.gov/compound/5280343

86. Bule M, Abdurahman A, Nikfar S, Abdollahi M, Amini M. Antidiabetic effect of quercetin: A systematic review and meta-analysis of animal studies. Food Chem

Toxicol. 2019;125(February):494–502.

87. Nabavi SF, Russo GL, Daglia M, Nabavi SM. Role of quercetin as an alternative for obesity treatment: You are what you eat! Food Chem. 2015;179:305–10.

88. Phenol-Explorer. Polyphenol Classes, Flavonoids, Flavonols, Quercetin 3-O-rutinoside [Internet]. [cited 2022 Jul 27]. Available from: http://phenol-explorer.eu/compounds/296

89. Phenol-Explorer. Polyphenol Classes, Flavonoids, Flavonols, Quercetin 3-O-rhamnoside [Internet]. [cited 2022 Jul 27]. Available from: http://phenol-explorer.eu/compounds/295

90. Peñalva R, Esparza I, Morales-Gracia J, González-Navarro CJ, Larrañeta E, Irache JM. Casein nanoparticles in combination with 2-hydroxypropyl-β-cyclodextrin improves the oral bioavailability of quercetin. Int J Pharm. 2019;570(August):118652.

91. Lesjak M, Beara I, Simin N, Pintać D, Majkić T, Bekvalac K, et al. Antioxidant and anti-inflammatory activities of quercetin and its derivatives. J Funct Foods. 2018;40(November 2017):68–75.

92. Agencia Española de Seguridad Alimentaria y Nutrición (AESAN). Informe del Comité Científico de la Agencia Española de Seguridad Alimentaria y Nutrición (AESAN) sobre condiciones de uso de determinadas sustancias distintas de vitaminas, minerales y plantas para ser empleadas en complementos alimenticios - 1. 2012;11–234.

93. Lozano-Pérez AA, Rivero HC, Pérez Hernández M del C, Pagán A, Montalbán MG, Víllora G, et al. Silk fibroin nanoparticles: Efficient vehicles for the natural antioxidant quercetin. Int J Pharm. 2017;518(1–2):11–9.

94. Almeida AF, Borge GIA, Piskula M, Tudose A, Tudoreanu L, Valentová K, et al. Bioavailability of Quercetin in Humans with a Focus on Interindividual Variation. Compr Rev Food Sci Food Saf. 2018;17(3):714–31.

95. Murota K, Nakamura Y, Uehara M. Flavonoid metabolism: The interaction of metabolites and gut microbiota. Biosci Biotechnol Biochem. 2018;82(4):600–10.

96. Pinheiro RGR, Pinheiro M, Neves AR. Nanotechnology innovations to enhance the therapeutic efficacy of quercetin. Nanomaterials. 2021;11(10):1–26.

97. Luca SV, Macovei I, Bujor A, Miron A, Skalicka-Woźniak K, Aprotosoaie AC, et al. Bioactivity of dietary polyphenols: The role of metabolites. Crit Rev Food Sci Nutr. 2020;60(4):626–59.

98. D'Andrea G. Quercetin: A flavonol with multifaceted therapeutic applications? Fitoterapia. 2015;106:256–71.

99. Ulusoy HG, Sanlier N. A minireview of quercetin: from its metabolism to possible mechanisms of its biological activities. Crit Rev Food Sci Nutr. 2020;60(19):3290–303.

100. Xu D, Hu MJ, Wang YQ, Cui YL. Antioxidant activities of quercetin and its

complexes for medicinal application. Molecules. 2019;24(6).

101. Li Y, Yao J, Han C, Yang J, Chaudhry MT, Wang S, et al. Quercetin, inflammation and immunity. Nutrients. 2016;8(3):1–14.

102. Tang SM, Deng XT, Zhou J, Li QP, Ge XX, Miao L. Pharmacological basis and new insights of quercetin action in respect to its anti-cancer effects. Biomed Pharmacother. 2020;121(July 2019):109604.

103. Kukongviriyapan U, Sompamit K, Pannangpetch P, Kukongviriyapan V, Donpunha W. Preventive and therapeutic effects of quercetin on lipopolysaccharide-induced oxidative stress and vascular dysfunction in mice. Can J Physiol Pharmacol. 2012;90(10):1345–53.

104. Tzankova V, Aluani D, Kondeva-Burdina M, Yordanov Y, Odzhakov F, Apostolov A, et al. Hepatoprotective and antioxidant activity of quercetin loaded chitosan/alginate particles in vitro and in vivo in a model of paracetamol-induced toxicity. Biomed Pharmacother. 2017;92:569–79.

105. Kalantari H, Foruozandeh H, Khodayar MJ, Siahpoosh A, Saki N, Kheradmand P. Antioxidant and hepatoprotective effects of Capparis spinosa L. fractions and Quercetin on tert-butyl hydroperoxide- induced acute liver damage in mice. J Tradit Complement Med. 2018;8(1):120–7.

106. Morikawa K, Nonaka M, Narahara M, Torii I, Kawaguchi K, Yoshikawa T, et al. Inhibitory effect of quercetin on carrageenan-induced inflammation in rats. Life Sci. 2003;74(6):709–21.

107. Mamani-Matsuda M, Kauss T, Al-Kharrat A, Rambert J, Fawaz F, Thiolat D, et al. Therapeutic and preventive properties of quercetin in experimental arthritis correlate with decreased macrophage inflammatory mediators. Biochem Pharmacol. 2006;72(10):1304–10.

108. Penalva R, González-Navarro CJ, Gamazo C, Esparza I, Irache JM. Zein nanoparticles for oral delivery of quercetin: Pharmacokinetic studies and preventive anti-inflammatory effects in a mouse model of endotoxemia. Nanomedicine Nanotechnology, Biol Med. 2017 Jan;13(1):103–10.

109. Hashemzaei M, Far AD, Yari A, Heravi RE, Tabrizian K, Taghdisi SM, et al. Anticancer and apoptosis-inducing effects of quercetin in vitro and in vivo. Oncol Rep. 2017;38(2):819–28.

110. Rivera Rivera A, Castillo-Pichardo L, Gerena Y, Dharmawardhane S. Anti-Breast Cancer Potential of Quercetin via the Akt/AMPK/Mammalian Target of Rapamycin (mTOR) Signaling Cascade. Tan M, editor. PLoS One. 2016 Jun 10;11(6):e0157251.

111. Ragab SMM, Abd Elghaffar SK, El-Metwally TH, Badr G, Mahmoud MH, Omar HM. Effect of a high fat, high sucrose diet on the promotion of non-alcoholic fatty liver disease in male rats: The ameliorative role of three natural compounds. Lipids Health Dis. 2015;14(1):1–11.

112. Arias N, MacArulla MT, Aguirre L, Martínez-Castaño MG, Portillo MP. Quercetin

can reduce insulin resistance without decreasing adipose tissue and skeletal muscle fat accumulation. Genes Nutr. 2014;9(1).

113. Rivera L, Morón R, Sánchez M, Zarzuelo A, Galisteo M. Quercetin ameliorates metabolic syndrome and improves the inflammatory status in obese Zucker rats. Obesity. 2008;16(9):2081–7.

114. Kuipers EN, van Dam AD, Held NM, Mol IM, Houtkooper RH, Rensen PCN, et al. Quercetin lowers plasma triglycerides accompanied by white adipose tissue browning in diet-induced obese mice. Int J Mol Sci. 2018;19(6):1–14.

115. Kobori M, Masumoto S, Akimoto Y, Oike H. Chronic dietary intake of quercetin alleviates hepatic fat accumulation associated with consumption of a Western-style diet in C57/BL6J mice. Mol Nutr Food Res. 2011;55(4):530–40.

116. Seo MJ, Lee YJ, Hwang JH, Kim KJ, Lee BY. The inhibitory effects of quercetin on obesity and obesity-induced inflammation by regulation of MAPK signaling. J Nutr Biochem. 2015;26(11):1308–16.

117. Strobel P, Allard C, Perez-Acle T, Calderon R, Aldunate R, Leighton F. Myricetin, quercetin and catechin-gallate inhibit glucose uptake in isolated rat adipocytes. Biochem J. 2005 Mar 15;386(3):471–8.

118. Panchal SK, Poudyal H, Brown L. Quercetin Ameliorates Cardiovascular, Hepatic, and Metabolic Changes in Diet-Induced Metabolic Syndrome in Rats. J Nutr. 2012 Jun 1;142(6):1026–32.

119. Maciel RM, Costa MM, Martins DB, França RT, Schmatz R, Graça DL, et al. Antioxidant and anti-inflammatory effects of quercetin in functional and morphological alterations in streptozotocin-induced diabetic rats. Res Vet Sci. 2013 Oct;95(2):389–97.

120. Velescu BŞ, Anuţa V, Aldea A, Jinga M, Cobeleschi PC, Zbârcea CE, et al. Evaluation of protective effects of quercetin and vanadyl sulphate in alloxan induced diabetes model. Farmacia. 2017;65(2):200–6.

121. Luangaram S, Kukongviriyapan U, Pakdeechote P, Kukongviriyapan V, Pannangpetch P. Protective effects of quercetin against phenylhydrazine-induced vascular dysfunction and oxidative stress in rats. Food Chem Toxicol. 2007;45(3):448–55.

122. Porcu EP, Cossu M, Rassu G, Giunchedi P, Cerri G, Pourová J, et al. Aqueous injection of quercetin: An approach for confirmation of its direct in vivo cardiovascular effects. Int J Pharm. 2018;541(1–2):224–33.

123. Srinivasan P, Vijayakumar S, Kothandaraman S, Palani M. Anti-diabetic activity of quercetin extracted from Phyllanthus emblica L. fruit: In silico and in vivo approaches. J Pharm Anal. 2018;8(2):109–18.

124. DeFelice SL. The nutraceutical revolution: its impact on food industry R&D. Trends Food Sci Technol. 1995;6(2):59–61.

125. Schmitt J, Ferro A. Nutraceuticals: Is there good science behind the hype? Br J Clin

Pharmacol. 2013;75(3):585–7.

126. Piccolella S, Crescente G, Candela L, Pacifico S. Nutraceutical polyphenols: New analytical challenges and opportunities. J Pharm Biomed Anal. 2019;175:112774.

127. Williamson EM, Liu X, Izzo AA. Trends in use, pharmacology, and clinical applications of emerging herbal nutraceuticals. Br J Pharmacol. 2020 Mar 6;177(6):1227–40.

128. Vozza G, Khalid M, Byrne HJ, Ryan S, Frias J. Nutrition—nutrient delivery. In: Nutrient Delivery. Elsevier; 2017. p. 1–42.

129. Liyanage C, Hettiarachchi M. Food fortification. Ceylon Med J. 2011 Oct 1;56(3):124–7.

130. U.S. Food & Drug Administration (FDA). Dietary Supplement Products & Ingredients [Internet]. 2022 [cited 2022 Jul 26]. Available from: https://www.fda.gov/food/dietary-supplements/dietary-supplement-products-ingredients

131. European Medicines Agency (EMA). Glossary of regulatory terms [Internet]. [cited 2022 Jul 21]. Available from: https://www.ema.europa.eu/en/about-us/about-website/glossary/name_az/M

132. FDA Reader. How the FDA Regulates Nutraceuticals [Internet]. 2019 [cited 2022 Jul 26]. Available from: https://www.fdareader.com/blog/how-the-fda-regulates-nutraceuticals

133. U.S. Food & Drug Administration (FDA). Dietary Supplements [Internet]. 2022 [cited 2022 Jul 26]. Available from: https://www.fda.gov/food/dietary-supplements

134. European Food Safety Authority (EFSA). Food supplements [Internet]. [cited 2022 Jul 26]. Available from: https://www.efsa.europa.eu/en/topics/topic/food-supplements

135. BCC Research. FOD013H Nutraceuticals: Global Markets to 2026, Report overview [Internet]. 2021 [cited 2022 Jul 25]. Available from: https://www.bccresearch.com/market-research/food-and-beverage/nutraceuticals-global-markets.html

136. Rambaran TF. A patent review of polyphenol nano-formulations and their commercialization. Trends Food Sci Technol. 2022;120(January):111–22.

137. Singh T, Shukla S, Kumar P, Wahla V, Bajpai VK. Application of nanotechnology in food science: Perception and overview. Front Microbiol. 2017;8(AUG):1–7.

138. He X, Deng H, Hwang H min. The current application of nanotechnology in food and agriculture. J Food Drug Anal. 2019;27(1):1–21.

139. Ameta SK, Rai AK, Hiran D, Ameta R, Ameta SC. Use of Nanomaterials in Food Science. In: Biogenic Nano-Particles and their Use in Agro-ecosystems. Singapore: Springer Singapore; 2020. p. 457–88.

140. Singh H. Nanotechnology applications in functional foods; Opportunities and challenges. Prev Nutr Food Sci. 2016;21(1):1–8.

141. Singh R, Mann B, Sharma R, Singh S. Application of Nanotechnology in Functional Foods. In: Nanoscience for Sustainable Agriculture. Cham: Springer International Publishing; 2019. p. 547–79.

142. Flores FC, de Lima JA, Ribeiro RF, Alves SH, Rolim CMB, Beck RCR, et al. Antifungal Activity of Nanocapsule Suspensions Containing Tea Tree Oil on the Growth of Trichophyton rubrum. Mycopathologia. 2013 Apr 8;175(3–4):281–6.

143. Ghosh V, Mukherjee A, Chandrasekaran N. Ultrasonic emulsification of food-grade nanoemulsion formulation and evaluation of its bactericidal activity. Ultrason Sonochem. 2013;20(1):338–44.

144. Lucock M, Jones P, Martin C, Yates Z, Veysey M, Furst J, et al. Photobiology of vitamins. Nutr Rev. 2018;76(7):512–25.

145. Zhou W, Liu W, Zou L, Liu W, Liu C, Liang R, et al. Storage stability and skin permeation of vitamin C liposomes improved by pectin coating. Colloids Surfaces B Biointerfaces. 2014;117:330–7.

146. Azevedo MA, Bourbon AI, Vicente AA, Cerqueira MA. Alginate/chitosan nanoparticles for encapsulation and controlled release of vitamin B2. Int J Biol Macromol. 2014;71:141–6.

147. Soottitantawat A, Takayama K, Okamura K, Muranaka D, Yoshii H, Furuta T, et al. Microencapsulation of l-menthol by spray drying and its release characteristics. Innov Food Sci Emerg Technol. 2005;6(2):163–70.

148. Kayaci F, Uyar T. Encapsulation of vanillin/cyclodextrin inclusion complex in electrospun polyvinyl alcohol (PVA) nanowebs: Prolonged shelf-life and high temperature stability of vanillin. Food Chem. 2012;133(3):641–9.

149. Liu Y, Wang L, Zhao Y, He M, Zhang X, Niu M, et al. Nanostructured lipid carriers versus microemulsions for delivery of the poorly water-soluble drug luteolin. Int J Pharm. 2014;476(1):169–77.

150. Tripathi S, Kushwah V, Thanki K, Jain S. Triple antioxidant SNEDDS formulation with enhanced oral bioavailability: Implication of chemoprevention of breast cancer. Nanomedicine Nanotechnology, Biol Med. 2016;12(6):1431–43.

151. Maoka T. Carotenoids as natural functional pigments. J Nat Med. 2020;74(1):1–16.

152. Pan X, Yu S, Yao P, Shao Z. Self-assembly of β-casein and lysozyme. J Colloid Interface Sci. 2007;316(2):405–12.

153. Wang X, Jiang Y, Wang YW, Huang MT, Ho CT, Huang Q. Enhancing anti-inflammation activity of curcumin through O/W nanoemulsions. Food Chem. 2008;108(2):419–24.

154. Gramlich L, Ireton-Jones C, Miles JM, Morrison M, Pontes-Arruda A. Essential Fatty Acid Requirements and Intravenous Lipid Emulsions. J Parenter Enter Nutr.

2019;43(6):697–707.

155. Zimet P, Livney YD. Beta-lactoglobulin and its nanocomplexes with pectin as vehicles for ω-3 polyunsaturated fatty acids. Food Hydrocoll. 2009;23(4):1120–6.

156. Ghorbanzade T, Jafari SM, Akhavan S, Hadavi R. Nano-encapsulation of fish oil in nano-liposomes and its application in fortification of yogurt. Food Chem. 2017;216:146–52.

157. Peters R, Brandhoff P, Weigel S, Marvin H, Bouwmeester H, Aschberger K, et al. Inventory of Nanotechnology applications in the agricultural, feed and food sector. EFSA Support Publ. 2014;EN-621:125 pp.

158. Akbarzadeh A, Rezaei-Sadabady R, Davaran S, Joo SW, Zarghami N, Hanifehpour Y, et al. Liposome: Classification, preparation, and applications. Nanoscale Res Lett. 2013;8(1):1.

159. Jaiswal M, Dudhe R, Sharma PK. Nanoemulsion: an advanced mode of drug delivery system. 3 Biotech. 2015;5(2):123–7.

160. Duan Y, Dhar A, Patel C, Khimani M, Neogi S, Sharma P, et al. A brief review on solid lipid nanoparticles: Part and parcel of contemporary drug delivery systems. RSC Adv. 2020;10(45):26777–91.

161. Martínez-López AL, Pangua C, Reboredo C, Campión R, Morales-Gracia J, Irache JM. Protein-based nanoparticles for drug delivery purposes. Int J Pharm. 2020;581(March):119289.

162. Kianfar E. Protein nanoparticles in drug delivery: animal protein, plant proteins and protein cages, albumin nanoparticles. J Nanobiotechnology. 2021;19(1):1–32.

163. European Union Observatory for Nanomaterials (EUON). Food [Internet]. [cited 2022 Jun 28]. Available from: https://euon.echa.europa.eu/food

164. European Food Safety Authority (EFSA). Nanotechnology [Internet]. [cited 2022 Jun 28]. Available from: https://www.efsa.europa.eu/en/topics/topic/nanotechnology

165. Commission of the European Communities. Regulatory aspects of nanomaterials. Communication from the Commission to the European Parliament, the Council and the European Economic and Social Committee. Brussels; 2008.

166. Nile SH, Baskar V, Selvaraj D, Nile A, Xiao J, Kai G. Nanotechnologies in Food Science: Applications, Recent Trends, and Future Perspectives. Nano-Micro Lett. 2020 Dec 4;12(1):45.

167. The Project on Emerging Nanotechnologies. Consumer Products Inventory: Canola Active Oil [Internet]. [cited 2022 Jun 29]. Available from: https://www.nanotechproject.tech/cpi/products/canola-active-oil/

168. The Project on Emerging Nanotechnologies. Consumer Products Inventory: Nanotea [Internet]. [cited 2022 Jun 29]. Available from: https://www.nanotechproject.tech/cpi/products/nanotea/

169. The Project on Emerging Nanotechnologies. Consumer Products Inventory: Nanoceuticals Slim Shake Chocolate [Internet]. [cited 2022 Jun 29]. Available from: https://www.nanotechproject.tech/cpi/products/nanoceuticalstm-slim-shake-chocolate/

170. Rothen-Rutishauser B, Bogdanovich M, Harter R, Milosevic A, Petri-Fink A. Use of nanoparticles in food industry: current legislation, health risk discussions and public perception with a focus on Switzerland. Toxicol Environ Chem. 2021;103(4):420–34.

171. One planet nutrition. Nano Quercetin [Internet]. [cited 2022 Jun 9]. Available from: https://www.oneplanetnutrition.com/shop#!/Nano-Quercetin-120-Caps-250-mg/p/135605345/category=27372415

172. ActiNovo. Liposomal quercetin [Internet]. [cited 2022 Jun 9]. Available from: https://www.actinovo.com/en/liposomal-quercetin?number=LF0024.4&gclid=CjwKCAjwtIaVBhBkEiwAsr7-cxUsDHCbU_f7rmjJfxHdfU0gu7uo5wuJInX0XyfwV7KHq9m4tJU5rxoCpLwQAvD_BwE

173. Natural Factors. Quercetin LipoMicel Matrix [Internet]. [cited 2022 Sep 22]. Available from: https://ca.naturalfactors.com/products/quercetin-lipomicel-matrix

174. IHerb. Quercetin LipoMicel.Matrix [Internet]. [cited 2022 Jun 9]. Available from: https://es.iherb.com/pr/natural-factors-quercetin-lipomicel-matrix-60-liquid-softgels/101704?gclid=CjwKCAjwtIaVBhBkEiwAsr7-cwreNGbXqFMW5AMPzHBD6mRqSA7u4shTlVTArANMgzpp_J4X0f2dWxoCKtoQAvD_BwE&gclsrc=aw.ds

175. Anwer MK, Al-Mansoor MA, Jamil S, Al-Shdefat R, Ansari MN, Shakeel F. Development and evaluation of PLGA polymer based nanoparticles of quercetin. Int J Biol Macromol. 2016;92:213–9.

176. Arasoğlu T, Derman S, Mansuroğlu B, Uzunoğlu D, Koçyiğit B, Gümüş B, et al. Preparation, characterization, and enhanced antimicrobial activity: Quercetin-loaded PLGA nanoparticles against foodborne pathogens. Turkish J Biol. 2017;41(1):127–40.

177. Chitkara D, Nikalaje SK, Mittal A, Chand M, Kumar N. Development of quercetin nanoformulation and in vivo evaluation using streptozotocin induced diabetic rat model. Drug Deliv Transl Res. 2012;2(2):112–23.

178. Pool H, Quintanar D, Figueroa J de D, Bechara JEH, McClements DJ, Mendoza S. Polymeric Nanoparticles as Oral Delivery Systems for Encapsulation and Release of Polyphenolic Compounds: Impact on Quercetin Antioxidant Activity & Bioaccessibility. Food Biophys. 2012;7(3):276–88.

179. Sunoqrot S, Abujamous L. pH-sensitive polymeric nanoparticles of quercetin as a potential colon cancer-targeted nanomedicine. J Drug Deliv Sci Technol. 2019;52(April):670–6.

180. Kumar VD, Verma PRP, Singh SK, Viswanathan S. LC-ESI-MS/MS analysis of quercetin in rat plasma after oral administration of biodegradable nanoparticles. Biomed Chromatogr. 2015;29(11):1731–6.

181. Dinesh Kumar V, Verma PRP, Singh SK. Development and evaluation of biodegradable polymeric nanoparticles for the effective delivery of quercetin using a quality by design approach. LWT - Food Sci Technol. 2015;61(2):330–8.

182. Rifaai RA, Mokhemer SA, Saber EA, El-Aleem SAA, El-Tahawy NFG. Neuroprotective effect of quercetin nanoparticles: A possible prophylactic and therapeutic role in alzheimer's disease. J Chem Neuroanat. 2020;107(March):101795.

183. Bagad M, Khan ZA. Poly(n-butylcyanoacrylate) nanoparticles for oral delivery of quercetin: Preparation, characterization, and pharmacokinetics and biodistribution studies in Wistar rats. Int J Nanomedicine. 2015;10:3921–35.

184. Zhang Y, Yang Y, Tang K, Hu X, Zou G. Physicochemical characterization and antioxidant activity of quercetin-loaded chitosan nanoparticles. J Appl Polym Sci. 2008 Jan 15;107(2):891–7.

185. Aluani D, Tzankova V, Kondeva-Burdina M, Yordanov Y, Nikolova E, Odzhakov F, et al. Evaluation of Biocompatibility and Antioxidant Efficiency of Chitosan-Alginate Nanoparticles Loaded With Quercetin. Int J Biol Macromol. 2017;103:771–82.

186. Barbosa AI, Costa Lima SA, Reis S. Application of pH-responsive fucoidan/chitosan nanoparticles to improve oral quercetin delivery. Molecules. 2019;24(2).

187. Kim ES, Kim DY, Lee JS, Lee HG. Mucoadhesive chitosan-gum arabic nanoparticles enhance the absorption and antioxidant activity of quercetin in the intestinal cellular environment. J Agric Food Chem. 2019;67(31):8609–16.

188. Yan L, Wang R, Wang H, Sheng K, Liu C, Qu H, et al. Formulation and characterization of chitosan hydrochloride and carboxymethyl chitosan encapsulated quercetin nanoparticles for controlled applications in foods system and simulated gastrointestinal condition. Food Hydrocoll. 2018;84(June):450–7.

189. Selvaraj S, Shanmugasundaram S, Maruthamuthu M, Venkidasamy B, Shanmugasundaram S. Facile Synthesis and Characterization of Quercetin-Loaded Alginate Nanoparticles for Enhanced In Vitro Anticancer Effect Against Human Leukemic Cancer U937 Cells. J Clust Sci. 2020;32(6):1507–18.

190. Farrag Y, Ide W, Montero B, Rico M, Rodríguez-Llamazares S, Barral L, et al. Preparation of starch nanoparticles loaded with quercetin using nanoprecipitation technique. Int J Biol Macromol. 2018;114:426–33.

191. Wang T, Wu C, Li T, Fan G, Gong H, Liu P, et al. Comparison of two nanocarriers for quercetin in morphology, loading behavior, release kinetics and cell inhibitory activity. Mater Express. 2020;10(10):1589–98.

192. Li HL, Zhao X Bin, Ma YK, Zhai GX, Li LB, Lou HX. Enhancement of gastrointestinal absorption of quercetin by solid lipid nanoparticles. J Control Release.

2009;133(3):238–44.

193. Ahmad N, Banala VT, Kushwaha P, Karvande A, Sharma S, Tripathi AK, et al. Quercetin-loaded solid lipid nanoparticles improve osteoprotective activity in an ovariectomized rat model: A preventive strategy for post-menopausal osteoporosis. RSC Adv. 2016;6(100):97613–28.

194. Rodríguez-Félix F, Del-Toro-Sánchez CL, Javier Cinco-Moroyoqui F, Juárez J, Ruiz-Cruz S, López-Ahumada GA, et al. Preparation and Characterization of Quercetin-Loaded Zein Nanoparticles by Electrospraying and Study of In Vitro Bioavailability. J Food Sci. 2019;84(10):2883–97.

195. Moreno LCG e I, Puerta E, Suárez-Santiago JE, Santos-Magalhães NS, Ramirez MJ, Irache JM. Effect of the oral administration of nanoencapsulated quercetin on a mouse model of Alzheimer's disease. Int J Pharm. 2017 Jan;517(1–2):50–7.

196. Giannouli M, Karagkiozaki V, Pappa F, Moutsios I, Gravalidis C, Logothetidis S. Fabrication of quercetin-loaded PLGA nanoparticles via electrohydrodynamic atomization for cardiovascular disease. Mater Today Proc. 2018;5(8):15998–6005.

197. Zhou Y, Chen D, Xue G, Yu S, Yuan C, Huang M, et al. Improved therapeutic efficacy of quercetin-loaded polymeric nanoparticles on triple-negative breast cancer by inhibiting uPA. RSC Adv. 2020;10(57):34517–26.

198. Li H, Wang D, Liu C, Zhu J, Fan M, Sun X, et al. Fabrication of stable zein nanoparticles coated with soluble soybean polysaccharide for encapsulation of quercetin. Food Hydrocoll. 2019;87(August 2018):342–51.

199. Zhou JF, Zheng GD, Wang WJ, Yin ZP, Chen JG, Li JE, et al. Physicochemical properties and bioavailability comparison of two quercetin loading zein nanoparticles with outer shell of caseinate and chitosan. Food Hydrocoll. 2021;120(March):106959.

200. Chavoshpour-Natanzi Z, Sahihi M. Encapsulation of quercetin-loaded β-lactoglobulin for drug delivery using modified anti-solvent method. Food Hydrocoll. 2019;96(May):493–502.

201. Reboredo C, González-Navarro CJ, Martínez-Oharriz C, Martínez-López AL, Irache JM. Preparation and evaluation of PEG-coated zein nanoparticles for oral drug delivery purposes. Int J Pharm. 2021;597(January).

202. Doktorovova S, Shegokar R, Martins-Lopes P, Silva AM, Lopes CM, Müller RH, et al. Modified Rose Bengal assay for surface hydrophobicity evaluation of cationic solid lipid nanoparticles (cSLN). Eur J Pharm Sci. 2012;45(5):606–12.

203. Martínez-López AL, González-Navarro CJ, Vizmanos JL, Irache JM. Zein-based nanocarriers for the oral delivery of insulin. In vivo evaluation in Caenorhabditis elegans. Drug Deliv Transl Res. 2021 Apr 29;11(2):647–58.

204. Abdulkarim M, Agulló N, Cattoz B, Griffiths P, Bernkop-Schnürch A, Gómez Borros S, et al. Nanoparticle diffusion within intestinal mucus: Three-dimensional response analysis dissecting the impact of particle surface charge, size and

heterogeneity across polyelectrolyte, pegylated and viral particles. Eur J Pharm Biopharm. 2015;97:230–8.

205. Schindelin J, Arganda-Carreras I, Frise E, Kaynig V, Longair M, Pietzsch T, et al. Fiji: an open-source platform for biological-image analysis. Nat Methods. 2012 Jul 28;9(7):676–82.

206. Brenner S. The genetics of Caenorhabditis elegans. Genetics. 1974;77(1):71–94.

207. Stiernagle T. Maintenance of C. elegans. WormBook. 2006;(1999):1–11.

208. Navarro-Herrera D, Aranaz P, Eder-Azanza L, Zabala M, Hurtado C, Romo-Hualde A, et al. Dihomo-gamma-linolenic acid induces fat loss in: C. Elegans in an omega-3-independent manner by promoting peroxisomal fatty acid β-oxidation. Food Funct. 2018;9(3):1621–37.

209. Inchaurraga L, Martín-Arbella N, Zabaleta V, Quincoces G, Peñuelas I, Irache JM. In vivo study of the mucus-permeating properties of PEG-coated nanoparticles following oral administration. Eur J Pharm Biopharm. 2015;97:280–9.

210. Zhang Y, Huo M, Zhou J, Xie S. PKSolver: An add-in program for pharmacokinetic and pharmacodynamic data analysis in Microsoft Excel. Comput Methods Programs Biomed. 2010;99(3):306–14.

211. Aranaz P, Navarro-Herrera D, Romo-Hualde A, Zabala M, López-Yoldi M, González-Ferrero C, et al. Broccoli extract improves high fat diet-induced obesity, hepatic steatosis and glucose intolerance in Wistar rats. J Funct Foods. 2019;59(June):319–28.

212. Heinemann L. Insulin Assay Standardization: Leading to Measures of Insulin Sensitivity and Secretion for Practical Clinical Care. Diabetes Care. 2010;33(6):e83.

213. Matthews DR, Hosker JP, Rudenski AS, Naylor BA, Treacher DF, Turner RC. Homeostasis model assessment: insulin resistance and β-cell function from fasting plasma glucose and insulin concentrations in man. Diabetologia. 1985;28(7):412–9.

214. Staten MA, Stern MP, Miller WG, Steffes MW, Campbell SE. Insulin assay standardization: Leading to measures of insulin sensitivity and secretion for practical clinical care. Diabetes Care. 2010;33(1):205–6.

215. Navarro-Herrera D, Aranaz P, Eder-Azanza L, Zabala M, Romo-Hualde A, Hurtado C, et al. Borago officinalis seed oil (BSO), a natural source of omega-6 fatty acids, attenuates fat accumulation by activating peroxisomal beta-oxidation both in C. elegans and in diet-induced obese rats. Food Funct. 2018;9(8):4340–51.

216. Cui A, Hu Z, Han Y, Yang Y, Li Y. Optimized analysis of in vivo and in vitro hepatic steatosis. J Vis Exp. 2017;2017(121):1–6.

217. Livak KJ, Schmittgen TD. Analysis of relative gene expression data using real-time quantitative PCR and the $2^{-\Delta\Delta CT}$ method. Methods. 2001;25(4):402–8.

218. Kiratli PO, Aksoy T, Bozkurt MF, Orhan D. Detection of ectopic gastric mucosa

using ^{99m}Tc pertechnetate: Review of the literature. Ann Nucl Med. 2009;23(2):97–105.

219. Chusyd DE, Wang D, Huffman DM, Nagy TR. Relationships between Rodent White Adipose Fat Pads and Human White Adipose Fat Depots. Front Nutr. 2016;3(April).

220. Bhanu Prakash KN, Gopalan V, Lee SS, Velan SS. Quantification of abdominal fat depots in rats and mice during obesity and weight loss interventions. PLoS One. 2014;9(10):1–9.

221. Sebo ZL, Rodeheffer MS. Assembling the adipose organ: Adipocyte lineage segregation and adipogenesis in vivo. Dev. 2019;146(7).

222. Nijhuis THJ, de Boer SAS, Wahegaonkar AL, Bishop AT, Shin AY, Hovius SER, et al. A New Approach to Assess the Gastrocnemius Muscle Volume in Rodents Using Ultrasound; Comparison with the Gastrocnemius Muscle Index. Kincaid AE, editor. PLoS One. 2013 Jan 10;8(1):e54041.

223. Ulrich Welsch. Sobotta. Histología. 3rd editio. Editorial Médica Panamericana; 2013. 588 p.

224. Tillander V, Alexson SEH, Cohen DE. Deactivating Fatty Acids: Acyl-CoA Thioesterase-Mediated Control of Lipid Metabolism. Trends Endocrinol Metab. 2017;28(7):473–84.

225. Poirier Y, Antonenkov VD, Glumoff T, Hiltunen JK. Peroxisomal β-oxidation-A metabolic pathway with multiple functions. Biochim Biophys Acta - Mol Cell Res. 2006;1763(12):1413–26.

226. Wang J, Xiang H, Lu Y, Wu T, Ji G. The role and therapeutic implication of CPTs in fatty acid oxidation and cancers progression. Am J Cancer Res. 2021;11(6):2477–94.

227. Pecka-Kiełb E, Kowalewska-Łuczak I, Czerniawska-Piątkowska E, Króliczewska B. FASN, SCD1 and ANXA9 gene polymorphism as genetic predictors of the fatty acid profile of sheep milk. Sci Rep. 2021;11(1):1–11.

228. Rui L. Brown and beige adipose tissues in health and disease. Compr Physiol. 2017;7(4):1281–306.

229. DeBose-Boyd RA, Ye J. SREBPs in Lipid Metabolism, Insulin Signaling, and Beyond. Trends Biochem Sci. 2018;43(5):358–68.

230. Hillard CJ, Huang H, Vogt CD, Rodrigues BE, Neumann TS, Sem DS, et al. Endocannabinoid Transport Proteins: Discovery of Tools to Study Sterol Carrier Protein-2. Methods Enzymol. 2017;593:99–121.

231. Enns JE, Taylor CG, Zahradka P. Variations in adipokine genes AdipoQ, Lep, and LepR are associated with risk for obesity-related metabolic disease: The modulatory role of gene-nutrient interactions. J Obes. 2011;2011.

232. Osuna-Prieto FJ, Martinez-Tellez B, Segura-Carretero A, Ruiz JR. Activation of Brown Adipose Tissue and Promotion of White Adipose Tissue Browning by Plant-

based Dietary Components in Rodents: A Systematic Review. Adv Nutr. 2021;12(6):2147–56.

233. Irache JM, González-Navarro CJ. Zein nanoparticles as vehicles for oral delivery purposes. Nanomedicine. 2017 Jun;12(11):1209–11.

234. Berardi A, Bisharat L, AlKhatib HS, Cespi M. Zein as a Pharmaceutical Excipient in Oral Solid Dosage Forms: State of the Art and Future Perspectives. AAPS PharmSciTech. 2018;19(5):2009–22.

235. Reboredo C, González-Navarro CJ, Martínez-López AL, Martínez-Oharriz C, Sarmento B, Irache JM. Zein-Based Nanoparticles as Oral Carriers for Insulin Delivery. Pharmaceutics. 2022 Dec 24;14(1):39.

236. Brotons-Canto A, Gonzalez-Navarro CJ, Gurrea J, González-Ferrero C, Irache JM. Zein nanoparticles improve the oral bioavailability of resveratrol in humans. J Drug Deliv Sci Technol. 2020;57(March):101704.

237. Ghafoor K, Özcan MM, AL-Juhaımı F, Babıker EE, Sarker ZI, Ahmed IAM, et al. Nutritional composition, extraction, and utilization of wheat germ oil: A review. Eur J Lipid Sci Technol. 2017;119(7):1–9.

238. Agencia Española de Seguridad Alimentaria y Nutrición (AESAN). Food for specific groups, food supplements and natural mineral waters notified in Spain [Internet]. [cited 2022 Jul 29]. Available from: https://rgsa-web-aesan.mscbs.es/rgsa/resultado_producto.jsp

239. More S, Bampidis V, Benford D, Bragard C, Halldorsson T, Hernández-Jerez A, et al. Guidance on risk assessment of nanomaterials to be applied in the food and feed chain: human and animal health. EFSA J. 2021;19(8):111 pp.

240. Pangua C, Reboredo C, Campión R, Gracia JM, Martínez-López AL, Irache JM. Mucus-penetrating nanocarriers. In: Theory and Applications of Nonparenteral Nanomedicines. Elsevier; 2021. p. 137–52.

241. Suk JS, Xu Q, Kim N, Hanes J, Ensign LM. PEGylation as a strategy for improving nanoparticle-based drug and gene delivery. Adv Drug Deliv Rev. 2016 Apr;99(1):28–51.

242. D'souza AA, Shegokar R. Polyethylene glycol (PEG): a versatile polymer for pharmaceutical applications. Expert Opin Drug Deliv. 2016 Sep 1;13(9):1257–75.

243. Shi L, Zhang J, Zhao M, Tang S, Cheng X, Zhang W, et al. Effects of polyethylene glycol on the surface of nanoparticles for targeted drug delivery. Nanoscale. 2021;13(24):10748–64.

244. Yuan H, Chen CY, Chai GH, Du YZ, Hu FQ. Improved transport and absorption through gastrointestinal tract by pegylated solid lipid nanoparticles. Mol Pharm. 2013;10(5):1865–73.

245. Liao VHC. Use of Caenorhabditis elegans to Study the Potential Bioactivity of Natural Compounds. J Agric Food Chem. 2018;66(8):1737–42.

246. Corsi AK, Wightman B, Chalfie M. A Transparent window into biology: A primer

on Caenorhabditis elegans. WormBook. 2015;1–31.

247. Dimov I, Maduro MF. The C. elegans intestine: organogenesis, digestion, and physiology. Cell Tissue Res. 2019;377(3):383–96.

248. Hunt PR. The C. elegans model in toxicity testing. J Appl Toxicol. 2017;37(1):50–9.

249. Lin Y, Yang N, Bao B, Wang L, Chen J, Liu J. Luteolin reduces fat storage in Caenorhabditis elegans by promoting the central serotonin pathway. Food Funct. 2020;11(1):730–40.

250. Shen P, Yue Y, Zheng J, Park Y. Caenorhabditis elegans: A Convenient In Vivo Model for Assessing the Impact of Food Bioactive Compounds on Obesity, Aging, and Alzheimer's Disease. Annu Rev Food Sci Technol. 2018;9:1–22.

251. Peng H, Wei Z, Luo H, Yang Y, Wu Z, Gan L, et al. Inhibition of Fat Accumulation by Hesperidin in Caenorhabditis elegans. J Agric Food Chem. 2016 Jun 29;64(25):5207–14.

252. Aranaz P, Peña A, Vettorazzi A, Fabra MJ, Martínez-Abad A, López-Rubio A, et al. Grifola frondosa (Maitake) Extract Reduces Fat Accumulation and Improves Health Span in C. elegans through the DAF-16/FOXO and SKN-1/NRF2 Signalling Pathways. Nutrients. 2021 Nov 7;13(11):3968.

253. Lin Y, Bao B, Yin H, Wang X, Feng A, Zhao L, et al. Peripheral cathepsin L inhibition induces fat loss in C. elegans and mice through promoting central serotonin synthesis. BMC Biol. 2019;17(1):1–19.

254. Shen P, Yue Y, Kim KH, Park Y. Piceatannol Reduces Fat Accumulation in Caenorhabditis elegans. J Med Food. 2017;20(9):887–94.

255. Aranaz P, Navarro-Herrera D, Zabala M, Romo-Hualde A, López-Yoldi M, Vizmanos JL, et al. Phenolic compounds reduce the fat content in caenorhabditis elegans by affecting lipogenesis, lipolysis, and different stress responses. Pharmaceuticals. 2020;13(11):1–33.

256. Shen P, Hsieh TH, Yue Y, Sun Q, Clark JM, Park Y. Deltamethrin increases the fat accumulation in 3T3-L1 adipocytes and Caenorhabditis elegans. Food Chem Toxicol. 2017;101:149–56.

257. Martínez-López AL, González-Navarro CJ, Aranaz P, Vizmanos JL, Irache JM. In vivo testing of mucus-permeating nanoparticles for oral insulin delivery using Caenorhabditis elegans as a model under hyperglycemic conditions. Acta Pharm Sin B. 2021 Apr;11(4):989–1002.

258. Lucio D, Martínez-Ohárriz MC, Jaras G, Aranaz P, González-Navarro CJ, Radulescu A, et al. Optimization and evaluation of zein nanoparticles to improve the oral delivery of glibenclamide. In vivo study using C. elegans. Eur J Pharm Biopharm. 2017 Dec;121:104–12.

259. Inchaurraga L, Martínez-López AL, Martin-Arbella N, Irache JM. Zein-based nanoparticles for the oral delivery of insulin. Drug Deliv Transl Res. 2020;10(6):1601–11.

260. Lucio D, Martínez-Ohárriz MC, Gu Z, He Y, Aranaz P, Vizmanos JL, et al. Cyclodextrin-grafted poly(anhydride) nanoparticles for oral glibenclamide administration. In vivo evaluation using C. elegans. Int J Pharm. 2018;547(1–2):97–105.

261. Lucio D, Martínez-Ohárriz MC, González-Navarro CJ, Navarro-Herrera D, González-Gaitano G, Radulescu A, et al. Coencapsulation of cyclodextrins into poly(anhydride) nanoparticles to improve the oral administration of glibenclamide. A screening on C. elegans. Colloids Surfaces B Biointerfaces. 2018;163:64–72.

262. Shen P, Zhang R, McClements DJ, Park Y. Nanoemulsion-based delivery systems for testing nutraceutical efficacy using Caenorhabditis elegans: Demonstration of curcumin bioaccumulation and body-fat reduction. Food Res Int. 2019;120(December 2018):157–66.

263. Escorcia W, Ruter DL, Nhan J, Curran SP. Quantification of Lipid Abundance and Evaluation of Lipid Distribution in Caenorhabditis elegans by Nile Red and Oil Red O Staining. J Vis Exp. 2018;2018(133):1–6.

264. Chen X, Yin OQP, Zuo Z, Chow MSS. Pharmacokinetics and modeling of quercetin and metabolites. Vol. 22, Pharmaceutical Research. 2005. p. 892–901.

265. Li H, Li M, Fu J, Ao H, Wang W, Wang X. Enhancement of oral bioavailability of quercetin by metabolic inhibitory nanosuspensions compared to conventional nanosuspensions. Drug Deliv. 2021;28(1):1226–36.

266. Malek M, Yousefi R, Safari S, Seyyedi SHS, Mottaghi A. Dietary Intakes and Biochemical Parameters of Morbidly Obese Patients Prior to Bariatric Surgery. Obes Surg. 2019;29(6):1816–22.

267. Ben-Porat T, Weiss R, Sherf-Dagan S, Nabulsi N, Maayani A, Khalaileh A, et al. Nutritional Deficiencies in Patients with Severe Obesity before Bariatric Surgery: What Should Be the Focus During the Preoperative Assessment? J Acad Nutr Diet. 2020;120(5):874–84.

268. Salazar Lugo R, Nicolalde Saavedra J, Maldonado Noboa V, Santamaría Coronado M, Barahona Meneses A, Salas Salas H, et al. Prevalencia de parámetros nutricionales, bioquímicos y estilos de vida en adultos con fenotipos cardiometabólicos de Imbabura, Ecuador / Nutritional, biochemical parameters and life styles associated with developed of in adults of Imbabura, Ecuador. Nutr Clin y Diet Hosp. 2016;36(3):153–61.

269. Molina-Ayala M, Rodríguez-González A, Albarrán-Sánchez A, Ferreira-Hermosillo A, Ramírez-Rentería C, Luque-de León E, et al. Características clínicas y bioquímicas de pacientes con obesidad extrema al ingreso y un año después de someterse a cirugía bariátrica / Clinical and biochemical characteristics of patients with morbid obesity at the time of hospital admission and one year after undergoing bariatric surgery. Rev Med Inst Mex Seguro Soc. 2016;54:S118–23.

270. Catalán V, Gómez-Ambrosi J, Ramirez B, Rotellar F, Pastor C, Silva C, et al. Proinflammatory cytokines in obesity: Impact of type 2 diabetes mellitus and

gastric bypass. Obes Surg. 2007;17(11):1464–74.

271. Sorlí Guerola JV. Obesidad y alteraciones metabólicas: Factores genéticos y ambientales en población mediterránea. University of Valencia; 2008.

272. Huang XJ, Choi YK, Im HS, Yarimaga O, Yoon E, Kim HS. Aspartate aminotransferase (AST/GOT) and alanine aminotransferase (ALT/GPT) detection techniques. Sensors. 2006;6(7):756–82.

273. Sattar N, Forrest E, Preiss D. Non-alcoholic fatty liver disease. BMJ. 2014;349(July):1–8.

274. Sanyal D, Mukherjee P, Raychaudhuri M, Ghosh S, Mukherjee S, Chowdhury S. Profile of liver enzymes in non-alcoholic fatty liver disease in patients with impaired glucose tolerance and newly detected untreated type 2 diabetes. Indian J Endocrinol Metab. 2015;19(5):597–601.

275. Iser D, Ryan M. Fatty Liver Disease A practical guide for GPs. Aust Fam Physician. 2013 Nov 27;42(7):444–7.

276. Chiuman V, Chiuman L, Tanjung DS, Miftahulaila M, Erawati S, Florenly. Oral Ulcer Healing Activity of Lemon Pepper Ethanol Extract Gel in Streptozotocin-Induced Diabetic Wistar Rats. Maj Kedokt Bandung. 2022 Jun;52(2):80–8.

277. Irudayaraj SS, Jincy J, Sunil C, Duraipandiyan V, Ignacimuthu S, Chandramohan G, et al. Antidiabetic with antilipidemic and antioxidant effects of flindersine by enhanced glucose uptake through GLUT4 translocation and PPARγ agonism in type 2 diabetic rats. J Ethnopharmacol. 2022 Mar;285:114883.

278. Mukhopadhyay P, Maity S, Mandal S, Chakraborti AS, Prajapati AK, Kundu PP. Preparation, characterization and in vivo evaluation of pH sensitive, safe quercetin-succinylated chitosan-alginate core-shell-corona nanoparticle for diabetes treatment. Carbohydr Polym. 2018;182(August 2017):42–51.

279. Okyar A, Can A, Akev N, Baktir G, Sütlüpinar N. Effect of Aloe vera leaves on blood glucose level in type I and type II diabetic rat models. Phyther Res. 2001;15(2):157–61.

280. Tang Q, Li X, Song P, Xu L. Optimal cut-off values for the homeostasis model assessment of insulin resistance (HOMA-IR) and pre-diabetes screening: Developments in research and prospects for the future. Drug Discov Ther. 2015;9(6):380–5.

281. Aranaz P, Romo-Hualde A, Navarro-Herrera D, Zabala M, López-Yoldi M, González-Ferrero C, et al. Low doses of cocoa extract supplementation ameliorate diet-induced obesity and insulin resistance in rats. Food Funct. 2019;10(8):4811–22.

282. Papandreou C, García-Gavilán J, Camacho-Barcia L, Hansen TT, Sjödin A, Harrold JA, et al. Circulating metabolites associated with body fat and lean mass in adults with overweight/obesity. Metabolites. 2021;11(5):1–11.

283. Panee J. Monocyte Chemoattractant Protein 1 (MCP-1) in obesity and diabetes.

Cytokine. 2012;60(1):1–12.

284. Mandal A. Blood Sugar Glucose Measurement [Internet]. News-Medical. 2019 [cited 2022 Aug 16]. Available from: https://www.news-medical.net/health/Blood-Sugar-Glucose-Measurement.aspx#:~:text=Whole blood and serum blood,it is multiplied by 1.15.

285. Sato S, Mukai Y. Modulation of chronic inflammation by quercetin: The beneficial effects on obesity. J Inflamm Res. 2020;13:421–31.

286. Melgarejo E, Medina MÁ, Sánchez-Jiménez F, Urdiales JL. Monocyte chemoattractant protein-1: A key mediator in inflammatory processes. Int J Biochem Cell Biol. 2009;41(5):998–1001.

287. Kim CS, Park HS, Kawada T, Kim JH, Lim D, Hubbard NE, et al. Circulating levels of MCP-1 and IL-8 are elevated in human obese subjects and associated with obesity-related parameters. Int J Obes. 2006;30(9):1347–55.

288. Sartipy P, Loskutoff DJ. Monocyte chemoattractant protein 1 in obesity and insulin resistance. Proc Natl Acad Sci. 2003 Jun 10;100(12):7265–70.

289. Fernández-Sánchez A, Madrigal-Santillán E, Bautista M, Esquivel-Soto J, Morales-González Á, Esquivel-Chirino C, et al. Inflammation, oxidative stress, and obesity. Int J Mol Sci. 2011;12(5):3117–32.

290. Indra MR, Karyono S, Ratnawati R, Malik SG. Quercetin suppresses inflammation by reducing ERK1/2 phosphorylation and NF kappa B activation in Leptin-induced Human Umbilical Vein Endothelial Cells (HUVECs). BMC Res Notes. 2013;6(1):0–7.

291. Comalada M, Camuesco D, Sierra S, Ballester I, Xaus J, Gálvez J, et al. In vivo quercitrin anti-inflammatory effect involves release of quercetin, which inhibits inflammation through down-regulation of the NF-κB pathway. Eur J Immunol. 2005;35(2):584–92.

292. Houten SM, Wanders RJA. A general introduction to the biochemistry of mitochondrial fatty acid β-oxidation. J Inherit Metab Dis. 2010;33(5):469–77.

293. Hunt MC, Solaas K, Frode Kase B, Alexson SEH. Characterization of an acyl-CoA thioesterase that functions as a major regulator of peroxisomal lipid metabolism. J Biol Chem. 2002;277(2):1128–38.

294. Hunt MC, Siponen MI, Alexson SEH. The emerging role of acyl-CoA thioesterases and acyltransferases in regulating peroxisomal lipid metabolism. Biochim Biophys Acta - Mol Basis Dis. 2012;1822(9):1397–410.

295. Hunt MC, Alexson SEH. The role Acyl-CoA thioesterases play in mediating intracellular lipid metabolism. Prog Lipid Res. 2002;41(2):99–130.

296. Aires V, Delmas D, Djouadi F, Bastin J, Cherkaoui-Malki M, Latruffe N. Resveratrol-induced changes in MicroRNA expression in primary human fibroblasts harboring carnitine-palmitoyl transferase-2 gene mutation, leading to fatty acid oxidation deficiency. Molecules. 2018;23(1).

297. Zeng J, Deng S, Wang Y, Li P, Tang L, Pang Y. Specific inhibition of acyl-CoA oxidase-1 by an acetylenic acid improves hepatic lipid and Reactive Oxygen Species (ROS) metabolism in rats fed a high fat diet. J Biol Chem. 2017;292(9):3800–9.

298. Meyer K, Jia Y, Cao W-Q, Kashireddy P, Ra M. Expression of peroxisome proliferator-activated receptor α, and PPARα regulated genes in spontaneously developed hepatocellular carcinomas in fatty acyl-CoA oxidase null mice. Int J Oncol. 2002 Dec 1;

299. Sheridan R, Lampe K, Shanmukhappa SK, Putnam P, Keddache M, Divanovic S, et al. Lampe1: An ENU-Germline Mutation Causing Spontaneous Hepatosteatosis Identified through Targeted Exon-Enrichment and Next-Generation Sequencing. Silver DL, editor. PLoS One. 2011 Jul 7;6(7):e21979.

300. Moreno-Fernandez ME, Giles DA, Stankiewicz TE, Sheridan R, Karns R, Cappelletti M, et al. Peroxisomal β-oxidation regulates whole body metabolism, inflammatory vigor, and pathogenesis of nonalcoholic fatty liver disease. JCI insight. 2018;3(6).

301. Pierce SB, Walsh T, Chisholm KM, Lee MK, Thornton AM, Fiumara A, et al. Mutations in the DBP-deficiency protein HSD17B4 cause ovarian dysgenesis, hearing loss, and ataxia of perrault syndrome. Am J Hum Genet. 2010;87(2):282–8.

302. Huyghe S, Mannaerts GP, Baes M, Van Veldhoven PP. Peroxisomal multifunctional protein-2: The enzyme, the patients and the knockout mouse model. Biochim Biophys Acta - Mol Cell Biol Lipids. 2006;1761(9):973–94.

303. Obradovic M, Sudar-Milovanovic E, Soskic S, Essack M, Arya S, Stewart AJ, et al. Leptin and Obesity: Role and Clinical Implication. Front Endocrinol (Lausanne). 2021;12(May):1–14.

304. Brondani L de A, Assmann TS, Duarte GCK, Gross JL, Canani LH, Crispim D. The role of the uncoupling protein 1 (UCP1) on the development of obesity and type 2 diabetes mellitus. Vol. 56, Arquivos Brasileiros de Endocrinologia & Metabologia. 2012. p. 215–25.

305. Herz CT, Kiefer FW. Adipose tissue browning in mice and humans. J Endocrinol. 2019;241(3):R97–109.

306. Choi H, Kim CS, Yu R. Quercetin upregulates uncoupling protein 1 in white/brown adipose tissues through sympathetic stimulation. J Obes Metab Syndr. 2018;27(2):102–9.

307. Faghfouri AH, Khajebishak Y, Payahoo L, Faghfuri E, Alivand M. PPAR-gamma agonists: Potential modulators of autophagy in obesity. Eur J Pharmacol. 2021;912(October):174562.

308. Janani C, Ranjitha Kumari BD. PPAR gamma gene - A review. Diabetes Metab Syndr Clin Res Rev. 2015;9(1):46–50.

309. Vluggens A, K. Reddy J. Nuclear Receptors and Transcription Factors in the Development of Fatty Liver Disease. Curr Drug Metab. 2012;13(10):1422–35.

310. Cano-Martínez A, Bautista-Pérez R, Castrejón-Téllez V, Carreón-Torres E, Pérez-Torres I, Díaz-Díaz E, et al. Resveratrol and quercetin as regulators of inflammatory and purinergic receptors to attenuate liver damage associated to metabolic syndrome. Int J Mol Sci. 2021;22(16):1–16.

311. Oberkofler H, Fukushima N, Esterbauer H, Krempler F, Patsch W. Sterol regulatory element binding proteins: Relationship of adipose tissue gene expression with obesity in humans. Biochim Biophys Acta - Gene Struct Expr. 2002;1575(1–3):75–81.

312. Shimano H, Sato R. SREBP-regulated lipid metabolism: Convergent physiology-divergent pathophysiology. Nat Rev Endocrinol. 2017;13(12):710–30.

313. Menendez JA, Vazquez-Martin A, Ortega FJ, Fernandez-Real JM. Fatty acid synthase: Association with insulin resistance, type 2 diabetes, and cancer. Clin Chem. 2009;55(3):425–38.

314. Fhu CW, Ali A. Fatty Acid Synthase: An Emerging Target in Cancer. Molecules. 2020;25(17):1–22.

315. Ansari P, Choudhury ST, Seidel V, Rahman A Bin, Aziz MA, Richi AE, et al. Therapeutic Potential of Quercetin in the Management of Type-2 Diabetes Mellitus. Life. 2022 Jul 28;12(8):1146.

316. Kriska T, Pilat A, Schmitt JC, Girotti AW. Sterol carrier protein-2 (SCP-2) involvement in cholesterol hydroperoxide cytotoxicity as revealed by SCP-2 inhibitor effects. J Lipid Res. 2010;51(11):3174–84.

317. Xu C, Li H, Tang CK. Sterol carrier protein 2 in lipid metabolism and non-alcoholic fatty liver disease: Pathophysiology, molecular biology, and potential clinical implications. Metabolism. 2022;131(November 2021):155180.

318. Smith DA, Beaumont K, Maurer TS, Di L. Relevance of Half-Life in Drug Design. J Med Chem. 2018;61(10):4273–82.

319. Schrag M, Regal K. Pharmacokinetics and Toxicokinetics. In: A Comprehensive Guide to Toxicology in Nonclinical Drug Development. Elsevier; 2013. p. 69–106.

320. McKenney JM. A comparison of the efficacy and toxic effects of sustained- vs immediate-release niacin in hypercholesterolemic patients. JAMA J Am Med Assoc. 1994 Mar 2;271(9):672–7.

321. Yadav SK, Mishra S, Mishra B. Eudragit-based nanosuspension of poorly water-soluble drug: Formulation and in vitro-in vivo evaluation. AAPS PharmSciTech. 2012;13(4):1031–44.

322. Elmotasem H, Farag HK, Salama AAA. In vitro and in vivo evaluation of an oral sustained release hepatoprotective caffeine loaded w/o Pickering emulsion formula – Containing wheat germ oil and stabilized by magnesium oxide nanoparticles. Int J Pharm. 2018;547(1–2):83–96.

323. Tang Y, Nakashima S, Saiki S, Myoi Y, Abe N, Kuwazuru S, et al. 3,4-Dihydroxyphenylacetic acid is a predominant biologically-active catabolite of

quercetin glycosides. Food Res Int. 2016;89:716–23.

324. Liu Y, Myojin T, Li K, Kurita A, Seto M, Motoyama A, et al. A Major Intestinal Catabolite of Quercetin Glycosides, 3-Hydroxyphenylacetic Acid, Protects the Hepatocytes from the Acetaldehyde-Induced Cytotoxicity through the Enhancement of the Total Aldehyde Dehydrogenase Activity. Int J Mol Sci. 2022;23(3):1–13.

325. Catalán M, Ferreira J, Carrasco-Pozo C. The Microbiota-Derived Metabolite of Quercetin, 3,4-Dihydroxyphenylacetic Acid Prevents Malignant Transformation and Mitochondrial Dysfunction Induced by Hemin in Colon Cancer and Normal Colon Epithelia Cell Lines. Molecules. 2020;25(18).

326. Liu M, Wang L, Huang B, Lu Q, Liu R. 3,4-Dihydroxyphenylacetic acid ameliorates gut barrier dysfunction via regulation of MAPK-MLCK pathway in type 2 diabetes mice. Life Sci. 2022;305(June):120742.